PAUL SCHERRER INSTITUT

PSI

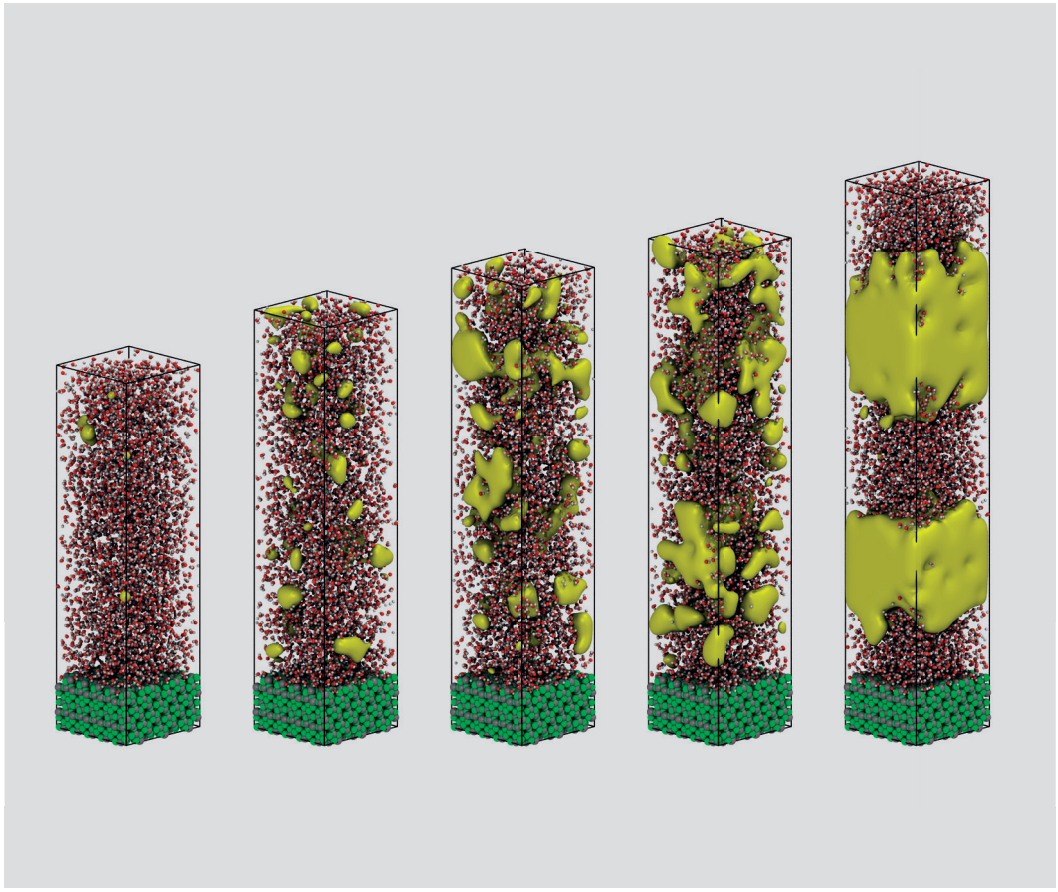

Progress Report 2019

Laboratory for Waste Management :: Nuclear Energy and Safety Department

Cover
Air bubble nucleation at a boiling water-ZrO_2 interface obtained by transition path sampling molecular dynamics simulations.

swiss safety center
ISO 9001
certified system

PAUL SCHERRER INSTITUT

PSI

Progress Report 2019

Laboratory for Waste Management
Nuclear Energy and Safety Department

See also our web-page
http://www.psi.ch/les/

Preface

The mission of the Laboratory for Waste Management (LES) is to carry out a comprehensive research and development (R&D) programme in support of Swiss radioactive waste disposal options. In particular, the aim is to be one of the world-leading laboratories in the fields of geochemistry of disposal systems and transport mechanisms of radionuclides, including geochemical retardation and immobilisation.

The laboratory serves an important national role by supporting the Swiss Federal Government and Nagra in their tasks to safely dispose of radioactive wastes from medical, industrial and research applications as well as from nuclear power plants. The research activities cover fundamental aspects of repository geochemistry, chemistry and physics of radionuclides at geological interfaces, and radionuclide transport and retardation in geological and technical barriers. The work performed is a balanced combination of experimental activities conducted in dedicated laboratories for handling radioactive isotopes, field experiments and computer simulations. The work is directed towards repository implementation and the results are used by Nagra in their comprehensive performance assessments studies. The finalisation of the site selection process and the implementation of a repository in the next decades will require strong expertise in model-based assessments of the repository *in situ* conditions for specific repository designs. The long-term strategy of LES is thus to develop experimental and modelling expertise necessary for fully coupled description of relevant processes in a repository in order to assist safety driven implementation of disposal options in Switzerland.

Together with two other laboratories in the department of Nuclear Energy and Safety, LES maintains best practices and standards in the laboratory management and data processing according to the ISO9001:2015 certified Integrated Quality Management System. In 2019, LES has successfully passed the monitoring audit conducted by the Swiss Safety Center (www.safetycenter.ch). The certification covers the research and scientific services for agencies in the area of nuclear waste disposal and environmental sciences.

The present report summarises the research activities and results achieved in 2019. It gives a detailed overview of research projects, personnel management, national and international collaborations, and individual contributions achieved by scientists in the four research groups at PSI and the Chair of Mineralogy at the University of Bern.

We gratefully acknowledge the support of our work by the PSI management, Nagra, and numerous research programmes within National and European Funding agencies (e.g. SNSF, ERC).

Table of Contents

1 OVERVIEW

Churakov S.V.

1.1 Introduction

The overall progress made in the Laboratory for Waste Management (LES) from January 1st, 2019 to December 31th, 2019 is summarised in the first part of the report. The report is organised thematically according to the eight overarching research topics. These topics are multidisciplinary in nature and include contributions from different research groups at LES and the Mineralogy Group in the Institute of Geological Sciences at the University of Bern.

1.2 General

The site selection process for geological disposal of radioactive waste in Switzerland has entered its final stage. On November 22nd, 2018, the Swiss Federal Government has approved the further investigation of the "Jura Ost", "Nördlich Lägern" and "Zürich Nordost" areas for the final selection of a disposal site for a nuclear waste repository in Switzerland. All proposed siting regions are located in the Opalinus Clay formation. In 2019, Nagra has started a deep drilling campaign for the characterisation of the local geological and hydrological conditions at these sites. Lithological data will be used to improve the stratigraphic and tectonic models of disposal sites currently available from a 3D seismic exploration campaign. *In situ* hydraulic tests and core samples analysis will be used to confirm *in situ* transport and retention properties of the host rocks and their confining units. These data will provide an important basis for the performance assessment of the selected sites.

The ultimate aim of the current site selection stage is to identify one disposal site for the Spent Fuel/High Level Waste (SF/HLW) and one disposal site for the Low/Intermediate Level Waste (L/ILW). Both repositories can, in principle, be placed in different locations of the same region, as a so-called "Kombi-Lager" option, given that all necessary safety criteria are fulfilled. In particular, the mutual effects of SF/HLW and L/ILW in the "Kombi-Lager" option have to be carefully evaluated. For either option, safety has the highest priority.

Between April and November 2019, Nagra has been conducting a drilling campaign in Bülach – Herrenwis, located in the "Nördlich Lägern" siting region. The drilling has been completed and core samples have been characterised for mineralogy and lithology in the Institute of Geological Sciences at the University of Bern. Samples of Opalinus Clay and its confining units have been delivered to LES for further laboratory characterisation. LES conducts cation exchange capacity measurements as well as sorption and diffusion studies with selected radionuclides.

In August 2019, the second drilling campaign has started in Trüllikon (ZH) to complete the overall picture of the geological conditions in the potential siting region "Zürich Nordost". The samples from this campaign will be transferred to LES in the middle of 2020 for further investigations.

In the context of the site selection process and the preparation of a general licence application, the focus and priorities of the waste disposal implementor are shifting from fundamental research towards synthesis of technical documentation and building defendable chains of arguments for the site selection. In this context, LES' national role is to maintain know-how in the field of waste disposal chemistry and physics, independent of the short-term priorities of the sectoral plan. Accordingly, LES continues research aimed at filling existing knowledge gaps in understanding the sorption and transport behaviour of radionuclides and provide scientific justification for model assumptions made in safety assessment studies. Present and future research activities focus on the behaviour of modern spent fuel under repository conditions, the chemical evolution of the repository near field, sorption competition phenomena, the behaviour of redox-sensitive elements, the role of mineral surface-induced redox reactions, and the transfer of sorption models and data from dispersed to compacted systems. LES further strengthens and builds up its experimental and modelling expertise in reactive transport simulations. These capabilities are particularly important for understanding the long-term evolution of *in situ* repository conditions and the interaction between repository barriers causing an alteration of their retention and transport properties. Special attention is paid to understanding the role of heterogeneities in the waste forms, which can lead locally to very specific chemical conditions. In this context, LES develops a state-of-the-art expertise in multi-scale reactive transport modelling which enables rigorous stepwise upscaling of model parameters from atomistic to repository scale. LES' long-term goal is to maintain existing datasets for safety analysis, including sorption, diffusion and thermodynamics and to develop beyond state-of-the-art expertise in the quantitative description of the long-term repository evolution. LES' vision is to

obtain a fully coupled description of *in situ* repository conditions and THMC-transport phenomena.

All siting regions currently considered in the selection process are located in the Opalinus Clay formations. Opalinus Clay has a high sorption capacity and an exceptionally low hydraulic conductivity favourable for radionuclide retention. However, degradation of organic materials, corrosion of metallic waste forms and metal-based reinforcement in the engineered barriers lead to the accumulation of volatile species (e.g. CO_2, CH_4, H_2). Potential pressure build up may have negative consequences for the integrity of the low permeability barrier such as Opalinus Clay. Accordingly, LES has initiated an experimental and theoretical research programme aimed at better understanding gas migration phenomena in compacted clays and argillaceous rocks.

In 2019, the Joint European Research Proposal COFUND-EJP NFRP-2018-6: *"European Joint Research Programme in the management and disposal of radioactive waste Eurad"* has been approved by the European Commission. This project is a joint venture of 52 mandated research agencies, waste management organisations and technical safety organisations focusing on the most urgent research issues of nuclear waste disposal in Europe. Within the Eurad framework, LES participates in six individual work packages (WP):

FUTURE: Fundamental understanding of radionuclide retention (WP Lead)

DONUT: Modelling of process couplings and numerical tools applied to performance assessment (Task co-Lead)

ACED: Assessment of chemical evolution of ILW and HLW disposal cells (Task Lead)

GAS: Mechanistic understanding of gas transport in clay materials (Contributor)

CORI: Cement organics radionuclide interactions (Contributor)

UMAN: Uncertainty management multi-actor network (Contributor)

Our long-term scientific collaborator Prof. Kenichiro Nakarai from the Hiroshima University and his colleague from Tokyo University, Prof. Takahashi, have conducted a 6 months research stay at LES. This scientific exchange is a part of the 4-years research project *"Advanced technology development for treatment/disposal of hazardous materials with unified evaluation of cementitious and geotechnical materials"* supported by the Japanese Society for the Promotion of Science. Within this project Prof. Nakarai and his research team collaborates with LES on experimental and modelling studies of cement-clay interaction in waste disposal systems.

The extension phase of the collaborative project *"Thermodynamik und Speziation von Aktiniden bei höheren Temperaturen"* (ThermAc) funded by the German Ministry of Education and Finances (BMBF) has been approved. The project activities within this phase are focused on the development of a database for high temperature properties of actinides.

LES continues participation in the follow-up phase of the THEREDA project coordinated by GRS (Gesellschaft für Anlagen- und Reaktorsicherheit GmbH, Germany). This project aims at a critical evaluation of thermodynamic data for high saline environments. The thermodynamic data for cement minerals in the THEREDA database were updated with the new CEMDATA18 dataset.

The development and testing of an experimental set-up for compound-specific analysis of ^{14}C released by the corrosion of irradiated steel is ongoing. In 2019, the development of analytical techniques for compound-specific analysis of ^{14}C-bearing molecules in the gaseous phase has been successfully completed.

LES actively maintains collaborations with national and international research institutes in the field of waste management and environmental research. The main multi- and bi-lateral co-operations with external institutions and universities are summarised in Table 1.1.

Participation in international research projects and independent acquisition of project funding for PhD and postdoc projects is particularly important for developing state-of-the-art research capabilities, knowledge transfer and education of young generation scientists. New PhD projects and postdoc fellowships approved or started in 2019 are listed below along with ongoing ones.

L. Hax Damiani (PhD student): *"Modelling transport across reactive interfaces with the Nernst-Planck approach"*. Start date: January 2016 (Funding: EU).

P. Krejci (PhD student): *"Multispecies cation transport in compacted clays"*. Start date: December 2016 (Funding: Swiss National Science Foundation, SNSF).

P. Luraschi (PhD student): *"Evolution of transport properties, mineralogy and porosity of cement-clay interfaces"*. Start date: April 2017 (Funding: Nagra, PSI).

M. Mahrous (PhD student): *"Resolving dissolution-precipitation processes in porous media: Pore-scale lattice Boltzmann modelling combined with synchrotron-based X-ray characterisation"*. Start date: March 2018 (Funding: SNSF).

A. Mancini (PhD student): *"Thermodynamic and spectroscopic investigations of the Fe and S speciation in anoxic cementitious systems"*. Start date: April 2016 (Funding: SNSF).

J. Owusu (PhD student): *"Pore-scale simulations of gas molecules in saturated and partially saturated clays"*. Start date: Nov 2019 (Funding: HORIZON 2020, Eurad).

Tab. 1.1: National and international co-operations.

Co-operations
National Nagra* (Major financial contribution, Various technical working groups) Swissnuclear* (Reactor safety, material aging)
Multinational NEA Thermodynamic Database Project EURATOM HORIZON2020 (EURAD) EURATOM HORIZON2020 (CEBAMA) EURATOM HORIZON2020 (DISCO) Mont Terri Projects* (diffusion retardation, clay-cement interaction)
Universities University of Bern*, Switzerland (mineralogy, petrography, water chemistry, C-14 AMS) EPFL, Switzerland (cement systems) Université de Bourgogne, Dijon, France (molecular modelling) ETH*, Zurich, Switzerland (GEMS) Hiroshima University, Japan (clay-cement interaction) University of Luxembourg* (porous media) Sino-French Institute of Nuclear Engineering and Technology, Sun Yatsen University (diffusion) Uppsala University, Sweden (atomistic simulations)
Research Centres CEA*, France (chemistry of near and far field) EMPA*, Switzerland (cement) IFR, HZDR*, Germany (XAS, TRLFS, atomistic modelling, reactive transport) INE, KIT*, Germany (near and far field; TRLFS) FZJ, Germany (sorption/diffusion of Ra, reactive transport, thermodynamics of solid solutions) SCK/CEN, Belgium (clay and cement systems) UFZ*, Germany (reactive transport, clay systems)
Industrial Partners GlaxoSmithKline NanoCem

**formal co-operation agreements*

Y. Qian (PhD student): *"Adsorption of redox sensitive radionuclides on Fe-bearing clay minerals"*. Start date: Nov 2019 (Funding: HORIZON 2020, Eurad).

R. Schliemann (PhD student): *"Dissolution, growth and ion uptake at phyllosilicate surfaces: Coupling atomistic interactions at the mineral water interface with Kinetic Monte Carlo model"*. Start date: July 2016 (Funding: SNSF).

S. Wick (PhD student): *"Sorption of thallium on illite and birnessite and its impact on thallium solubility in soils"*. Start date: April 2016 (Funding: SNSF).

Dr. Y. Chen (postdoc): *"Diffusive transport of gaseous species at saturated and partially saturated conditions"*. Start date: September 2019 (Funding: EU Horizon 2020 Marie Skłodowska-Curie grant, PSI-FELLOW-II-3i).

Dr. P. Cruz Hernandez (postdoc): *"Sorption mechanisms of Zn and U on Opalinus Clay"*. Start date: August 2019 (EU Horizon 2020 Marie Skłodowska-Curie grant, PSI-FELLOW-II-3i).

Dr. G. Geng (PSI-FELLOW-II-3i postdoc): *"Alkali-silica reaction in concrete"*. Start date: July 2017 (Funding: SNSF, EU Horizon 2020 Marie Skłodowska-Curie grant, PSI-FELLOW-II-3i).

Dr. T.L. Guillemot (postdoc) *"Development of C-14 AMS based analytical methods for the identification and quantification of dissolved and volatile organic compounds"* Start date: January 2019 (Funding Nagra).

Dr. F. Marafatto (postdoc): *"Cryo-microspectroscopy at the microXAS beamline for the investigation of redox- and radiation-sensitive samples"*. Start date: June 2017 (Funding: PSI, EAWAG).

Dr. D. Miron (postdoc): *"Effect of aluminum on C-S-H structure, stability and solubility"*. Start date: December 2017 (Funding: SNSF).

Dr. R. Patel (postdoc): *"Resolving carbonation mechanisms of cement-based materials through multi-scale microstructural simulations"*. Start date: August 2017. Completed: July 2019 (Funding: EU Horizon 2020 Marie Skłodowska-Curie grant, PSI-FELLOW-II-3i).
"Boiling crisis in nuclear reactor". Start date: August 2019 (Funding: Swissnuclear).

Dr. G. Yang (postdoc): *"Pore-scale control of mineral precipitation: from atomistic model to macroscopic modelling and experimental observations"*. Start date: July 2017. Completed: June 2019 (Funding: EU Horizon 2020 Marie Skłodowska-Curie grant, PSI-FELLOW-II-3i).

Several LES PhD students have defended their PhD thesis in 2019:

Dr. A. Keri: *"Shedding light on metal adsorption processes on clay minerals inferred from atomistic simulations and X-ray absorption spectroscopy"*. PhD Defence 14 June 2019, University of Bern (Funding: SNSF).

Dr. L. Nedyalkova *"A structural and thermodynamic study of the intercalation of selenium(IV), selenium(-II), sulfur(-II) and I(-I) in AFm-phases"*. PhD Defence 9 November 2019, University of Bern (Funding: EU).

Dr. A. Shafizadeh *"Porosity and structural changes at clay-cement interfaces and their relations to transport properties"*. PhD Defence 30 July 2019, University of Bern (Funding: Nagra, PSI).

The organisational chart of LES comprises four research groups located at PSI (organisation chart, Fig. 1.1). A fifth research group is located in the Institute of Geological Sciences (IfG) at the University of Bern. The mineralogy group at IfG is complementing the expertise in the field of mineral dissolution kinetics, structural studies of high porous materials and X-ray diffraction-based structure refinement and the geochemistry of conventional waste disposal. In particular, the mineralogy group hosts the Competence Centre for Secondary Raw Materials conducting applied research in the field of environmental geochemistry and secondary raw materials recycling.

The LES annual report 2019 is organised in seven thematic research projects addressing specific aspects of repository geochemistry and radionuclide transport:

Chapter 2: Geochemical evolution of repository near field

Chapter 3: Development of mechanistic sorption models and experimental validation

Chapter 4: Radionuclide transport and retention in compacted systems at full and partial saturation

Chapter 5: Cement-waste interaction and upscaling to the field scale

Chapter 6: Radioactive waste characterisation

Chapter 7: Thermodynamic models and databases

Chapter 8: Fundamental aspects of mineral reactivity and structural transformations

Chapter 9: Geochemical aspects of conventional waste materials and their disposal

The following section provides an overview of activities related to the Sectoral Plan for Deep Geological Disposal, repository near and far field, reactivity of barrier systems and code benchmarking activities.

1.3 Sectoral plan for deep geological disposal

The potential radiological impact of a repository is one of the main safety relevant criteria employed in the site selection process. Sorption and diffusion data are the basis for such calculations. The sorption databases are derived based on thermodynamic calculations. Therefore, a reference Thermodynamic Data Base (TDB) must be available before the development of the sorption databases and the modelling of the *in situ* repository conditions can start. The ongoing review of the thermodynamic data continues with the aim to release a new updated TDB in 2020. This database will be the reference for all subsequent thermodynamic calculations to be conducted within the SGT-E3 ("Sachplan Geologische Tiefenlager, Etappe 3"). A critical evaluation of thermodynamic data for Cd, Pd, silicates, the rare earth elements Sm, Eu, Ho, as well as data for major elements of ground and pore water including the models for elevated temperatures was conducted in 2019 (see section 7.2).

To be available for the use in the safety assessments for RBG ("Rahmenbewilligungsgesuch"), the cement sorption database has to be updated by the end of 2022. To fill the gaps in the data, an experimental study was launched in 2019 to determine the sorption values (R_d) for ^{26}Al, ^{32}Si and ^{41}Ca, safety-relevant radionuclides that have not been taken into account in previous sorption databases (see section 7.3).

Calcium silicate hydrates (C-S-H) determine the most relevant properties and the durability of hydrated cement pastes and concretes. C-S-H shows a complex structure and a wide variation of chemical compositions. Accurate thermodynamic predictions of stability, density, composition and solubility of C-S-H in response to changes in cement recipe, water addition, humidity, temperature, carbonation, leaching, and other factors are still one of the major challenges in cement chemistry. Recently, an advanced self-consistent model for the C-N-K-A-S-H system has been developed. In 2019, the model has been extended to account for Al uptake and for retention of radionuclides (U, Np) and fission products (Ba, Sr) (see section 7.4).

1.4 Repository near field

1.4.1 Repository chemistry

Dissolution of spent fuel and vitrified nuclear waste defines the radionuclides release after breaching of the disposal casks containing high-level radioactive waste. Because of its high importance, this source term has been intensively studied for decades. The manu-

facturing recipe of nuclear fuels is evolving to improve reactor performance. In recent years, nuclear power plants have started using chromium-doped UO_2 fuels in commercial light water reactors. Such Cr-doped fuel has a larger grain size and allows the reactors to operate at higher power in a more efficient energy production regime compared with the performance of conventional fuel. In the framework of the Horizon 2020 EU programme, a collaborative scientific project is running under the acronym DISCO (Modern spent fuel DISsolution and chemistry in failed COntainer conditions). Within this project, LES investigates redox conditions in Cr-doped spent fuel under reactor operation conditions as well as under dry storage and geological repository conditions after failure of the steel containment. To this end, a multicomponent solid solution model has been developed and implemented in the GEMS geochemical solver. The comparison of the model predictions with available experimental data, revealed that the fuel oxygen potential is particularly sensitive to the activity of Mo in metallic inclusions (ε-particles). Therefore, future investigations should focus on the study of mixing properties in such phases. The developed model further indicates that the addition of small amounts of Cr in UO_2 fuels should have no adverse effect under geological storage conditions, such as enhanced radionuclide release due to faster UO_2 dissolution or due to oxidation of redox-sensitive nuclides (see section 6.3).

^{79}Se and ^{129}I are released from the radioactive waste under real repository conditions, after the cement curing stage. These radionuclides primarily interact with AFm phases via sorption mechanism and not through co-precipitation. In the framework of the Horizon 2020 EC Project "CEBAMA", the mechanisms controlling the Se and I uptake by AFm phases have been investigated. In 2019, a modelling exercise was undertaken to test whether the thermodynamic solid solution models developed in previous years were capable of describing I and Se sorption isotherms onto AFm-SO_4, AFm-HS, AFm-CO_3 and AFm-$OHCO_3$ measured previously (see section 3.5).

The anoxic corrosion of activated steel in the near field of a L/ILW repository leads to the release of ^{14}C-containing low molecular weight (LMW) carbon compounds, such as ^{14}C-containing formate and acetate. Both the batch-type corrosion studies with non-activated zero-valent iron powders and the corrosion experiments with activated steel support the hypothesis that the latter compounds will be present in the alkaline pore water of a cement-based repository. At ambient temperature and pressure, however, these LMW organics are expected to be metastable in accordance with presently available thermodynamic data, and are expected to decompose into $^{14}CO_2$ and $^{14}CH_4$. Accordingly, chemical stability and decomposition kinetics of organic compounds in repository relevant conditions are investigated in gas-tight pressurised reactors with particular focus on the effects of temperature and the presence of iron (see section 6.2.5).

1.4.2 Clay systems

Solid/liquid distribution coefficients (K_d values) are applied to estimate the retention of radionuclides in the engineered barriers and host rocks in the safety analysis of deep geological radioactive waste repositories. In order to derive adsorption values for argillaceous rocks under a wide range of porewater and mineralogical compositions, the so-called bottom-up approach is often used. This approach assumes that the uptake of radionuclides in complex mineral/porewater systems can be quantitatively predicted from the knowledge and understanding of the mechanistic adsorption processes on single minerals, and the models developed to describe them. Sorption on the Opalinus Clay is described with the assumption that the 2:1 clay minerals illite and illite-smectite mixed layers are the dominant sorbents. Scaling the site capacities to the clay mineral content of the rocks and including the radionuclide speciation in the different porewaters allows calculating their adsorption isotherms in natural rocks.

In the reporting year, the approach has been tested for blind predictions of the adsorption isotherms for Cs, Ni, Co, Eu, Th and U on two Opalinus Clay samples. Results of the tests strongly support the bottom-up approach and methodology for developing state-of-the-art sorption databases for argillaceous rocks to be used in safety analysis. Furthermore, an approach has been elaborated for the evaluation of the upper and lower uncertainty bands for the calculations of the K_d values in safety analysis (see section 3.2).

Success of the bottom-up approach depends on the correct assignment of the solid phases responsible for radionuclides uptake. Within an EU funded project, the micro-XRF measurements were applied to identify the dominant sorbing phases for U(VI) in the Boda claystone formation, which is the selected potential host rock for a HLW repository in Hungary. The study showed that not only the argillaceous matrix is responsible for uranium uptake. Contrary to conventional assumption of clay mineral controlled retention, U-rich fringes were observed around carbonate fillings which contribute to the U retention in the rock (see section 3.6).

Thallium (Tl) is a highly toxic trace element predominantly occurring in the environment as Tl^{+}, but it can also exist as Tl^{3+}. The former is highly soluble and mobile, whereas the latter is highly insoluble, strongly hydrolysing and normally occurring in oxide form. Literature data suggest that the clay mineral illite is a key sorbent for Tl^{+} in soils and sediments. A sorption model for Tl adsorption on illite has been developed in the framework of a SNSF funded PhD project (collaboration with Eawag). As a next step, the bottom-up approach has been validated for the adsorption behaviour of thallium in top soil samples from the Erzmatt region in Switzerland (see section 3.3).

The development of a mechanistic sorption model for safety relevant radionuclides and competing elements is ongoing with the aim to fill existing gaps in the sorption databases. Mn is an omnipresent element in environmental systems and can be a potential competing metal for radionuclides in the near and far field of a radioactive waste repository. In this context, adsorption of Mn^{2+} on illite and the modelling of the experimental data has been completed (see section 3.4).

Atomic-scale information about the sorption mechanism of ions on mineral surfaces is essential for the development of a mechanistic sorption model. Recently, a combination of spectroscopic studies and atomistic simulations was used to reveal the nature of high and low affinity sorption sites on clay mineral surfaces. The success of the approach is very promising and has potential for applications to more complicated systems. In a SNSF PhD project, "*Detailed understanding of metal adsorption on clay minerals obtained by combining atomistic simulations and X-ray absorption spectroscopy*", the structural mechanism of iron and uranyl adsorption on clay minerals were studied. The combination of *ab initio* simulations and X-ray absorption spectroscopy allowed to reveal the oxidation state and the structural characteristic of Fe surface complexes formed on a montmorillonite surface as a function of the metal concentration in solution (see section 3.7).

The molecular-scale understanding of clay minerals dissolution is essential for the development of mechanistic models for toxic metals and radionuclides retention in soils and waste disposal sites. In the framework of a SNSF PhD project (PhD student R. Schliemann) an *ab initio* metadynamics simulation approach is applied to investigate the free energy surface and the reaction mechanism associated with the removal of tetrahedral and octahedral units from pristine edge faces of smectite minerals. The results of the simulations show a complex free energy surface with multiple local minima corresponding to the intermediate reaction products formed during the dissolution process. The saddle points connecting the local minima represent the energies of the activated complexes corresponding to the individual reaction steps. Analysis of data for different edge surfaces indicate that a complete detachment of silanol and aluminol groups from the surface requires up to four elementary reaction steps (see section 8.3)

The transferability of sorption data derived in disperse clay suspensions to the compacted systems is addressed in diffusion experiments on a model mono-mineral system. The presence of competing cations in the equilibrium pore water solution is one of the most important factors influencing the sorption behaviour of the cations in compacted systems. Specifically the impact of ferrous iron (Fe(II)), a product of the anaerobic corrosion of iron and steel, on radionuclide sorption is being investigated. Owing to difficulties in the handling and maintaining the stability of the ferrous iron form, Mn(II) was used as a chemical analogues in the diffusion and sorption experiments with compacted illite. An excellent agreement between the experimental data and the simulations could be obtained using a modified 2SPNE SC/CE model taking into account cation enrichment in the EDL. In particular, the assumption of mobile surface metal cations in the diffuse layer was found to be indispensable for a valuable description of the experimental tracer profiles (see section 4.2).

Large amounts of gas will be produced in a repository due to the corrosion of iron and steel and the degradation of organic waste forms. Potential negative effects of gas pressure build up on the integrity of barrier systems depend strongly on the permeability of the barriers with respect to gaseous molecules. An institutional Marie-Currie EU-COFUND postdoc project investigates the diffusion of selected gases in partially saturated clay systems such as compacted bentonite, bentonite/sand mixtures and Opalinus Clay. In a first phase, the re-saturation characteristics of compacted bentonite and Opalinus Clay are studied. First measurements with bentonite and Opalinus Clay indicate that re-saturation takes place in two steps, an initial fast process followed by a slow process. Furthermore, strong similarity in the behaviour of compacted and loose bentonite could be observed (see section 4.5).

1.4.3 Cement systems

Carbon-14 has been identified as a major contributor to the long-term release of radioactivity from a cement-based repository into the host rocks. Corrosion of activated steel is the main source of ^{14}C in the Swiss waste disposal system. The mobility of ^{14}C depends on its speciation. While the overall ^{14}C inventory in the radioactive waste is well known, the chemical form of

^{14}C-bearing compounds is poorly understood. The aim of the ^{14}C project is to investigate i) the release of ^{14}C-bearing organic compounds from waste materials (e.g. during the corrosion of activated steel) and their speciation, ii) the chemical stability of these organic compounds in repository relevant conditions, and iii) the retardation of the organics in the near field of a repository for radioactive waste.

One of the major difficulties associated with the compound-specific analysis of ^{14}C-bearing species is their extremely low concentration, which is far below the detection limit of the conventional analytical techniques, such as gas and liquid chromatography. Accelerator mass spectrometry is the most powerful technique, which would allow detection of ^{14}C species in the system. A combination of liquid and gas chromatography with accelerator mass spectrometry measurements techniques for the compound-specific analysis of ^{14}C species at ultra-low concentrations in the gas and liquid phase is being developed and tested (see section 6.2).

Batch-type corrosion experiments with non-activated steel powders provide information on the carbon compounds produced in iron-water-systems during anoxic iron corrosion. In the current stage of the project, the release of carbon compounds from pre-corroded carbon-containing zero-valent iron powders were studied. The good agreement of predicted and experimental data provides evidence that hydro-carbons are formed by a Fischer-Tropsch-type mechanism in the course of anoxic iron corrosion (see section 6.2.1).

A well-controlled corrosion experiment with activated steel that is immersed in anoxic alkaline solution under a N_2 atmosphere in a gas-tight reactor is currently running. Several samplings of the liquid phase have been carried out since the beginning of the experiment in May 2016. A very sensitive analytical method based on compound-specific radiocarbon analysis has been developed to determine the total organic ^{14}C content (TO^{14}C) of the solution and to identify and quantify the ^{14}C-bearing compounds present in the liquid phase (see section 6.2.2).

The development of compound-specific radiocarbon analysis for the gaseous ^{14}C-containing compounds has been completed in 2019. Using the new analytical method, the ^{14}C-bearing gaseous compounds and the total ^{14}C concentration in the gas phase resulting from the anoxic corrosion of activated steel were identified for the first time. ^{14}C-bearing methane was identified and quantified as the main ^{14}C carrier in the gas phase. The concentration of ^{14}C-bearing ethane was found to be close to the detection limit of the analytical method. Furthermore, the total ^{14}C content in the gas phase agreed well with the concentration of ^{14}C-bearing methane. Check of the mass balance corroborates that ^{14}C-bearing methane was the only relevant ^{14}C carrier in the gas phase (see section 6.2.3 and 6.2.4).

Iron/steel and cement are important components of the planned deep geological L/ILW repository in Switzerland. Within a short period free oxygen is consumed and *in situ* conditions are strongly reducing. Anoxic corrosion of metallic iron at the interface between cement paste and iron/steel produces Fe(II,III) corrosion products. The corrosion products can interact with the cement paste and can affect the long-term barrier performance of cementitious materials in the L/ILW repository. In the current safety assessment concepts, the cement paste is assumed to be the only sorbing material in the near field and solely responsible for radionuclide retention. A PhD project funded by the SNSF aims at developing a mechanistic understanding of Fe(II,III) interaction with C-S-H phases. In this project, Fe(II,III) interaction with single cement phases and with a polymineral matrix in aged Fe(0)-containing slag cements sampled from concrete structures that had been exposed to environmental conditions for several years is investigated by using wet chemistry experiments and by synchrotron-based techniques. The results of the project show that Fe(II) and Fe(III) interact with C-S-H phases. These observation rises the question whether or not sorption competition between Fe(II), Fe(III) and radionuclides preferentially taken up by C-S-H phases could occur. For example, the present study shows that Fe(III) occupies structural positions in the interlayer that may also be accommodated by actinides (see section 5.2).

The alkali-silica reaction (ASR) is a deterioration mechanism, which can severely shorten the durability of concrete structures. The ASR takes place between the siliceous component of concrete aggregates and the alkaline pore solution. The formation of the ASR products is often accompanied by significant internal expansion and cracking of concrete, which severely shortens the service life of the affected infrastructure. Understanding the structure and mechanism of ASR formation is essential for the control and mitigation of the ASR in cementitious systems. The structural and thermodynamic properties of ASR are investigated in the framework of the SNSF Sinergia project “Alkali-silica reaction (ASR) in concrete”, by a team of researchers from Empa, EPFL and PSI. Additional support to this project is provided by the Marie Skłodowska-Curie European Union’s Horizon 2020 research and innovation programme. Detailed analysis of ASR samples from different locations and from laboratory synthesis could demonstrate that crystalline ASR products resemble the structure of shlykovite, which is a layer silicate with a Ca layer between silicate sheets and K/Na imbedded within the sheets. The

amorphous ASR products highly resemble the structure of C-S-H phases, although they seem to have a different nano-morphology (see section 5.3).

1.4.4 Interface processes

Cement and clay materials have different porewater chemistry. Chemical interaction between these materials results in dissolution-precipitation reactions that may alter the transport properties at the interface. The evolution of these interface properties is of relevance for the long-term safety assessment of underground radioactive waste repositories. Several samples with cement-clay interfaces were investigated by means of through-diffusion experiments using HTO and chloride radiotracers. They provide information on the diffusivities of an uncharged and of a negatively charged tracer, which are related to the evolution of the total and the anion-accessible porosity. The collected data and earlier observations allow to draw the following conclusions about the evolution of transport properties across the interface: i) The HTO flux does not approach zero, which means that a part of the porosity is still available for diffusion after 6 years of reaction. ii) Most of the reactions take place during the first 1.5 years, suggesting that the observed decrease of D_e slows down the further reactivity of the interface. iii) The reduction of the D_e with respect to unaltered Na-montmorillonite samples is much stronger for chloride (96% within 17 months) than for HTO (45% after 17 months). The observations suggest that the precipitation reactions take place preferentially in the porosity domain accessible by anions (free porosity) leading to a very strong decrease of the chloride diffusivity (see section 2.2.1).

1.5 Repository far field

The diffusion mechanism of strongly sorbing tracers in Opalinus Clay is still not fully understood. Diffusion of Eu(III) in Opalinus Clay has been investigated in order to improve the description of strongly sorbing radionuclides transport in compacted systems. Preliminary results from the diffusion studies indicate larger disagreement between the theoretically calculated time evolution of the Eu(III) concentration in the reservoir and the measured data. Unexpectedly, the measured decrease of the Eu(III) reservoir concentration was found to be much faster than predictions by currently applied models. Further experiments are necessary to identify the nature of Eu(III) retention mechanism in Opalinus Clay (see section 4.3).

Enhanced cation fluxes of clays cannot be described by simple Fick's law consistently. A surface diffusion model has been developed and applied to describe Na and Sr diffusion in Opalinus Clay. Sorption site-specific surface mobilities are the model parameters. Their parameters were estimated for Na and Sr ions based on radial diffusion experiments in Opalinus Clay (see section 4.4).

Fate and transport of inert and reactive gases in the Opalinus Clay formation is investigated at field scale in the HT-experiment. A borehole was filled with a gas mixture, and the evolution of gas pressure and gas phase composition was monitored. In addition, the inflow of formation water and its composition in the borehole was measured. In order to improve the description of the experimental results and to better constrain the model parameter a new model for gas flux calculations across the borehole/Opalinus Clay interface has been set up. The model assumes the existence of a very thin film of water covering the Opalinus Clay surface, which is in thermodynamic equilibrium with the gas phase in the borehole. With this model assumption, the calculated equilibrium concentration of dissolved gases in the borehole is used as a boundary condition for the transport model in Opalinus Clay. The transport model calculates fluxes for dissolved species across the borehole wall using the concentration gradients at the boundary. Optimised numerical implementation allows efficient parameter variation studies for the relevant transport parameters. The new modelling approach significantly simplifies the handling of gas and water fluxes across the borehole interface and at the same time improves the agreement of the modelling results with the experimental data. Remarkably, this implementation provides a good description of the experimental data without invoking artificially enhanced hydrogen fluxes into the Opalinus Clay to explain the observed decrease of hydrogen concentrations in the borehole (see section 2.2.2).

1.6 Model development, code benchmarking, advanced analytical tools, thermodynamic databases

Benchmarking and verification of reactive transport codes is an ongoing activity, which is necessary to demonstrate the credibility of numerical simulations, and to improve the description of complex geochemical interactions and radionuclide transport in a nuclear waste repository. The SeS benchmark on the modelling of Cs diffusion through clay for single species and multi-species reactive transport has been finalised in 2019. The simulation codes MCOTAC, FLOTRAN, CORE2D, PHREEQC and PHREEQC-COMSOL were included in the multispecies reactive transport benchmark. In general, a good agreement between Cs breakthrough curves simulated with different codes could be obtained. Substantial deviations between the calculated breakthrough times have been reported between PHREEQC-COMSOL and other codes. The

numerical performance of the codes, e.g. the calculation time necessary to complete the benchmark, varied between different codes by several orders of magnitude (see section 2.3.3).

Reactive transport simulations include a number of strongly non-linear couplings between the sorption and transport parameters. A comprehensive uncertainty and sensitivity analysis study has been performed to evaluate the importance of sorption and transport parameters for the evaluation of radionuclide breakthrough curves for a simplified repository design. Extensive realisations and calculations of Cs migration in clay have been produced as a basis for the sensitivity analysis, aiming to quantify the effect of uncertainties on site-specific sorption reactions equilibrium constants and pore-water cations' concentrations, i.e. uncertain sorption model parameters. The sensitivity analysis allowed to further generate a classification tree to show combinations of uncertain sorption model parameters' values controlling the uncertainty (see section 2.4).

A new numerical simulation method describing the mass transport, nucleation, mineral precipitation and dissolution within a confinement has been developed and tested against experimental data, in collaboration with the Nuclear Waste Management and Reactor Safety Laboratory at Forschungszentrum Jülich (FZ-Jülich, Germany). In this project, an advanced multiscale modelling and numerical diagnostics approach was applied to simulate a microfluidic lab-on-chip experiment conducted at the experimental facilities of the FZ-Jülich. The experimental set-up describes flow and diffusion controlled precipitation and subsequent dissolution of $SrSO_4$ (celestine). Accurate models and advanced computational algorithms allowed to create an off-line digital twin to provide an insight into the underlying processes at an unprecedented level of detail and to predict near-future evolution steps of the system (see section 2.3.1).

Pore-level reactive transport modelling provides a link between elementary atomistic-scale chemical processes at mineral fluid interfaces and the field scale simulations of subsurface geotechnical systems. Accurate prediction of *in situ* conditions and transport properties of evolving geotechnical systems require representative and detailed information regarding the pore structure and the connectivity of the pore space. An innovative methodology for the extraction of petro physical parameters from numerical modelling and core-scale reactive transport experiments has been developed in collaboration with the King Fahd University of Petroleum and Minerals (KFUPM), in Saudi Arabia. Seven limestone cores have been scanned using high-resolution micro computed tomography before and after an acid injection experiment at the KFUPM. The resulting tomograms were segmented and several petrophysical parameters needed for reactive transport simulations, such as the reactive surface area, the definition of the Representative Elementary Volume (REV), the porosity and the permeability fields, have been extracted. This petrophysical information is used in both pore-scale and continuum-scale simulations, which will be further compared with experimental results. This project aims at enhancing the reliability of multi-scale reactive transport simulations, and improvement of the upscaling strategies for transport parameters from small-scale experiments and simulations to the field scale observations at geological time scales (see section 2.3.2).

A coupled thermo-hydraulic-chemical (THC) lattice Boltzmann based reactive transport model has been developed to describe the pore-scale evolution of the microstructure and porosity distribution in cement paste reacting with carbonated brine. The simulations show a good quantitative agreement between modelling and experimental observations at the initial stages of the system evolution. For longer times, however, the modelling results and experimental observations start to diverge significantly. The main reason for this deviation are the large uncertainties in the kinetics of C-S-H dissolution and calcite precipitation (see section 5.4).

Mineral reactivity depends strongly on molecular-scale mass transport and ion-solvent interactions at the mineral fluid interface. Molecular dynamics (MD) simulations provide an accurate description of the mineral fluid interface taking into account all-atom-interactions. This simulation approach is computationally expensive, if applied to large molecular systems. Classical Density Functional Theory (DFT) delivers structural and thermodynamic information at comparatively low computational costs. In the PSI-FELLOW-II-3i project "*Pore-scale control of mineral precipitation: from an atomistic model to macroscopic modelling and experimental observations*" (G. Yang), the classical density functional theory (f-DFT) was applied to model water and ion distributions at the charged mineral/water interface. The DFT calculations are 3-4 orders of magnitude faster than conventional MD simulations. The DFT/LJ-3CM model provides a robust approach, which can be further used for upscaling reactive transport simulations under more complex thermo-chemo-hydro-mechanical conditions (see section 2.3.5).

Synchrotron-based X-ray absorption spectroscopy (XAS) is currently the only available technique to probe the chemical redox state of trace elements in complex environmental matrices. The combination of

XAS with a micro-focused beam and a scanning sample stage allows us to obtain such information with spatial resolution down to the micrometer scale. Modern synchrotron light sources provide smaller and more brilliant beams with a high photon flux density dump on the samples, which can alter the oxidation state of the measured elements. To improve the measurement protocol of redox sensitive samples a cryostat cooling of samples has been developed to reduce sample exposure to the beam (see section 3.8).

In the realm of a collaborative project with the Laboratory for Scientific Computing and Modelling at PSI (LSM-PSI) and under the umbrella of the Swissnuclear funding agency through the project "*Multi-scale numerical prediction of boiling crisis*", the fundamental understanding of boiling processes from atomistic to reactor scale is pursued. LES is conducting research at the micrometer level, and at the same time supervises the modelling at the atomistic level, aiming to provide a bottom-up parametrisation of the macroscopic boiling code, developed at PSI, PSI-Boil (https://www.psi.ch/en/lsm/psi-boil). Atomistic simulations are applied to investigate the molecular-scale mechanism of gas bubble nucleation. The pseudo-potential based lattice Boltzmann scheme simulates a single component two-phase fluid system by addition of attractive or repulsive forces, added to the standard lattice Boltzmann model to incorporate a non-ideal pressure tensor. The implementation has been benchmarked by reproducing the Laplace law. In addition, the implemented model can account for different contact angles between fluid phases and solid and surface roughness (see section 2.6.1).

In the framework of a collaboration between the Institute for Mechanical Process Engineering and Mechanics at the Karlsruhe Institute of Technology and LES, phosphate removal from water using colloidal C-S-H particles has been investigated. A multi-scale two way coupled lattice Boltzmann-Discrete Element Method (LB-DEM) model for dense reactive particle flows has been implemented and tested. In this model, fluid flow and reactive transport processes are treated within the continuum framework and solved using the lattice Boltzmann method. This technique enables the simulation of large systems with a large number of particles. The dynamics of the suspended particles is modelled by a Discrete Element Method (DEM) (see section 2.6.2).

1.7 Environmental impact of conventional waste disposal, secondary raw material recycling and fundamental aspects of mineral reactivity and structural transformations

Since 2015, PSI/LES and the Institute for Geological Science at the University of Bern (UBERN/IfG) have established a research collaboration in the field of mineralogy and crystallography. The research of the Mineralogy Group at the University of Bern covers fundamental aspects of mineral dissolution and precipitation, chemical factors of crystal structure stability and temperature driven phase transitions in minerals. The dedicated laboratories operated by the group are equipped with powder and single crystal diffractometers for structural studies of minerals, and with an atomic force microscope for *in situ* characterisation of mineral surfaces. The experimental studies are widely supported by modelling activities.

A zero waste society is a long-term vision of circular economy. Full implementation of sustainable recycling technologies will take several decades. During this transition period, waste disposal in landfill sites will continue and the long-term stability of waste materials under disposal conditions will be an essential aspect for environmental protection. The Competence Centre for Secondary Raw Materials (CCSRM) at the Institute of Geological Sciences (IfG) conducts applied research in the field of environmental geochemistry and secondary raw materials. The core competences of the CCSRM cover topics of circular economy and disposal quality of conventional non-radioactive waste materials. Geochemical aspects and challenges related to the *in situ* conditions in conventional and radioactive waste disposal rely on common scientific background and modelling tools. Common expert knowledge provides the necessary basis for collaboration and mutual synergies between LES/PSI and CCSRM/UniBern. The CCSRM is imbedded in the Mineralogy Group at the IfG. The projects of the CCSRM are coordinated by Dr. U. Eggenberger (see section 9.1).

Heavy-metal-exchanged zeolites are attractive materials that find applications in several research fields, from environmental remediation to catalysis. The SNSF-AMBIZIONE project, led by Dr. G. Cametti, investigates the structural changes taking place in natural zeolites as a function of heavy metal uptake by combing experimental methods (X-ray diffraction, X-ray absorption spectroscopy) and theoretical computations (MD simulations). These complementary approaches are highly successful in structural characterisation of complex systems where the charge compensating cations are usually affected by strong positional disorder (see section 8.2).

Waste water contains large quantities of phosphorus and nitrogen that could be used for soil fertilisation. On the other hand, the presence of heavy metals poses a serious environmental risk to waste water reutilisation for agricultural purposes. The two most common calcium carbonate minerals (calcite, trigonal; and aragonite, orthorhombic) have been proposed as a remediation agent for water contaminated with lead

(Pb). Accordingly, batch recrystallisation experiments have been performed to assess the efficiency of these materials. The atomic-scale mechanism of calcite dissolution in presence of $Pb(NO_3)_2$ solutions was revealed using atomic force microscopy in a flow-through reactor. Despite their similar solubility, the calcite system shows substantially higher efficiency for Pb uptake compared to the aragonite one due to the crystallographic relationships between substrates and product. Aragonite and cerussite ($PbCO_3$, orthorhombic) share the same crystallographic structure. Structural similarities favour formation of a continuous layer of cerussite on aragonite that hinders reaction and prevents the replacement of the whole substrate grains (see section 8.4).

Recycling of secondary raw materials from industrial processes is one of the basic waste minimisation approaches. The potential of recycling of gravel wash mud in cement production has been investigated in a pilot project in collaboration with the Cornaux cement plant of the Jura-Cement-Fabriken AG. The results show that gravel wash mud materials can be used as raw material substitutes for cement production. Within this project, a numerical tool was developed, which provides an optimal mixing recipe for the cement plant based on material properties and chemical composition of components. After successful laboratory investigations, factory-scale tests have been implemented in the Cornaux pilot plant facility. The testing programme included a critical evaluation of the clinker composition, the different aspects of quality management, and the economic and ecological benefits (see section 9.2).

At present, 4.2 Mio tons of municipal solid waste are incinerated in Switzerland every year. The incineration allows mass and volume reduction, destruction of organic compounds, energy recovery and a transformation of waste into inert residues. Per year 750'000 tons of bottom ash and 75'000 tons of fly ash are produced in the incineration plants. In addition, similar quantities of wood ash from wood-burning stoves are produced. According to the revised Swiss Waste Ordinance from the year 2015, metal recovery must be implemented for municipal solid waste incineration plants producing fly ash by the year 2021, and for the wood ash by the year 2023, respectively. To comply with the new requirements, alternative options for metal extraction from the bottom and the fly ash as well as for the wood ash is being evaluated (see sections 9.3.1-9.3.3).

In addition to metals, fly ashes contain a number of toxic organic compounds, in particular polychlorinated dibenzo-p-dioxins and dibenzofurans (PCDD and PCDF). Dioxins are formed in the boiler area according to the "de novo" synthesis. It has been shown that PCDD/PCDF can be completely destroyed by reprocessing of the fly ash in municipal solid waste incineration plants using the so-called "ReFire" process. A fully automated ReFire process has been implemented in the kiln lines at KEBAG. Further process optimisation could be obtained via improvement of the flue gas cleaning system (see section 9.4).

Currently, a number of hazardous wastes produced in Switzerland are exported and disposed off in underground repositories abroad. If, for any reason, such disposal routes become no longer feasible, these materials will have to be treated and/or deposited in Switzerland. To fulfil the requirements of the Swiss Waste Ordinance, solidification and stabilization of such waste materials need to be implemented. Solidification of waste aims at converting a liquid or semi-solid waste to a solid, monolithic form that allows for an easier handling and disposal. Stabilization on the other hand focuses on producing a less toxic or less mobile waste form. Both solidification and stabilization are usually implemented in one single process. The integral assessment protocol comprises four "modules" aiming to provide a fundamental understanding of the processes and mechanisms promoting or inhibiting contaminant release: a) compressive strength, b) availability of contaminant release, c) long-term elution, and d) computer modelling (see section 9.5).

Time evolution of solid waste materials, leachate and gas emissions in the surroundings of a landfill are the key parameters for the evaluation of landfill *in situ* conditions. A comprehensive monitoring of a landfill site for disposal of incineration waste in Canton Zurich has been initiated in October 2018. The monitoring aims to analyse the long-term landfill behaviour and to make recommendations for the aftercare options. Preliminary analysis of collected time series data shows that reliable forecast of the long-term behaviour of dry bottom ash deposits requires longer landfill observation data. For the long-term environmental risk assessment, the prognosis has to be carried out considering a change in hydrological conditions. The influence of temperature, pH, redox conditions, sorption and biological activity is planned to be investigated in a follow-up project using reactive transport models (see section 9.6).

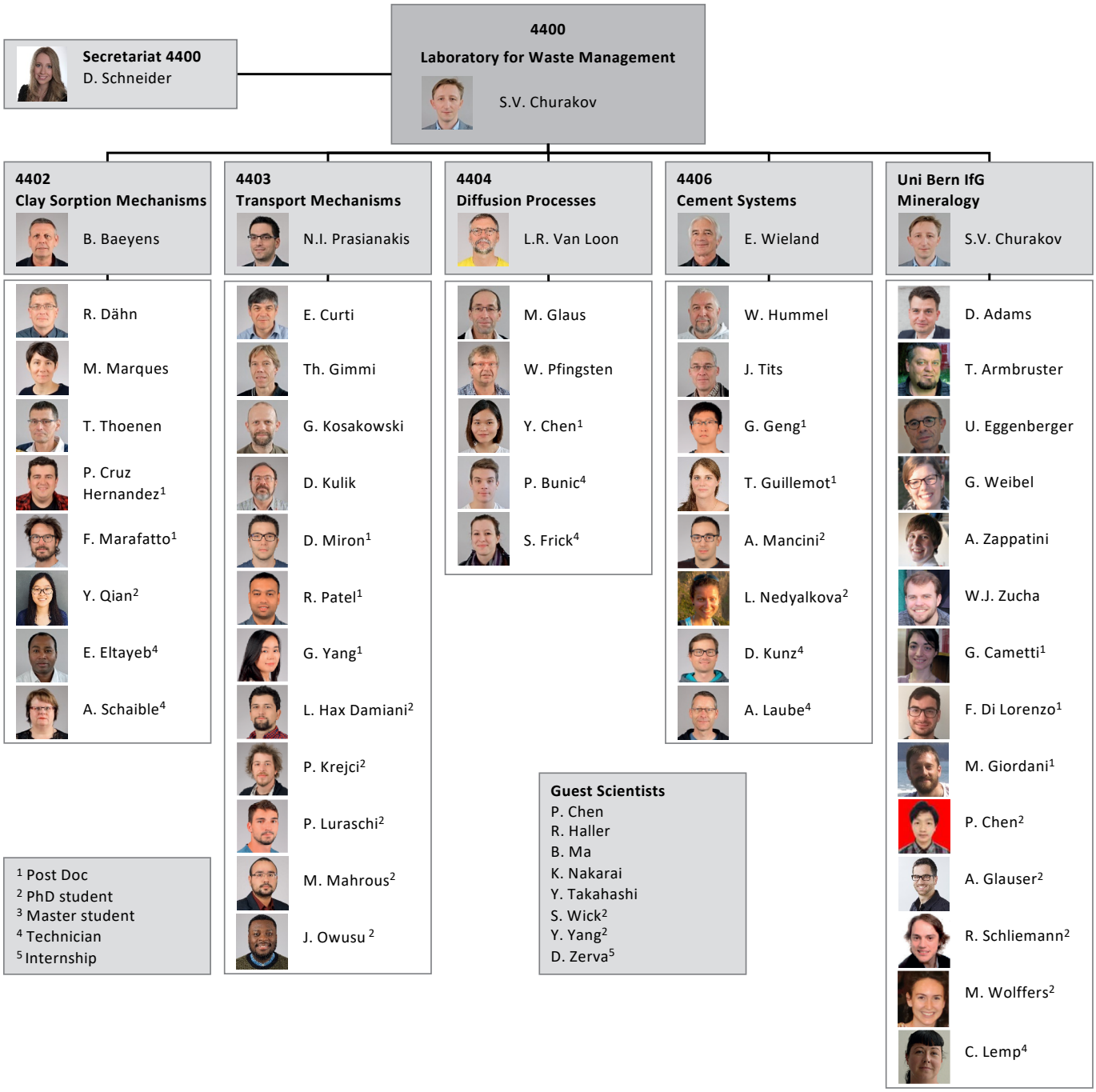

Fig. 1.1: Organisation chart of LES.

2 GEOCHEMICAL EVOLUTION OF REPOSITORY SYSTEMS

Prasianakis N.I., Churakov S.V., Curti E., Gimmi T., Jakob A., Kosakowksi G., Pfingsten W., Kulik D., Miron D. (postdoc), Yang G. (postdoc), Patel R.(postdoc), Karalis K. (postdoc-LSM), Luraschi P.(PhD student), Hax Damiani L. (PhD student), Maier M.L. (visiting PhD student), R. Haller (master student)

2.1 Introduction

This project aims at developing cross-scale THMC-numerical models and simulation tools for describing the long-term evolution of the multi-barrier repository and geotechnical engineering systems. This expertise is essential for the safety assessment and cross comparison of various repository designs as a part of the site selection process in the Sectoral Plan for Deep Geological Disposal (SGT) Stage 3, and the following general license application. Geotechnical engineering is a steadily growing research field focused on the optimal use of the subsurface reservoirs properties for geothermal energy production and for resource exploration. The project is focusing on three main topics: 1) Experimental characterisation and numerical modelling of the evolution of the technical barriers and their respective interfaces e.g. cement evolution and cement-clay interaction; 2) Fundamental understanding of reactive transport mechanisms, including sorption through multiscale modelling and upscaling techniques; 3) The benchmarking and application of state-of-the-art coupled codes as well as the development and coupling of thermodynamic modelling and database tools. Overarching thematic contributions and modelling support is provided in the area of contaminants retention and transport in host rock, heterogeneities, uncertainties and diffusion in disperse/compacted systems.

In the area of repository design and the temporal evolution of the repository *in situ* conditions, the study of the evolution of cement-clay interfaces, as well as the transport of inert and reactive gases were conducted. Within the Nagra supported PhD project: "*Evolution of transport properties, mineralogy, and porosity of cement-clay interfaces*" (P. Luraschi), the interaction between various cement types and clay materials is investigated. A detailed understanding of the reactive processes at the interface was obtained by combining diffusion experiments, SEM, and neutron imaging observations. Several samples of cement-clay interfaces are investigated by means of through-diffusion experiments using HTO and chloride ($^{36}Cl^-$) radiotracers. These experiments provide information on the diffusivities of an uncharged and of a negatively charged tracer, which are related to the evolution of the total and the anion-accessible porosity, over a period of 6 years of interface evolution. LES participates in the modelling of the Hydrogen-Transfer (HT) experiment in the Mont Terri rock laboratory. This field experiment aims at process understanding of inert and reactive gases transport in the Opalinus Clay formation. A new model developed within the project provides a very good agreement with the experimental observations. This model considers among others, the coupling of the involved transport and biochemical processes.

To investigate the interplay between reactive fluid transport, nucleation, precipitation and porosity evolution, several microfluidic experiments have been set up at FZ-Jülich in collaboration with LES. Such microfluidic lab-on-chip reactors have the potential to miniaturize laboratory experiments and observe the processes at the microscale. The experimental data were successfully modelled with advanced numerical simulation codes (digital twin) taking into account explicit coupling, between fluid flow, mineral reactivity and the time evolution of porosity. Use of advanced cross-scale algorithms provided an insight into the underlying processes at an unprecedented level of detail, including the shape and the rate of formation of the precipitates, which were largely influenced by the experimental conditions.

Within the SNSF PhD project "*Resolving dissolution-precipitation processes in porous media: Pore-scale lattice Boltzmann modelling combined with synchrotron based X-ray characterisation*" (M. Mahrous), the pore-level reactive transport modelling capabilities are extended. Pore-level models require detailed information regarding the pore structure and the connectivity of the pores. In collaboration with the King Fahd University of Petroleum and Minerals (KFUPM), in Saudi-Arabia, seven limestone cores, which have been scanned using high resolution micro computed tomography (CT), before and after an acid injection experiment, have been analysed in depth. The petrophysical parameters (porosity and permeability) have been extracted and used as input for direct pore-level (full core) simulations, as well as for the initialisation of macroscopic codes.

Machine learning techniques have been implemented for multiscale multiphysics modelling. First results suggest that efficient upscaling of results, from pore-scale to field scale, can be accomplished via the use of well trained artificial neural networks.

The SeS benchmarking exercise on the performance of several coupled transport codes for Cs diffusion through clays has been finalised in 2019.

In the PSI-FELLOW-II-3i project "*Pore-scale control of mineral precipitation: from atomistic model to macroscopic modelling and experimental observations*" (G. Yang) classical fluid-Density Functional Theory (f-DFT) was applied to obtain structural and thermodynamic properties of (Na,Ca) montmorillonite-fluid interface and to bridge atomistic and pore-level simulations.

A comprehensive analysis of parameter uncertainty propagation in reactive transport modelling of radionuclide sorption processes in clay has been performed by considering Cs migration through clay as a model system. The macroscopic code MCOTAC has been used to generate the space of possible solutions by varying the transport and sorption parameters of the model. Among other, an uncertainty classification tree has been generated which can help to identify critical parameters in the transport and sorption models relevant for performance assessment.

GEM software development (GEMS, lead scientist D. Kulik) has been continued and the improvement of the GEM2MT module for simplified reactive transport simulations has been extended in collaboration with the Colorado School of Mines, USA. The improved module has been applied in the case of NaCl solution and seawater diffusive ingress into cement mortar samples. The mineral zoning developed in the seawater ingress appears to resemble the one observed in experiments for clay-cement interaction conducted in the context of radioactive waste disposal.

Several on-going diversification projects are using advanced modelling capabilities developed at LES. In the realms of a collaborative project with the Laboratory for Scientific Computing and Modelling at PSI (LSM-PSI) and under the umbrella of the Swissnuclear funding agency through the project "*Multi-scale numerical prediction of boiling crisis*" (R. Patel & K. Karalis), the fundamental aspects of boiling processes are investigated from atomistic to reactor scale. The simulation of heterogeneous water boiling (bubble nucleation) at nano-scale was performed with the classical Molecular Dynamics (MD) method using the Transition Path Sampling (TPS) technique. The capabilities of lattice Boltzmann codes have been extended to reactive particle flows by coupling with discrete element method for adsorption on moving reactive particles. Finally, a collaborative research project with the pharmaceutical company "*GlaxoSmithKline*" has been initiated in 2019.

2.2 *In situ* conditions in repository near field

2.2.1 Interactions at cement-clay interfaces: 6 years of interface evolution and of the respective transport properties: diffusion of HTO and $^{36}Cl^-$

Cement and clay materials are characterised by different porewater chemistry. Chemical interaction between these materials results in dissolution-precipitation reactions of minerals that may alter the transport properties at their interface. The evolution of these interface properties is of relevance for the long-term safety assessment of the underground radioactive waste repositories. As a continuation of the former PhD project on cement-clay interaction, a new series of experiments with 5 mm long plugs of ordinary Portland cement and Na montmorillonite, both connected to the corresponding pore water solutions were performed to follow the time evolution of diffusivity and porosity at these interfaces. Several samples with cement-clay interfaces were investigated by means of through-diffusion experiments using HTO and chloride radiotracers. This provides information on the diffusivities of an uncharged and of a negatively charged tracer, which are related to the evolution of the total and the anion- accessible porosity.

The experiments with HTO indicate a strong decrease of the diffusive flux (and of the corresponding effective diffusion coefficient D_e of the clay plug only) during the first 1.5 years of interaction. This phase is followed by a second period, from 1.5 to 6 years, where the D_e reduction is less remarkable (Fig. 2.1a). The evolution of $^{36}Cl^-$ flux shows similar behaviour (Fig. 2.1b): a strong reduction of the effective diffusion coefficient during the first 1.5 years and a subsequent relatively small further reduction of the D_e. Interestingly, for some interface samples, no chloride flux could be measured anymore after long experimental times. The chloride flux shows a relatively strong scatter, which is related to the larger sensitivity of this negatively charged tracer to small variations in porosity or bulk-dry density, or also to local heterogeneities in the sample. Such small variations more strongly affect the effective diffusion coefficient of $^{36}Cl^-$ than that of HTO.

In earlier neutron imaging experiments it could be shown that, in these samples, a zone of reduced porosity has been developed on the Na montmorillonite side (Shafizadeh et al. 2019). The present data combined with these earlier observations allow to make the following conclusions: i) The HTO flux does not approach zero, which means that a part of the porosity is still available for diffusion after 6 years of reaction. ii) Most of the reaction took place during the first 1.5 years, suggesting that the observed decrease of D_e

slows down the further reactivity of the interface, that is, slowdown of further precipitation processes. iii) The reduction of the D_e with respect to unaltered Na-montmorillonite samples (Fig. 2.1, green symbols) is much stronger for chloride (96% within 17 months) than for HTO (45% after 17 months). This suggests that the precipitation reactions took place preferentially in the porosity domain accessible by anions (free porosity) leading to a very strong decrease of the chloride diffusivity.

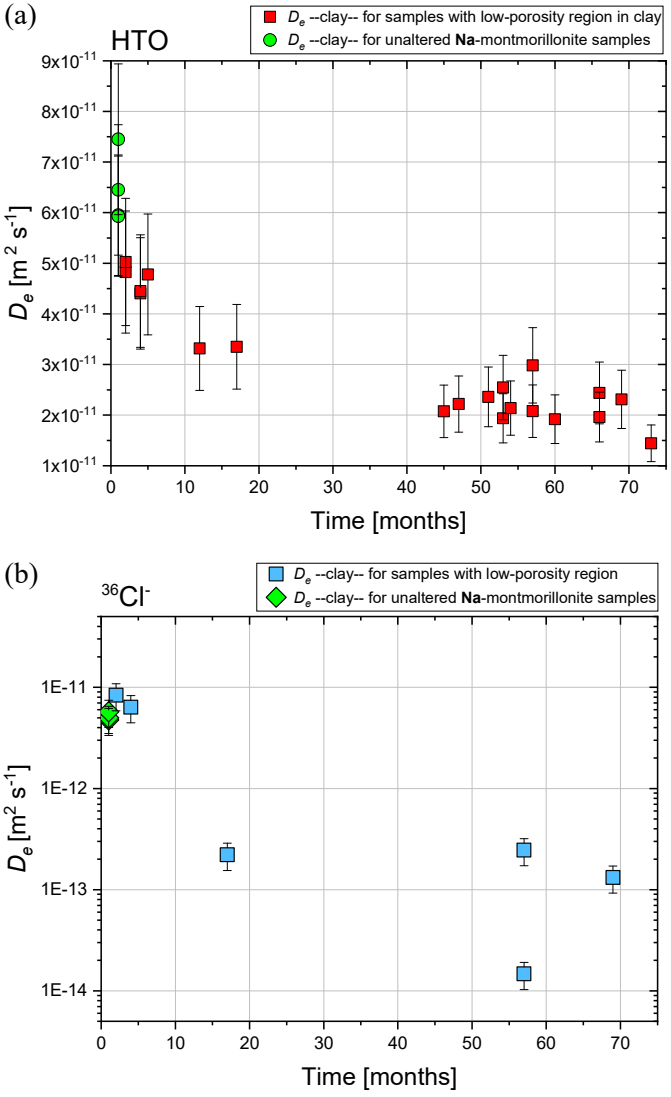

Fig. 2.1: Evolution of the average diffusion coefficient (D_e) of (a) HTO and (b) $^{36}Cl^-$.

2.2.2 Modelling of gas transport for the Mont Terri HT experiment

The Hydrogen-Transfer (HT) experiment in the Opalinus Clay formation at the Mont Terri rock laboratory is aimed at investigations of gas exchange and transport between the gas-filled borehole and the adjacent clay rock. This experiment improves understanding and provides information about the fate and transport of the inert and reactive gases in the Opalinus Clay formation. A borehole was filled with gas mixtures, and the evolution of gas pressure and gas phase composition were monitored. In addition, the inflow of formation water and its composition in the borehole was measured. Using this information, the transport properties of the gases in the rock adjacent to the borehole have to be assessed. For reactive gases, and more specifically for hydrogen, also the assessment of the consumption/degradation rates and mechanisms are of great interest. The coupling of the involved transport and biochemical processes requires inverse modelling of observations using reactive transport models.

Previous models have been extended as follow:

- a new conceptual description of mass transfer between the gas-filled borehole and the water-saturated rock has been implemented,
- equilibrium pore water chemistry consistent with the Opalinus Clay mineralogy was used,
- Python3 based implementation of the model using the coupling between FEniCS (http://www.fenicsproject.org), a software for solving the transport equations with the Finite Element method, and xGEMS (http://gems.web.psi.ch/), a Gibbs Energy Minimization (GEM) software for calculation of thermodynamic equilibria.

The new model for gas flux calculations across the borehole/Opalinus Clay interface assumes the existence of a very thin film of water covering the Opalinus Clay surface, which is in thermodynamic equilibrium with the gas phase in the borehole. With this model assumption, the calculated equilibrium concentration of dissolved gas in the borehole is used as a boundary condition for the transport model in Opalinus Clay (Fig. 2.2). The transport model calculates fluxes for dissolved species across the borehole wall using the concentration gradients at the boundary. Because of the optimisation of the numerical solution of the transport in the Opalinus Clay it is now feasible to conduct parameter variations for the relevant transport parameters. Fig. 2.3 shows the influence of the parameterisation of the porosity-diffusivity correlation for the Opalinus Clay formation, which gives the effective diffusion coefficient for species in the Opalinus Clay pore water, i.e. dissolved gases.

The thermodynamic equilibrium between gas, aqueous, and mineral phases for the borehole and the Opalinus Clay was calculated with the xGEMS solver using the Thermoddem geochemical database. This model set-up specifically facilitates the inverse calculation of gas pressures in the borehole caused by mass fluxes

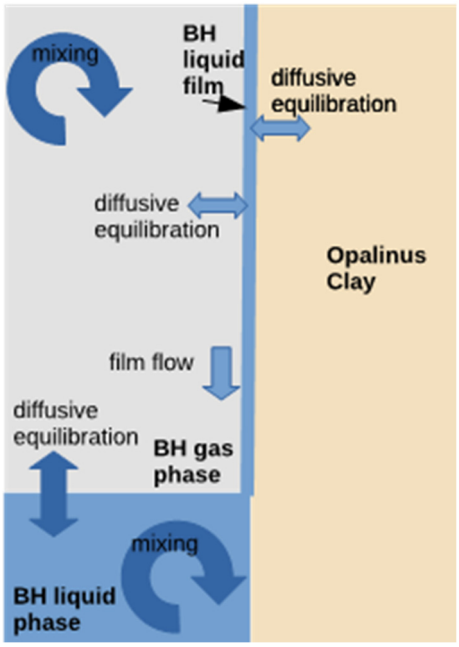

Fig. 2.2: Conceptual model for gas and water fluxes in the borehole and across the borehole(BH)-Opalinus Clay interface.

(dissolved gases and water influx) across the borehole wall and bio-chemical consumption of hydrogen in the borehole and/or in the Opalinus Clay.

The new modelling approach significantly simplifies the handling of gas and water fluxes across the borehole interface and at the same time improves the agreement of the modelling results with the experimental data. In contrast to the previous model, the consumption of hydrogen due to microbiologically mediated sulphate reduction is implemented in the borehole (instead of in the Opalinus Clay). Remarkably, this implementation provides a good description of the experiment without invoking artificially enhanced hydrogen fluxes into the Opalinus Clay and explains the observed decrease of hydrogen concentrations in the borehole. A small mismatch exists for CO_2 profiles (Fig. 2.3 upper-right) because of the Opalinus Clay pore water definition, which is in equilibrium with certain carbonate minerals. However, this difference does not have a significant impact on the overall system evolution.

2.3 Fundamental understanding of reactive transport and sorption mechanisms

2.3.1 Microfluidic experiments and pore-scale modelling diagnostics for assessing mineral precipitation and dissolution in confined spaces.

A new numerical simulation method describing the mass transport, nucleation, mineral precipitation and dissolution in confinement has been developed and tested against experimental data in collaboration with the Institute of Energy and Climate Research (IEK-6): Nuclear Waste Management and Reactor Safety at

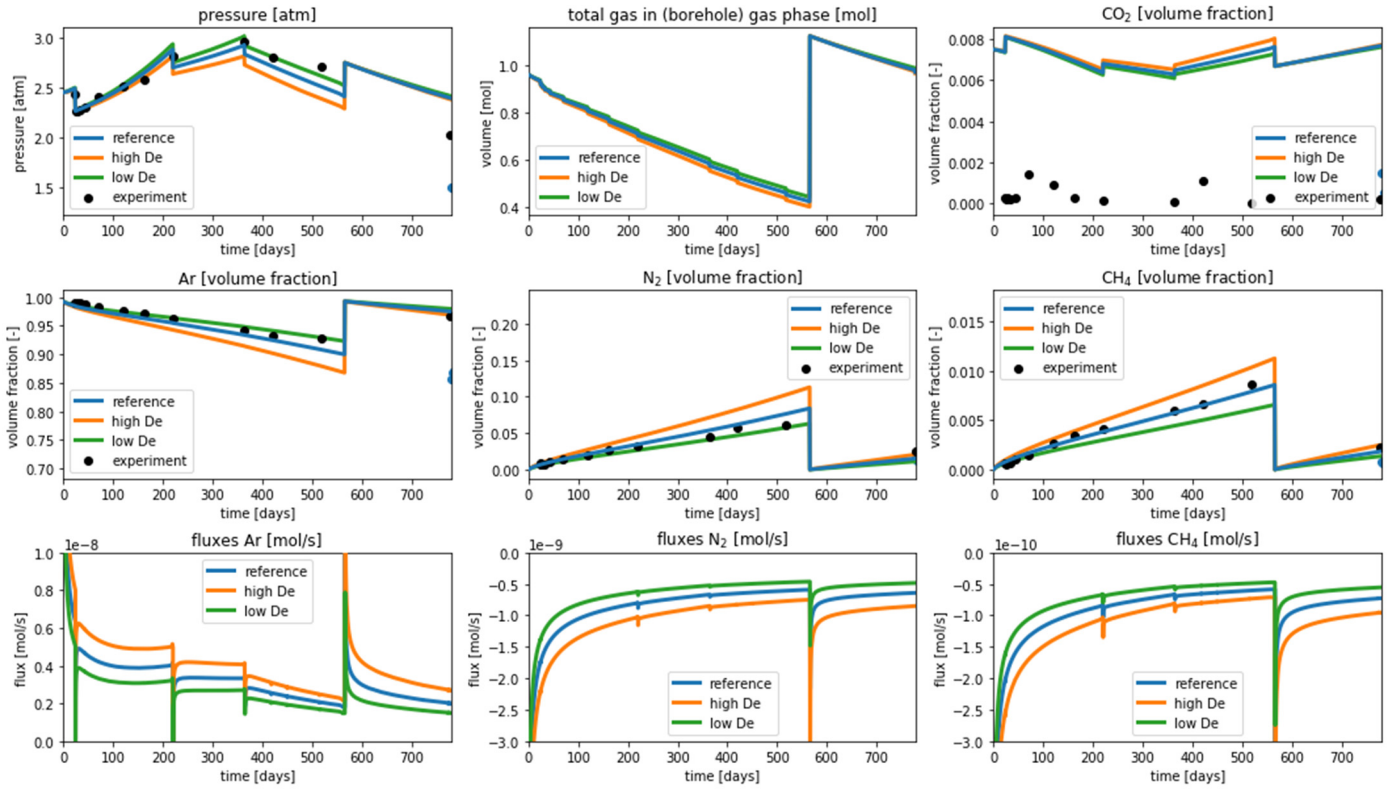

Fig. 2.3: Influence of porosity – diffusivity correlation (effective diffusion coefficients) on borehole gas pressure and gas phase composition calculated with the updated model.

Forschungszentrum Jülich (FZ-Jülich), Germany. In this project, an advanced multiscale modelling and numerical diagnostics approach has been applied to simulate a microfluidic lab-on-chip experiment conducted at the experimental facilities of the FZ-Jülich. The reactive transport processes conceived in the experimental set-up involve the flow and the diffusion controlled precipitation and the subsequent dissolution of $SrSO_4$ (celestine). The experimental set-up is depicted in Fig. 2.4. Mixing of $SrCl_2$ and Na_2SO_4 rich fluid occurs in a mixed advection-diffusion flow regime. Celestine growth has been monitored using optical microscopes. The measured rates and direction of crystal growth depend on local mass transport, concentrations and reaction kinetics, all of them varying continuously in time and space. Full spatial and temporal resolution of the respective fields is only possible using advanced cross-scale reactive transport modelling, in this case based on the lattice Boltzmann method (Prasianakis et al. 2017). Accurate models and advanced computational algorithms allowed to create an offline digital twin with the capacity to provide an insight into the underlying processes at an unprecedented level of detail, and to predict near-future evolution steps of the system (Poonoosamy et al. 2019).

2.3.2 Obtaining petrophysical parameters from micro-CT scans for reactive transport simulations

Pore-level reactive transport modelling provides the link between the elementary atomistic-scale chemical processes at mineral fluid interface, and the field scale long-time modelling of subsurface geotechnical systems. Accurate prediction of *in situ* conditions and transport properties of evolving geotechnical systems require representative and detailed information regarding the pore structure and the connectivity of the pore space. Particularly challenging is the experimental characterisation of such a phenomena. Innovative

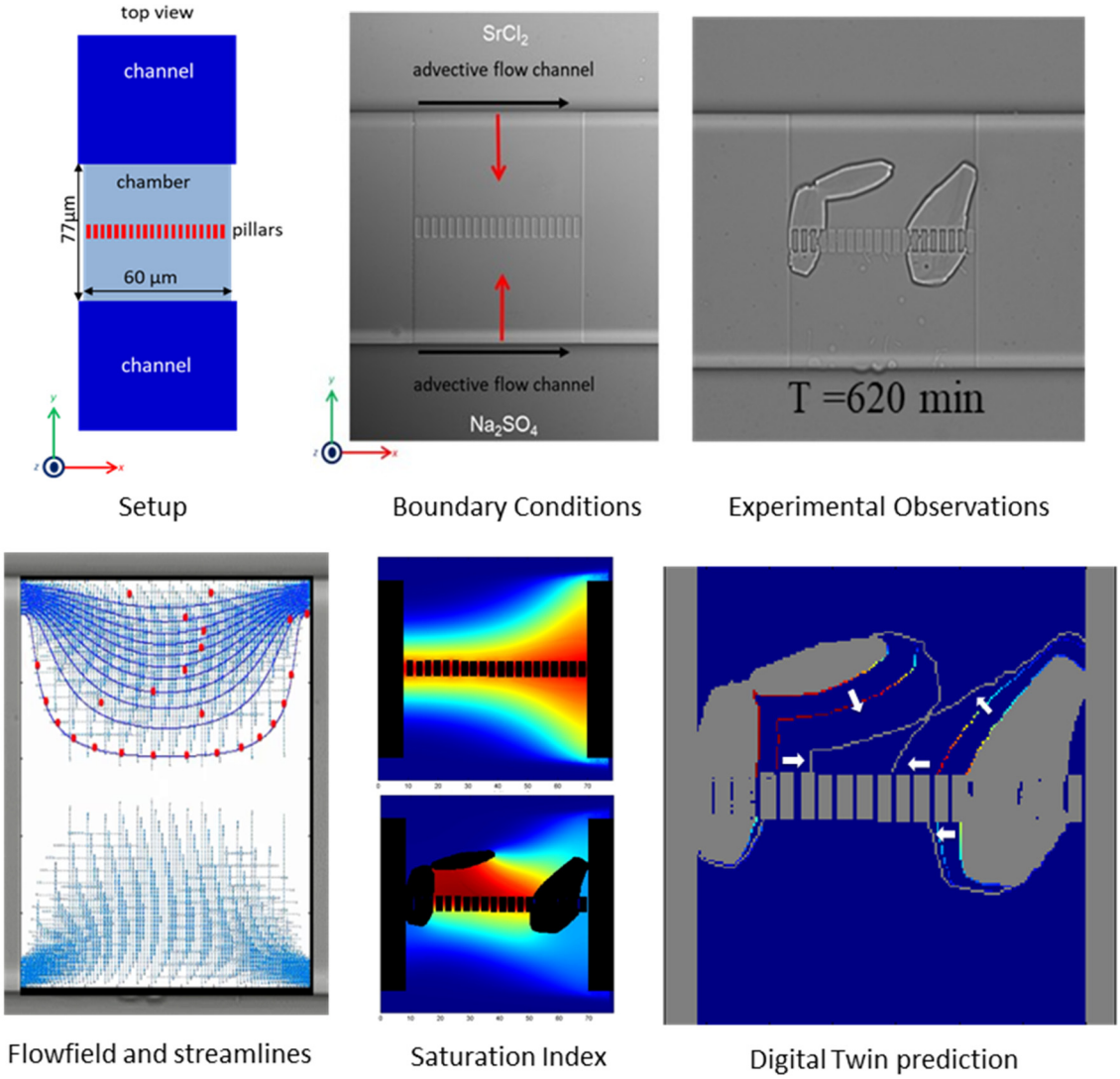

Fig. 2.4: Combining lab-on-chip experiments and advanced cross-scale numerical diagnostics. Top: microfluidic experimental set-up and observations of celestine growth. (Bottom) Digital twin based on cross-scale reactive transport models providing information of local velocities, concentrations (saturation index) and predictions of rates and directions of crystal growth (Poonoosamy et al. 2019).

methodology for extraction of petro physical parameters from numerical modelling and core-scale reactive transport experiments are conducted in collaboration with the King Fahd University of Petroleum and Minerals (KFUPM) in Saudi-Arabia. Seven limestone cores were scanned using high-resolution micro computed tomography before and after an acid injection experiment at the KFUPM. The resulting tomograms were segmented and several petrophysical parameters needed for reactive transport simulations such as the reactive surface area, the definition of the Representative Elementary Volume (REV), the porosity and the permeability fields were extracted. The stepwise approach for processing micro-CT scans for continuum-scale and pore-scale simulations is described in Fig. 2.5. In Fig 2.5a the original 8-bit grayscale image of the limestone rock from the micro-CT machine is depicted, where each voxel has been assigned a value between 0 and 255. Fig. 2.5b is the segmented image where each voxel is defined as either rock or pore. The 3D construction of the segmented image serves as a direct input for lattice Boltzmann pore-scale simulations. Fig. 2.5c shows the calculation of the reactive surface (interface between pore and rock) area used as input in both continuum-scale and pore-scale simulations. Fig. 2.5d shows the REV analysis used to determine the grid cell size for the continuum-scale simulations. The graph shows that the grid cell size of 1 mm^3 is the lower limit for REV representing the core porosity. Fig. 2.5e shows the discretisation of the segmented image into cubic grid cells of 1 mm length. By computing the porosity and the permeability of each grid cell, the porosity field (Fig. 2.5e, f.1) and the permeability field (Fig. 2.5e, f.2) are constructed and used as an input to the continuum-scale simulations.

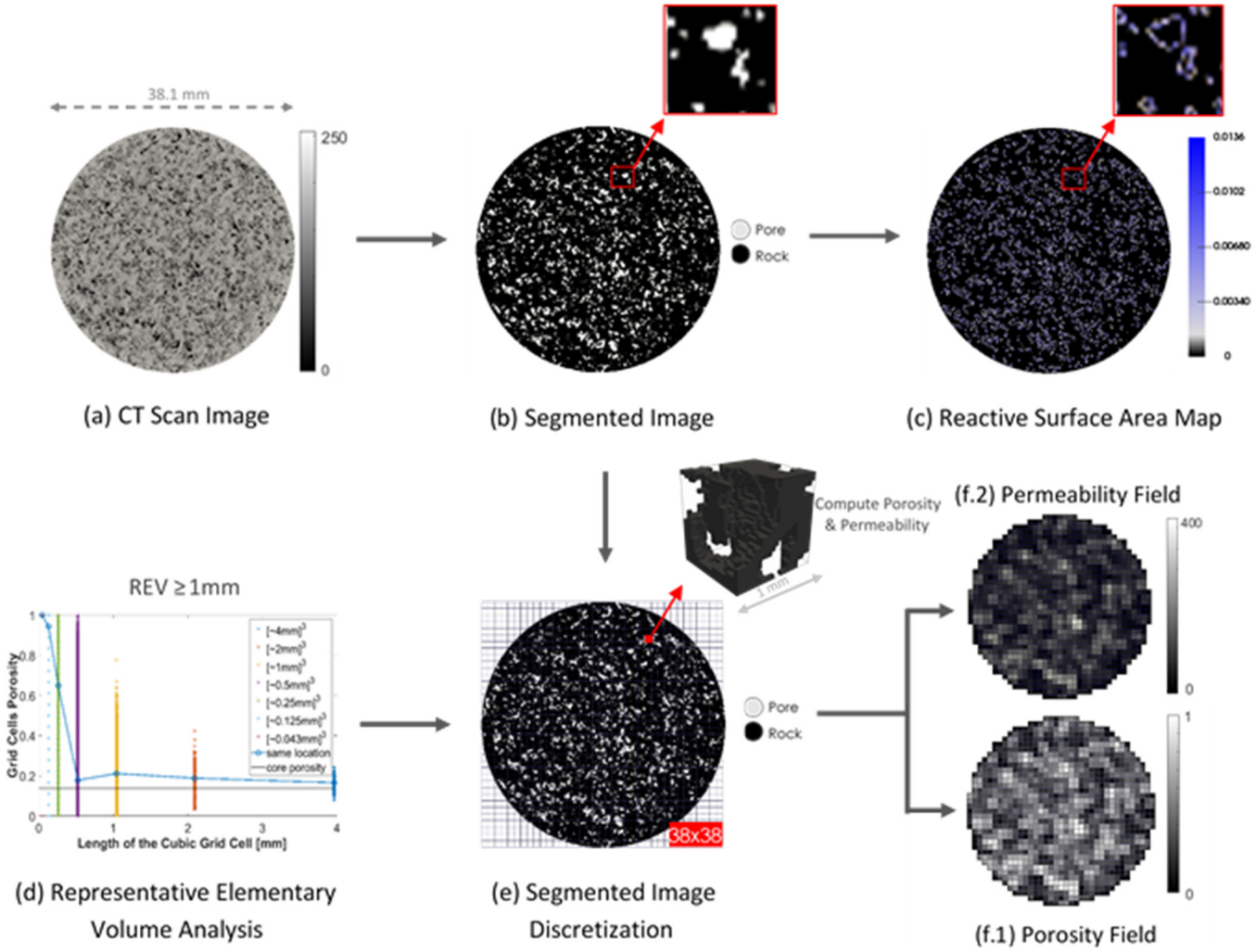

Fig. 2.5: Multiscale processing of µCT scans and upscaling of transport parameters for continuum-scan and pore-scale simulations. (a) Original 8-bit grayscale image of the limestone rock from the µCT. (b) The segmented image where each voxel is defined as either rock or pore. (c) Calculation of the reactive surface (interface between pore and rock) area used as input in both continuum-scale and pore-scale simulations. (d) REV analysis used to determine the minimal grid cell size for the continuum-scale simulations. (e) The discretisation of the segmented image into cubic grid cells of 1 mm length. The porosity field (f.1) and permeability field (f.2) are constructed and used as an input to the continuum-scale simulations.

It should be noted that 2D cross-section images are shown here just for illustrative purposes. In practice these processing steps are completed in 3D. The extracted petrophysical information will be used in both pore-scale and continuum-scale simulations, which will be further compared with experimental results. The resulting digitally reconstructed pore-structures are composed by more than 1.5 billion voxels as shown in Fig. 2.6. Simulations using these structures are computationally intensive and are conducted using a dedicated in-house developed CPU/GPGPU lattice Boltzmann code. The corresponding simulations were performed at the Swiss Supercomputer Center (www.cscs.ch). This project will enhance the reliability of multi-scale reactive transport simulations, and will shed light on the upscaling of transport parameters from small-scale experiments/simulations to the field scale observation at geological time scales.

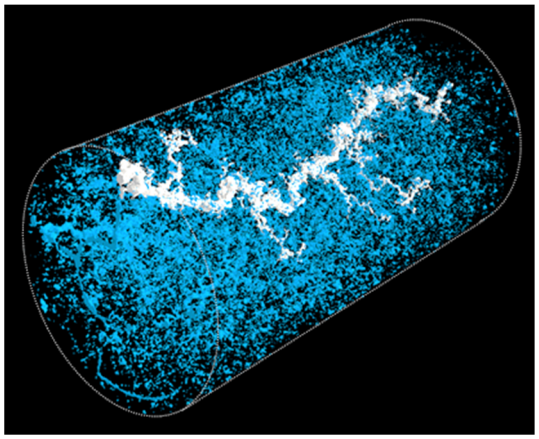

Fig. 2.6: Pore network of limestone core after acid injection obtained from μCT scan. The resulting wormhole from calcite dissolution is highlighted in white.

2.3.3 Modelling of Cs diffusion through clays

The SeS benchmark on the modelling of Cs diffusion through clay for single species and multi species reactive transport has been finalised in 2019. The simulation codes MCOTAC, FLOTRAN, CORE2D, PHREEQC and PHREEQC-COMSOL participated to the multispecies benchmark. In general, a good agreement between Cs breakthrough curves simulated with different codes could be obtained. The calculation time for this benchmark example varies within an order of magnitude for the different codes. Substantial deviations between the calculated break-through times have been reported between PHREEQC-COMSOL and other codes. It should be further noted that the calculated Cs breakthrough curves and calculation times of PHREEQC-COMSOL depend extremely on the set-up of the PHREEQC-COMSOL coupling itself. The smaller the assumed Cs concentration at the high-concentration boundary, the larger the deviations for the calculated Cs breakthrough, especially for the PHREEQC-COMSOL coupling as shown in Fig. 2.7, where the first Cs arrival time was calculated to be much earlier compared to all other code involved in the benchmark.

2.3.4 Machine learning for multiscale couplings

In continuum-scale models, the simulation domain is represented by grid cells that are equal to or larger than the "Representative Elementary Volume" (REV). Inside this REV macroscopic property of a material is represented by a statistical average. However, dissolution and precipitation processes act at a large range of scales, from atomistic to field scale, so that the exact definition of REV is very challenging. To better model the processes occurring within the elementary volumes of a continuum-scale algorithm, an input describing the microscopic processes is necessary. Such information can be derived using atomistic and pore-level simulators along with a subsequent upscaling step. Such an example is the effect of dissolution and precipitation on the permeability and diffusivity of a porous medium. Empirical porosity permeability-correlations have limited applicability in reactive transport simulations especially in the cases of high reactivity, as for example in the dissolution of a calcite rock during the injection of a low pH fluid.

In (Prasianakis et al. 2018) porosity-permeability correlations in reacting porous media have been extracted via pore-scale lattice Boltzmann simulations.

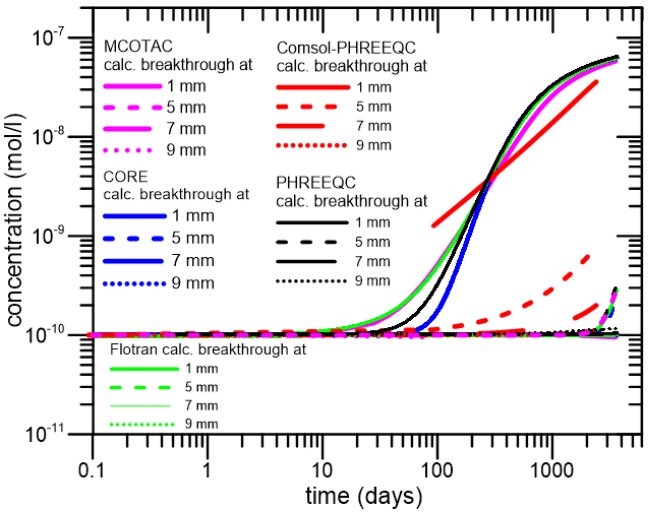

Fig. 2.7: Cs breakthrough curves calculated with the multi species transport models at different locations in the Opalinus Clay samples (x = 1, 5, 7 and 9 mm) by using five reactive transport codes (CORE2DV5, FLOTRAN, MCOTAC, PHREEQC and COMSOL-PHREEQC) for a Cs concentration of 10^{-7} mol/L at the high-concentration boundary.

Fitting of these correlations to the simulation results is not a straightforward task and cannot be successfully automated. Artificial neural networks (see Fig. 2.8) have been implemented to describe porosity-permeability relationships in the simulated system, The accuracy of the neural network outperforms the accuracy obtained by closed form correlations. In addition, training and subsequent upscaling could be automated. First upscaling results are very promising and suggest that machine-learning techniques can be used to automate cross-scale transfer of physical parameter in numerical algorithms.

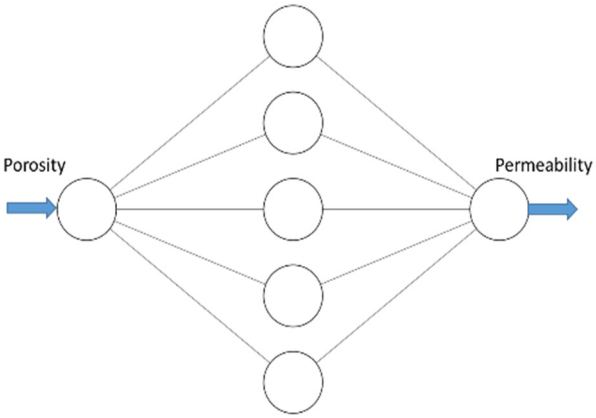

Fig. 2.8: Topology of a neural network trained to reproduce the pore-level simulation porosity-permeability output. Input is the porosity and output is the permeability value. An artificial neural network is able to represent complex relationships in multi-dimension spaces.

2.3.5 Modelling Ca-Na ion exchange in montmorillonite by atomistic simulations and fluid density functional theory

Mineral reactivity depends strongly on molecular-scale mass transport and elementary ion solvent interactions at the mineral fluid interface. Molecular dynamics (MD) simulations provide an accurate description of the mineral fluid interface taking into account all-atom-interactions. This simulation approach is computationally expensive, if applied to large molecular systems. Classical Density Functional Theory (DFT) delivers structural and thermodynamic information at comparatively low computational costs. In the PSI-FELLOW-II-3i project "*Pore-scale control of mineral precipitation: from atomistic model to macroscopic modelling and experimental observations*" (G. Yang), classical density functional theory (f-DFT) was applied to model water and ion distribution at the charged mineral water interface. In our f-DFT model for the montmorillonite–electrolyte interface, the solvent molecules and ions were included in the system of equation as neutral and charged Lennard-Jones particles respectively. The model was referred to as DFT/LJ-3CM. The performance of this 3 component classical DFT model was compared with the atomistic simulations for montmorillonite (MMT) in different state of hydration for NaCl and $CaCl_2$ in electrolyte solution. The predictions of DFT/LJ-3CM model were found to be in good agreement with the atomistic simulations and with experiments under a wide range of conditions. The calibrated DFT/LJ-3CM model for Na and Ca MMT was able to provide a semi-

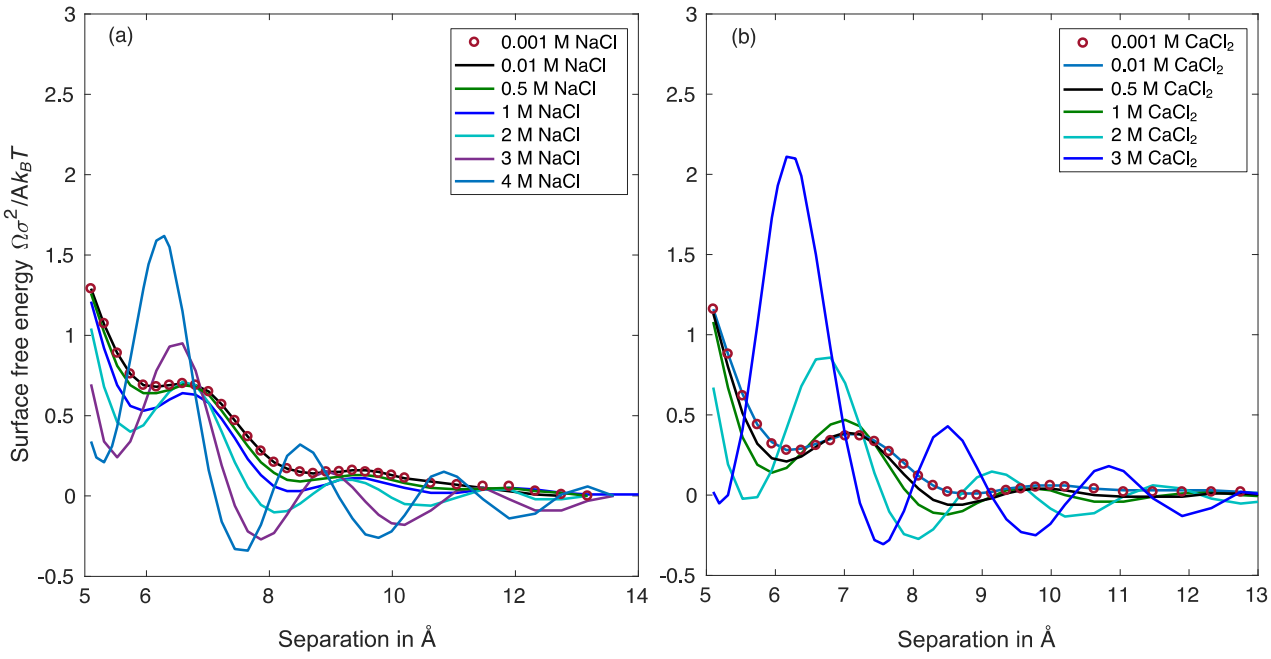

Fig. 2.9: The free energy per unit surface area as function of the equilibrium interlayer separation between two smectite TOT layers in (a) NaCl; (b) $CaCl_2$ bulk solutions. The ionic concentrations are indicated in the plots. Minima of the free energy correspond to the stable hydration state of the MMT.

quantitative estimate of the cation selectivity for the ion exchange equilibrium and swelling behaviour of MMT (Fig. 2.9). At the same time, the DFT calculations are 3-4 orders of magnitude faster than conventional MD simulations. The DFT/LJ-3CM model provides a robust approach, which can be used for upscaling in reactive transport simulators and modelling ion migration taking place under more complex thermo-chemo-hydro-mechanical conditions.

2.4 Decision trees and parameter uncertainty propagation as a tool to identify critical parameters for performance assessment

Cooperation with Ali Ahoub, Giovanni Sansavini (both Risk Center, ETHZ) and Luca Podofillini (LEA, PSI)

The sorption model parameters (Bradbury & Baeyens 2002, 2005) uncertainty propagation in reactive transport modelling of radionuclide transport has been estimated for Cs migration models through clay (MCOTAC, Pfingsten 2002). Extensive realisations of Cs breakthrough curves in clay have been produced as the basis for the sensitivity analysis, aiming to the quantification of the effect of the uncertainties of site-specific sorption reactions equilibrium constants and pore-water cations' concentrations, i.e. uncertain sorption model parameters. The sensitivity analysis allowed to further generate a classification tree to show combinations of uncertain sorption model parameters' values.

For the construction of the classification tree shown in Fig. 2.10, a predefined maximum Cs concentration value equal to 95% of the Cs boundary concentration was defined for the calculated Cs breakthrough at a specified location. Calculated Cs breakthrough values lower and higher than 95% of the Cs boundary concentration are labelled "Low Concentration" and "High Concentration" values, respectively.

For the current example, the classification tree can be interpreted as follows: The most important model parameter influencing the uncertainty of the simulations, which is the Type2-K-Cs (ion exchange equilibrium constant for K^+ exchange with Cs^+ on Type2 surface sites) in the considered system, is placed on the top of the diagram. If this sorption model parameter is larger than 1.39, the Cs breakthrough reaches "High Concentration" and the tree branch should be followed to the next relevant uncertain model parameter, i.e. the Na^+ concentration. If the Na^+ concentration is lower than 0.43 mol/L, the Cs breakthrough will not reach the defined maximum Cs concentration, then a "Low Concentration" result is expected, and the condition of "Low Concentration" is

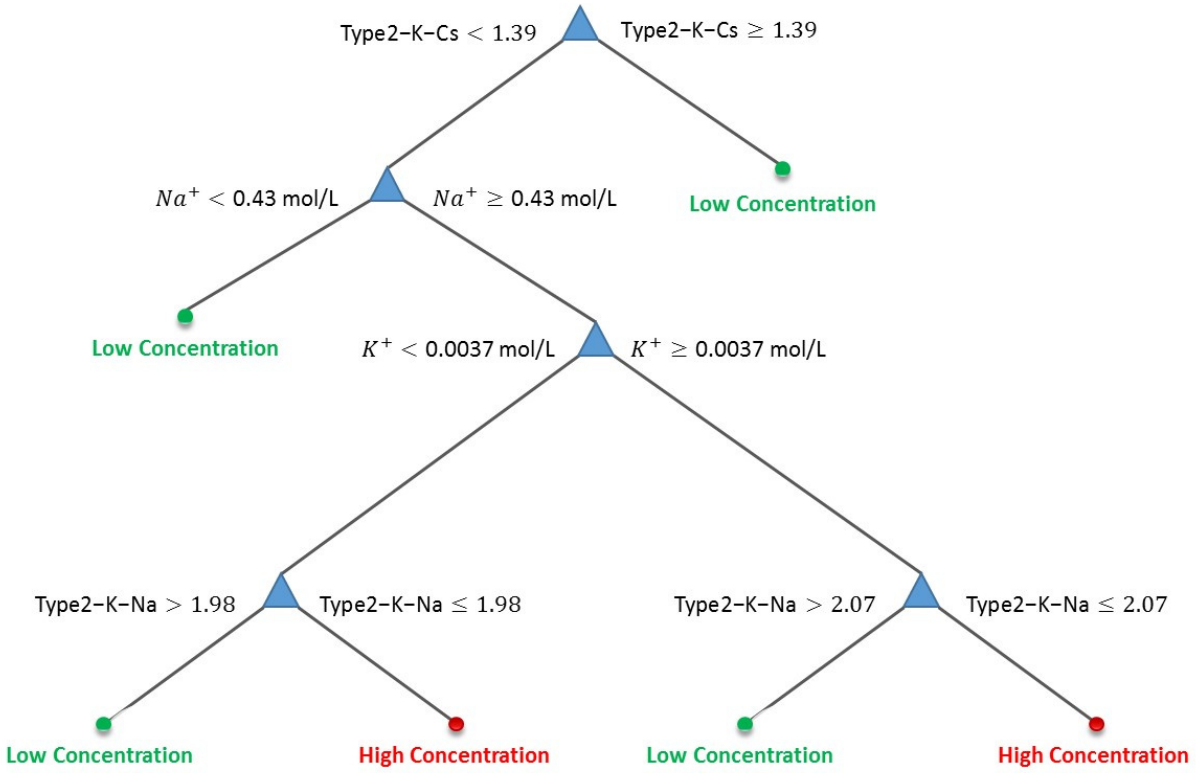

Fig. 2.10: Classification tree for an assumed up-stream boundary caesium concentration of 10^{-3} mol/L and uncertain parameter values for the sorption model (major ion concentration levels and equilibrium sorption constants). "High concentration" indicates an arbitrarily pre-defined Cs concentration of 95% of the Cs boundary concentration for calculated breakthroughs.

valid for the combination of the two most influencing parameters responsible for Cs sorption in this system. However, if the Na^+ concentration is higher than 0.43 mol/L, then the tree branches again to the next relevant uncertain sorption model parameter, which is the K^+ concentration. This procedure continues until the last uncertain sorption model parameter with branches of "Low Concentration" and "High Concentration", indicating whether an uncertain parameter combination is acceptable ("Low Concentration") or not ("High Concentration").

It is clear that such classification trees can be constructed for "worst case parameter values" in order to judge about site-specific critical parameter values in performance assessment, especially when comparing different sites and waste repository designs.

2.5 Improvement of GEM2MT module (GEM-Selektor code) for simplified reactive transport simulations with applications to cement degradation (NaCl solution and seawater ingress)

The GEM2MT module of the GEM-Selektor code package (http://gems.web.psi.ch) has been largely developed in 2005-2007 in collaboration with W. Pfingsten, F. Enzmann (Uni.Mainz), G. Kosakowski and S. Dmytrieva as a tool for simplified reactive transport simulations (mainly 1-D columns with advection, dispersion and diffusion) in an integrated graphical environment. Initially, two numerical methods were implemented using the GEMS3K API at TNodeArray level: Finite Differences (FD) for simulating advection with hydrodynamic dispersion, following Rausch et al. (2005), and Random-Walk (RW) capable of modelling diffusion with or without advection, following the MCOTAC code (Pfingsten 1996). Also, the generic box-flux scheme (with mobile phase group fluxes and ODE box mass integration) was implemented using Kulik et al. (1993). Later on, in 2010, in collaboration with T. Wagner (ETHZ at that time), the so-called "sequential reactor chain/wave" scheme was added for benchmarking with the HCh code. The coupling with chemistry was made in non-iterative operator-splitting fashion, in most cases moving the bulk composition of aqueous phase between nodes/boxes at transport step, and re-computing equilibria in nodes/boxes with the GEM IPM-3 algorithm at the equilibration step.

The demand for a modern GEM2MT has been increased since 2015, mainly from the side of cement and hydrothermal geochemistry communities of GEMS users. Several user guides along with some bug-fixing and improved wizards and template scripts were added in 2019 during D. Kulik's stay at Colorado School of Mines (May 2019, Golden CO, USA) in collaboration with Prof. A. Gysi, who distributes the MINES thermodynamic database and tutorials for GEMS (http://tdb.mines.edu). The Colorado School of Mines actively uses the GEM-Selektor code for modelling hydrothermal systems. Prof. Gysi's group uses the GEM2MT module for simulating hydrothermal water-rock interaction in applications to ore formation and geological CO_2 disposal. The resulting version 3.5.0 of the GEM-Selektor code has been released in May 2019.

As a relevant application of the improved GEM2MT module, in collaboration with Prof. B. Lothenbach (Empa, NTNU), 1-D reactive transport (RT) models of NaCl solution and seawater diffusive ingress into cement mortar samples has been set up and computed. The goal was to compare and verify the RT simulations by the random-walk method using the chloride retention and mineralogical profile data from recent experiments performed in Prof. K. De Weerdt's group (NTNU) (De Weerdt et al. 2019). The transport parameters (for pure diffusion case) could be calibrated against the Cl-retention profiles for 21 days for both NaCl solution and seawater ingress. The RT simulations reproduced the formation of the same mineral zoning as that observed in the experiments and discussed in literature (Jakobsen et al. 2016). The mineral zoning developed in the seawater ingress case appears to resemble the one observed in experiments for clay-cement interaction (Jenni et al. 2017) conducted in the context of radioactive waste disposal.

The Chemical part of RT simulations has been set up using cement and mortar compositions from De Weerdt et al. (2019), with respective selection of thermodynamic data from the PSI/Nagra (Thoenen et al. 2014) and Cemdata18 (Lothenbach et al. 2019) databases in GEMS format. All calculations were conducted at 1 bar, 20 °C. The extended Debye-Hueckel activity model for aqueous phase was used. Three initial systems were created and checked: (1a) Sand-0.55 *m* NaCl solution (with trace concentrations of other elements set to 10^{-9} *m* or less); (1b) Sand-SW – the normative seawater with salinity of 35 g/kg; (2) Mortar with inert quartz and porewater occupying 10% of total volume (i.e. with porosity 10%). The volume of aqueous solution in (1a) and (1b) systems was adjusted to be the same as that in the mortar system (2).

The transport part of the reactive transport simulations was set as a 1-D column of 20 mm length. The left-hand side was declared a constant-flux boundary condition and initialised with the system 1a or 1b. The rest of the column was initialised with the system 2 (mortar with its porewater), and the right boundary was declared as constant-flux sink and cell. For the random-walk simulations, the advection velocity was set to zero, and the tortuosity τ with the aqueous diffusion

coefficient D_c adjusted in trial simulations to reproduce the Cl uptake curves for 21 days (Figure 2.11). Reasonable prediction of Cl uptake was obtained by setting $D_c = 2.3\times10^{-9}$ m^2/s (for all species as for water) and tortuosity $\boldsymbol{\tau} = 10$ (or effective diffusion coefficient $D_{eff} = 2.3\times10^{-10}$ m^2/s assuming $\boldsymbol{\tau} = 10$ or bulk diffusivity $D = 2.3\times10^{-11}$ m^2/s). These numbers agree with literature values for Cl^- diffusion coefficients and bulk diffusivity in concrete. The resulting mineralogical changes are shown in Figure 2.12. This successful modelling exercise demonstrates that the GEM2MT module of GEMS has become a useful tool for running and validating RT simulations of various kinds of degradation of cementitious materials, by induction also in geological repository environments.

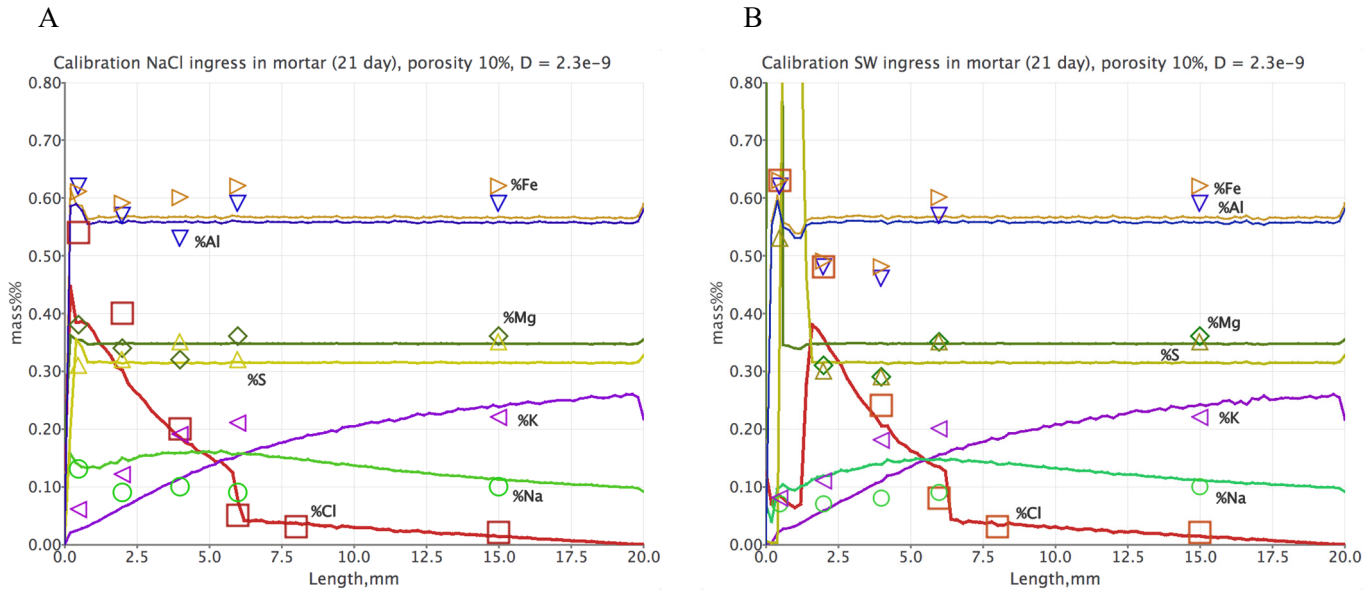

Fig. 2.11: Bulk element content profiles (in mortar dried at 105 °C) predicted by random-walk simulations for 21-day ingress of NaCl solution (A) and seawater (B) cases, against experimental data (De Weerdt et al., 2019) shown as scattered symbols.

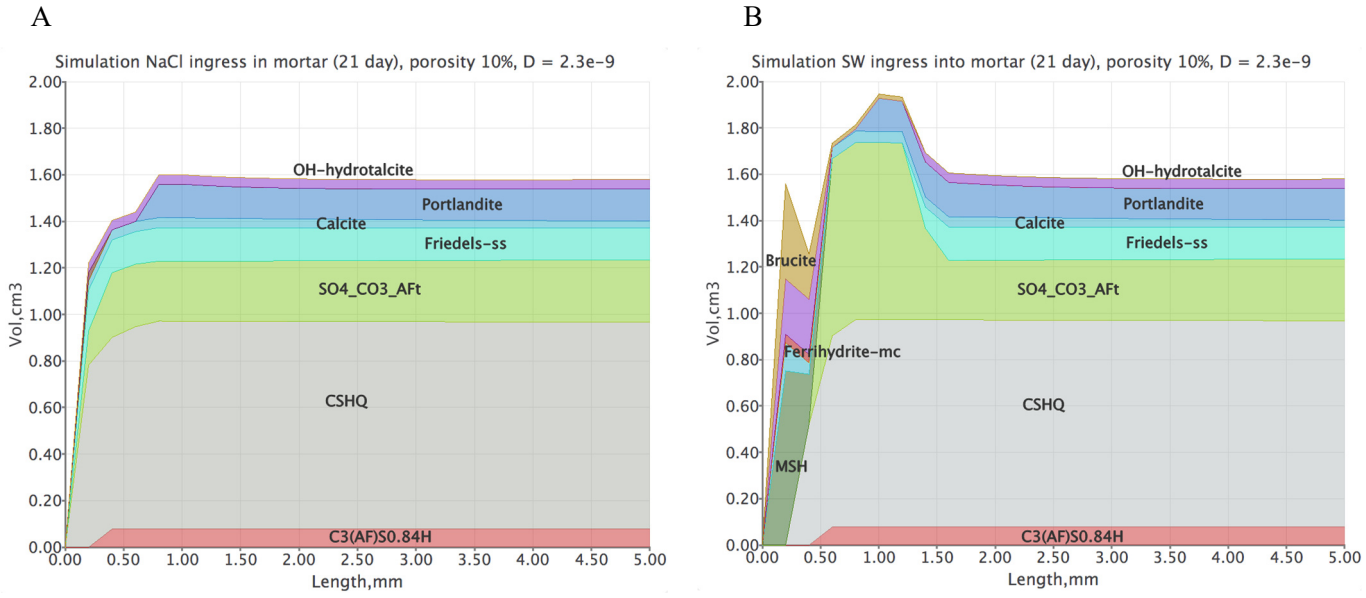

Fig. 2.12: Volumes of reactive mineral phases predicted in the first 5 mm (fluid ingress side) of the 1-D column for 21-day ingress of NaCl solution (A) and seawater (B) cases. Inert sand (quartz) of the mortar is not shown.

2.6 Diversification projects

2.6.1 Multi-scale numerical prediction of boiling crisis

In the realms of a collaborative project with the Laboratory for Scientific Computing and Modelling at PSI (LSM-PSI) and under the umbrella of the Swissnuclear funding agency through the project "*Multi-scale numerical prediction of boiling crisis*", the fundamental understanding of boiling processes from atomistic to reactor scale is pursued. LES is conducting the research at the micrometer level, and at the same time supervises the modelling at the atomistic level, aiming at providing bottom-up parametrisation to the macroscopic boiling code, developed at PSI, PSI-Boil (https://www.psi.ch/en/lsm/psi-boil).

A pseudo-potential lattice Boltzmann scheme (Li et al. 2016) which has been widely used for simulating boiling problems was implemented in the open source lattice Boltzmann method framework *Yantra* (lead scientist: R. Patel). The pseudo-potential based lattice Boltzmann scheme simulates a single component two-phase fluid system by addition of attractive or repulsive forces, added to the standard lattice Boltzmann model to incorporate a non-ideal pressure tensor. The implementation has been benchmarked by reproducing the Laplace law. In addition, the implemented model can account for different contact angles between fluid phases and solid walls and can also accept as an input a segmented image of the surface roughness. First parametric studies on the effect of surface roughness on bubble dynamics have been conducted. Fig. 2.13 shows the interaction and bubble dynamics of a bubble with a rough wall for several timesteps, using the developed model. Due to buoyancy forces, the bubble moves from bottom to top (top-bottom periodic boundary condition is applied). Depending on the conditions, a scenario were a bubble is entrapped may occur.

The simulation of heterogeneous water boiling (bubble nucleation) at nano-scale was performed with the classical Molecular Dynamics (MD) method using the Transition Path Sampling (TPS) technique. Molecular insights into the first stages of the bubble formation in water in contract with the zirconia alloy and at the same time the location where nucleation is likely to occur were determined. The interactions between water molecules were described using the SPC/E water model (Berendsen et al. 1987) and between the

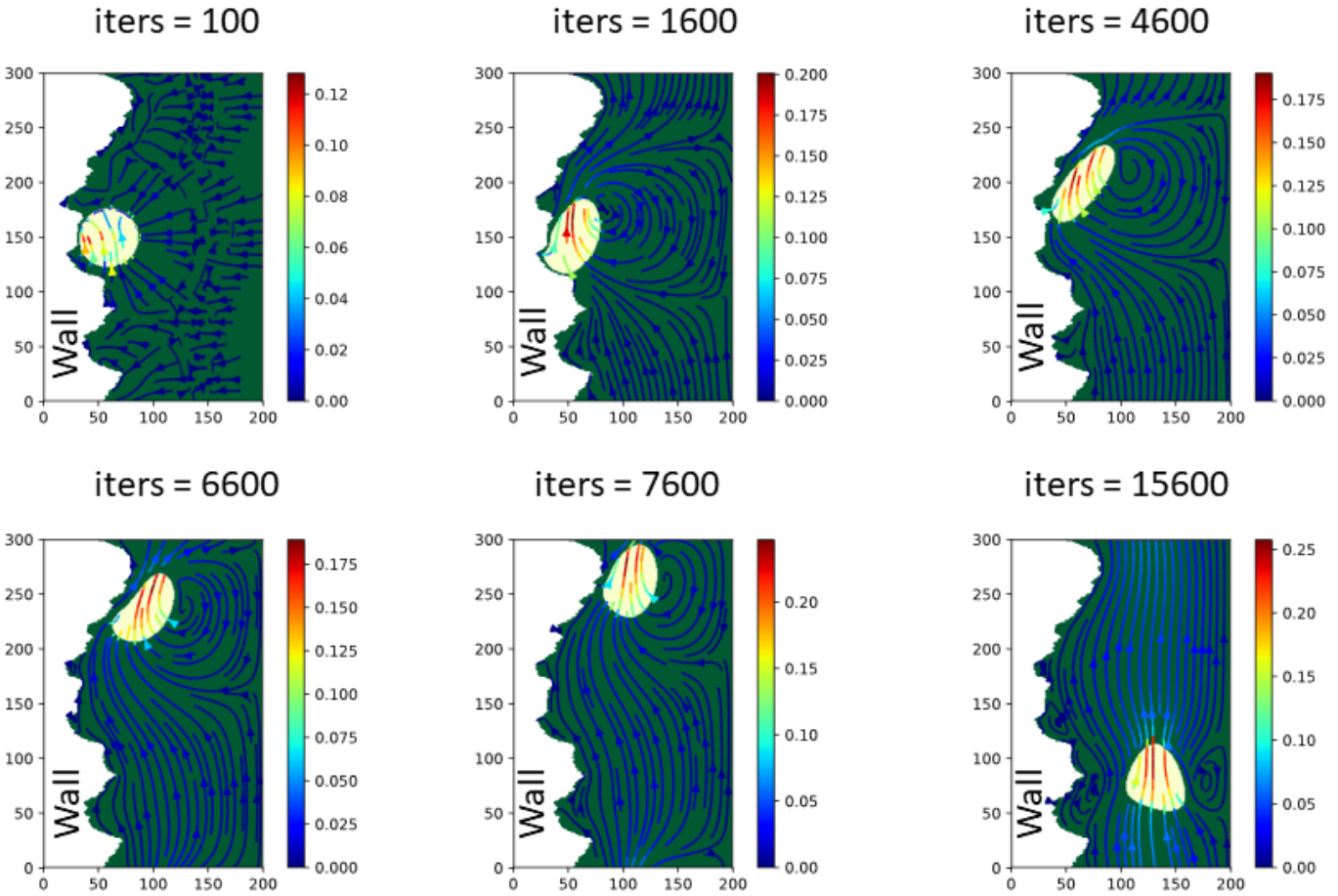

Fig. 2.13: Bubble dynamics in a boiling water fluid near rough wall simulated using the implemented pseudo-potential lattice Boltzmann method. Wall is treated as hydrophilic material. Body force of 1×10^{-3} LU^2/TU (non-dimensional lattice units) applied on the vapour phase (in light yellow). The streamlines and their colour reveal critical information about the flow and the magnitude of the velocity field.

Zr-alloy molecules using the interatomic potential developed by Martins et al. (2004). The Lorentz-Berthelot combining rule was used to determine the unlike Lennard-Jones parameters.

Fig. 2.14 demonstrates the nucleation of vapor during the heterogeneous boiling of water in contact with a layer of monoclinic mineral baddeleyite ($mZrO_2$). The zirconium alloy surface was represented by the most stable hydrophilic facet (-111) (Motta et al. 2015; Ciszak et al. 2019). Multiple small cavities (vapor bubbles) are initially formed in the liquid domain (Fig. 2.14a) and start merging, leading to the formation of successively growing vacuum domains (i.e. vapor phase, Fig. 2.14b and 2.14c). The surface orientation plane defines the hydrophobicity/hydrophilicity of the interface plane and consequently affect the bubble nucleation mechanism (Hens et al. 2014; Motta et al. 2015). The (-111) facet of Zr-alloy is hydrophilic leading to the formation of a thin water liquid film on the interface plane. The latter suggests a better heat exchange between the solid and the liquid and the absence of vapor bubbles (Fig. 2.14c) (Hens et al. 2014).

2.6.2 Coupled lattice Boltzmann - discrete element method for adsorption on moving particles

A PhD student from the Institute for Mechanical Process Engineering and Mechanics at the Karlsruhe Institute of Technology, (Germany), Marie-Luise Maier, has conducted her research exchange visit at LES during March-June 2019. The visit was realised in the framework of know-how exchange between KIT (OpenLB software) and lattice Boltzmann simulation tools available at PSI. The main aim of the visit was to develop a model describing the process of phosphate removal from water using colloidal C-S-H particles. In the first step, a one way coupled lattice Boltzmann-Discrete Element Method (LB-DEM) reactive particulate flow model, developed within the OpenLB framework, was validated through a series of analytical benchmarks.

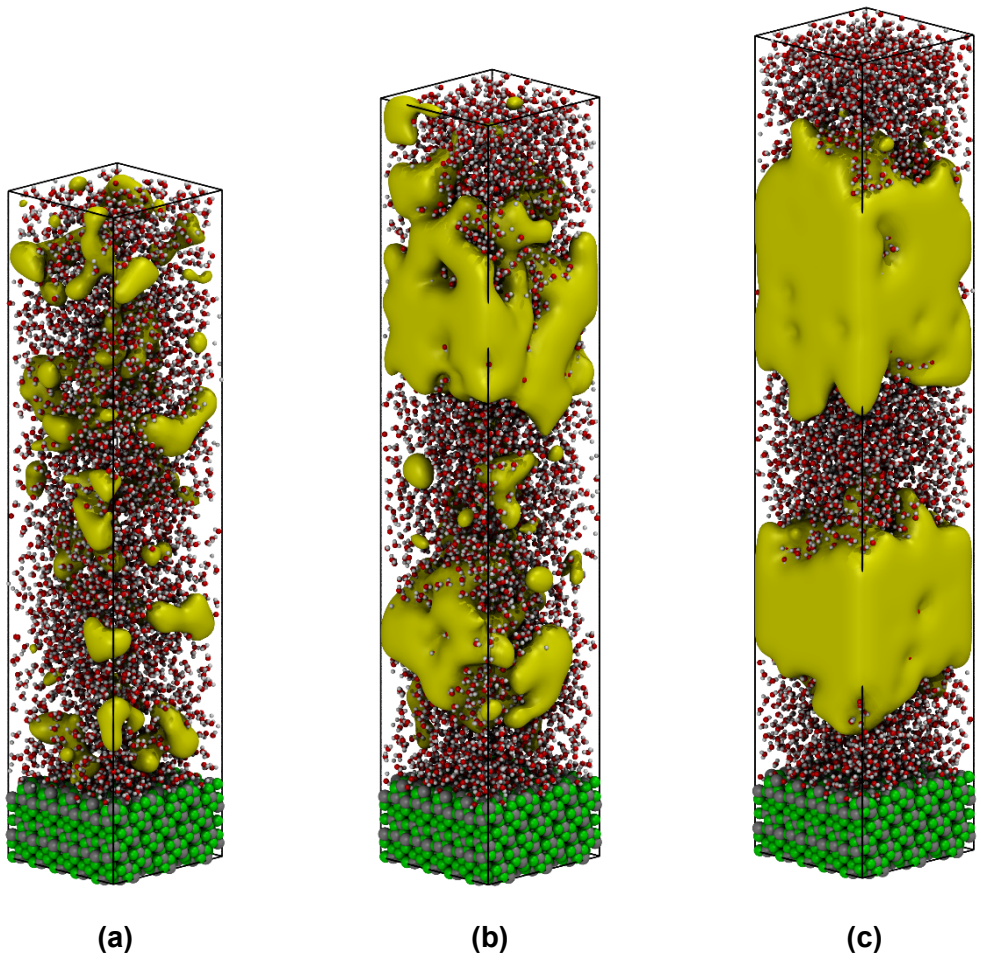

Fig. 2.14: Massive boiling of water in contact with the (-111) plane of monoclinic zirconia computed with MD. The (a), (b) and (c) configurations correspond to different bubble nucleation times (400, 600 and 800 ps, respectively). The green colour represents the oxygen atoms of the zirconia, the silver the zirconium atoms, the red the oxygen atoms of water and the light grey the hydrogen atoms of water. The yellow iso-surfaces represent the voids inside the supercell (voids are defined as set of points separated by at least 3Å distance from any water molecule (Zahn 2004).

In the second step, a multi-scale two way coupled LB-DEM model for dense reactive particulate flows has been implemented. In this model, fluid flow and reactive transport processes are treated within the continuum framework and solved using the lattice Boltzmann method. In a voxel of the flow simulation (LB-grid) several particles co-exist and the coupling of fluid and particles interaction is accounted for, through a volume averaging. This technique enables the simulations of large systems with a large number of particles. The dynamics of the suspended particles is modelled by the DEM. Special care has been taken to have a correct coupling between the models to ensure a grid convergent solution. The model has been implemented and demonstrated by combining two open source codes *Yantra* (lead developer: R. Patel) and *Yade* (Šmilauer et al. 2015). Fig 2.15 shows exemplary simulation results from the developed model.

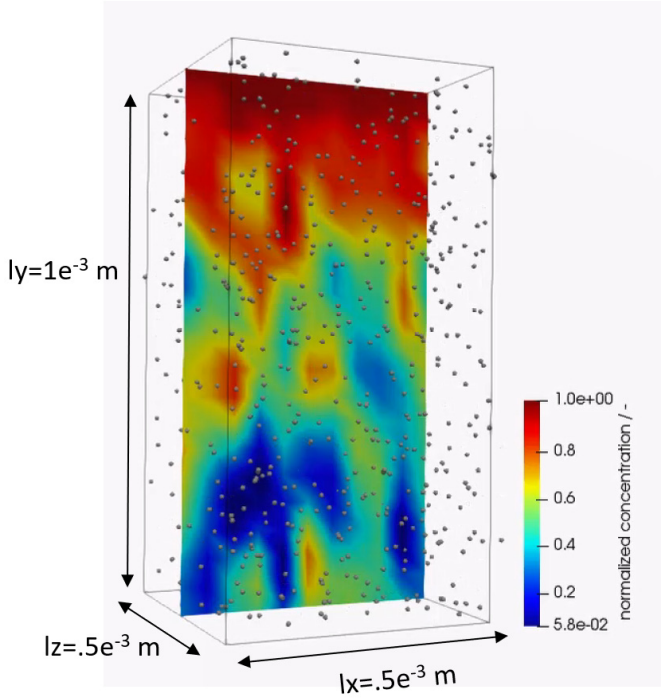

Fig. 2.15: Representative simulation output of the multiscale two-way coupled lattice Boltzmann- discrete element model for reactive particulate flows. As particles flow from top to bottom, they react with solution and they deplete the dissolved phosphate concentration (blue: low concentration, red: high concentration).

2.6.3 Research project with GlaxoSmithKline vaccines

In 2019, an industrial project with the pharmaceutical company GlaxoSmithKline Vaccines, Belgium (GSK) has been initiated (PI: N. Prasianakis). GSK is a science-led global healthcare company focused on the research, development and manufacturing of innovative pharmaceutical medicines, vaccines and consumer healthcare products. This project embark on the state-of-the-art multiscale models and methods developed at LES in the recent years.

2.7 References

Berendsen H. J. C., Grigera J. R., Straatsma T. P. (1987)
The missing term in effective pair potentials. The Journal of Physical Chemistry 91, 6269-6271.

Bradbury M. H., Baeyens B. (2002)
Sorption of Eu on Na- and Ca-montmorillonites: experimental investigations and modelling with cation exchange and surface complexation. Geochimica et Cosmochimica Acta 66, 2325-2334.

Bradbury M. H., Baeyens B. (2005)
Modelling the sorption of Mn(II), Co(II), Ni(II), Zn(II), Cd(II), Eu(III), Am(III), Sn(IV), Th(IV), Np(V) and U(VI) on montmorillonite: Linear free energy relationships and estimates of surface binding constants for some selected heavy metals and actinides. Geochimica et Cosmochimica Acta 69, 875-892.

Ciszak C., Desgranges L., Garcia P., Sabathier C., Fayette L., Chevalier S. (2019)
On the origins and the evolution of the fuel-cladding bonding phenomenon in PWR fuel rods. Journal of Nuclear Materials 520, 110-120.

De Weerdt K., Lothenbach B., Geiker M. R. (2017)
Comparing chloride ingress from seawater and NaCl solution in Portland cement mortar. Cement and Concrete Research 115, 80-89.

Hens A., Agarwal R., Biswas G. (2014)
Nanoscale study of boiling and evaporation in a liquid Ar film on a Pt heater using molecular dynamics simulation. International Journal of Heat and Mass Transfer 71, 303-312.

Jakobsen U. H., De Weerdt K., Geiker M. R. (2016)
Elemental zonation in marine concrete. Cement and Concrete Research 85, 12-27.

Jenni A., Gimmi T., Alt-Epping P., Mäder U., Cloet V. (2017)
Interaction of ordinary Portland cement and Opalinus Clay: Dual porosity modelling compared to experimental data. Physics and Chemistry of the Earth 99, 22-37.

Kulik D. A., Miron G. D., Lothenbach B. (2018)
A realistic three-site solid solution model of C-S-H. Goldschmidt 2018 Conference, Boston MA, USA.

L'Hôpital E., Lothenbach B., Le Saout G., Kulik D., Scrivener K. (2015)
Incorporation of aluminium in calcium-silicate-hydrates. Cement and Concrete Research 75, 91–103.

Li Q., Luo K. H., Kang Q. J., He Y. L., Chen Q., Liu Q. (2016)
Lattice Boltzmann methods for multiphase flow and phase-change heat transfer. Progress in Energy and Combustion Science 52, 62-105.

Lothenbach B., Kulik D. A., Matschei T., Balonis M., Baquerizo L., Dilnesa B. Z., Miron G. D., Myers R. (2019)
Cemdata18: A chemical thermodynamic database for hydrated Portland cements and alkali-activated materials. Cement and Concrete Research 115, 472-506.

Martins L. R., Skaf M. S., Ladanyi B. M. (2004)
Solvation dynamics at the water/zirconia interface: Molecular dynamics simulations. The Journal of Physical Chemistry B 108, 19687-19697.

Miron G. D., Kulik D. A., Dmytrieva S. V., Wagner T. (2015)
GEMSFITS: Code package for optimisation of geochemical model parameters and inverse modeling. Applied Geochemistry 55, 28-45

Missana T., García-Gutiérrez M., Mingarro M., Alonso U. (2017)
Analysis of barium retention mechanisms on calcium silicate hydrate phases. Cement and Concrete Research 93, 8–16.

Motta A. T., Couet A., Comstock R. J. (2015)
Corrosion of zirconium alloys used for nuclear fuel cladding. Annual Review of Materials Research 45, 311-343.

Prasianakis N. I., Curti E., Kosakowski G., Poonoosamy J., Churakov S. V. (2017)
Deciphering pore-level precipitation mechanisms. Scientific Reports 7, 13765.

Prasianakis N. I., Gatschet M., Abbasi A., Churakov S.V. (2018)
Upscaling strategies of porosity-permeability correlations in reacting environments from pore-scale simulations. Geofluids, 9260603-9260608.

Poonoosamy J., Westerwalbesloh C., Deissmann G., Mahrous M., Curti E., Churakov S. V., Klinkenberg M., Kohlheyer D., von Lieres E., Bosbach D., Prasianakis N. I. (2019)
A microfluidic experiment and pore-scale modelling diagnostics for assessing mineral precipitation and dissolution in confined spaces. Chemical Geology 528, 119264.

Pfingsten W. (2002)
Experimental and modelling indications for self-sealing of a cementitious low- and intermediate-level waste repository by calcite precipitation. Nuclear Technology 140, 63 – 82.

Pfingsten W. (1996)
Efficient modeling of reactive transport phenomena by a multispecies random walk coupled to chemical equilibrium. Nuclear Technology 116, 208-221.

Shafizadeh A., Gimmi T., Van Loon L. R., Kaestner A. P., Mäder U. K., Churakov S. V. (2019)
Time-resolved porosity changes at cement-clay interfaces derived from neutron imaging. Cement and Concrete Research (in press).

Šmilauer V. et al. (2015)
Yade Documentation 2nd edition. The Yade Project. DOI 10.5281/zenodo.34073 (http://yade-dem.org/doc/)

Tits J., Fujita T., Harfouche M., Dähn R.,
Tsukamoto M., Wieland E. (2014)
Radionuclide uptake by calcium silicate hydrates: case studies with Th(IV) and U(VI). PSI Bericht Nr. 14-03, Paul Scherrer Institut, Villigen PSI, Switzerland.

Thoenen T., Hummel W., Berner U., Curti E. (2014)
The PSI/Nagra chemical thermodynamic database 12/07. PSI Bericht 14-04, Paul Scherrer Institut, Villigen PSI, Switzerland.

Tits J., Fujita T., Tsukamoto M., Wieland E. (2007)
Uranium(VI) uptake by synthetic calcium silicate hydrates. Material Research Society Symposium Proceedings 1107, 467–474.

Tits J., Wieland E., Müller C. J., Landesman C., Bradbury M. H. (2006)
Strontium binding by calcium silicate hydrates. Journal of Colloid and Interface Science 300, 78-87.

Tits J., Stumpf T., Rabung T., Wieland E., Fanghänel (2003)
Uptake of Cm(III) and Eu(III) by calcium silicate hydrates: a solution chemistry and time-resolved laser fluorescence spectroscopy study. Environmental Science and Technology 37, 3568-3573.

Zahn D. (2004)
How does water boil? Physical Review Letters 93, 227801.

Zhang Z. Q., Matin M. A., Ha M. Y., Jang J. (2016)
Molecular dynamics study of the hydrophilic-to-hydrophobic switching in the wettability of a gold surface corrugated with spherical cavities. Langmuir 32, 9658-9663.

3 DEVELOPMENT OF MECHANISTIC SORPTION MODELS AND EXPERIMENTAL VALIDATION

Baeyens B., Dähn R., Marques Fernandes M., Tits J., Churakov S.V., Schaible A., Eltayeb E., Marafatto F. (postdoc), Nedyalkova L. (PhD student), Kéri A. (PhD student), Wick S. (PhD student)

3.1 Introduction

The aim of this project is to improve the mechanistic understanding of the uptake processes of (radio-) contaminants onto 2:1 clay minerals, argillaceous rocks and soils, and on AFm phases, one of the main products formed during the hydration of Portland and calcium aluminate cement-based systems. An important activity related to the safety analyses foreseen in SGT-E3 is the development of sorption data bases (SDB). In preparation of this task a modified approach will be applied compared to previous performance assessments, i.e. the bottom-up approach will be applied to calculate K_d values in argillaceous rock systems for a range of geochemical "*in situ*" conditions. The approach was tested for blind prediction of the adsorption isotherms of Cs, Ni, Co, Eu, Th and U on two Opalinus Clay (OPA) samples. In the framework of the SNSF funded PhD project (SNSF Nr. 200021_162364) on the adsorption behaviour of thallium in soils, the bottom-up approach on the exchangeability of geogenic Tl in soils could be validated. A further related activity was the quantification of the adsorption of Mn(II) on illite and the modelling of the experimental data with the 2SPNE SC/CE model. Mn is ubiquitous in the near and far fields of radioactive waste repositories and can be a potential competing metal for the adsorption of divalent fission products. To account for such processes an adsorption model needs to be in place.

A number of projects have started in 2019 related to the mechanistic understanding of adsorption processes. The most important one is part of the pan-European research project EURAD (HORIZON 2020 GA ID: 847593) and started on 1 July 2019. The first kick-off meeting of the work package on the *Fundamental understanding of radionuclide retention* (FUTURE) took place on 8-9 October 2019 at PSI. The tasks 2.3 and 3 on sorption reversibility and redox-controlled uptake of radionuclides on clay mineral surfaces, respectively, are the most relevant to this project. A PhD student has start on 1 November 2019 within task 3 on adsorption of redox-sensitive elements. In the framework of COFUND, a postdoc project on the validation of adsorption models on argillaceous rocks using advanced surface spectroscopic techniques has started on 1 September 2019.

The PhD projects on the immobilisation of Se and I in cementitious systems by AFm phases (Cebama project) and atomistic modelling of Fe and uranyl adsorption on montmorillonite (SNSF project) have been finalised in 2019. The postdoc project on the development of cryo-microspectroscopic techniques for redox- and radiation-sensitive samples developed at the microXAS beamline of the SLS (CROSS project) has also been completed in 2019.

3.2 Validation of experimental radionuclide adsorption data onto Opalinus Clay from Mont Terri and Schlattingen by mechanistic models

For the safety analysis of deep geological radioactive waste repositories solid liquid distribution coefficients (K_d values) are required. In order to derive adsorption values for argillaceous rocks under a wide range of porewater and mineralogical compositions, the so-called bottom-up approach can be used (e.g. Bradbury & Baeyens 2000; Bradbury & Baeyens 2011; Marques Fernandes et al. 2015). This approach hypothesis that the uptake of radionuclides in complex mineral/porewater systems can be quantitatively predicted from a knowledge and understanding of the mechanistic adsorption processes on single minerals, and the models developed to describe them. In the case of Opalinus Clay the assumption is that the 2:1 clay minerals illite and illite-smectite mixed layers are the dominant sorbents. Scaling the site capacities to the clay mineral content of the rocks and including the radionuclide speciation in the different porewaters allows calculating the adsorption isotherms in the natural rocks.

Adsorption isotherms of Cs, Ni, Co, Eu, Th and U determined onto different Opalinus Clay samples in the frame of previous safety assessments (Entsorgungs-nachweis 2002, SGT-E2) are available to test the aforementioned approach. The experimental datasets were modelled using the generalised Cs adsorption model (Bradbury & Baeyens 2000) and the 2SPNE SC/CE adsorption model (Bradbury & Baeyens 2009) both developed for illite. The model calculations have been performed in the following way. In a first step blind model predictions have been calculated using the selectivity coefficients (K_c) and surface complexation constants (K_{SC}) derived for pure illite. In a second step K_c and K_{SC} have been optimised for the specific Opalinus Clay systems. In both calculations, the basic

non-adjustable parameters of the illite adsorption model (site capacities, protolysis constants) and associated auxiliary thermodynamic data for the aqueous speciation have been fixed throughout.

The results of the adsorption measurements and modelling on the two different Opalinus Clay samples (Mt Terri & Schlattingen) are illustrated in Fig. 3.1. The broken lines in Fig. 3.1 are the blind predictions using the K_c and K_{SC} constants for illite tabulated in Tab. 3.1. In a number of cases the correspondence between the blind prediction and the experimental data is good and falls within the experimental errors of the measurements. In other cases, the blind predictions (broken curves) deviate up to 0.5 and in one single case up to 1 log unit. For these cases the K_c and K_{SC} constants for the dominant adsorption reactions have been optimised and their values are included in Tab. 3.1. The reasons for the deviation in the case of Cs and divalent metals might be multiple. We assume that the illite in the Opalinus Clay behaves identical to the Illite du Puy (IdP) for which the 2SPNE SC/CE model was developed. However, for Cs at least, Bradbury & Baeyens (2000) showed that depending on the illite, the adsorption on the frayed edge sites varies within ± 0.5 log units. For the other elements the assumption that illite/smectite mixed layers behave similar to the pure IdP is likely valid but has never been verified. For Ni, Bradbury & Baeyens (2009) observed a "natural" scatter of the experiment data (different data sets) in the range pH 7 to 9 of up to 1 log units. Also competition with e.g., Mn or Fe (which has not been considered here) might contribute to the observed discrepancies (Bradbury & Baeyens 2005; Marques Fernandes & Baeyens 2019) in the lower $[Me^{II}]_{eql.}$ range. In one case the data could not be quantified (grey area for Ni adsorption on Opalinus Clay from Schlattingen) at the higher Ni equilibrium concentrations. The black line in this figure represent full site saturation of the weak edge sites and increasing the K_{SC} constant will not result in higher Ni loadings. Clearly, a different uptake process of Ni is taking place. This anomalous behaviour was further investigated using X-ray absorption spectroscopy (Marques Fernandes et al. 2015) and is summarised below. All in all, however, the experimental data can be satisfactorily modelled over the entirely concentration range represented by the isotherms.

From the information presented in this study a substantial body of evidence is present which strongly supports the bottom-up approach and methodology for developing state-of-the-art sorption databases for argillaceous rocks to be used in future safety analyses. The variation of the K_c and K_{SC} constants obtained for the Opalinus Clay systems can be used as upper and lower uncertainty bands for the calculations of the K_d values in the safety analysis.

In Marques Fernandes et al. (2015), the adsorption of Ni on Opalinus Clay was addressed by extended X-ray absorption fine structure (EXAFS) spectroscopy. EXAFS measurements were carried out on samples with two different Ni loadings *i.e.,* Ni-OPA_1 and Ni-OPA_2 with 13 and 27 $mmol \cdot kg^{-1}$ Ni, respectively, and on one illite sample Ni-IdP (as reference for a Ni inner-sphere surface complex) with 21 $mmol \cdot kg^{-1}$ Ni. The Ni-OPA loadings lie on the isotherms where experimental data and modelling strongly deviate. The Ni-K edge EXAFS (k^3-weighted $\chi(k)$ spectra and the corresponding radial structure functions spectra) of the Opalinus Clay samples, along with 3 reference spectra: Ni-IdP, Ni-layered double hydroxides (LDH) from Scheinost & Sparks (2000) and Ni-phyllosilicate (Ford et al. 1999) are shown in Fig. 3.2. The k^3-weighted $\chi(k)$-spectra of the two Ni-OPA samples are similar and exhibit distinct features at ~5.2 and 7.3 $Å^{-1}$. These features are characteristic for Ni-solids (Scheinost & Sparks 2000) and can be used as a fingerprint to discriminate adsorption from precipitation. The spectrum of Ni-IdP, however, does not exhibit any of these features. On the other hand, the radial structure functions of Ni-OPA exhibit a backscattering contribution at 2.7 Å (R + ΔR) originating from Ni-Ni interaction, similar to the spectra of the Ni-solids. This contribution is absent in the spectra of Ni–IdP sample. The similarities of the Ni-OPA spectra with the Ni-solids and the difference with Ni-IdP clearly indicate that deviation between modelled and measured Ni-isotherm should be explain by a surface induced precipitation of Ni-solids.

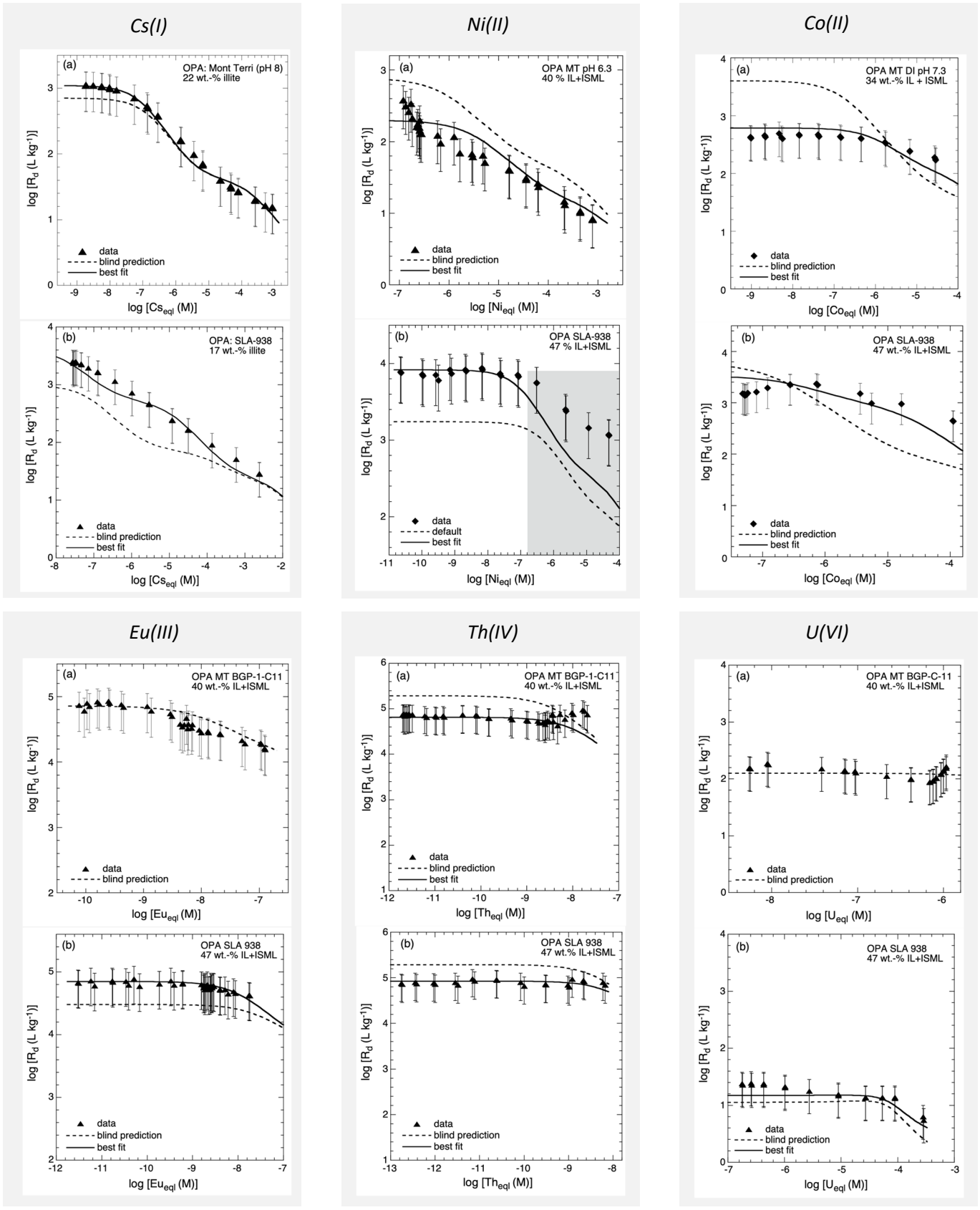

Fig. 3.1: R_d values determined from sorption isotherms of Cs, Ni, Co, Eu, Th and U on Opalinus Clay from (a) Mont Terri and (b) Schlattingen. Experimental and modelling. The broken lines are blind predictions using the illite model. The solid lines are the best fit parameters for the Opalinus Clay. The modelling parameters are summarised in Tab. 3.1.

Tab. 3.1: Summary of cation exchange and surface complexation reactions and corresponding thermodynamic constants for the sorption of Cs, Ni, Co, Eu, Th and U^{VI} on illite and the 2 Opalinus Clay samples.

Sorption reaction	Illite	Mt Terri OPA	SLA OPA
Caesium		log K_c	
$Na\text{-}FES + Cs^+ \Leftrightarrow Cs\text{-}FES + Na^+$	7.0	7.2	7.6
$Na\text{-}T2S + Cs^+ \Leftrightarrow Cs\text{-}T2S + Na^+$	3.6	3.6	4.6
Nickel		*log* K_{SC}	
$\equiv S^SOH + Ni^{2+} \Leftrightarrow \equiv S^SONi^+ + H^+$	0.7	0.1	1.4
$\equiv S^{W1}OH + Ni^{2+} \Leftrightarrow \equiv S^{W1}ONi^+ + H^+$	-1.8	-2.3	-1.3
Cobalt			
$\equiv S^SOH + Co^{2+} \Leftrightarrow \equiv S^SOCo^+ + H^+$	1.3	0.4	0.9
$\equiv S^{W1}OH + Co^{2+} \Leftrightarrow \equiv S^{W1}OCo^+ + H^+$	-2.0	-1.6	-0.8
Europium			
$\equiv S^SOH + Eu^{3+} + H_2O \Leftrightarrow \equiv S^SOEuOH^+ + 2H^+$	-4.4	-4.4	-3.9
$\equiv S^{W1}OH + Eu^{3+} + H_2O \Leftrightarrow \equiv S^{W1}OEuOH^+ + 2H^+$	-6.2	-6.2	-6.2
Thorium			
$\equiv S^SOH + Th^{4+} + 4\ H_2O \Leftrightarrow \equiv S^SOTh(OH)_4^- + 5H^+$	-15.3	-15.8	-15.7
Uranyl			
$S^SOH + UO_2^{2+} + 2\ H_2O \Leftrightarrow \equiv S^SOUO_2(OH)_2^- + 3H^+$	-10.8	-10.8	-10.8
$S^{W1}OH + UO_2^{2+} + 2\ H_2O \Leftrightarrow \equiv S^{W1}OUO_2(OH)_2^- + 3H^+$	-12.3	-12.3	-12.3

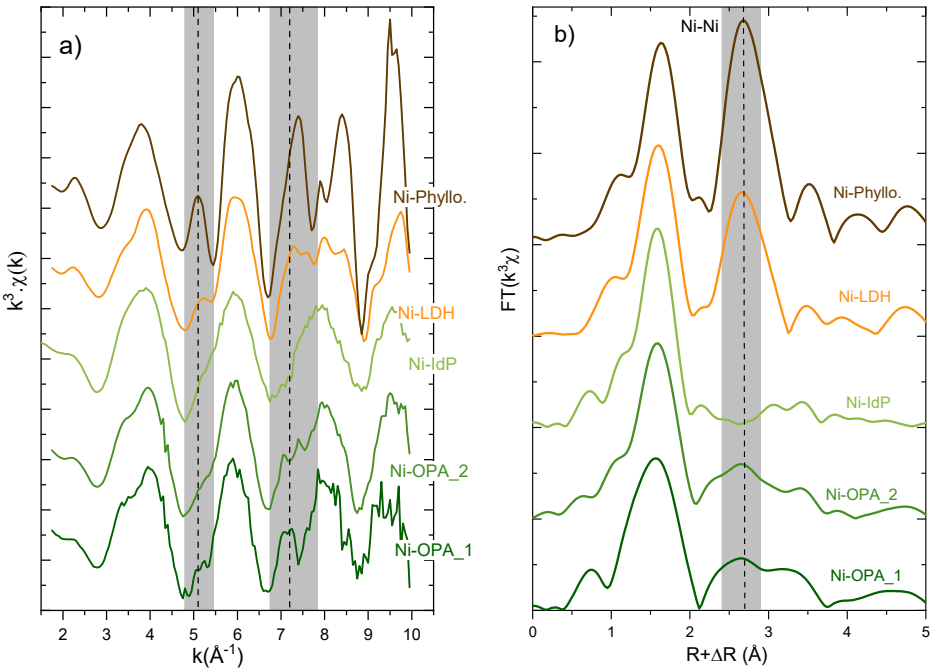

Fig. 3.2: a) Raw k^3-weighted χ(k) spectra of Ni sorbed on Opalinus Clay and of Ni–reference samples and b) the corresponding radial structure functions. Shaded areas indicate the appearance of distinct features arising from Ni-Ni single and multiple scattering interactions characteristic for specific Ni-precipitates (data taken from Marques Fernandes et al. 2015).

3.3 Thallium adsorption in soils

Thallium (Tl) is a highly toxic trace element and occurs in the environment predominantly as Tl^+, but it can also exist as Tl^{3+}. The former is highly soluble and more mobile whereas the latter is highly insoluble, strongly hydrolysing and occurs normally in oxide form. Special geological conditions can result in increased Tl concentrations in soils formed from rocks hosting Tl-rich minerals (Voegelin et al. 2015). Topsoils from the Erzmatt site (community Buus, Kanton Basel-Landschaft, Switzerland) are particularly rich in geogenic Tl and were investigated in the framework of a SNSF funded PhD project (SNSF Nr. 200021_162364).

There is substantial evidence in the open literature that the clay mineral illite is a key sorbent for Tl^+ in soils and sediments (e.g. Voegelin et al. 2015). A sorption model for Tl^+ on illite has recently been developed (Wick et al. 2018) and the so-called bottom-up approach has been tested on top soil samples from the Erzmatt site. From six selected topsoil samples, with geogenic Tl contents between 3.1 and 346.6 mg/kg, the concentration of Tl in the soil porewater (obtained from 0.01 M $CaCl_2$ extractions) and the exchangeable Tl from the clay minerals (obtained from 1 M NH_4 extractions) are plotted in Fig. 3.3 representing a Tl^+ adsorption isotherm.

The blind prediction of the geogenic Tl behaviour of these soil samples has been carried out as outlined in the following. In a first step the adsorption of Tl on pure illite (in 0.1 M NaCl) as proposed in Wick et al. (2018) is calculated and shown in Fig. 3.3 by the red line. In a second step the Tl isotherm on Na-illite is scaled to the mica content of the soil samples gained by XRD and given as blue line in Fig. 3.3. The average dioctahedral mica content of the 6 samples is 14.4 ±3.4 wt.% consisting of 6.5 wt.% muscovite $2M_1$ and 7.9 wt.% illite. These 2 types of mica minerals are considered to be the main sorbents w.r.t. to Tl^+ adsorption in the topsoil samples. In the third step calculations further include the soil porewater composition and the competitive adsorption of Na^+, K^+, NH_4^+ and Ca^{2+}. The average concentrations measured in the $CaCl_2$ extractions of the six soil samples are Na^+ = $3.1\pm0.5\times10^{-5}$ M, K^+ = $1.7\pm0.5\times10^{-4}$ M, Mg^{2+} = $1.5\pm0.4\times10^{-3}$ M, Ca^{2+} = $8.5\pm0.5\times10^{-3}$ M and $6.1\pm2.8\times10^{-5}$ M NH_4^+. The selectivity coefficients for Tl-Na, Tl-K, Tl-NH_4 and Tl-Ca exchange for illite were derived by Wick et al. (2018). The results of this calculation are shown by the black line in Fig. 3.3. The good agreement between the model and the measurement of the adsorbed Tl confirms the hypothesis that Tl^+ is strongly associated with mica-type minerals in soils. For the considered concentration range (10^{-9} M - 4×10^{-7} M) Tl^+ is predominantly adsorbed at the frayed edge sites.

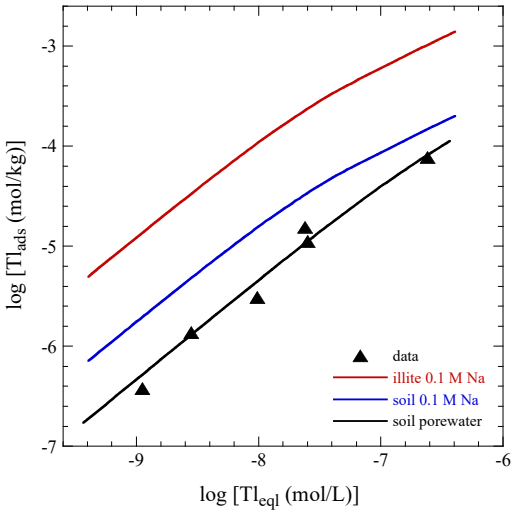

Fig. 3.3: Illustration of the bottom-up approach for the geogenic Tl behaviour in 6 selected topsoil samples from the Erzmatt site (Swiss Jura Mountains). The red line is the model prediction of Tl on pure illite in 0.1 M NaCl. The blue line is the scaling of the Tl isotherm to the average mica content of the soil samples. The black line is the model prediction calculated in the soil porewater under consideration of the competitive adsorption behaviour of mainly K^+ and NH_4^+.

3.4 Manganese adsorption on illite

Mn is an omnipresent element in the environment and can be a potential competing metal for radionuclides in the near and far fields of a radioactive waste repository. In order to quantify its competitive adsorption behaviour, a surface complexation model for Mn(II) on 2:1 clay minerals needs to be established. In the open literature no such model is available as well as reliable sorption data on clay minerals. One sorption edge and 3 sorption isotherms of Mn on Na-illite (IdP) in 0.1 M NaCl background were measured. The experimental results are summarised in Fig. 3.4. The data have been modelled using the 2SPNE SC/CE sorption model (Bradbury & Baeyens 2009) and the model parameters given in Tab. 3.2. The experimental results could be quantitatively well described. The K_c and the K_{SC} summarised in Tab. 3.2 are important basic data and will be used in future SDBs for the safety analysis in SGT-E3. This work has been recently published by Marques Fernandes & Baeyens (2019).

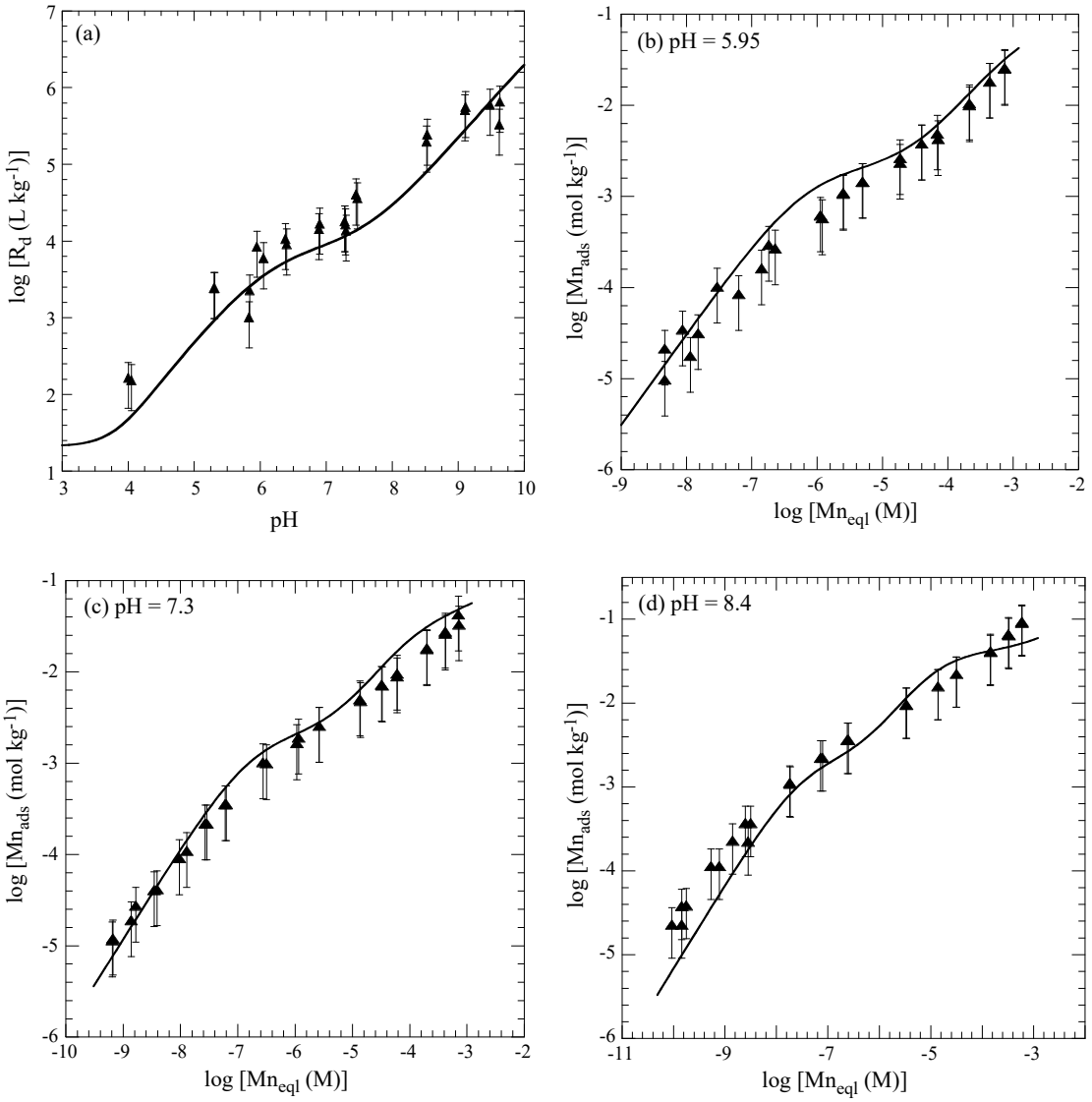

Fig. 3.4: (a) Mn(II) sorption edge in 0.1 M NaCl and sorption isotherms at (b) pH 6, (c) pH 7 and (d) pH 8 in 0.1 M NaCl on Na-IdP. Experimental data and modelling.

Tab. 3.2: Surface complexation constants on strong and weak sites and selectivity coefficients for Mn adsorption on Na-IdP.

Surface complexation on strong sites	log K_{SC}
$\equiv S^{S}OH + Mn^{2+} \Leftrightarrow \equiv S^{S}OMn^{+} + H^{+}$	0.9
$\equiv S^{S}OH + Mn^{2+} + H_2O \Leftrightarrow \equiv S^{S}OMnOH^{0} + 2H^{+}$	-6.7
Surface complexation on weak sites	
$\equiv S^{W1}OH + Mn^{2+} \Leftrightarrow \equiv S^{W1}OMn^{+} + H^{+}$	-2.3
$\equiv S^{W1}OH + Mn^{2+} + H_2O \Leftrightarrow \equiv S^{W1}OMnOH^{0} + 2H^{+}$	-9.2
Cation exchange on planar sites	K_c
2 Na-illite + $Mn^{2+} \Leftrightarrow$ Mn-illite + $2Na^{+}$	3.6

3.5 Immobilisation of selenium and iodine by AFm phases

This PhD study is carried out in the framework of the Horizon 2020 EC Project "Cebama". The objectives of the study are 1) to improve the insight into the mechanisms controlling the Se and I uptake by AFm phases, 2) to evaluate the effects of sulfur as a competitor for the Se and I uptake by AFm phases and 3) to develop thermodynamic models based on a solid solution approach describing the Se and I uptake by AFm phases and the competition with S.

During the first three years of the PhD study, pure AFm phases containing Se, I or S in various redox states as intercalating anion were synthesised and characterised and their composition, structure and solubility was determined using various techniques such as X-ray diffraction (XRD), Thermogravimetric Analysis (TGA), Fourier-transform Infrared (FTIR), Dynamic

Vapour Sorption (DVS) analysis, as well as aqueous phase analysis (Nedyalkova et al. 2019a). In addition, the formation of AFm phases intercalated by binary mixtures of Se or I, and the anions commonly found in cement (CO_3^{2-}, OH^- and HS^-) was investigated in co-precipitation experiments under a broad range of redox conditions. With the help of these experimental data, thermodynamic solid solution models were developed for the studied AFm pairs (Nedyalkova et al. 2019b).

Under real repository conditions, ^{79}Se and ^{129}I will mainly be released from the radioactive waste after the cement curing process has been completed. These radionuclides will thus primarily interact with AFm phases through sorption processes and not through co-precipitation. Thus, in 2018, Se and I sorption experiments were carried out onto AFm phases commonly found in hardened cement paste such as monocarbonate (AFm-CO_3), hemicarbonate (AFm-$OHCO_3$), monosulfate (AFm-SO_4), but also AFm-HS to cover also AFm phases expected to exist under strongly reducing conditions. Sorption isotherms with I^-, SeO_4^{2-}, and SeO_3^{2-} were measured in an equilibrium concentration range from ~10^{-7} M up to 0.1 M. Both the I^- sorption and the Se sorption on AFm phases were found to depend strongly on the type of intercalating anion in the sorbing AFm interlayer. Overall, the largest R_d values were found for both cations onto hemicarbonate, and the lowest R_d values onto monocarbonate.

In 2019, a modelling exercise was undertaken to test whether the thermodynamic solid solution models developed in previous years were capable of describing the I and Se sorption isotherms onto AFm-SO_4, AFm-HS, AFm-CO_3 and AFm-$OHCO_3$ measured previously. Based on the modelling results the following conclusions could be drawn:

I^- sorption isotherms onto AFm-SO_4, AFm-HS and AFm-$OHCO_3$ could be described very well with solid solution models assuming complete miscibility between I^- and $[OHCO_3]^-$ (Fig. 3.5a) and between $2I^-$ and SO_4^{2-}, and assuming only partial miscibility between I^- and HS^- with two small miscibility gaps close to each of the end members.

Se(VI) sorption by AFm phases predominantly takes place via adsorption processes on AFm surface sites. Indeed, the sorption isotherm of Se(IV) onto AFm-CO_3 in Fig. 3.5b. reveals linear sorption up to full loading of the surface site capacity (~10^{-3} mol kg^{-1}) followed by precipitation of AFm-SeO_4 with further increase of the aqueous SeO_4^{2-} concentration. XRD studies performed in previous years showed that SeO_4^{2-} does not mix homogeneously with CO_3^{2-} in the AFm interlayers and AFm co-precipitation experiments with mixtures of both anions result in the formation of the two pure end members. The sorption isotherm for Se(IV) on AFm-SO_4 could be modelled using a non-ideal solid solution model with the end members being AFm-SeO_4 and AFm-$SO_4(16H_2O)$ assuming a very large miscibility gap with composition $0.1 \leq x_{SeO4} \leq 0.99$. The co-precipitation experiments performed in the previous years had shown that AFm-SeO_4 forms only a partial solid solution with the fully hydrated AFm-SO_4 containing 16 H_2O molecules per unit cell in its interlayers and not with less hydrated AFm-SO_4 phases. However, even when the AFm-SO_4 interlayer is maximally expanded by 16 H_2O molecules, mixing between SeO_4^{2-} and SO_4^{2-} was only observed at the lowest SeO_4^{2-} : SO_4^{2-} ratios.

The Se(IV) sorption behaviour onto AFm phases was only tested for the case of AFm-SO_4. The Se(IV) sorption isotherm on this AFm phase could be described in three steps: 1) At low loadings a (SeO_3^{2-} - SO_4^{2-})-AFm solid solution forms with x_{SeO4} increasing with increasing Se loading. 2) With further increase of the Se loading, simultaneous precipitation of the (SeO_3^{2-} - SO_4^{2-})-AFm solid solution and $CaSeO_3$ is observed. 3) The final step at the highest Se(IV) loadings finally is characterised by precipitation of pure $CaSeO_3$. This model is supported by the XRD patterns of the co-precipitation experiments demonstrating that the predominant Se(IV) sorption mechanism on this AFm phase is intercalation in the interlayers by charge-balanced substitution of SO_4^{2-} for SeO_3^{2-}. The Se(IV) sorption behaviour observed in our study confirms experimental observations made by Ma and co-workers on the same system (Ma et al. 2018). These authors, however, failed to find evidence for the formation of a solid solution between AFm-SO_4 and AFm-SeO_3 in their high energy X-ray diffraction (HEXD) and pair distribution function (PDF) studies.

In summary, it can be concluded that the process controlling uptake of I^- by the common AFm phases in hardened cement paste under oxidising and reducing conditions, is anion exchange with anions present in the AFm interlayers and this process can be described very well with the help of thermodynamic solid solutions models. Se(IV) sorption onto AFm phases is mainly controlled by a surface adsorption process whereas Se(IV) sorption onto AFm-SO_4 is controlled by two processes: anion exchange with SO_4^{2-} in the interlayer and precipitation of $CaSeO_3$(s).

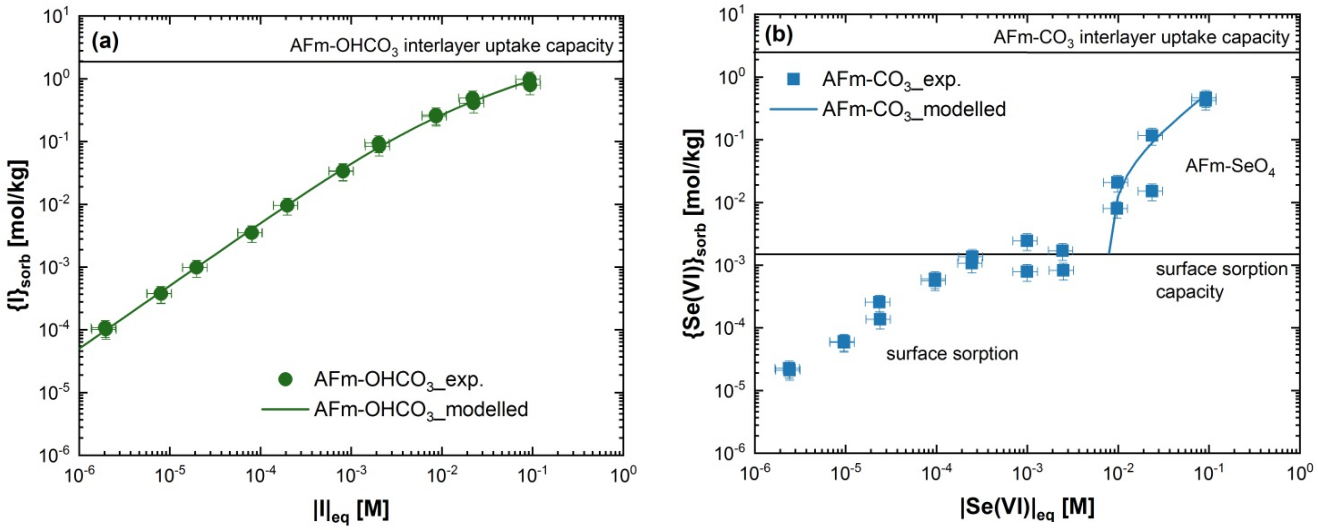

Fig. 3.5: a) I⁻ sorption isotherm onto AFm-$OHCO_3$ at pH = 13.0. Solid lines represent model prediction using thermodynamic solid solution model and assuming a complete miscibility between I⁻ and $[OHCO_3]^-$. b) Se(VI) sorption onto AFm-CO_3 at pH = 13.0. The solid line represents the model prediction assuming precipitation of the AFm-SeO_4 end member.

3.6 Microspectroscopic study of uranyl uptake on Boda claystone formation

One of the main pillars on which the safety analysis is built on, is the retention of radionuclides on the buffer material and host rocks of the near and far fields, respectively, of a radioactive waste repository. Understanding the mechanism of the uptake processes of radionuclides on the solid phases is crucial. In clay repositories, due to the low water content, the movement of the radionuclides is driven by diffusive processes, but adsorption and precipitation of newly formed phases are the key limiting processes in case of cations. In this study, the uptake of U(VI) on the Boda Claystone Formation (BCF), the selected potential host rock in Hungary for a HLW repository, was exemplarily investigated within an EU funded project.

The investigated rocks were prepared from mineralogical and geochemical characterised cores from drillings in BCF (depth below 500 m). Polished thin (~50 µm) rock sections were prepared on high-purity Si wafers. The thin sections were exposed to an U(VI) containing solution with an ionic strength similar to that of the porewater of the host rock (0.1 M NaCl). Positions of interest were carefully pre-selected using Scanning Electron Microscopy (SEM). These positions were investigated at the microXAS beamline at the Swiss Light Source (SLS), using a spot size down to 1×1 μm^2. In order to re-locate the positions of interest, elemental distribution maps were collected for the adsorbed element (U) as well as for the major and minor elements of the rock (e.g. K, Ca, Fe). In parallel, 2D micro-XRD images were collected in transmission mode at an excitation energy of 17300 eV for each pixel.

The micro-X-ray fluorescence (XRF) measurements showed that not only the argillaceous matrix (indicated by the K-rich regions) is responsible for uranium uptake. Instead, additional 5-10 µm thick U-rich fringes were observed around carbonate fillings (Fig. 3.6). High-resolution micro-XRF/XRD investigations clearly showed that the fracture-infilling region of the BCF samples contained zoned dolomite rhombohedra with outer Mn-rich areas. Micro-XRD demonstrated that these rhombohedra mainly consist of ankerite. The ankerite rims coincident with U enrichment (Fig. 3.7). Based on SEM/EDX and micro-XRD mapping ~25 ±10 % of the U(VI) uptake could be attributed to secondary phases (Fig. 3.7), proofing that minor phases can contribute to the uptake in such complex systems.

Similar examples, in which the so-called bottom-up approach fails, include Pu uptake by Yucca Mountain tuff (Powell et al. 2006) and Opalinus Clay (Kaplan et al. 2017), Np by Opalinus Clay (Fröhlich et al. 2012). These studies demonstrated the limitations of the bottom-up approach. However, as long as redox reactions on the minor phases present in the uptake system lead to less mobile species and/or the neoformed phases which are stable over geological time scales, the results of the bottom-up approach are still useful in performance assessments as they represent conservative sorption values.

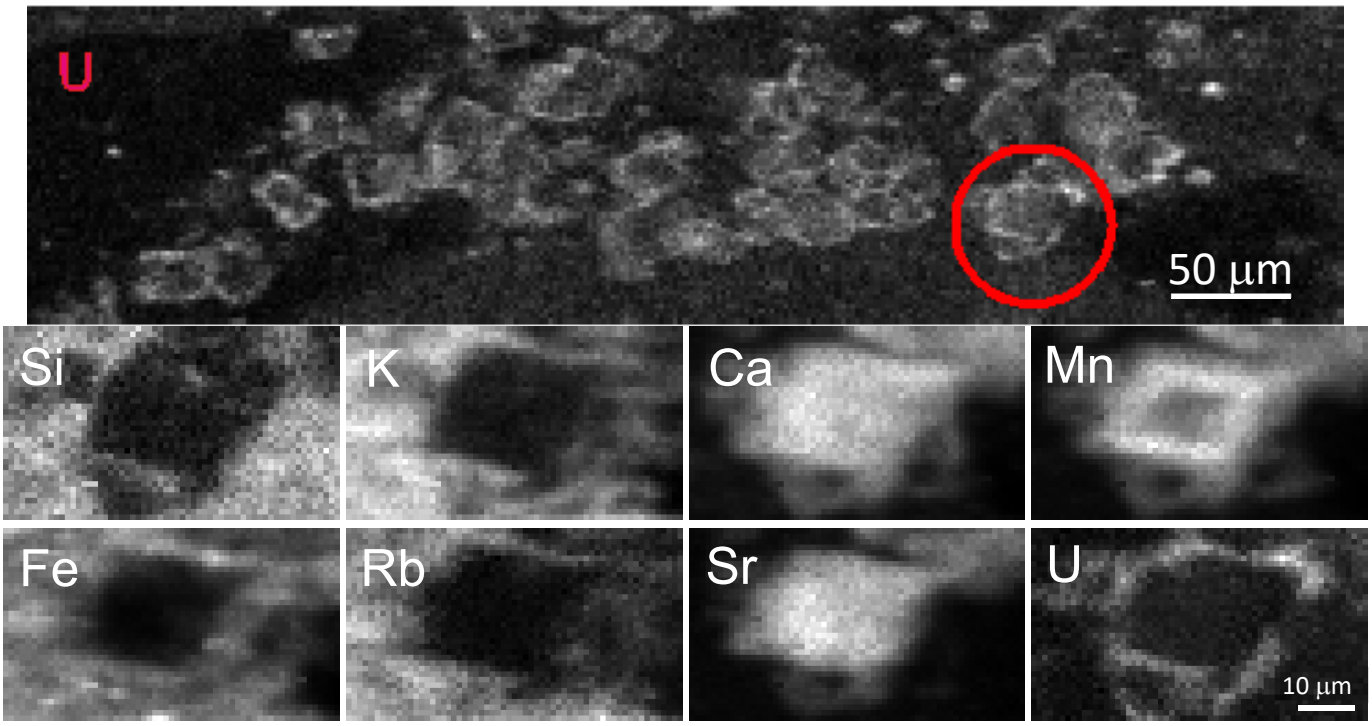

Fig. 3.6: Overview micro-XRF map of U distribution (top) collected with a beam and step size of 1×1 µm². Enlargement of the particle marked by a red circle (bottom) with a beam and step size of 1×1µm².

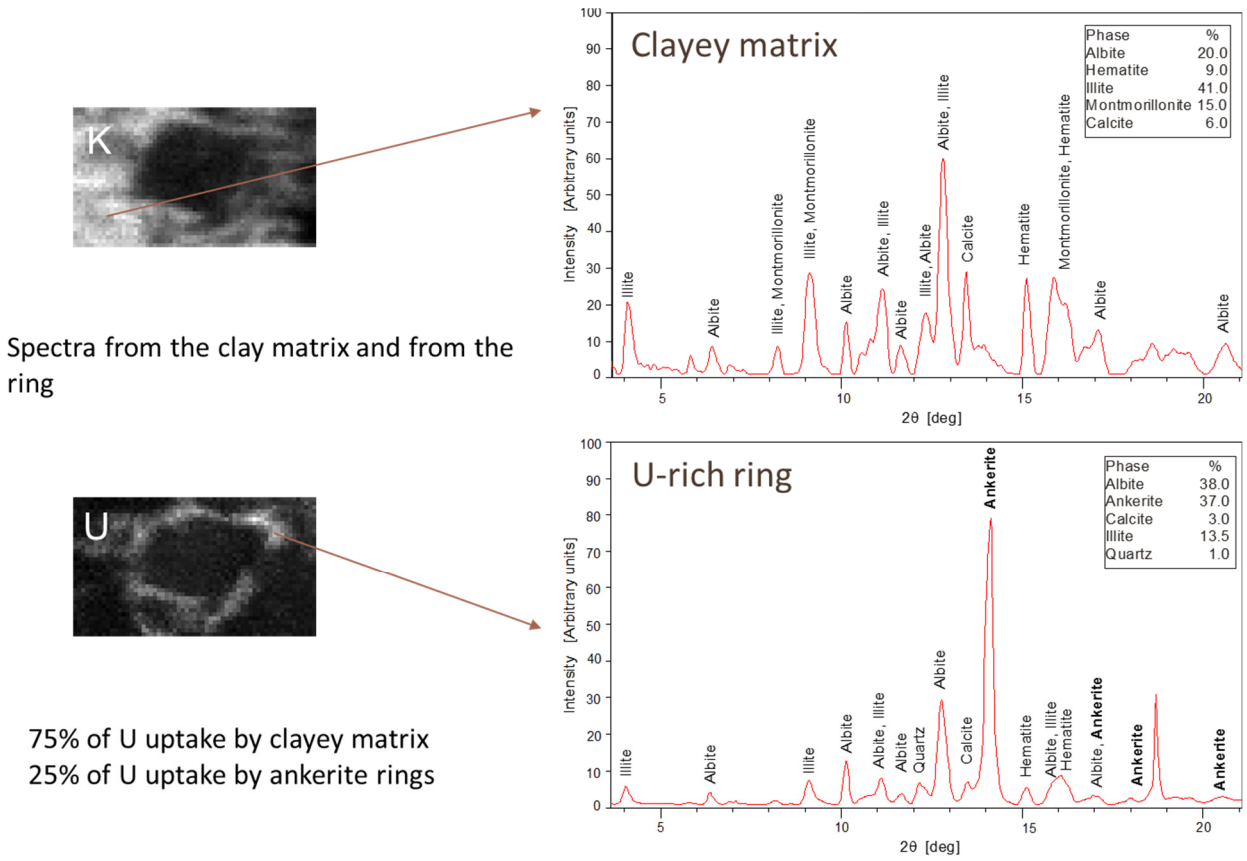

Fig. 3.7: Micro-XRD pattern collected from the clay rich regions and the rims.

3.7 Fe and U sorption on montmorillonite

In the last year of the SNSF funded PhD project, "*Detailed understanding of metal adsorption on clay minerals obtained by combining atomistic simulations and X-ray absorption spectroscopy*", the structural mechanism of iron and uranyl adsorption on clay minerals were studied. The combination of *ab initio* simulations and X-ray absorption spectroscopy (XAS) allowed to reveal the oxidation state and the structural characteristic of Fe surface complexes formed on montmorillonite surface at different loadings (Fig. 3.8). The quantitative interpretation of the atomistic modelling based XAS spectra (Fig. 3.9) indicated a particularly complex surface uptake of aqueous Fe(II). At low loading Fe is adsorbed at the surface in Fe(III) oxidation state at both strong and weak sites. With increasing Fe(II) concentration in solution, Fe(II) co-adsorb with Fe(III) at weak sites, medium loading, and also at strong sites, high loading (Kéri 2019).

The energy comparison of the relaxed structures of various bidentate uranyl surface complexes revealed that the stability of the uranyl species are essentially determined by the speciation and structural arrangement of surface chemical groups (e.g. OH^-) forming the adsorption site. The comparison of the basic structural parameters (of U–O shell) indicates an agreement with the most stable models. Furthermore an affinity of complexes to Fe(III) could be confirmed by calculations (Kéri 2019).

The thesis was successfully defended with "summa cum laude" on the 14 June 2019 at the University of Bern.

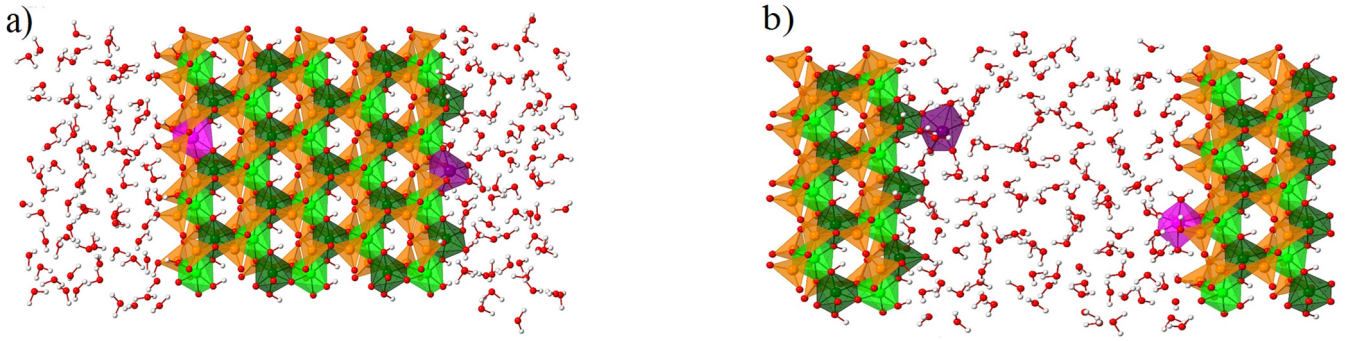

Fig. 3.8: Views of bidentate inner-sphere Fe(III)-sorption complexes on edge sites of cis-vacant montmorillonite. The complexes referred to in the thermodynamic sorption model as "strong-site" are shown in panel a, while the structure shown in panel b represents "weak-site" complexes.

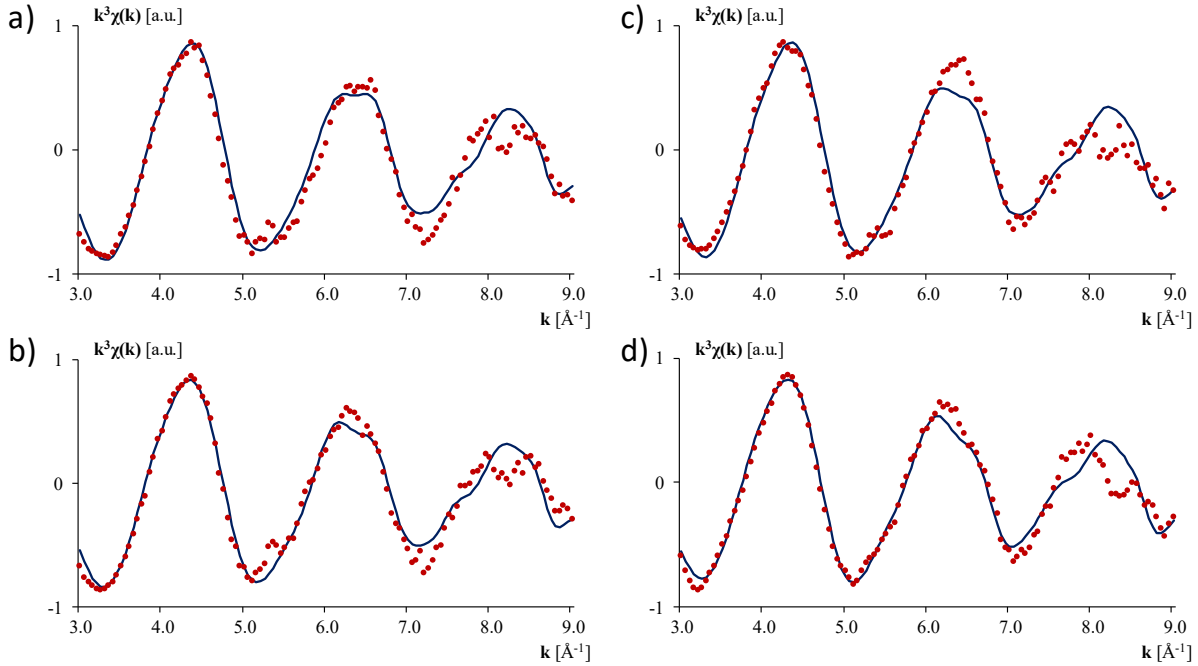

Fig. 3.9: Experimental EXAFS spectra (red dots) with the corresponding best fits based on the reference atomic structures and theoretical EXAFS spectra obtained by ab initio molecular dynamic simulations (solid lines). In the panels, the measured EXAFS spectra were collected from montmorillonite samples at different Fe loadings 6, 9, 17, 37 mmol/kg shown in panel a-d, respectively.

3.8 Cryo-µ-spectroscopy at the microXAS beamline for the investigation of redox- and radiation-sensitive samples and its application to environmental research

Synchrotron-based absorption spectroscopy is currently the only available technique to probe the chemical redox state of trace elements in complex environmental matrices. The combination of XAS with a micro-focused beam and a scanning sample stage allow us to obtain such information with spatial resolution down to the micrometer scale. However, synchrotron light sources are undergoing upgrades, which will bring smaller and more brilliant beams, increasing the photon flux density delivered onto the samples. This can be a challenge to radiation-sensitive samples such as environmental ones, altering their state during the measurement. To resolve this issue, different strategies have been developed such as reducing sample temperature with cryostat solutions and reducing sample exposure to the beam with novel measurement strategies. In the context of this project, we purchased and installed a cryostat solution at the microXAS beamline (X05LA) of the SLS, developed new sample preparation and measurement protocols to ensure the measurement of trace element speciation in environmental samples while minimising radiation induced changes in the specimen. We tested these protocols to investigate the speciation of Tl in Tl-contaminated soils from the Swiss Jura mountains (Fig. 3.10). Two peer-reviewed papers are underway on this subject as well as a third one investigating data quality and statistics of these approaches, fruit of a collaboration between PSI and another group at Eawag, is in preparation.

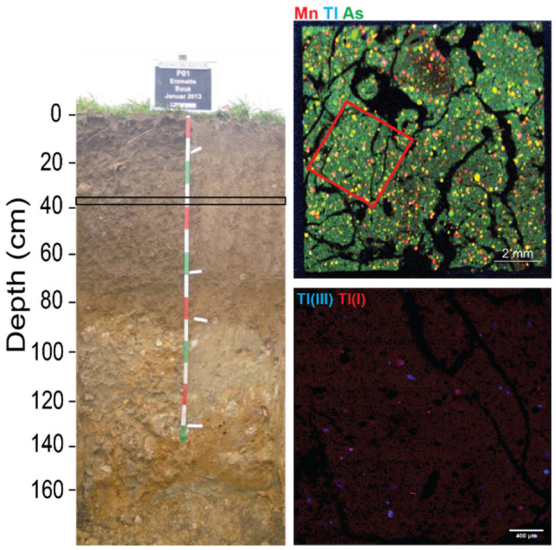

Fig. 3.10: (left) soil profile where the samples were collected; (top right) tabletop XRF image of a thin section showing Tl, Mn and As distribution; (bottom right) synchrotron-based chemical imaging of the distribution of reduced and oxidised Tl in the sample.

3.9 References

Bradbury M. H., Baeyens B. (1997a)
A mechanistic description of Ni and Zn sorption on Na-montmorillonite. 2. Modelling. Journal of Contaminant Hydrology 27, 223-248.

Bradbury M. H., Baeyens B. (2000)
A generalised sorption model for the concentration dependent uptake of caesium by argillaceous rocks. Journal of Contaminant Hydrology 42, 141-163.

Bradbury M. H., Baeyens B. (2009)
Sorption modelling on illite Part I: Titration measurements and the sorption of Ni, Co, Eu and Sn. Geochimica et Cosmochimica Acta 73, 990-1003.

Bradbury M. H, Baeyens B. (2011)
Predictive sorption modelling of Ni(II), Co(II), Eu(IIII), Th(IV) and U(VI) on MX-80 bentonite and Opalinus Clay: A bottom-up approach. Applied Clay Science 52, 27-33.

Ford, R. G., Scheinost, A. C., Scheckel, K. G., Sparks, D. L. (1999)
The link between clay mineral weathering and the stabilization of Ni surface precipitates. Environmental Science and Technology 33, 3140-3144.

Fröhlich D. R., Amayri S., Drebert J., Grolimund D., Huth J., Kaplan U., Krause J., Reich T. (2012)
Speciation of Np(V) uptake by Opalinus Clay using synchrotron microbeam techniques. Analytical and Bioanalytical Chemistry 404, 2151-2162.

Kaplan U., Amayri S., Drebert J., Rossberg A., Grolimund D., Reich T. (2017)
Geochemical interactions of plutonium with Opalinus Clay studied by spatially resolved synchrotron radiation techniques. Environmental Science and Technology 51, 7892-7902.

Kéri A. G. (2019)
Mechanism of metal uptake by clay minerals - X-ray spectroscopy and molecular modelling study. PhD Thesis, University of Bern, Bern, Switzerland.

Ma B., Fernandez-Martinez A., Grangeon S., Tournassat C., Findling N., Carrero S., Tisserand D., Bureau S., Elkaïm E., Marini C., Aquilanti G. (2018)
Selenite uptake by Ca–Al LDH: a description of intercalated anion coordination geometries. Environmental Science and Technology 52, 1624-1632.

Marques Fernandes M., Baeyens B. (2019)
Cation exchange and surface complexation of lead on montmorillonite and illite including competitive adsorption effects. Applied Geochemistry 100, 190-202.

Marques Fernandes M., Vér N., Baeyens B. (2015)
Predicting the uptake of Cs, Co, Ni, Eu, Th and U on argillaceous rocks using sorption models for illite. Applied Geochemistry 59, 189-199.

Nedyalkova L., Lothenbach B., Renaudin G., Mäder U., Tits J. (2019a)
Effect of redox conditions on the structure and solubility of sulfur-and selenium-AFm phases. Cement and Concrete Research 123, 105803.

Nedyalkova L., Lothenbach B., Geng G., Mäder U., Tits J.(2019b)
Uptake of iodine by calcium aluminate phases (AFm phases). Applied Geochemistry (submitted).

Powell B. A., Duff M. C., Kaplan D. I., Fjeld R. A., Newville M., Hunter D. B., Bertsch P. M., Coates J. T., Eng P., Rivers M. L., Serkiz S. M., Sutton S. R., Triay I. R., Vaniman D. T. (2006)
Plutonium oxidation and subsequent reduction by Mn(IV) minerals in Yucca Mountain tuff. Environmental Science and Technology 40, 3508-3514.

Scheinost A. C., Sparks D. L. (2000).
Formation of layered single-and double-metal hydroxide precipitates at the mineral/water interface: A multiple-scattering XAFS analysis. Journal of Colloid and Interface Science 223, 167-178.

Voegelin A., Pfenninger N., Petrikis J., Majzlan J., Plötze M., Senn A. C., Mangold S., Steininger R., Göttlicher J. (2015)
Thallium speciation and extractability in a thallium-and arsenic-rich soil developed from mineralized carbonate rock. Environmental Science and Technology 49, 5390-5398.

4 RADIONUCLIDES TRANSPORT AND RETENTION IN COMPACTED SYSTEMS AT FULL AND PARTIAL SATURATION

Van Loon L.R., Glaus M.A., Pfingsten W., Baeyens B., Marques Fernandes M., Frick S., Bunic P., Gimmi T., Churakov S.V., Chen Y. (postdoc), Krejci P. (PhD student), Chen P. (PhD student)

4.1 Introduction

The retention of radionuclides by clay minerals in engineered and geological barrier systems is a key safety function in the deep geological disposal of radioactive waste. Reliable sorption data (R_d values) and a mechanistic understanding of sorption and transport processes are thus mandatory for a proper evaluation of the barrier safety function. Sorption studies are mainly performed in batch systems using dispersed clay with a low solid-to-liquid ratio. In such an experimental set-up the composition of the solution can be well controlled (e.g. pH, Eh, concentrations of anions and cations, organic and inorganic ligands) and/or varied in order to study its effect on the sorption. Real clay systems, however, are very dense and are characterised by a high solid-to-liquid ratio. It is still an unanswered question whether the data and models derived from dilute dispersed systems can be transferred to the real, compact system. The aim of this project is to resolve conceptual difficulties in applying the existing sorption models to diffusion in compacted argillaceous rocks.

A second focus of the project deals with the question whether adsorbed ions should be treated as immobile or partially mobile. These two conceptual model assumptions have fundamental implications for the transport behaviour of ions in compacted systems. In the case of fully immobilisation, a pore diffusion model can describe transport whereas in the case of partial immobilisation surface diffusion models have to be applied.

Diffusion studies of gas molecules in fully and partial saturated compacted clay systems was started in the framework of a institutional Marie Skłodowska-Curie COFUND fellowship partially financed by the EU.

4.2 Sorption and diffusion in compacted illite

Diffusion experiments in model clay systems were carried out to address the transferability of sorption data derived in disperse clay suspensions to the compacted systems. Out of the several influencing factors that may potentially lead to systematic differences between the disperse and the compacted system is the presence of competing cations in the equilibrium pore water solution. Note that in the experiments with compacted model clay minerals such species can purposefully be present both in the equilibrium solution in the external reservoir and in the intrinsic pore water sample of the clay. Moreover, the surface of the clay minerals can be easily brought into equilibrium with a selected pore water solution in a preconditioning step. This is different from experiments with pristine clay rock, where differences between the composition of the pore water and the external synthetic porewater may exist owing to slow exchange processes, such as the dissolution of minor accessory minerals to components, which may not be present in the artificial pore water maintained in the external reservoirs in diffusion experiments.

Specifically the impact of ferrous iron (Fe(II)), a product of the anaerobic corrosion of iron and steel, on radionuclide sorption shall be investigated. Included in these activities are the measurements of the diffusion of Fe(II) in compacted clay minerals. Owing to difficulties in the handling and maintaining the stability of the ferrous iron form, Mn(II) was used as a chemical analogue in the diffusion and sorption in compacted illite. Mn(II) has a slightly higher pK_a than Fe(II), from which it can be expected that its sorption behaviour is somewhat weaker than that of Fe(II) (Baes & Mesmer 1976). Otherwise no fundamental differences between these two metal cations are expected regarding the diffusion in and sorption on compacted illite. The diffusion measurements were carried out (i) at trace Mn(II) concentrations under variable pH and ionic strength conditions and (ii) at fixed pH and ionic strength, but using large background concentrations of the stable isotope of Mn(II). The entirety of the results obtained from these measurements allows to derive a multi-site sorption model along with the identification of potentially mobile surface species. Fig. 4.1 shows selected results for the pH dependence of sorption distribution ratios (R_d) and effective diffusion coefficients (D_e) derived from the diffusion experiments in the compacted systems. The model curves were calculated using a set of thermodynamic sorption data (cf. Table 4.1) optimised (by eye) with respect to the entirety of the experimental results. The dependence of R_d values on the Mn(II) concentration could not be readily reproduced using strong and weak edge sorption sites only. Additional auxiliary sites (denoted to as *wx*) were introduced to overcome this difficulty. Currently, these sites are considered as pure fitting parameters. However, such sites could also be invoked to improve the validity of the two site protolysis non-electrostatic surface complexation and

cation exchange model (2SPNE SC/CE) to describe the sorption of Co^{2+} and Zn^{2+} in disperse illite (Montoya et al. 2018). In the future, the results of the sorption modelling derived from the experiments carried out using compacted clay samples may be compared to the measurements using disperse clay samples at low solid-to-liquid ratios (cf. chapter 3 LES Progress Report 2019). Such a comparison will prove ultimately whether significant differences exist regarding the sorption behaviour of disperse versus compacted clay samples.

Regarding the diffusive properties of representatives of the transition metal series, the electrical double layer theory, involving mobile surface species in the diffuse layer, has been successfully applied to explain the

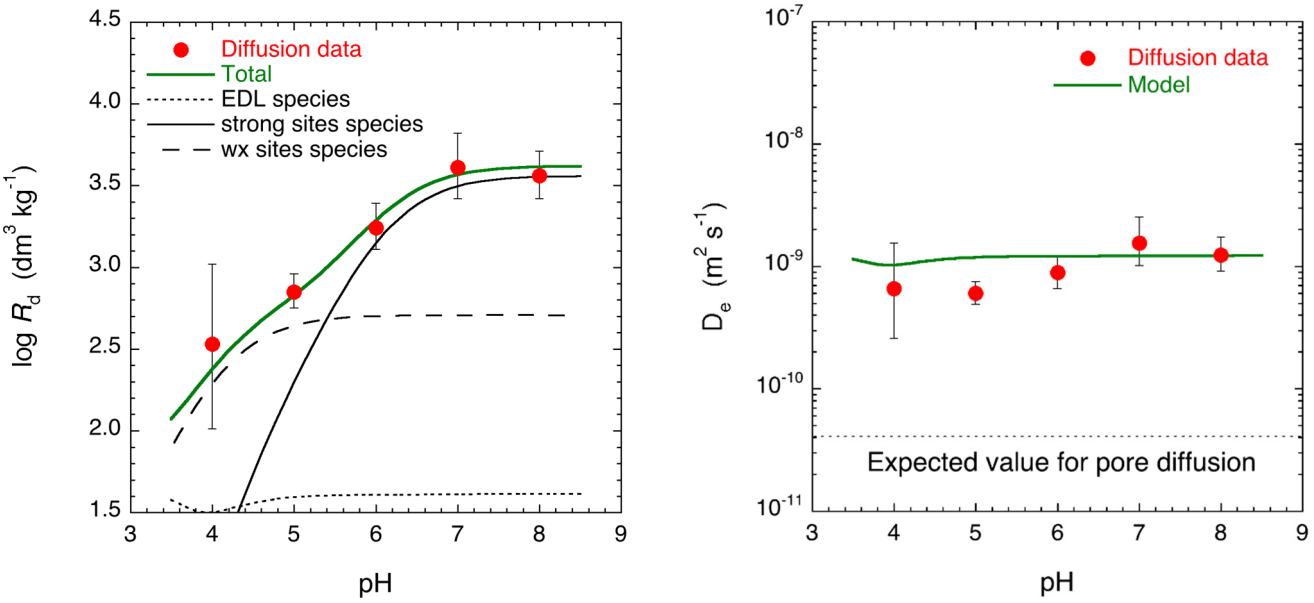

Fig. 4.1: Mn(II) sorption and diffusion data measured in illite compacted to a bulk dry density of 1700 kg m^{-3} at trace Mn(II) concentrations and 0.1 M ionic strength. The model curves were calculated using the thermodynamic data given in Table 4.1 and assuming that cationic species in the diffuse layer near the planar surfaces are mobile. The 'pore diffusion' model assumes that only aqueous phase species are mobile.

Tab. 4.1: Thermodynamic data used for modelling the in-diffusion data of Mn(II) in illite compacted to bulk-dry density of 1700 kg m^{-3}. The values of the interaction constants of Mn^{2+} were fitted to the experimental data. All other constants are literature values (Bradbury & Baeyens 2009; Glaus et al. 2015; Montoya et al. 2018).

Site types	Strong sites	Weak sites #1	Auxiliary sites	Stern layer sites
Site capacities (mol kg^{-1})	2×10^{-3}	4×10^{-2}	5×10^{-4}	1.9×10^{-1}
Formation constants [a] for the addition of	$^{s}\beta$	$^{w\#1}\beta$	$^{wx}\beta$	^{Su}K
H^+	6.2 / 4.0 [b]	6.2 / 4.0 [b]	4.2 / (2.5) [b]	-0.8
Na^+	–	–	–	-0.7 [c]
K^+	–	–	–	0.654
Mg^{2+}	–	–	–	0.107
Ca^{2+}	–	–	–	0.104
Al^{3+}	–	–	–	0.3
Mn^{2+}	0.55 [d]	(-2.5 [e])	2.3 [e]	0.3

[a] ^{10}log values

[b] Stepwise protonation of strong and weak sites (≡SO$^-$), viz. ≡SO$^-$ + H$^+$ = ≡SOH and ≡SOH + H$^+$ = ≡SOH$_2^+$

[c] Appelo and Wersin (2007)

[d] ≡S^{s}OH + Me^{2+} = ≡S^{s}OMe(OH)$_{j-1}^{2-j}$ + jH$^+$; j = 1,2,3, where ≡S^{s}OH is the mono-protonated strong surface site and Me a divalent metal cation.

[e] ≡S^{w}OH + Me^{2+} = ≡S^{w}OMe(OH)$_{j-1}^{2-j}$ + jH$^+$; j = 1,2, where ≡S^{w}OH is the mono-protonated weak surface sites.

specific parameter dependencies observed for the diffusion of such species in illite compacted to bulk-dry densities of ~1700 kg m^{-3} (Glaus et al. 2015; Glaus et al. 2019). Whether these results can be directly transferred to the diffusive behaviour of Opalinus Clay, in which illite is compacted to bulk-dry densities larger than 2000 kg m^{-3}, cannot readily be concluded. A representative Co(II) through-diffusion experiment was carried out with illite compacted to ~2100 kg m^{-3}. The swelling pressure of such strongly compacted illite samples is so strong that it was not possible to use the membrane-confined diffusion cells, in which the solution is separated from the clay sample by a very thin polymeric membrane, only. The illite samples were encased in stainless steel cells, confined by porous stainless-steel disks. This set-up allowed also for the measurement of through-diffusion of HTO to be made, for which no experimental results are available at such high compaction degrees. Fig. 4.2 shows a comparison of the experimental data (^{57}Co tracer profile) and a blind prediction based on the HTO diffusion measurements and the electrical double layer diffusion and sorption model according to Glaus et al. (2015). The agreement between the experimental data and the model curve is excellent, suggesting that this model is readily applicable to compaction degrees outside the scope of previous measurements. In particular the assumption of mobile surface metal cations in the diffuse layer is indispensable for a valuable description of the experimental profile depth of the tracer.

A new PhD student (Ping Chen) started a project on the behaviour of Technetium-99 in compacted illite in presence of Fe(II). Illite is the main clay mineral in Opalinus Clay and thus represents a model system for Opalinus Clay. In a first phase of the project the diffusion of HTO and $^{99}TcO_4^-$ in Na-illite was studied (Fig. 4.3). In Na-illite, $^{99}TcO_4^-$ stays in the oxidised state and behaves as an anion, similarly to $^{36}Cl^-$ (Glaus et al. 2010). Fe(II) plays a key role in the redox behaviour of ^{99}Tc (Pearce et al. 2018; Peretyazhko et al. 2009). To this end, the sorption behaviour of Fe(II) in illite will be investigated in more detail (Baeyens & Marques Fernandes 2018).

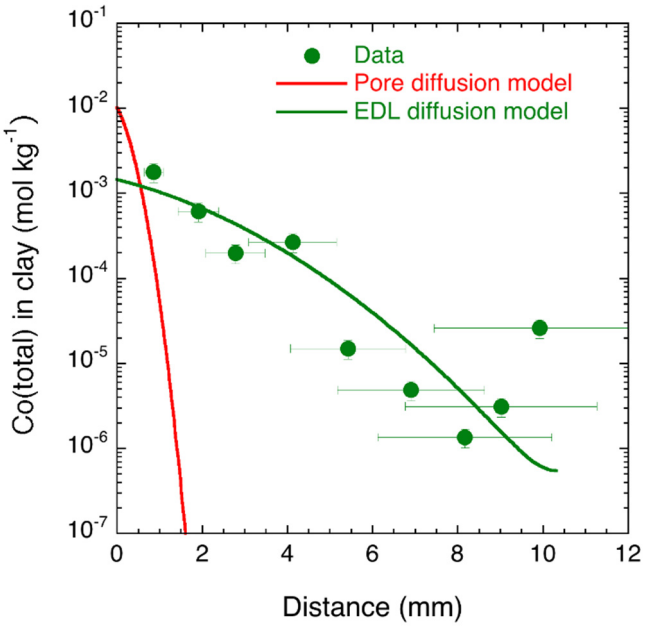

Fig. 4.2: Tracer profile of Co(II) in an in-diffusion experiment in illite compacted to a bulk-dry density of ~2100 kg m^{-3} at pH 5 and ionic strength of 0.1 M. The green model curve shows a blind prediction using the electrical double layer diffusion and sorption model proposed in Glaus et al. (2015). This model assumes that Co^{2+} cations present in the diffuse layer near the planar surfaces are mobile. The respective blind prediction without the assumption of mobile surface species is shown as a red model curve.

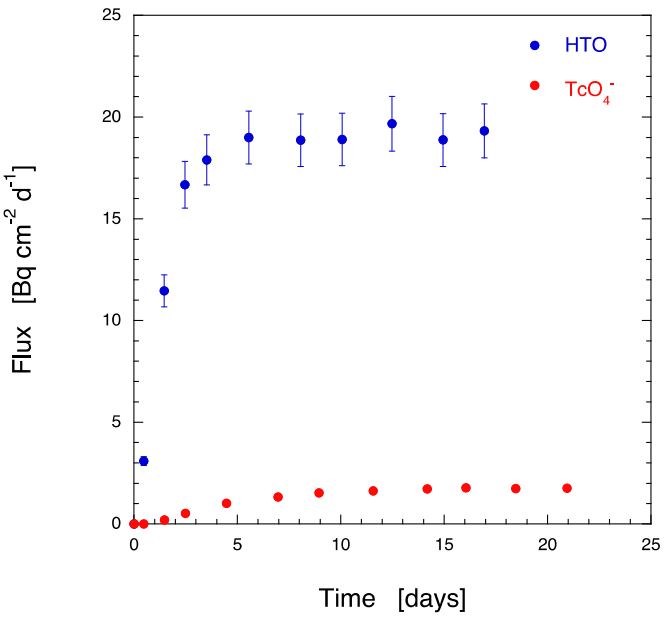

Fig. 4.3: Flux vs time curves (downstream reservoir) for the diffusion of HTO and TcO_4^- in compacted illite at a background electrolyte concentration of 0.1 M NaCl (Illite de Puy; ρ_b = 1600 kg m^{-3}). The calculated effective diffusion coefficients for HTO and TcO_4^- are 8×10^{-11} m^2 s^{-1} and 6×10^{-12} m^2 s^{-1}, respectively. Calculated diffusion accessible porosities for HTO and TcO_4^- are 0.6 and 0.15, respectively.

4.3 Sorption/diffusion in Opalinus Clay

The diffusion of strongly sorbing tracers in Opalinus Clay is still not fully understood. In order to improve our understanding of the behaviour of strongly sorbing radionuclides, the diffusion of Eu(III) in Opalinus Clay was investigated. An Opalinus Clay core was pre-equilibrated with pore water and contacted thereafter with a ^{152}Eu doped pore water at a total Eu concentration of ≅10^{-8} M. After 200 days of in-diffusion, the concentration profile in the rock sample was measured with the modified abrasive peeling method (Van Loon & Müller 2014). Fig 4.4 shows the concentration profile of Eu(III) in Opalinus Clay together with the evolution of the concentration of Eu(III) in the source reservoir as a function of time. The diffusion distance is only 400 µm after 200 days. Although the profile can be modelled with a simple pore diffusion model with $D_e = 5\times10^{-11}$ m^2 s^{-1} and a K_d of 60'000 cm^3 g^{-1}, mass balance calculations show that only 50 % of the mass loss in solution could be found back in the clay core. Calculating the evolution of the Eu(III) concentration in solution as a function of time with a model which accounts assuming for sorption and diffusion processes only, indicates that the concentration of Eu(III) in solution should be ca. 50% of the initial value. The experiment showed an almost complete depletion of the reservoir. This indicates that another, yet unknown, sink for Eu(III) exists. Further experiments are necessary to identify the nature of this additional Eu(III) sink.

4.4 Na and Sr diffusion modelling in Opalinus Clay

Enhanced mass fluxes of cations in clays cannot be described by simple Fick's law consistently. Therefore, we apply a surface diffusion model (Gimmi & Kosakowski 2011) to describe Na and Sr diffusion in Opalinus Clay. Sorption site-specific surface mobilities are the model parameters. For the estimation of the surface mobilities of Na and Sr the surface diffusion model was applied to a radial diffusion experiment in Opalinus Clay (Figure 4.5). The initial Na and Sr concentrations in the reservoir decreased during the experiment and the tracer fluxes were measured at the outer boundary of the Opalinus Clay sample.

A detailed description of the experimental set-up can be found in Van Loon et al. (2004). For modelling we used a 1-site cation exchange model describing exchange on the planar sites of the illite clay fraction in the Opalinus Clay. The selectivity coefficient of Sr had to be adapted, similar to the value found by Appelo et al. (2010). Figure 4.6 shows the modelling results. For Na and Sr the model (red line) matches the data (black dots with error bars) very well. The estimated surface mobilities (μ_s) for Na and Sr, (Na: μ_s = 0.4; Sr: μ_s = 0.05) are in good agreement with literature values (Gimmi & Kosakowski 2011). In summary, the surface diffusion model is able to successfully describe enhanced Na and Sr diffusion in Opalinus Clay.

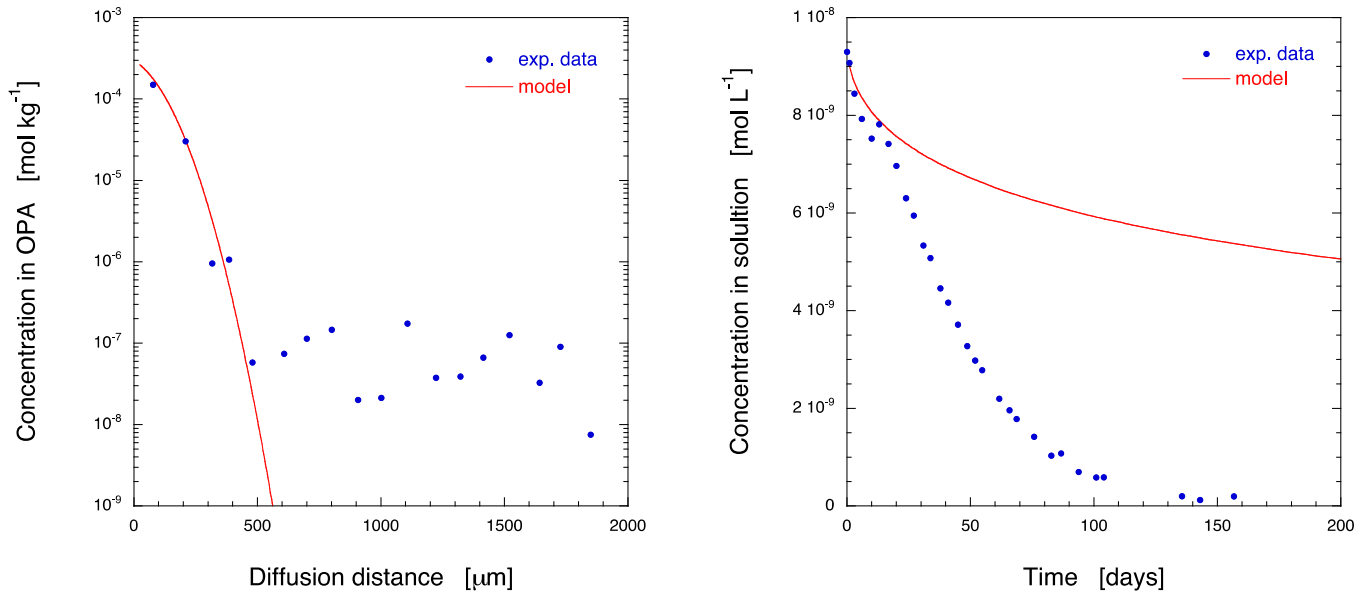

Fig. 4.4: Concentration profile of Eu(III) in Opalinus Clay (OPA) after 200 days of in-diffusion (left) and the evolution of the concentration of Eu(III) in the source solution of the in-diffusion experiment (right).

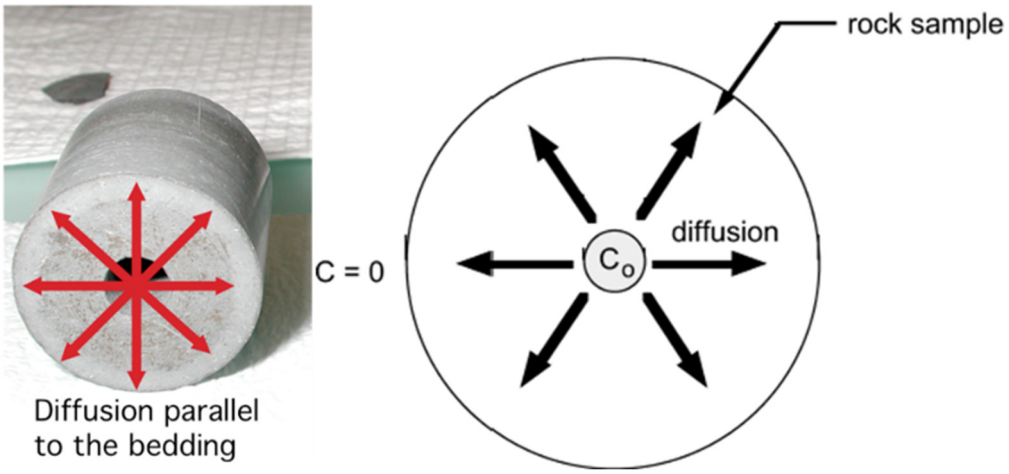

Fig. 4.5: Experimental set-up of the radial diffusion experiment from Van Loon et al. (2004).

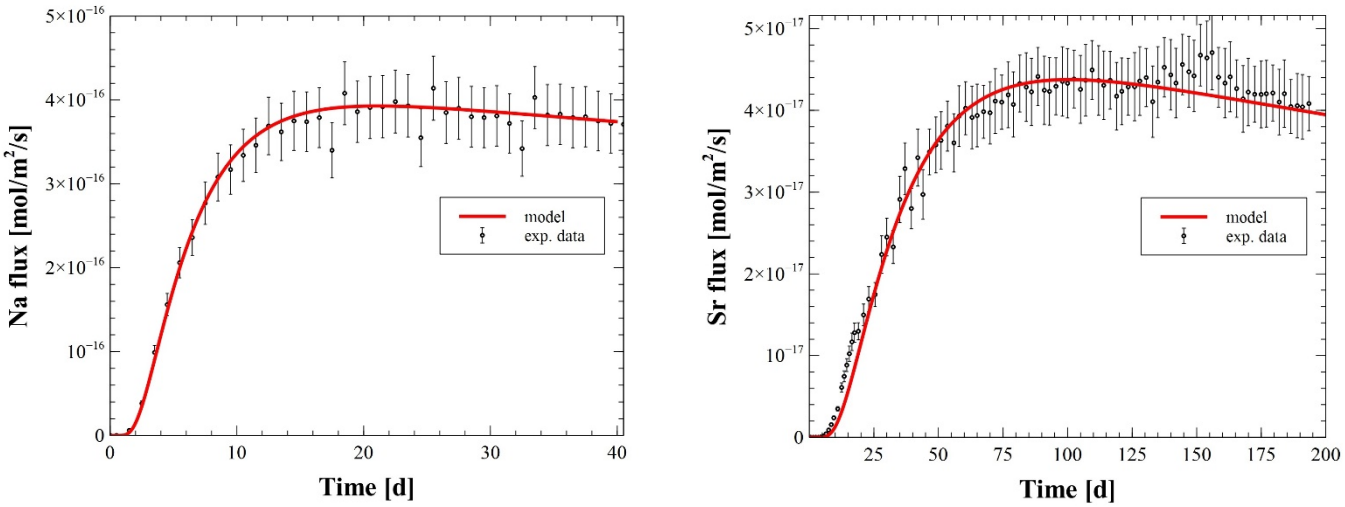

Fig. 4.6: Results of the radial diffusion experiment: Na flux (left) and Sr flux (right) on the outer boundary of the Opalinus Clay sample. Red line: surface diffusion model; black dots with error bars: experimental data.

4.5 Gas diffusion in partially saturated clay systems

Large amounts of gas will be produced in a repository due to corrosion of steel and degradation of organic waste forms (Diomidis et al. 2016). Whether these gases have a negative effect on the barrier system depends strongly on the permeability of the barrier systems for gases. An institutional Marie-Currie EU-COFUND postdoc project (Yanhua Chen) on gas diffusion in compacted clay systems has started in August 2019. The main emphasis of the project is on measuring the diffusion of selected gases in partially saturated clay systems such as compacted bentonite, bentonite/sand mixtures and Opalinus Clay. In a first phase, the resaturation characteristics of bentonite powder, compacted bentonite and Opalinus Clay are studied. In the case of compacted bentonite, two systems were studied: one sample was sandwiched between two filter plates and confined so that the total volume was constant; another sample was compacted but not confined so that the volume could change in one direction (along the axis of the sample holder) during water uptake. All clay systems were placed in a closed chamber with a given relative humidity (rh) that is fixed by saturated salt solutions (saturated NaCl solution, rh = 75 % or saturated KCl, rh = 85 %). The evolution of the weight is monitored as a function of time. First measurements (Fig 4.7) with bentonite (Volclay KWK) and Opalinus Clay indicate that resaturation takes place in two steps, an initial fast process followed by a slow process. In the case of bentonite, no large difference was observed between the powder, the confined compacted sample and the unconfined compacted sample.

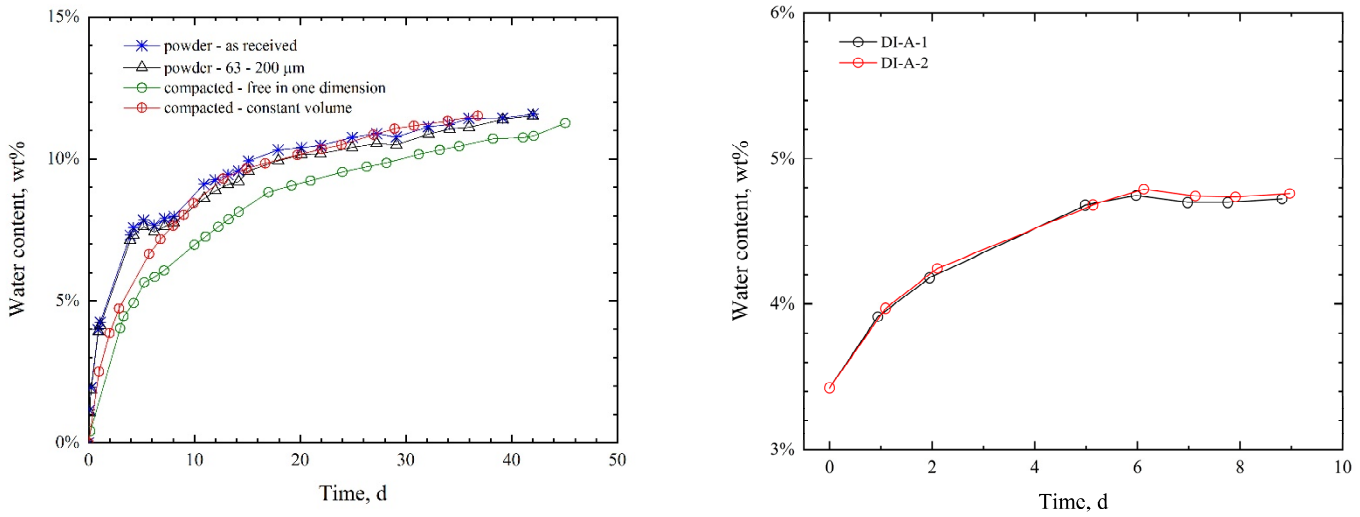

Fig. 4.7: Resaturation of compacted clay systems as a function of time: (left) bentonite Volclay KWK (rh 75%; saturated NaCl solution; T = 22 °C) and (right) Opalinus Clay (rh 85%; saturated KCl solution; T = 22 °C). The initial water content of the systems was 0 wt. % for bentonite and 3.3 wt. % for Opalinus Clay.

4.6 References

Appelo C. A. J., Van Loon L. R., Wersin P. (2010)
Multicomponent diffusion of a suite of tracers (HTO, Cl, Br, I, Na, Sr, Cs) in a single sample of Opalinus Clay. Geochimica et Cosmochimica Acta 74, 1201-1219.

Appelo C. A. J., Wersin P. (2007)
Multicomponent diffusion modeling in clay systems with application to the diffusion of tritium, iodide, and sodium in Opalinus Clay. Environmental Science and Technology 41, 5002-5007.

Baes C. F. J., Mesmer R. E. (1976)
The hydrolysis of cations. John Wiley & Sons, Inc., New York, USA.

Baeyens B., Marques Fernandes M. (2018)
Adsorption of heavy metals including radionuclides. Developments in Clay Science 9, 125-172.

Bradbury M. H., Baeyens B. (2009)
Sorption modelling on illite Part I: Titration measurements and the sorption of Ni, Co, Eu and Sn. Geochimica et Cosmochimica Acta 73, 990-1003.

Diomidis N., Cloet V., Leupin O. X., Marschall P., Poller A., Stein M. (2016)
Production, consumption and transport of gases in deep geological repositories according to the Swiss disposal concept. Nagra Technical Report NTB 16-03, Nagra, Wettingen, Switzerland.

Gimmi T., Kosakowski G. (2011)
How mobile are sorbed cations in clays and clay rocks? Environmental Science and Technology 45, 1443-1449.

Glaus M. A., Aertsens M., Appelo C. A. J., Kupcik T., Maes N., Van Laer L., Van Loon L. R. (2015)
Cation diffusion in the electrical double layer enhances the mass transfer rates for Sr^{2+}, Co^{2+} and Zn^{2+} in compacted illite. Geochimica et Cosmochimica Acta 165, 376-388.

Glaus M. A., Frick S., Rossé R., Van Loon L. R. (2010)
Comparative study of tracer diffusion of HTO, $^{22}Na^{+}$ and $^{36}Cl^{-}$ in compacted kaolinite, illite and montmorillonite. Geochimica et Cosmochimica Acta 74, 1999-2010.

Glaus M. A., Frick S., Van Loon L. R. (2019)
A coherent approach for cation surface diffusion in clay minerals and cation sorption models: Diffusion of Cs^{+} and Eu^{3+} in compacted illite as case examples. Submitted to Geochimica et Cosmochimica Acta.

Montoya V., Baeyens B., Glaus M. A., Kupcik T., Marques Fernandes M., Van Laer L., Bruggeman C., Maes N., Schäfer T. (2018)
Sorption of Sr, Co and Zn on illite: Batch experiments and modelling including Co in-diffusion measurements on compacted samples. Geochimica et Cosmochimica Acta 223, 1-20.

Pearce C. I., Icenhower J. P., Asmussen R. M., Tratnyek P. G., Rosso K. M., Lukens W. W., Qafoku N. P. (2018)
Technetium stabilization in low-solubility sulfide phases: A review. ACS Earth and Space Chemistry 2, 532-547.

Peretyazhko T., Zachara J. M., Heald S. M., Jeon B. H., Kukkadapu R. K., Liu C., Moore D., Resch C. T. (2009)
Heterogeneous reduction of Tc(VII) by Fe(II) at the solid-water interface. Geochimica et Cosmochimica Acta 72, 1521-1539.

Van Loon L. R., Müller W. (2014)
A modified version of the combined in-diffusion/abrasive peeling technique for measuring diffusion of strongly sorbing radionuclides in argillaceous rocks: A test study on the diffusion of caesium in Opalinus Clay. Applied Radiation and Isotopes 90, 197-202.

Van Loon L. R., Soler J. M., Müller W., Bradbury M. H. (2004)
Anisotropic diffusion in layered argillaceous rocks: A case study with Opalinus Clay. Environmental Science and Technology 38, 5721–5728.

5 CEMENT-WASTE INTERACTION AND UPSCALING TO THE FIELD SCALE

Kosakowski G., Wieland E., Dähn R., Prasianakis N.I., Tits J., Churakov S.V., Geng G. (postdoc), Patel R. (postdoc), Mancini A. (PhD student)

5.1 Introduction

The Swiss geological waste disposal concept (Nagra 2016) foresees implementation of a multi-barrier system to ensure safe disposal of high-level waste (HLW), spent fuel, vitrified and long-lived intermediate-level waste, and low- and intermediate-level waste (L/ILW). Engineered and geological barriers of the L/ILW repository include the waste matrix, the waste packages, the emplacement containers, the cavern backfill and the host rock. The L/ILW repository near field will contain large amounts of cementitious materials, which will be major physical and chemical barriers to the release of radionuclides into the host rock. The barrier function of the cementitious near field is expected to change over time due to various (geo-)chemical processes taking place in cementitious systems (Kosakowski et al. 2014). It has been acknowledged that cement-waste interaction may additionally contribute to the degradation of cementitious materials and affect the long-term performance of the barriers.

The aim of this project is to identify the physico-chemical processes controlling the temporal evolution of the L/ILW (cement-based) repository and to assess the influence of processes and spatial heterogeneities on the evolution of the repository near field. In 2019, the main activities focused on i) interaction of iron corrosion products with cement paste, ii) alkali-silica reaction in concrete, and iii) carbonation mechanisms in cement-based materials. To this end, both experimental and modelling studies have been carried out.

5.2 Interaction of iron corrosion products with cement phases

Iron/steel and cement are important components of the planned deep geological L/ILW repository in Switzerland (Diomidis et al. 2016; Nagra 2014). Upon disposal, iron/steel will start corroding. Corrosion in oxic conditions will prevail in the early phase of the L/ILW repository. However, oxygen is quickly depleted from the near field by oxic corrosion of metallic iron after closure of the repository. As a result, conditions become strongly reducing and anoxic corrosion of metallic iron at the interface between cement paste and iron/steel starts to produce Fe(II,III) corrosion products. Magnetite (Fe_3O_4) and Fe sulphides (FeS, FeS_2) are expected to be the main products of iron/steel corrosion in anoxic alkaline conditions. Thus, it is assumed that iron corrosion products, in particular Fe(II), do not interact with cement phases. It was shown in earlier studies that Fe(III) interacts with Al(III)-bearing cement phases (e.g. Dilnesa et al. 2011; 2012, 2014; Vespa et al. 2015). Up to now, however, the interaction of Fe(II,III) with calcium silicate hydrates (C-S-H) has not yet been addressed. In particular, it is presently not clear whether or not interaction between the corrosion products and cement paste can occur and if so, whether or not this interaction will affect the long-term barrier performance of cementitious materials in the L/ILW repository. The aim of this project is to close the aforementioned gaps in our knowledge.

A PhD project funded by the Swiss National Science Foundation (SNSF) (grant No 200021_162342) was started in 2016. It aims to develop a mechanistic understanding of Fe(II,III) interaction with C-S-H phases in order to gain basic information required for improving the current understanding of iron/steel-cement interaction over the time scale of an L/ILW repository. In this project, the Fe speciation is being investigated a) upon the interaction of Fe(II,III) with single cement phases by using wet chemistry and synchrotron-based techniques, and b) in aged Fe(0)-containing slag cements sampled from concrete structures that had been exposed to environmental conditions for several years.

In 2019, studies on the interaction of Fe(II) and Fe(III) with calcium-silicate-hydrates (C-S-H) were continued by employing wet chemistry and spectroscopic techniques, in particular extended X-ray absorption fine structure spectroscopy (EXAFS). C-S-H phases are the main hydration products in Portland cements. These phases are important for controlling the mobility of radionuclides in a cementitious near field due to the high immobilisation potential for cations. Wet chemistry experiments with Fe(III) on C-S-H phases were performed by using the conventional batch sorption technique. The Fe(II) sorption experiments with C-S-H phases were carried out by controlling redox conditions in an electrochemical cell to avoid Fe(II) oxidation.

Sorption isotherm measurements show a linear uptake of both Fe(II) and Fe(III) by C-S-H phases with different Ca/Si ratios (e.g. 0.8 and 1.5) (Fig. 5.1a). However, the sorption value (K_d) of Fe(III) is considerably higher than that of Fe(II) indicating

stronger uptake of Fe(III) by C-S-H phases. Furthermore, the C-S-H composition does not have any notable effect on the uptake as the sorption isotherms determined on the C-S-H phases with Ca/Si ratios 0.8 and 1.5 lie upon each other within the experimental uncertainties for both oxidation states.

EXAFS spectroscopy measurements were performed on Fe(III)-doped C-S-H phases with the aim of identifying the sorption mechanisms. The EXAFS spectra collected on the Fe(III)-doped C-S-H phases with high Ca/Si ratios (1.2, 1.5) and low Fe(III) loadings (800 and 900 ppm) were found to be nearly identical, while the spectrum of the Fe(III)-C-S-H sample at low Ca/Si ratio (0.8) shows much weaker intensity of the backscattering contributions at larger distance (Fig. 5.1b). These differences suggest different coordination environments of Fe(III) at high and low Ca/Si ratios. Multi-shell fitting revealed that at high Ca/Si ratio (e.g. ≥ 1.2) Fe(III) is located in the interlayer of the C-S-H phases. In this location, Fe(III) is octahedrally coordinated and it is directly coordinated to the Si tetrahedra of the dreierketten silica chains adjacent to the interlayer space (Fig. 5.1c). The proposed structural model accounts for the large number of neighboring Ca, Si and O atoms (Tab. 5.1). It should be noted that complementary ^{29}Si NMR measurements indicated that Fe(III) is replacing the Q^2_b sites, which identifies silica in the bridging positions of the dreierketten structure (Mancini et al. 2019a). This finding corroborates the notion of interlayer binding of Fe(III) by C-S-H phases at high Ca/Si ratios.

In contrast, for Fe(III) C-S-H samples with a low Ca/Si ratio of 0.8, the ^{29}Si NMR data do not support significant Fe(III) uptake by the interlayer. According to the EXAFS data, also the backscattering and total number of neighboring atoms is different (Tab. 5.1). We interpret the structural parameters such that Fe(III) forms a separate, secondary Ca-Si-rich phase or clusters, respectively, on the surface of C-S-H phases as the number of neighboring Ca and Si is large. Note that the number of neighboring Ca and Si should be much lower (estimated ≤ 2), if surface complexation would be the dominant sorption mechanism.

Thermodynamic modelling suggested precipitation of microcrystalline $Fe(OH)_3$ in the Fe(III)-doped C-S-H samples at high Fe(III) concentrations. For example, the C-S-H suspensions were expected to be supersaturated with respect to $Fe(OH)_3$(mc) at pH 12.5 and above an aqueous Fe(III) concentration of 10^{-7} mol/L, corresponding to ~ 3000 ppm sorbed Fe. Nevertheless, the sorption isotherm data do not indicate precipitation of $Fe(OH)_3$(mc) in the Fe(III)-doped C-S-H systems at the latter loading (Fig. 5.1a). In addition, also the EXAFS data do not support the formation of a $Fe(OH)_3$ precipitate at this loading for Fe(III)-C-S-H with Ca/Si ratio = 1.5 (Tab. 5.1). These findings confirm that Fe(III)-doped C-S-H systems can be strongly supersaturated with respect to $Fe(OH)_3$. We also carried out EXAFS measurements on Fe(III)-doped C-S-H samples with loadings significantly ≥12,000 ppm in order to demonstrate $Fe(OH)_3$ precipitation. For example, presence of an amorphous $Fe(OH)_3$ precipitate was detected at 15,000 and 50,000 ppm Fe(III) loadings in case of the C-S-H phases with Ca/Si ratios 1.2 and 1.5, while precipitation was already observed at 12,000 ppm loading in case of the C-S-H phase with a Ca/Si ratio = 0.8 (Mancini et al. 2019a).

The sorption isotherm data suggest that Fe(II) bonding to C-S-H phases is much weaker than bonding of Fe(III). This is consistent with the lower sorption values reported in the literature for the uptake of bivalent earth-alkaline and transition metals by C-S-H phases (e.g. Wieland 2014). The EXAFS studies performed on Fe(II)-doped C-S-H phases do not show any spectroscopic difference at low and high Ca/Si ratios. This suggest identical coordination environments of Fe(II) irrespective of the C-S-H composition. Furthermore, the EXAFS data of Fe(II)-doped C-S-H phases revealed that uptake in the interlayer is highly unlikely due to the low coordination number of neighboring cations. Hence, the formation of a secondary phase or clusters on the surface of C-S-H phases, similar to Fe(III) at low Ca/Si ratio, is proposed. A publication on the Fe(II) uptake by C-S-H phases is in preparation (Mancini et al. 2019b).

The results from this PhD project show that Fe(II) and Fe(III) interact with C-S-H phases, the most important component of cement paste. It should be noted that in safety assessments cement paste is assumed to be the only sorbing material in the near field and solely responsible for radionuclide retention. In this context, one may pose the question whether or not sorption competition between Fe(II), Fe(III) and radionuclides preferentially taken up by C-S-H phases could occur. For example, the present study shows that Fe(III) occupies structural positions in the interlayer that may also be accommodated by actinides. Gaona et al. (2011) identified a large number of neighboring Ca, Si and O atoms of Np(IV) in Np(IV)-doped C-S-H samples, which prompted the authors to propose a structural model for Np(IV) uptake into the interlayer similar to that for the Fe(III) uptake proposed in this study. This implies that Np(IV) and Fe(III) may occupy the same crystallographic positions in the interlayer, which could result in competitive sorption of the two cations.

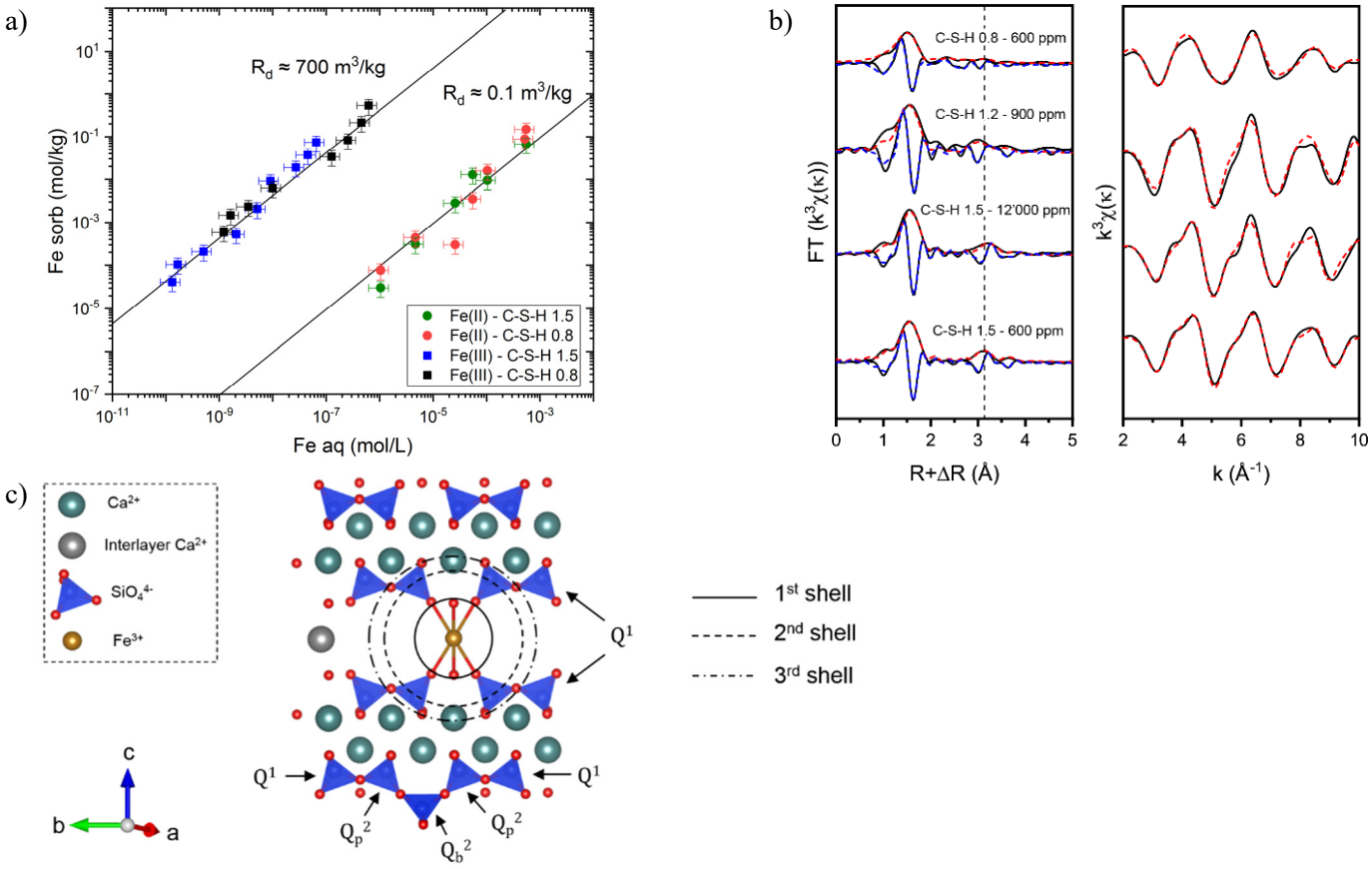

Fig 5.1: a) Comparison of Fe(II) and Fe(III) sorption on C-S-H phases with Ca/Si ratios 0.8 and 1.5 at pH 12.5, b) Experimental Fe K-edge spectra (Fourier transform of experimental (black solid line) and fitted (coloured dashed lines) k^3-weighted EXAFS functions) of Fe(III)-doped C-S-H phases. c) Proposed structural model for Fe(III) uptake by the interlayer at high Ca/Si ratios of C-S-H phases.

Tab. 5.1: Structural parameters derived from Fe K-edge EXAFS data analysis of C-S-H phases loaded with Fe(III). Calculated uncertainties are given in parentheses. N = number of neighboring atoms, R = interatomic distance, σ^2 = Debye-Waller factor, ΔE = energy shift, R-factor = residual factor.

Sample	**Fe(III)** (ppm)	**Shell**	**N**	**R** (Å)	**σ^2** (Å^2)	**ΔE** (eV)	**R-factor**
C-S-H 1.5	600	Fe-O`	5.8 (.5)	1.99 (.01)	0.006 (.001)	4.13 (1.1)	0.001
		Fe-Si	4.5 (1.0)	3.57 (.01)	0.008 (.002)		
		Fe-Ca	2.2 (.5)	4.36 (.03)	0.003 (.001)		
		Fe-O``	14.8 (2.5)	4.45 (.03)	0.005 (.002)		
C-S-H 1.5	12,000	Fe-O`	5.5 (.6)	2.02 (.01)	0.004 (.001)	4.53 (1.2)	0.002
		Fe-Si	4.8 (.7)	3.62 (.01)	0.008*		
		Fe-Ca	2*	4.35 (.04)	0.003*		
		Fe-O``	16.1 (2.9)	4.45 (.01)	0.007(.001)		
C-S-H 1.2	900	Fe-O`	6.7 (1.7)	2.00 (.01)	0.005 (.001)	-2.1 (1.5)	0.005
		Fe-Si	4*	3.56 (.03)	0.008 (.002)		
		Fe-Ca	2*	4.34 (.03)	0.003 (.001)		
		Fe-O``	15.3 (3.2)	4.43 (.01)	0.005 (.002)		
C-S-H 0.8	600	Fe-O	6*	1.97 (.02)	0.006 (.001)	3.28 (1.5)	0.022
		Fe-Si	4.6 (1.3)	3.15 (.07)	0.005 (.003)		
		Fe-Ca	2.8 (.8)	3.19 (.05)	0.003*		
		Fe-Fe	2*	3.34 (.05)	0.012 (.007)		

*) Fixed parameters.

5.3 Alkali-silica reaction in concrete

The alkali-silica reaction (ASR) is a deterioration mechanism, which can severely shorten the durability of concrete structures. The ASR takes place between the siliceous component of concrete aggregate and the alkaline pore solution. The formation of the ASR products is often accompanied by significant internal expansion and cracking of concrete, which severely shortens the service life of affected infrastructure (Merz et al. 2006). This project aims to elucidate molecular-scale mechanism of the ASR, i.e. the crystal structure and property of the ASR products (e.g. Dähn et al. 2016), and its correlation with the physical properties related to the expansion phenomena.

This project is a part of the Swiss SNSF Sinergia project "Alkali-silica reaction (ASR) in concrete", grant number CRSII5_17108, in which researchers from Empa, EPFL and PSI have teamed up with the aim to gain insights into the mechanisms of the reaction and to acquire knowledge about how ASR develops with time. Additional funding for this research topic was provided by the European Union's Horizon 2020 research and innovation programme under the Marie Skłodowska-Curie grant agreement No 701647.

In the year 2019, we analysed the micro X-ray absorption spectroscopy (XAS) data and High Pressure XRD (HP-XRD) data that were collected for ASR products from both the field and lab synthesis (Geng et al. 2019a, 2019b). Four ASR samples collected in the field were prepared for the microXAS study. 'Mels1' samples come from the abutment of a 50-year-old bridge in Mels, Switzerland. 'ES1' and 'ES2' samples are from laboratory produced concrete cubes exposed for 14 years to natural conditions in Valencia (Spain) and Milan (Italy), respectively. 'N1' samples are from a concrete subjected to Norwegian 38°C prism test for two years. The minerals shlykovite and mountainite were collected from Kola Peninsula, Russia (Zubkova et al. 2010). Lab ASR samples were synthesised by mixing SiO_2, CaO and (Na/K)OH in a molar ratio of 1:0.25:0.5 and at a water-to-solid ratio of 5:10. Obtained solids were filtered and dried after 80 days of reaction at 80℃. Two of them (SKC and SNC) were studied as reference phases (Shi et al. 2019).

The samples were analysed by Scanning Electron Microscopy (SEM) with a FEI Quanta 650 using an acceleration voltage of 12 kV. Chemical analysis was performed by energy-dispersive X-ray spectroscopy (EDS). The microXAS investigations of the ASR products were conducted at the PHOENIX beamline of the Swiss Light Source (SLS). Two-dimensional element mappings were obtained for field samples by scanning the sample through the micro-focussed beam with the incident beam energy fixed at 4050 eV (slightly above the Ca K-edge). The incident beam energy was scanned to obtain the absorption spectra from 3980 to 4200 eV for Ca K-edge, from 3520 to 3750 eV for K K-edge, and from 1000 to 1200 eV for Na K-edge. The XANES spectra were normalised and processed using the Athena package.

HP-XRD studies of the field samples (Mels_pore, ES1_pore, ES1_agg) were conducted at beamline P02.2 of the Deutsches Elektronen-Synchrotron (Hamburg, Germany) with a beam energy of 25.45 keV. The lab sample SKC was studied at beamline I15 of the Diamond Light Source (Oxfordshire, UK) with a beam energy of 29.2 keV. Hydrostatic pressure was applied with a Diamond Anvil Cell (DAC), from ambient (no applied pressure) to ~8 GPa, at a step size of 1-2 GPa, followed by an unloading of the DAC. The raw diffraction images were recorded by image plates and integrated to the normal diffractogram using the *Dioptas* software package.

The SEM images of concrete samples with ASR damage demonstrate a universal micro-morphology of reaction product veins running from inside the aggregate to the cementitious paste (Fig 5.2a). The product inside the aggregate is often crystalline with nano-platy morphology, while the product in the cementitious paste is often amorphous. Ca, K and Na K-edge XANES spectra were collected at spots within both crystalline and amorphous regions of the product vein, according to the fluorescence map of the microstructure (Fig. 5.2a). Examples of Ca K-edge XANES are displayed in Fig. 5.2b, which are compared with reference phases. Our results indicate that the crystalline ASR products exhibit identical chemical environment, despite their distinct sources and exposure conditions. Similarly, the amorphous ASR products from different field specimens are also identical. Furthermore, the crystalline ASR products resemble the structure of shlykovite, which is a layer silicate with Ca layer between silicate sheets and K/Na imbedded within the sheets (Fig. 5.2c). The amorphous ASR products highly resemble the structure of C-S-H phases, although they seem to have different nano-morphology (Geng et al. 2019a).

To understand the mechanical properties of the ASR products, HP-XRD measurements were conducted for the extracted powder of crystalline ASR products. An example is given in Fig. 5.3. With increasing hydrostatic load applied to the sample, its X-ray diffraction peaks shift towards smaller distance between crystal planes (Fig. 5.3a). Compared with the XRD of shlykovite, the ASR product exhibits several peak-splitting, e.g. at peak (002), (100) and (106), indicating that the product is composed of several phases with similar structure but slightly different lattice parameters. The two most abundant phases were identified and their lattice parameters were calculated

as a function of pressure, as shown in Figs. 5.3b-e. The dominant phase (phase_1) has an ambient basal spacing of 12.2 Å, yet it undergoes a rapid collapse at ~2 GPa (Fig. 5.3c), accompanied by a quick change of lattice parameter *a* as well (Fig. 5.3b). Meanwhile, the minor phase (phase_2) exhibits a rather elastic deformation with continuous change of lattice parameters when pressure increases, and a linear recovery when pressure is removed (Figs. 5.3d and e).

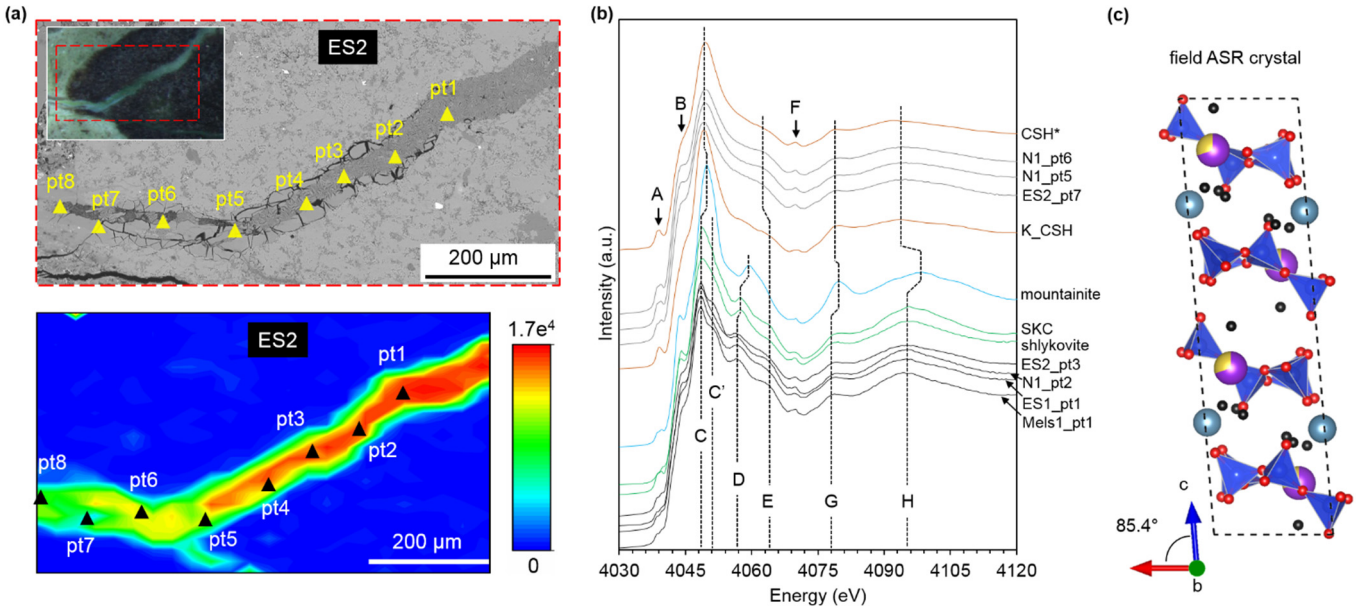

Fig. 5.2: MicroXAS study of field ASR samples: a) SEM (top) and fluorescence map (bottom) of a product vein in sample ES2, b) Ca K-edge XANES spectra of reference phases and ASR samples, c) the proposed crystal structure of ASR products in affected concrete.

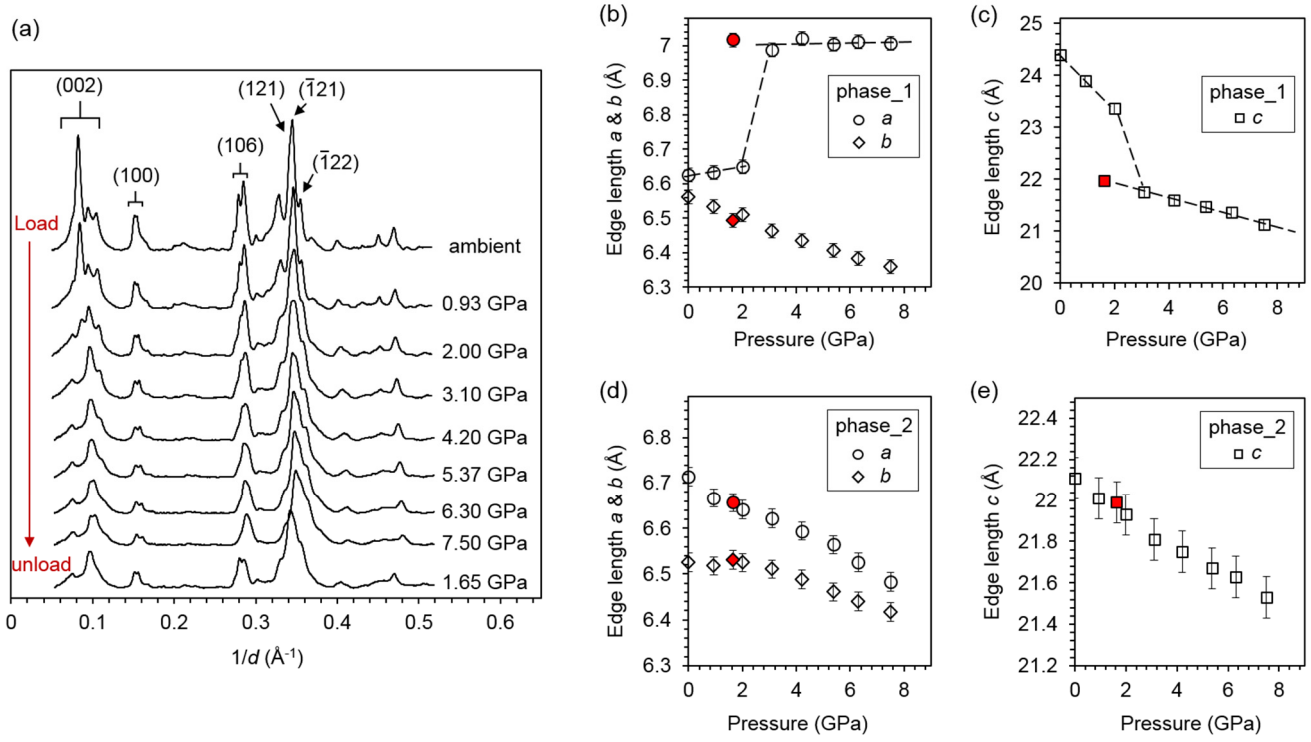

Fig. 5.3: High-pressure XRD study of sample ES1: a) XRD pattern as a function of applied pressure, b)-e) calculated lattice parameters as a function of pressure. The red data points correspond to unloaded cases.

Based on the refined lattice parameters, the volumetric changes of ASR products as well as the reference minerals were calculated as a function of pressure. Subsequently, their bulk moduli were calculated. The dominant phase in the studied field samples has a bulk modulus of 27±3 GPa. It undergoes a phase change at ~2 GPa to a high-pressure polymorph with a bulk modulus of 46±3 GPa. The minor phase in the studied field samples has a bulk modulus of 76±4 GPa. It exhibits no phase change during compression to ~8 GPa. The lab-synthesised ASR product (SKC) has a bulk modulus of 35±2 GPa. It also undergoes no phase change during compression. The presence of several phases with different bulk moduli in field ASR samples and the strong dependence on the porosity is consistent with the large range of elastic moduli obtained from nano-indentation (Geng et al. 2019b).

5.4 Resolving carbonation mechanisms of cement-based materials by multi-scale microstructural simulations

The PSI-fellow-3i project "*Resolving carbonation mechanisms of cement-based materials through multiscale microstructural simulations*" (R. Patel) was started in 2017 and finalised in 2019. The project received partial funding from the European Union's Horizon 2020 research and innovation programme under the Marie Sklodowska-Curie grant agreement No 701647.

In this project, a coupled thermo-hydraulic-chemical (THC) lattice Boltzmann based reactive transport model has been developed that describes the pore-scale evolution of the microstructure and porosity distribution of cement paste in contact with carbonated brine. Initial cement paste microstructures consistent with the experimental data of Duguid and Scherer (2010) were generated in 3D with the HYMOSTRUC code (Van Breugel 1995). Interaction of cement paste with the infiltrating brine causes dissolution of cement phases and re-precipitation of carbonate minerals. The corresponding evolution of microstructure and porosity was modelled with the in-house lattice Boltzmann code *Yantra* (Patel 2016).

The simulations show a good quantitative agreement between modelling and experimental observations at the initial stages of system evolution. For longer times, however, the modelling results and experimental observations start to diverge significantly. The main reason for the deviation are the large uncertainties in the kinetics of C-S-H dissolution and calcite precipitation. Fig. 5.4 shows typical distributions of mineral phases after 12 hours and 120 hours reaction time.

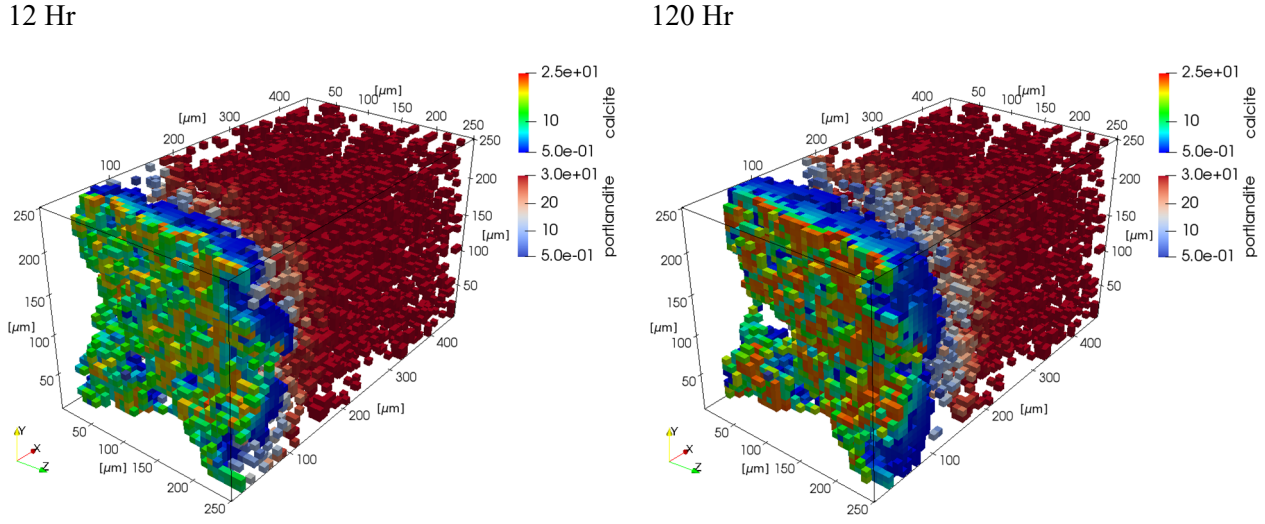

Fig. 5.4: Visualisation of calcite and portlandite molal concentrations after 12 and 120 hours of reaction in cement paste microstructure. Only volume elements containing calcite and portlandite higher than 0.5 M are shown (Patel et al. 2019).

5.5 References

Dähn R., Arakcheeva A., Schaub P., Pattison P., Chapuis G., Grolimund D., Wieland E., Leemann A. (2016)
Application of micro X-ray diffraction to investigate the reaction products formed by the alkali–silica reaction in concrete structures. Cement and Concrete Research 79, 49-56.

Dilnesa B. Z., Lothenbach B., Le Saout G., Renaudin G., Mesbah A., Filinchuk Y., Wichser A., Wieland E. (2011)
Iron in carbonate containing AFm phases. Cement and Concrete Research 41, 311-323.

Dilnesa B. Z., Lothenbach B., Renaudin G., Wichser A., Wieland E., Jennings H. (2012)
Stability of monosulfate in the presence of iron. Journal of the American Ceramic Society 95, 3305-3316.

Dilnesa B. Z., Lothenbach B., Renaudin G., Wichser A., Kulik D. A. (2014)
Synthesis and characterisation of hydrogarnet $Ca_3(Al_xFe_{1-x})_2(SiO_4)_y(OH)_{4(3-y)}$. Cement and Concrete Research 59, 96-111.

Diomidis N., Cloet V., Leupin O. X., Marschall P., Poller A., Stein M. (2016)
Production, consumption and transport of gases in deep geological repositories according to the Swiss disposal concept. Nagra Technical Report NTB 16-03, Nagra, Wettingen, Switzerland.

Duguid A., Scherer G. W. (2010)
Degradation of oilwell cement due to exposure to carbonated brine. International Journal of Greenhouse Gas Control 4, 546–60.

Gaona X., Dähn R., Tits J., Scheinost A. C., Wieland E. (2011)
Uptake of Np(IV) by C-S-H phases and cement paste: An EXAFS study. Environmental Science and Technology 45, 8765-8771.

Geng G., Shi Z., Leemann A., Glazyrin K., Kleppe A., Daisenberger D., Churakov S. V., Lothenbach B., Dähn R., Wieland E. (2019a)
Atomistic structure of alkali-silica reaction products refined from X-ray diffraction and micro X-ray absorption data. Cement and Concrete Research (in press).

Geng G., Shi Z., Leemann A., Borca C., Huthwelker T., Glazyrin K., Pekov I. V., Churakov S. V., Lothenbach B., Dähn R., Wieland E. (2019b)
Mechanical behavior and phase change of alkali-silica-reaction products under hydrostatic compression. Acta Crystallographica B (submitted).

Kosakowski G., Berner U., Wieland E., Glaus M., Degueldre C. (2014)
Geochemical evolution of the L/ILW near field. Nagra Technical Report NTB 14-11, Nagra, Wettingen, Switzerland.

Mancini A., Wieland E., Geng G., Dähn R., Skibsted J., Wehrli B., Lothenbach B. (2019a)
Fe(III) uptake by calcium silicate hydrates. Applied Geochemistry (in press).

Mancini A., Wieland E., Geng G., Dähn R., Wehrli B., Lothenbach B. (2019b)
Fe(II) interaction with cement phases. Cement and Concrete Research (in preparation).

Merz C., Hunkeler F., Griesser A. (2006)
UWEK, Forschungsauftrag AGB2001/471, Bericht Nr. 599, Bern.

Nagra (2014)
Modellhaftes Inventar für radioaktive Materialien MIRAM 14. Nagra Technical Report NTB 14-04, Nagra, Wettingen, Switzerland.

Nagra (2016)
Waste management programme 2016 of the waste producers. Nagra Technical Report NTB 16-01, Nagra, Wettingen, Switzerland.

Patel R. A. (2016)
Lattice Boltzmann method based framework for simulating physico-chemical processes in heterogeneous porous media and its application to cement paste, PhD thesis, Ghent University, Ghent, Belgium.

Patel R. A., Churakov S. V., Prasianakis N. I. (2019)
A multi-level pore-scale reactive transport model for the investigation of combined leaching and carbonation of cement paste. Cement and Concrete Composites (submitted).

Shi Z., Geng G., Leemann A., Lothenbach B. (2019)
Synthesis, characterisation, and water uptake property of alkali-silica reaction products. Cement and Concrete Research 121, 58-71.

Van Breugel K. (1995)
Numerical simulation of hydration and microstructural development in hardening cement paste (II): Applications. Cement and Concrete Research 25, 522-530.

Vespa M., Wieland E., Dähn R., Lothenbach B. (2015)
Identification of the thermodynamically stable Fe-containing phase in aged cement pastes. Journal of the American Ceramic Society 98, 2286-2294.

Wieland E. (2014)
Sorption data base for the cementitious near field of L/ILW and ILW repositories for performance assessment. Nagra Technical Report NTB 14-08, Nagra, Wettingen, Switzerland.

Zubkova N. V., Filinchuk Y. E., Pekov I. V., Pushcharovsky D. Y., Gobechiya E. R. (2010)
Crystal structures of shlykovite and cryptophyllite: comparative crystal chemistry of phyllosilicate minerals of the mountainite family. European Journal of Mineralogy 22, 547-555.

6 RADIOACTIVE WASTE CHARACTERISATION

Wieland E., Curti E., Kulik D.A., Tits J., Kunz D., Laube A., Guillemot T. (postdoc), Miron D.G. (postdoc)

6.1 Introduction

This chapter summarises the research activities related to the characterisation of radioactive waste materials, currently focusing on activated steel, spent fuel and vitrified high-level waste. This project aims at providing important information on the source term (e.g. release rates, speciation) of the radionuclides released from the waste materials in the planned repositories for high-level (HLW) and low- and intermediate-level waste (L/ILW). The source term influences directly and indirectly several safety assessment parameters and calculations related to the other repository compartments (near field, geosphere, biosphere). The source term is a time-dependent parameter strongly affected by the temporal evolution of the waste materials, which are subjected to chemical degradation processes, such as corrosion of irradiated (i.e. activated) steel, (bio-)chemical degradation of organic matter, or the dissolution of spent fuel and vitrified high-level waste. Besides changes caused by the evolution of the physical-chemical conditions, such as pH, temperature and redox potential, time dependence of radionuclide release from waste materials is thus a direct consequence of the degradation of waste materials themselves. For this reason, investigations into the waste properties have been identified as an area of research that is important for the Swiss waste disposal programme over the coming years and possibly also beyond the general licence application.

6.2 C-14 Project: Release and speciation of ^{14}C-bearing compounds

Carbon-14 (radiocarbon) is an important radionuclide in the inventory of radioactive waste produced worldwide and a significant dose-contributing radionuclide in safety assessments for deep geological L/ILW repositories due to its long half-life (5730 y) (Johnson & Schwyn 2008; Nagra 2002; Nuclear Decommissioning Authority 2012; Yim & Carron 2006). ^{14}C has to be taken into account in safety assessments for various reasons: i) ^{14}C can be present both as dissolved and gaseous species in the disposal facility and the host rock, ii) gaseous and dissolved ^{14}C-bearing organic compounds readily migrate in the near field and the geosphere due to weak interaction with mineral surfaces in alkaline to near neutral conditions, and iii) ^{14}C can be incorporated in the human food chain. Hence, the chemical form of the ^{14}C-containing species dictates the routes of ^{14}C migration in the engineered barrier system of a deep geological repository and the surrounding host rock, and therefore determines the long-term contribution of ^{14}C to dose release from a repository for radioactive waste.

Activated steel is the main source of ^{14}C in the radioactive waste produced in Switzerland. The formation of ^{14}C is primarily caused by the activation of nitrogen impurities contained in nuclear fuel and metal components of the core structural materials based on the nuclear reaction ^{14}N(n,p)^{14}C. Very limited information is available on the ^{14}C speciation upon release from corrosion of activated steel (Wieland & Hummel 2015; Swanton et al. 2015). Current safety assessments are still based on specific, simplifying assumptions regarding the ^{14}C speciation. The aim of this project is to determine i) the release of ^{14}C-bearing organic compounds from waste materials (e.g. during the corrosion of activated steel) and their speciation, and ii) the chemical stability of dissolved organic compounds in repository relevant conditions.

Acknowledgement: Compound-specific radiocarbon analysis (CSRA) is being developed in co-operation with Prof. Dr. S. Szidat, Dr. G. Salazar and M. Rauber (Department of Chemistry & Biochemistry at the University of Bern, Switzerland). The project has been partially funded by Nagra in the framework of an ongoing postdoc study (Dr. T. Guillemot: *"Carbon-14 project: Investigation of the C-14-containing species released during corrosion of irradiated steel"*).

6.2.1 Identification and quantification of organic compounds during anoxic iron corrosion

We have carried out batch-type corrosion experiments with non-activated steel powders that provide information on the carbon species produced in iron-water systems during anoxic iron corrosion. The results from this study support the development of analytical methods required in connection with the corrosion experiment with activated steel and give insight into the processes leading to the formation of reduced and oxidised carbon species during anoxic iron corrosion (Cvetković et al. 2018a). In the current stage of the project, the release of carbon compounds from pre-corroded carbon-containing zero-valent iron (ZVI) powders was studied in batch-type corrosion experiments (Guillemot et al. 2019). The ZVI powders were pre-corroded by different oxidative treatments. The commercially available ZVI powder was first pre-

treated by an acid wash in N_2-purged 1 M hydrochloric acid (HCl) for 30 min, supposed to impose mildly oxidative conditions. Portions of the pre-treated powder were further subjected to an accelerated oxidative treatment by suspending them in ultrapure water that was continuously purged with compressed air for one or two weeks, respectively. This led to the formation of increasing amounts of iron corrosion products on the surface. The powders were immersed in NaOH solution (pH = 11.0 and 12.5) prepared with N_2-purged ultrapure water to prepare head-space free samples. The carbon compounds formed during corrosion of the ZVI powders were monitored for 28 days. The results showed that the type of carbon species formed was influenced neither by the different types of oxidative pre-treatments nor by the pH of the alkaline solution. Furthermore, the same carbon species were observed in a previous study with the acid-treated ZVI powder immersed in Ca-containing cement-type pore solution at pH = 12.5 (Cvetković et al. 2018a). In the gas phase, hydrocarbons (HCs) containing up to 7 carbon atoms were identified, while in the liquid phase, carboxylic acids containing up to 3 carbon atoms were detected.

Deng et al. (1997) demonstrated that carbon initially present as impurity in ZVI powders is the source of the HCs produced during iron corrosion. The authors further speculated that the formation of HCs occurs according to a Fischer-Tropsch (F-T) type process. Nevertheless, conclusive evidence of this hypothesis was not provided. The F-T-type process corresponds to the polymerisation reaction of carbon on the surface of metal catalysts (Fischer & Tropsch 1923). The distribution of HCs consisting of *n* carbon atoms can be described by the Anderson-Schultz-Flory (ASF) equation (Anderson et al. 1956), which allows the mole fraction of the molecules having a chain length *n* to be predicted as function of the growth probability factor α of the chain. The latter factor is determined by the rates of propagation and termination of chain growth, which are independent of the chain length (Van der Laan & Beenackers 1999). Based on the ASF equation the HC mass fractions can be displayed as a function of the chain growth probability factor α (Fig. 6.1). In Fig. 6.1, the modelled distribution of HCs are shown along with the experimentally determined HC mass fractions for chain lengths C1, C2-C4 and C5-C7. The results show that experimental and modelled data agree well for α values ranging between 0.5 and 0.7. The latter range of the growth probability factor was determined for catalytic iron surfaces (e.g. Van der Laan & Beenackers 1999). The good agreement of predicted and experimental data within the α range representative of catalytic iron surfaces provides evidence that HCs are formed by a F-T-type mechanism during anoxic iron corrosion.

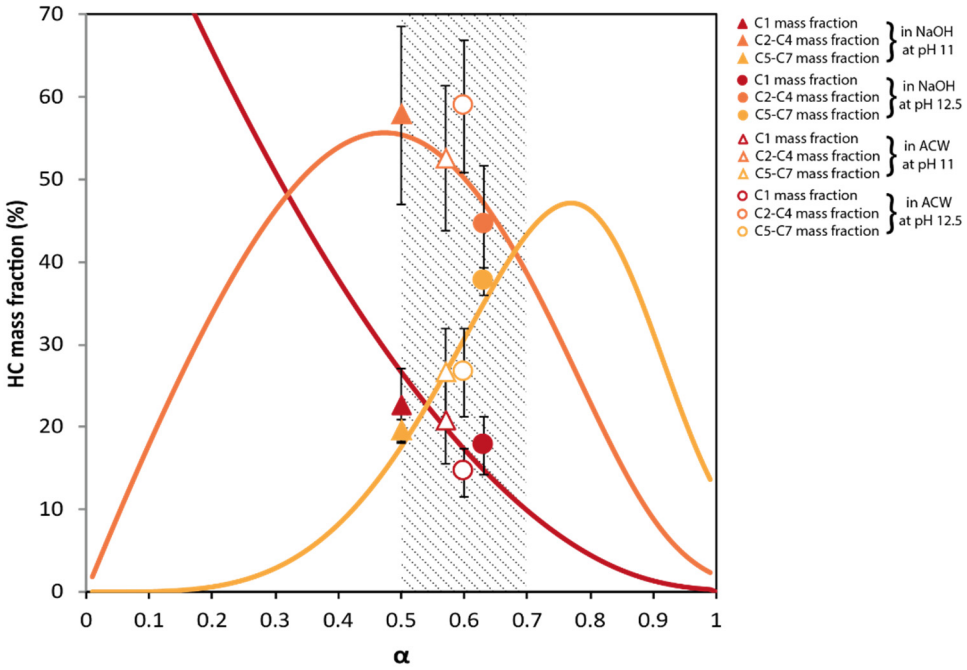

Fig. 6.1: HCs distribution as a function of the chain growth probability factor α. The lines represent the modelled data according to Van der Laan & Bernackers (1999). In red: the HC with one carbon atom (i.e. methane), in orange: the HCs with between two and four carbon atoms, and in yellow: the HCs with between five and eleven carbon atoms. Experimental data are illustrated by symbols with error bars: C1 (in red), C2-C4 (in orange), C5-C7 (in yellow). The mass fractions were calculated from HC concentrations determined during the corrosion of the acid-washed ZVI powder immersed in NaOH (full symbols) and Ca-containing cement-type pore solution (empty symbols) at pH 11 (triangles) and at pH 12.5 (circles) (data from Cvetković et al. (2018a) and Guillemot et al. (2019)). The shaded area highlights the expected range of α on catalytic iron/steel surfaces according to Van der Laan & Bernackers (1999).

In the previous study reported by Cvetković et al. (2018a), also the presence of oxidised compounds, in particular carboxylic acids, was observed during the anoxic corrosion of ZVI powders. So-called iron exchange and solution exchange experiments were carried out with the aim of identifying the process leading to the formation of the oxidised carbon compounds. In the iron exchange experiments, acid-treated ZVI powder was immersed in NaOH. After equilibration for three days, the solution was withdrawn from the vial and injected into a second vial containing fresh acid-treated ZVI powder. The procedure was repeated three times. It was expected that the first contact of ZVI with solution also removes residual oxygen possibly present in the N_2-purged ultrapure water used to prepare the NaOH solution by oxic corrosion. The concentration of carboxylic acids was determined in aliquots obtained from a parallel series of exchange experiments carried out in the same manner. The result show a steady increase in the concentrations of carboxylic acids after each exchange cycle (Fig. 6.2a). This finding indicates that the formation of carboxylic acids cannot be assigned to the oxidation of carbon bound in the ZVI powder as the presence of residual oxygen in solution after the first exchange can be excluded. In the solution exchange experiments the NaOH solution was replaced in the same vial containing the ZVI powder and analysed for carboxylic acids after each replacement. The results show that the latter compounds are released to solution by a rapid process of desorption accomplished within three days (Fig. 6.2b). The results from both studies agree with those reported by Cvetković et al. (2018a) who postulated that oxidised carbon compounds are formed during exposure of ZVI to oxic conditions, accommodated in the oxide layer on the surface of ZVI and then rapidly released from the oxide layer in contact with solution.

6.2.2 Corrosion experiment with activated steel

A well-controlled corrosion experiment with activated steel that is immersed in anoxic alkaline solution under a N_2 atmosphere in a gas-tight reactor is currently running (Wieland et al. 2018). Several samplings of the liquid phase have been carried out in the first two years of the experiment since it was started in May 2016. The development of a very sensitive analytical method based on compound-specific radiocarbon analysis (CSRA) was required due to the very low ^{14}C concentrations released to solution during corrosion of the two 1 g specimens prepared from an activated steel nut. The extremely low ^{14}C concentrations are due to the very low corrosion rate of activated steel in alkaline cement-type pore solution ($Ca(OH)_2$ saturated solution, pH = 12.5), the limited sample size (two 1 g specimens) and the relatively low ^{14}C inventory of the activated steel nut specimens mounted in the reactor. CSRA has been developed to determine the total organic ^{14}C content ($TO^{14}C$) of the solution and to identify and quantify the ^{14}C-bearing compounds present in the liquid phase. The analytical approach is based on the separation of individual compounds with liquid chromatography and ^{14}C quantification by ^{14}C accelerator mass spectrometry (AMS) (Cvetković et al. 2018b). CSRA allowed us to successfully determine the $TO^{14}C$ in several samplings and to identify and quantify ^{14}C-containing carboxylic acids as the main ^{14}C carriers present in the liquid phase (Cvetković et al. 2018c).

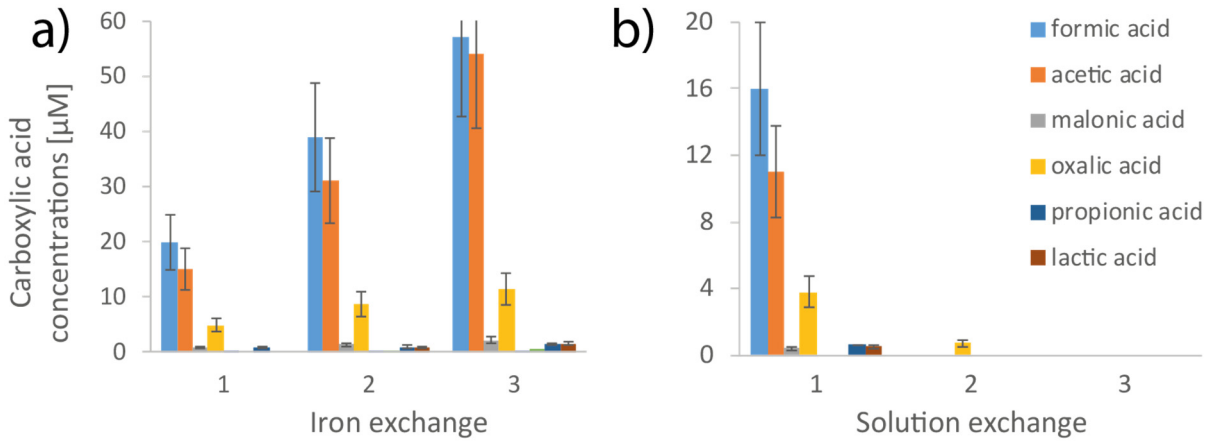

Fig. 6.2: a) Concentrations of dissolved carboxylic acids determined in the iron exchange experiments. b) Concentrations of carboxylic acids determined in the solution exchange experiments. Both graphs illustrate the experiments with ZVI pre-corroded in air-saturated water for one week and immersed in NaOH at pH 11.

6.2.3 Development of CSRA for gaseous compounds

In 2019, we focused on the final development of CSRA for the gaseous ^{14}C-containing compounds. It is expected that in addition to oxidised ^{14}C-bearing carbon species present in the liquid phase, also small ^{14}C-containing HCs, such as methane, ethane, etc. are formed in course of the corrosion of activated steel. The batch-type corrosion studies with non-activated steel powders showed that only a limited number of HCs are formed during steel corrosion (Cvetković et al. 2018a). It is further expected that only small HCs with less than 7 carbon atoms are present at significant concentrations (Guillemot et al. 2019).

The development of a CSRA for the gaseous compounds is based on the separation of individual ^{14}C-bearing compounds by gas chromatography (GC) and ^{14}C quantification by AMS. The AMS measurements were carried out with the MIni CArbon DAting System (MICADAS) operated at the Laboratory for Radiocarbon Analysis (LARA) at the University of Bern. Fig. 6.3 schematically shows the analytical set-up of the GC system operated by LES in the Hotlab of PSI. The use of GC allows us to separate the HCs from each other. The individual HCs compounds are oxidised in a combustion oven to $^{14}CO_2$ and collected in separate sampling loops of the fraction collector. The latter device can be connected to the AMS, and $^{14}CO_2$ directly injected into the AMS through the gas interface system (Fig. 6.3).

CSRA requires that a minimal amount of ^{12}C is injected into the GC, trapped in the fraction collector and finally released into the AMS in order to obtain reliable and reproducible measurements of the $^{14}C/^{12}C$ ratio by the AMS. First tests showed that injection of 20 µg stable carbon into the GC system was too low indicating that a portion of stable carbon was lost between the initial injection into the GC and ^{12}C detection by the AMS. This loss could occur either during passing through the oxidation oven connected to the GC, in the fraction collector or during release of stable carbon from the sampling loops of the fraction collector into the AMS. A series of tests were carried out to identify the reason for the loss of stable carbon and optimise injection of stable carbon. Once the gaseous compounds have passed the first separation column of the GC, they pass through the oxidation reactor to be oxidised to CO_2 (or $^{14}CO_2$, respectively) and a reduction oven, which eliminates traces of oxygen and nitrous oxides (Fig. 6.3). The efficiencies of both ovens were checked and no loss of stable carbon was quantified when passing these devices. Subsequently, CO_2 passes through a water separator to remove traces of water and through a second, short GC column, which allows CO_2 to be separated from non-oxidised hydrocarbons before being detected by the thermal conductivity detection system (TCD). Eventually, CO_2 is collected in the sampling loops of the fraction collector. Gas tightness of each loop was tested by injecting 20 µg CH_4 into the GC and by determining the resulting concentration of CO_2 in the each of the seven loops after 1 hour and 3 days of storage. The areas of the CO_2 peaks recorded by a NDIR CO_2 sensor (Non Dispersive Infra-Red sensor) were identical within the uncertainty, showing that all sampling loops were gas-tight. Eventually, injection of the gas samples into the GC was identified as the main source of stable carbon loss in the device, more specifically the setting of the split mode used before gas injection into the GC column. The setting was tested by filling the gas standard loop with 20 µg of fossil CH_4 and the sample loop with 0.5 mL N_2 (Fig. 6.3). CH_4 and N_2 were simultaneously injected into the

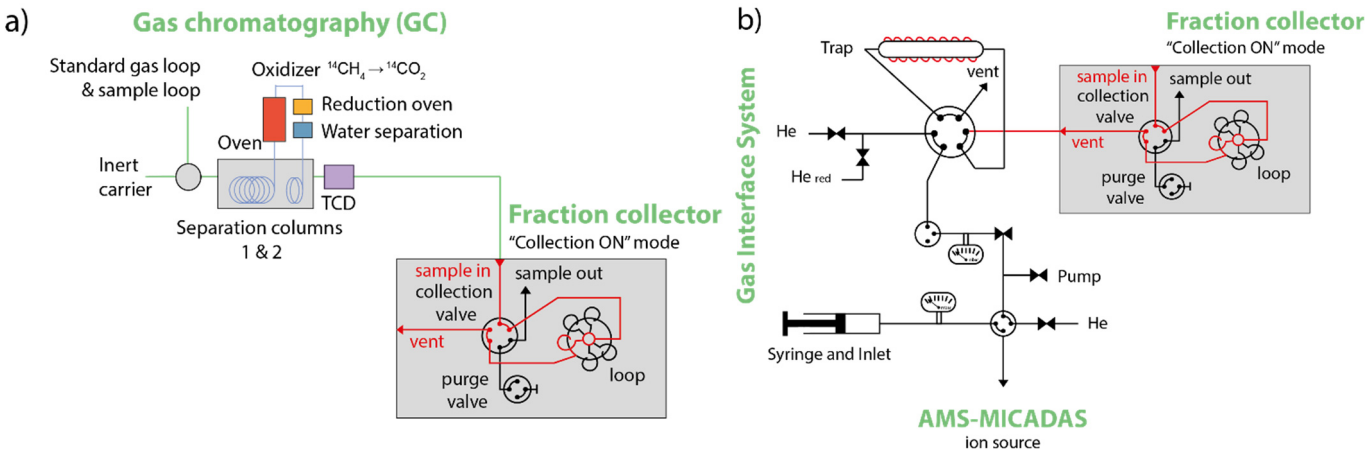

Fig. 6.3: a) Set-up of the GC system and fraction collector used to separate and collect the ^{14}C-bearing HCs. b) Connection between the fraction collector and the AMS through the gas interface system (GIS).

GC injector by applying a split mode with a splitless time of 1 min. During this time, the split line is closed and CH_4 and N_2 are stored in the liner before being injected into the GC column (Fig. 6.4a). After 1 min, the split line re-opens and CH_4 and N_2 present in the liner are flushed out through the split outlet. It was observed that a splitless time of 1 min resulted in a cut peak shape, both for CH_4 and N_2, as recorded by the TCD (Fig. 6.4b), which corresponds to the observed loss of stable carbon (~25%). Increasing the splitless time to 2 min, however, allowed us to collect the entire amount of 20 µg CH_4 injected via the standard loop as CO_2 in the AMS, thus avoiding any loss of stable carbon in the course of the separation and detection procedure. Nevertheless, as already indicated by Fig. 6.4b, the increased split time had a detrimental effect on the fractionation of the individual compounds as co-elution of some gaseous compounds occurred (data not shown). As a consequence, the split mode with a splitless time of 1 min was retained, while the amount of stable carbon injected was increased by developing a sample injection loop with a larger volume. Further optimisation of the procedure eventually showed that increasing the amount of injected stable carbon from 20 to 50 µg resulted in stable and reproducible measurements of the $^{14}C/^{12}C$ ratio by the AMS.

6.2.4 Speciation of ^{14}C during corrosion of activated steel

The development of CSRA for the gaseous compounds allowed us to determine the concentration of ^{14}C-containing carbon compounds both in the gas and in liquid phase, which were sampled in June 2019 after 1114 days corrosion experiment with the activated steel nut specimens.

CSRA of the solution was carried out as reported elsewhere (Cvetković et al. 2018b, 2018c). The total organic ^{14}C content ($TO^{14}C$) of the solution accounts for the total concentration of ^{14}C carried by the aqueous organic compounds. Formate, acetate, malonate, oxalate and lactate were identified as the ^{14}C-containing carboxylic acids (Fig. 6.5a). Interestingly, malonate had the highest concentration, while in the previous solution samplings ^{14}C-bearing formate, acetate and lactate were the most abundant carboxylates detected in solution (Cvetković et al. 2018c). In the current measurement, the $TO^{14}C$ corresponds to the sum of the concentrations of all ^{14}C-containing carboxylates (Fig. 6.5a). We were also able to quantify the inorganic ^{14}C fraction attributed to the presence of ^{14}C-bearing carbonate ($TI^{14}C$). The analytical method for $TI^{14}C$ measurements was developed at the University of Bern (Rauber 2018). The results show that the organic ^{14}C content ($TO^{14}C$) was higher as compared to the inorganic ^{14}C content ($TI^{14}C$), i.e. 55% versus 45% (Fig. 6.5a). By using the new analytical method described in the previous section, we were able to identify for the first time the ^{14}C-bearing gaseous compounds and the total ^{14}C concentration in the gas phase resulting from the anoxic corrosion of activated steel. ^{14}C-bearing methane was identified and quantified as the only ^{14}C carrier in the gas phase. The concentration of ^{14}C-bearing ethane was found to be close to the detection limit of the analytical method. Furthermore, the total ^{14}C content in the gas phase agreed well with the concentration of ^{14}C-bearing methane. Hence, check of the mass balance corroborates that ^{14}C-bearing methane was the only relevant ^{14}C carrier in the gas phase.

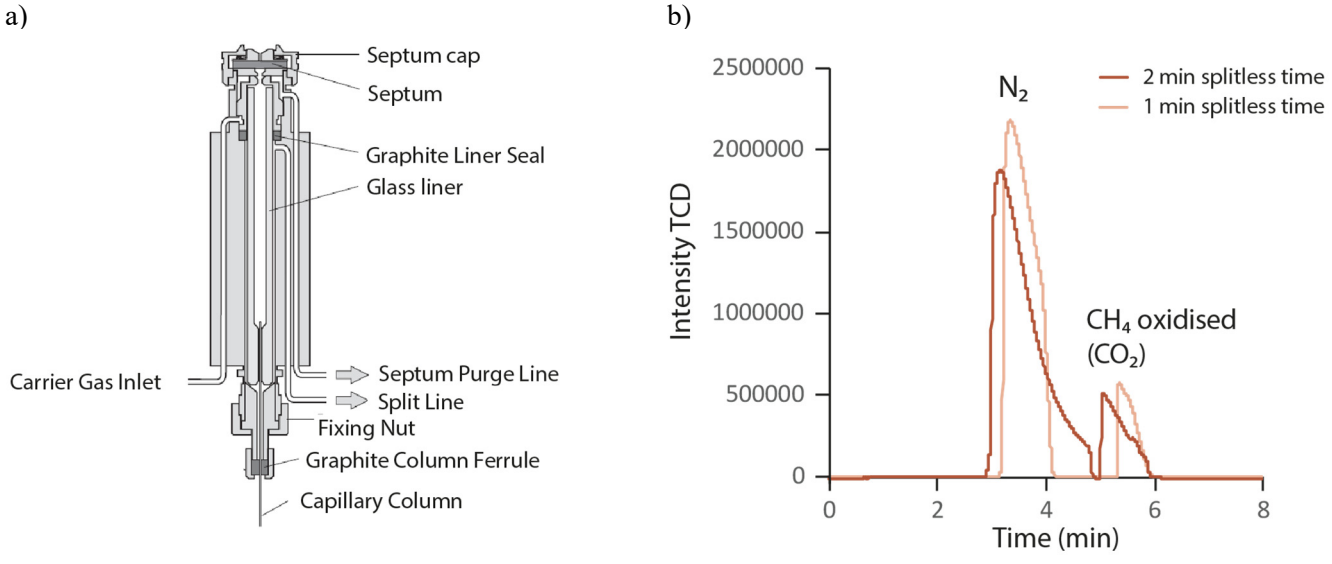

Fig. 6.4: a) Sketch of a split/splitless injector. B) Detection of N_2 and CO_2 peaks recorded by the TCD for two different splitless periods.

The ^{14}C inventory in the gas phase contributed to about 33% of the total ^{14}C inventory released to gas and liquid phase in the reactor after 1114 days corrosion of the activated steel nut specimens. Note, however, that the proportion of the ^{14}C inventory in the gas phase is expected to slowly increase with time in line with the very low corrosion rate of activated steel in highly alkaline conditions (estimated rate ≤ 1 nm/a based on our results). By contrast, the proportion of $TO^{14}C$, and presumably also $TI^{14}C$, is expected to be constant with time as the aqueous ^{14}C-containing carbon compounds result from instantaneous release of oxidised carbon species from the oxide layer of steel in the very first contact with solution rather than being the product of the continuous corrosion process of activated steel (see section 6.2.1). The latter conclusion has to be further substantiated by analysing the gaseous and aqueous ^{14}C-containing carbon compounds in future samplings.

6.2.5 Chemical stability of organic compounds in repository relevant conditions

The anoxic corrosion of activated steel in the near field of a L/ILW repository will be accompanied by the release of significant quantities of ^{14}C-containing low molecular weight (LMW) carbon compounds, such as ^{14}C-containing formate and acetate. Both the batch-type corrosion studies with non-activated ZVI powders and the corrosion experiments with activated steel reported in the previous sections support the hypothesis that the latter compounds will be present in the alkaline pore water of a cement-based L/ILW repository (Figs. 6.2 and 6.5). At ambient temperature and pressure, however, these LMW organics are expected to be metastable in accordance with presently available thermodynamic data, and they are expected to decompose into $^{14}CO_2$ and $^{14}CH_4$ (Wieland & Hummel 2015). The latter process would result in the undesired release of ^{14}C from the repository via the gas phase. It is generally accepted that, under the moderate temperatures (<65°C) and pressures (<8 MPa) prevailing in the cementitious near field of a L/ILW repository, the decomposition reaction will proceed very slowly. However, there are indications in the literature that the decomposition of formate and acetate via decarboxylation (formation of CO_2 and H_2 in the case of formate and CO_2 and CH_4 in the case of acetate) might be catalysed in presence of stainless steel surfaces and Fe oxides (Tits & Wieland 2019). Predictions based on decomposition rate constants extrapolated from high temperature (448K – 533K) kinetic experiments using the Arrhenius equation suggested that formate should decompose completely within a period of 50 years at an initial concentration of 10^{-3} M (Tits & Wieland 2019). However, extrapolations over such large temperature intervals bear very large uncertainties. The decomposition of formate and acetate under highly alkaline, anoxic and reducing conditions are currently being studied with the aim of gaining insight into the stability of formate and acetate under the conditions relevant to a cement-based L/ILW repository and into the effects of temperature and the presence of iron as a catalyst on the decomposition reactions.

In previous years, the stability of formate was investigated in pressurised reactors under anoxic conditions (N_2 atmosphere) and under slightly reducing conditions (2 atm forming gas (FG, 95% N_2/ 5% H_2)) at a total pressure of 5.5 bar and a temperature of 150°C to accelerate potential decomposition reactions. ^{13}C- and ^{14}C-labelled formate were used to allow differentiation between LMW organic compounds originating from the degradation of formate and those originating from organic contaminants present in the reactor (LES progress report 2018). These experiments

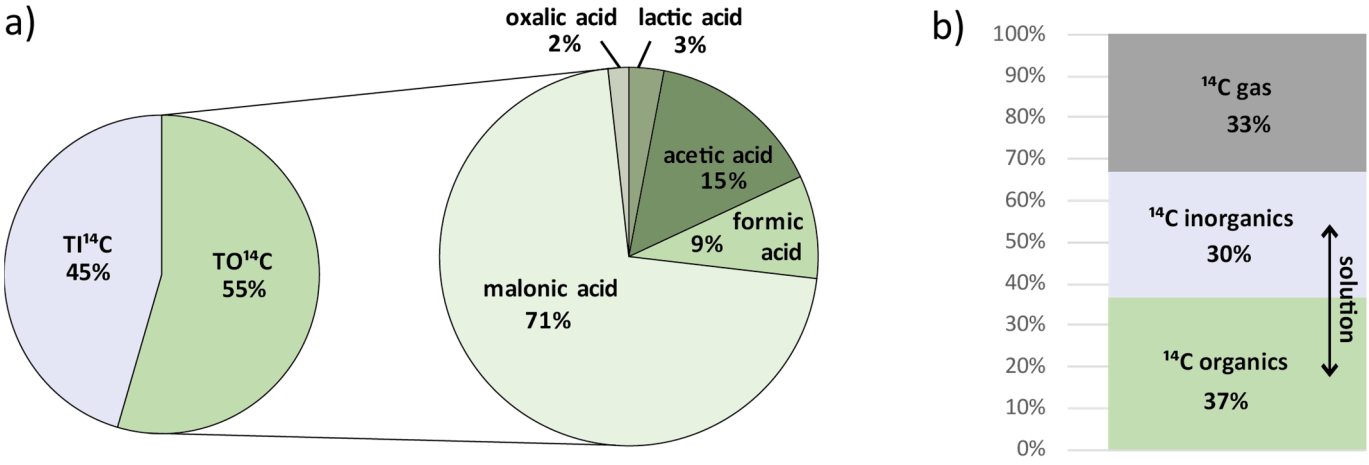

Fig. 6.5: a) Inventory of the ^{14}C species present in the solution sampled after 1114 days corrosion experiment with activated steel; b) proportion of ^{14}C-bearing, aqueous and gaseous compounds present in the reactor after 1114 days of corrosion of activated steel.

showed that ^{13}C-labelled formate was stable over a period up to eight months in deionised ultrapure water (Milli-Q H_2O) whereas under alkaline conditions, in the presence of $Ca(OH)_2$, a decrease of the concentration of ^{13}C-labelled formate was observed with time. This decrease was more pronounced at higher $Ca(OH)_2$ concentrations and became negligible at $Ca(OH)_2$ concentrations below the $Ca(OH)_2$ solubility limit (~3×10^{-3} M at a temperature of 150°C). It further appeared that the H_2 partial pressure in the reactor did not affect the stability of ^{13}C-labelled formate. The observed reduction in the aqueous concentrations of ^{13}C-labelled formate was tentatively interpreted in terms of the formation of ^{13}C-labelled carbonate originating from the decomposition of ^{13}C-labelled formate, and co-precipitation of $^{13}CO_3^{2-}$ with $Ca(OH)_2$ in the systems that were oversaturated w.r.t. $Ca(OH)_2$(s). Indeed, in an experimental system supersaturated with $Ca(OH)_2$(s) ([$Ca(OH)_2$] = 0.005 M), a significant portion of the missing ^{13}C-labelled compounds (~26 mol %) was recovered as $^{13}CO_2$ in the gas phase after thoroughly washing the reactor with 0.1 M HCl. However, 63 mol % of the initial ^{13}C-labelled formate could not be recovered. Further efforts undertaken in 2019 to retrieve the missing ^{13}C compounds were not successful.

In addition to the experiments carried out in gas-tight pressurised reactors, stability tests with ^{13}C- and ^{14}C-labelled formate were carried out in autoclaves to investigate the decomposition kinetics, the effects of temperature and the presence of iron. It should be noted that, in contrast to the sophisticated experiments in the pressurised reactors, the design of the autoclaves only allows us to monitor the stability of formate by determining the ^{13}C speciation and ^{14}C concentration (^{14}C-formate and their degradation products) in solution at the end of each experiment. Sampling of solution at different time intervals during the course of the experiment and sampling of the gas phase are not possible. These experiments confirmed the observations made in the stability test with ^{13}C-labelled formate performed in the pressurised reactors, that the aqueous concentration of ^{13}C-labelled formate only decreases in systems supersaturated w.r.t. $Ca(OH)_2$(s) (Fig. 6.6a). Under these conditions, the concentration of ^{13}C-labelled formate steadily decreased with time (Fig. 6.6a) and 70 % of the ^{13}C-labelled formate was degraded within 60 days reaction. It is unlikely that this observation is caused by formate sorption onto $Ca(OH)_2$(s) as formate is present in the anionic chemical form in alkaline conditions and thus sorbs very weakly onto cement phases (Wieland et al. 2016). Carbonate, on the other hand side, is known to show a strong affinity for hydroxide surfaces (e.g. Ruiz-Agudo et al. 2013). It is thus conceivable that ^{13}C-labelled formate is decomposed to carbonate which then reacts with precipitated $Ca(OH)_2$(s). Furthermore, it appears that the amount of Fe powder present in the system and the reaction temperature does not have a significant effect on the degradation of ^{13}C-labelled formate.

Degradation experiments with ^{13}C- and ^{14}C-labelled acetate under similar experimental conditions (20°C < T < 200°C, anoxic or slightly reducing conditions) are ongoing. First results suggest that acetate is stable over periods up to 180 days.

This study will be completed by the end of 2019 and the outcomes will be published in a PSI technical report (Tits et al. 2019).

6.3 Thermodynamics of Cr-doped UO_2 fuels (DISCO project)

In recent years, nuclear power plants have started using chromium-doped UO_2 fuels in commercial Light Water Reactors (LWR). The addition of small amounts of Cr_2O_3 during sintering induces coarsening of UO_2 grain

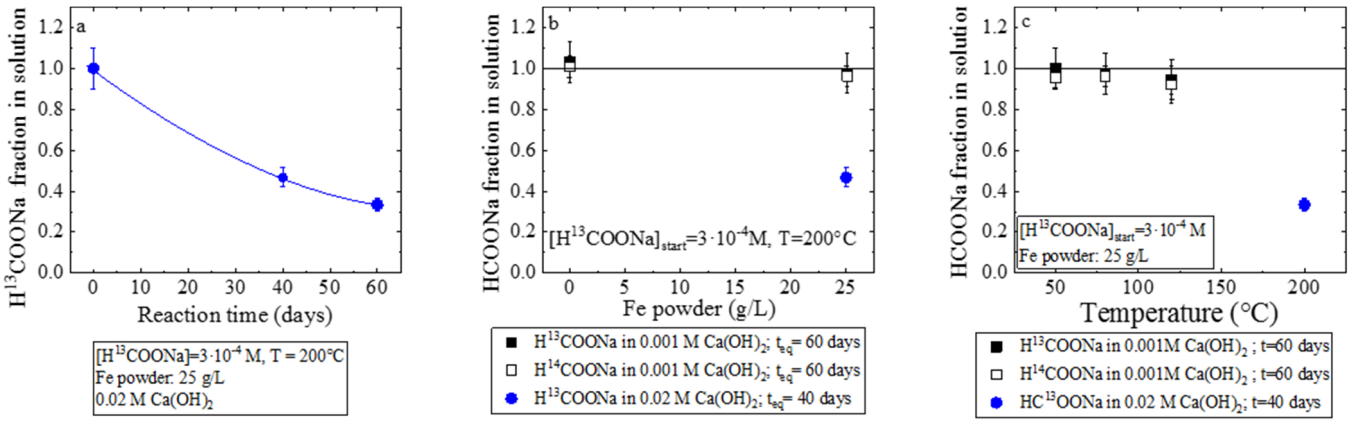

Fig. 6.6: Degradation of ^{13}C- and ^{14}C-labelled formate (HCOONa) under alkaline conditions in autoclaves at elevated temperature and pressure; a) degradation kinetics, b) effect of the presence of Fe(0), c) effect of temperature.

size up to about 60 μm and leads to a higher densification of the fuel material (97.3 % vs. 96.7% of the theoretical UO_2 density, see Arborelius et al. 2006). The larger grain size reduces Fission Gas Release (FGR), allowing the reactor to operate at higher power compared to operation with conventional UO_2 fuel and thus resulting in more efficient energy production.

This technology is recent, consequently scientific knowledge on the behaviour of doped fuels is limited, both under in-pile and out-of-pile conditions. In the framework of the Horizon 2020 EU programme, a collaborative scientific project is running under the acronym DISCO (Modern spent fuel DISsolution and chemistry in failed COntainer conditions) aiming at reducing this knowledge gap. The focus of the project is on fuel degradation in a geological repository for radioactive waste (Evins et al. 2019). The present contribution is embedded in DISCO's modelling package. The major objective is to compare Cr-doped and non-doped UO_2 fuel from the point of view of thermodynamic stability during irradiation in LWRs. Particular emphasis is put on possible consequences for spent fuel behaviour in a geological repository after containment failure.

This was achieved by developing and applying a comprehensive thermodynamic model for both types of fuel, taking into account the effects of solid solution formation, temperature, burnup, as well as internal cladding oxidation. The model allows calculating the fuel oxygen potential under in-pile conditions, from which the stoichiometry of the UO_2 phase (O/M ratio) and the oxidation state of redox-sensitive actinides and fission products (e.g. ^{93}Mo, ^{126}Sn, ^{99}Tc) can be derived. From this information, possible consequences on fuel dissolution rate and radionuclide release in a geological repository can be predicted. For instance, high oxygen potentials in Cr-doped fuel may conceivably lead to fast oxidative dissolution of the fuel and increased solubility of redox-sensitive nuclides, with potentially adverse results on the safety of geological repositories.

After reviewing the literature on Cr substitution in urania, a solid solution model was set up for UO_2 in the subsystem Cr^{III}-U^{IV}-U^{V}-O. This solid solution was then extended to include Pu, minor actinides (Am, Cm, Np) and soluble fission products (La, Nd, Ce). It was implemented by applying the sublattice model of Berman & Brown (1984) in the GEM-Selektor code (Kulik et al. 2013), using thermodynamic data from the in-house HERACLES database. Berman & Brown's model was selected because it allows defining end members compatible with the sublattice structure of UO_2 and with recognised substitution mechanisms. For instance, the selected Cr end member with bulk stoichiometry Cr_2O_3 can be defined with the sublattice formula $Cr_2O_3[Va]_{an}\,[Va]_{int}$ (where $[Va]_{an}$ and $[Va]_{int}$ are vacancies in the oxygen (anionic) and interstitial sublattice, respectively). This formulation is consistent with the fluorite structure of UO_2 and with the dominant Cr substitution mechanism identified in the literature (1 oxygen vacancy formed for each two Cr^{3+} ions substituting U^{4+}). The final UO_2 solid solution consists of 19 end members (Am_2O_3, $AmUO_4$, Ce_2O_3, $CeUO_4$, $(CeO_2)_2$, Cm_2O_3, $CmUO_4$, Cr_2O_3, La_2O_3, $LaUO_4$, Nd_2O_3, $NdUO_4$, $(NpO_2)_2$, $(NpO_{2.5})_2$, Pu_2O_3, $PuUO_4$, $(PuO_2)_2$, $(UO_2)_2$, $(UO_{2.25})_2$), describing mixing of 17 species (Am^{3+}, Ce^{3+}, Ce^{4+}, Cm^{3+}, Cr^{3+}, La^{3+}, Nd^{3+}, Np^{4+}, Np^{5+}, Pu^{3+}, Pu^{4+}, U^{4+}, U^{5+}, $[O^{2-}]_{an}$, $[Va]_{an}$, $[O^{2-}]_{int}$, $[Va]_{int}$) over the aforementioned three distinct sites. The full thermodynamic model for the fuel also includes ideal solid solutions for metallic inclusions (epsilon particles) and $(Sr,Ba)ZrO_3$, as well as a number of one-component phases.

A critical step in the development of the UO_2 solid solution was the calibration of mixing parameters (interaction coefficients) against published experimental data. To this aim, experimental oxygen partial pressure and oxygen potential data (Riglet-Martial et al. 2014; Matsui & Naito 1986; Hagemark & Broli 1967; Stadlbauer et al. 1974; Une & Oguma 1983) were fitted for selected subsystems, leading to the determination of coefficients describing non-ideality interactions of Cr^{3+}, Nd^{3+}, La^{3+} with U^{4+} or/and U^{5+}. Figs. 6.7 and 6.8 illustrate the fitting procedures applied to data for Cr-doped and La-doped urania. For the other species, chemical analogies had to be used to this purpose. A major finding was that a successful fitting of the data for Nd-doped urania was only possible by introducing, besides $Nd^{III}{}_2O_3$, an additional end member with stoichiometry $Nd^{III}U^{V}O_4$ (Fig. 6.9). These two end members reflect the two substitution mechanisms suggested by Ohmichi et al. (1981) for this type of compounds: (a) substitution of two Nd^{3+} into cationic sites, charge-compensated by oxygen vacancy formation (as in the case of Cr^{3+} substitution) and (b) substitution of a single Nd^{3+} with charge compensation by U^{5+}. Analogous end members were introduced for all trivalent species included in the UO_2 solid solution.

Thermodynamic calculations were carried out on model inventories for 1, 23, 42, 53 and 60 GWd/t_{iHM} over a temperature range (400 ºC – 1400 ºC) covering usual in-pile conditions from pellet center to pellet rim in LWRs. The calculated O/M ratios (where M is the sum of U and all dissolved metals) were always close to perfect stoichiometry (O/M = 1.993 to 2.000), in agreement with the experimental findings of Matzke (1994). The computed oxygen potential curves (Ellingham diagrams, Fig. 6.10) indicate that Cr-doping should have no significant effect on the oxidation state of the fuel, except at very low burnup. From 20 GWd/t_{iHM} upward, the calculated oxygen

potentials are well within the field of experimental values and increase with burnup. At burnups above 50 GWd/t_{iHM} the predicted potentials converge and reach maximum limiting values about 5-15 kJ/mol above the Mo-MoO_2 buffer. Further calculations indicated that Zircaloy oxidation at the internal cladding surface could lower the oxygen potential by 40-60 kJ/mol, shifting the calculated oxygen potential curve of 60 GWd/t_{iHM} fuel in Fig. 6.10 in the middle of the region A.

The comparison of the oxygen potential curves obtained with the optimised solid solution model with those obtained from simpler models, in which one-component solids replace the solid solution phases, revealed that the fuel oxygen potential is particularly sensitive to the activity of Mo in metallic inclusions (ε-particles). Therefore, future investigations should focus on the study of mixing properties in such phases.

In conclusion, our calculations indicate that the addition of small amounts of Cr in UO_2 fuels should have no adverse effect under geological storage conditions, such as enhanced radionuclide release due to faster UO_2 dissolution or oxidation of redox-sensitive nuclides.

Acknowledgment: This project has received funding from the European Union's Horizon 2020 research and innovation programme under grant agreement No 755443 - DISCO - NFRP-2016-2017/NFRP-2016-2017-1.

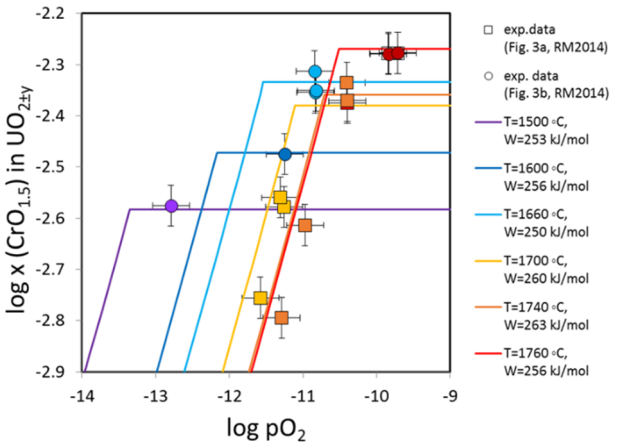

Fig. 6.7: Fits of Cr solubility data (Riglet-Martial et al. 2014). The mixing parameter W (describing the interaction between Cr^{3+} and U^{4+} in Cr-doped UO_2) was the only adjustable parameter in the GEM-Selektor calculations. The sharp kinks in the model curves correspond to the transition from Cr metal to Cr_2O_3 stability field at the specified temperature.

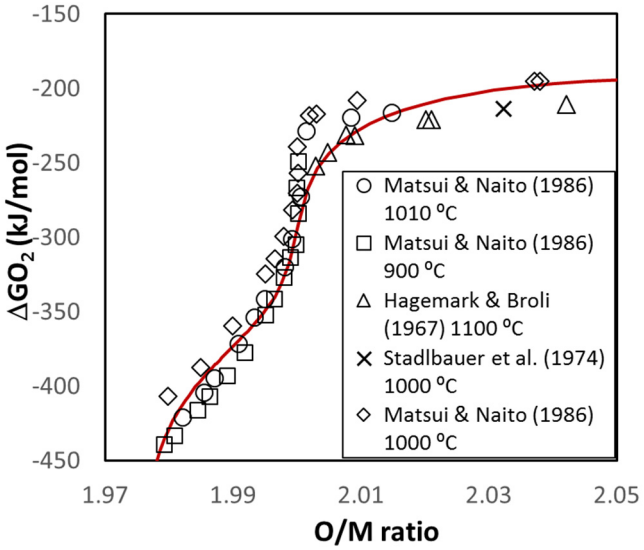

Fig. 6.8: Fit of oxygen potential data for $La_xU_{1-x}O_{2\pm y}$ (x=0.05) measured between 900 °C and 1100 °C. The fit was calculated at 1000 °C by adjusting simultaneously the interaction coefficient between La^{3+} and U^{5+} and the free energy of formation of the solid solution end member $La^{III}U^{V}O_4$, for which no thermodynamic data exist.

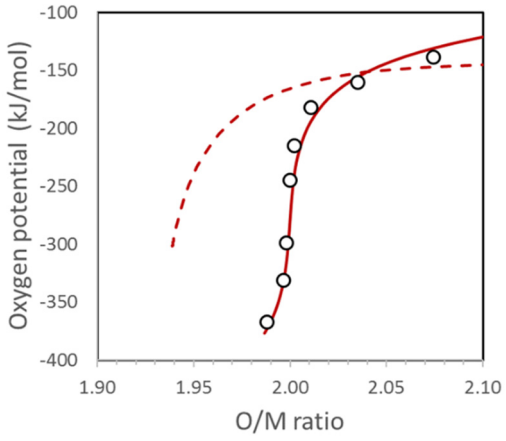

Fig. 6.9: Best fits of oxygen potential data from Une & Oguma (1983) for $Nd_{0.14}U_{0.86}O_{2\pm x}$ measured at 1500 °C, obtained omitting (broken line) or including (continuous line) the $La^{III}U^{V}O_4$ end member. This plot demonstrates that the latter component is necessary in order to model these data correctly.

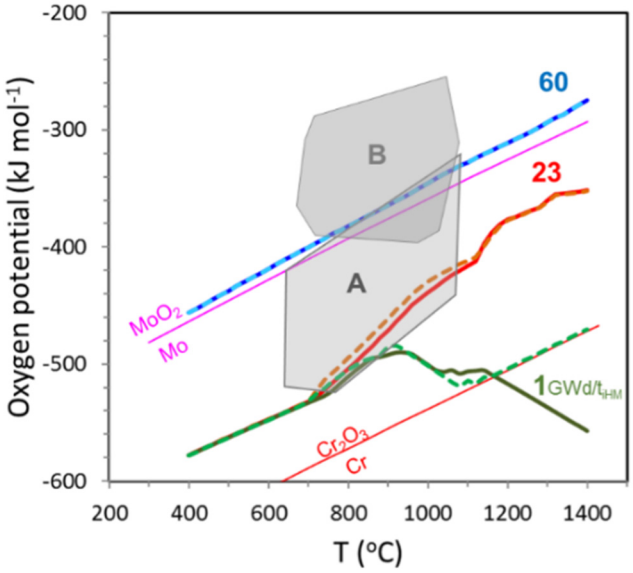

Fig. 6.10: Calculated burnup evolution of oxygen potential for conventional (thick continuous lines) and Cr-doped UO_2 fuel (thick broken lines). The grey fields delimit values of published experimental data for non-doped UO_2 fuels: (A) 13-58 GWd/t_{iHM} (Matzke 1994; Une et al. 1991); (B) 101 GWd/t_{iHM} (Walker et al. 2005). Thin continuous lines show oxygen potentials for selected pure metal/oxide pairs. Numbers on the right denote average fuel burnups assumed in the calculations.

6.4 References

Anderson R. B., Karn F. S., Shultz J. F. (1956)
Factors in sulfur poisoning of iron catalysts in Fischer-Tropsch synthesis. Journal of Catalysis 4, 56-63.

Arborelius J., Backman K., Hallstadius L., Limbäck M., Nilsson J., Rebensdorff B., Zhou G., Kitano K., Löfström R., Rönnberg G. (2006)
Advanced doped UO_2 pellets in LWR applications. Journal of Nuclear Science and Technology 43, 967–976.

Berman R. G., Brown T. H. (1984)
A thermodynamic model for multicomponent melts, with application to the system CaO-$A1_2O_3$-SiO_2. Geochimica et Cosmochimica Acta 48, 661-678.

Cvetković B. Z, Rothardt J., Büttler A., Kunz D., Schlotterbeck G., Wieland E. (2018a)
Formation of low-molecular-weight organic compounds during anoxic corrosion of zero-valent iron. Environmental Engineering Science 35, 447-461.

Cvetković B. Z., Salazar G., Kunz D., Szidat S., Wieland E. (2018b)
Analysis of ^{14}C-containing compounds released by corrosion of irradiated steel using accelerator mass spectrometry. Analyst 143, 3059-3067.

Cvetković B. Z., Salazar G., Kunz D., Tits J., Szidat S., Wieland E. (2018c)
Quantification of dissolved organic ^{14}C-containing compounds by accelerator mass spectrometry in a corrosion experiment with irradiated steel. Radiocarbon 60, 1711-1727.

Deng B. L., Campbell T. J., Burris D. R. (1997)
Hydrocarbon formation in metallic iron/water systems. Environmental Science and Technology 31, 1185-1190.

Evins L. Z., Duro L., Valls A., Corkhill C., Myllykylä E., Farnan I., Bosbach D., Metz V., Maldonado P. (2019)
Spent nuclear fuel dissolution (REDUPP and DISCO) Programme and Abstracts, EURADWASTE'19, 9th European Commission Conference on EURATOM Research and Training in Radioactive Waste Management, Pitesti, Romania, 4-7 June 2019, ISBN 978-92-79-98743-4.

Fischer F., Tropsch H. (1923)
The preparation of synthetic oil mixtures (synthol) from carbon monoxide and hydrogen. Brennstoff-Chemie 4, 276-285.

Guillemot T., Cvetković B. Z., Kunz D., Wieland E. (2019)
Processes leading to reduced and oxidised carbon compounds during corrosion of zero-valent iron in alkaline anoxic conditions. Chemosphere (submitted).

Hagemark K., Broli M. (1967)
Equilibrium oxygen pressures over solid solutions of urania-yttria and urania-lanthana at 1100" to 1400°C. Journal of the American Ceramic Society 50, 563–567.

Johnson L., Schwyn B. (2008)
Proceedings of a Nagra/RWMC workshop on the release and transport of C-14 in repository environments. Nagra Work Report NAB 08-22, Nagra, Wettingen, Switzerland.

Kulik D. A., Wagner T., Dmytrieva S. V., Kosakowski G., Hingerl F. F., Chudnenko K. V., Berner U. (2013)
GEM-Selektor geochemical modeling package: revised algorithm and GEMS3K numerical kernel for coupled simulation codes. Computational Geosciences 17, 1-24.

Matsui T., Naito K. (1986)
Electrical conductivity measurement and thermogravimetric study of lanthanum-doped uranium dioxide. Journal of Nuclear Materials 138, 19-26.

Matzke H. (1994)
Oxygen potential in the rim region of high burnup UO_2 fuel. Journal of Nuclear Materials 208, 18-26.

Nagra (2002)
Project Opalinus Clay - Safety Report. Demonstration of disposal feasibility for spent fuel, vitrified high-level waste and long-lived intermediate-level waste (Entsorgungsnachweis). Nagra Technical Report NTB 02-05, Nagra, Wettingen, Switzerland.

Nuclear Decommissioning Authority (2012)
Geological disposal. Carbon-14 project - Phase 1 Report. Technical Report NDA/RWMD/092, Harwell Oxford, United Kingdom.

Ohmichi T., Fukushima S., Maeda A., Watanabe H. (1981)
On the relation between lattice parameter and O/M ratio for uranium dioxide-trivalent rare earth oxide solid solution. Journal of Nuclear Materials 102, 40-46.

Rauber M. (2018)
Compound-specific radiocarbon analysis of aerosols, Master thesis, Faculty of Science, University of Bern, Bern, Switzerland.

Riglet-Martial Ch., Martin Ph., Testemale D., Sabathier-Devals C., Carlot G., Matheron P., Iltis X., Pasquet U., Valot C., Delafoy C., Largenton R. (2014)
Thermodynamics of chromium in UO_2 fuel: A solubility model. Journal of Nuclear Materials 447, 63-72.

Ruiz-Agudo E., Kudlacz K., Putnis C. V., Putnis A., Rodriguez-Navarro C. (2013)
Dissolution and carbonation of portlandite [$Ca(OH)_2$] single crystals. Environmental Science and Technology 47, 11342-11349.

Stadlbauer E., Wichmann U., Lott U., Keller C. (1974)
Thermodynamics and phase relationships of the ternary lanthanum- uranium-oxygen system. Journal of Solid State Chemistry 10, 341–350.

Swanton S. W., Baston G. M. N., Smart N. S. (2015)
Rates of steel corrosion and carbon-14 release from irradiated steels - state-of-the-art review, European Commission, Brussels, CAST WP2 Deliverable 2.1.

Tits J., Wieland E. (2019)
Stability of formic acid and acetic acid under cementitious near-field conditions. PSI Technical Report TM 44-18-21, Paul Scherrer Institut, Villigen PSI, Switzerland.

Tits J., Kunz D., Wieland E. (2019)
Experimental investigations on the stability of formic acid and acetic acid under cementitious near-field conditions. PSI Technical Report (in preparation).

Une K., Oguma M. (1983)
Oxygen potentials of $(U,Nd)O_{2\pm x}$ solid solutions in the temperature range 1000-1500 °C. Journal of Nuclear Materials 118, 189-194.

Une K., Tominaga Y., Kashibe S. (1991)
Oxygen potentials and lattice parameter of irradiated BWR fuels. Journal of Nuclear Science and Technology 28, 409-417.

Van der Laan G. P., Beenackers A. A. C. M. (1999)
Kinetics and selectivity of the Fischer-Tropsch synthesis. Catalysis Reviews: Science and Engineering 41, 255-318.

Walker C. T., Rondinella V. V., Papaioannou D., Van Winckel S., Goll W., Manzel R. (2005)
On the oxidation state of UO_2 nuclear fuel at a burn-up of around 100 MWd/kgHM. Journal of Nuclear Materials 345, 192-205.

Wieland E., Hummel W. (2015)
Formation and stability of carbon-14 containing organic compounds in alkaline iron-water systems: Preliminary assessment based on a literature survey and thermodynamic modelling. Mineralogical Magazine 79, 1275-86.

Wieland E., Jakob A., Tits J., Lothenbach B., Kunz D. (2016)
Sorption and diffusion studies with low molecular weight organic compounds in cementitious systems. Applied Geochemistry 67, 101-117.

Wieland E., Cvetković B. Z., Kunz D., Salazar G., Szidat S. (2018)
Carbon-14 speciation during anoxic corrosion of activated steel in a repository environment. ATW: international journal of nuclear power 63, 34-37.

Yim M. S., Caron F. (2006)
Life cycle and management of carbon-14 from nuclear power generation. Progress in Nuclear Energy 48, 2-36.

7 THERMODYNAMIC MODELS AND DATABASES

Hummel W., Kulik D.A., Thoenen T., Tits J., Miron G.D. (postdoc)

7.1 Introduction

The aim of this project is to develop thermodynamic models and databases to be applied in the preparation of various reports for the general license application (RBG). Solubility and sorption databases and synthesis reports are an important part of the documentation for RBG.

The timely finalisation of the thermodynamic database is an important task because the carefully selected thermodynamic data provide the basis for defining pore water models, for the solubility databases, the development of the sorption databases and simulation of the repository *in situ* conditions. The consistent and consequent use of the approved thermodynamic dataset throughout all types of thermodynamic calculations is of crucial importance.

The cement sorption database has to be updated by the end of 2022 for use in safety assessments for RBG. In preparation for this report, an experimental study was launched in 2019 to determine the sorption values (R_d) for ^{26}Al, ^{32}Si and ^{41}Ca, safety-relevant radionuclides that had not been taken into account in previous sorption databases.

In connection with the German project THEREDA (Thermodynamic Reference Database), presently funded by BGE (Bundesgesellschaft für Endlagerung), LES is in charge of maintaining the thermodynamic data of the cement system and was this year engaged in updating THEREDA with the thermodynamic data critically evaluated in CEMDATA18 (Lothenbach et al. 2019).

To support the thermodynamic calculations and maintenance of thermodynamic databases, the GEM-Selector (GEMS) code collection has been developed at PSI/LES since 2000 by a community team lead by D. Kulik. The most resent application of GEMS focuses on the development of new solid solution models for calcium silicate hydrate (C-S-H) phases of variable composition. These phases determine the most relevant properties and durability of hydrated cement pastes and concretes.

7.2 Update of the Thermodynamic Data Base (TDB)

A high quality Thermodynamic Data Base (TDB) is currently in place. This database needs to be kept state-of-the-art and remaining gaps need to be filled where this is safety relevant. As the availability of an approved TDB is an essential prerequisite for defining pore water models and for preparing solubility limits and sorption database reports for the next safety assessments related to Nagra's general license application. The TDB needs to be updated and existing gaps have to be filled before work on solubility and sorption databases commences. The development of the solubility and sorption databases is planned for 2021. The current update of the TDB to "TDB 2020" has been planned for the period 2017 – 2020 with a final document to be published in 2021.

The TDB update has been started in 2017 with reviews of Hg (Hummel 2017a), Cu (Thoenen 2017a), Pb (Hummel 2017b), Fe (Thoenen 2017b) and Po (Hummel 2017c). With the exception of Fe all the other elements are new in TDB 2020.

The review work has been continued in 2018 with the update of Sn (Thoenen 2018a) and Nb (Thoenen 2018b), and the review of data for Ti (Thoenen 2018c), Ag (Hummel 2018a), Ac (Hummel 2018b), Pa (Hummel 2018c) and Cf (Hummel 2018d) which are new elements in TDB 2020.

In 2019 the review work further continued with the reviews of Cd (Hummel 2019a), data for ground and pore water models (Hummel 2019b), Pd, silicates, and the rare earth elements Sm, Eu and Ho. Cd, Sm and Ho are new elements in TDB 2020. The TDB revision will be finalised in 2020 with a review of selected organic ligands.

7.2.1 Update of data for ground and pore water models

Chemical thermodynamic data for ground and pore water models in our original data base (Pearson & Berner 1991; Pearson et al. 1992) have been taken from the USGS review of data for major water-mineral reactions (Nordstrom et al. 1990) and basically have not been changed since then. However, a state-of-the-art data base including a complete set of temperature parameters is needed for properly defining Opalinus Clay pore waters in the temperature range 40 – 60 °C and for defining bentonite pore waters for even somewhat higher temperatures.

Thermodynamic data for species containing the metals Li, Na, K, Mg, Ca, Sr, Ba, Mn(II,III,IV), Al and the ligands OH^-, F^-, Cl^-, CO_3^{2-}, HCO_3^- and SO_4^{2-} have now been reviewed with special emphasis on temperature data (Hummel 2019b). Thermodynamic data for Fe have already been reviewed in 2017 (Thoenen 2017b).

In summary, a complete set of thermodynamic data for all relevant aqueous species and solids for ground and pore water models is now available (Tab 7.1).

Considering that the interactions of chloride with most cations, and of K with fluoride, are so weak that no complex formation could be defined, and that Mn(III) aqueous species may only be of relevance in fairly acidic solutions, the thermodynamic data sets for hydroxide, fluoride, chloride and sulphate aqueous species are complete.

In the case of carbonate, no experimental data for Li^{+}, Al^{3+} (and Mn^{3+}) complexation have been documented in the literature so far. However, Li and Al carbonate complexes are expected to be weak, and Fe(III) carbonate complexes may only play a role at fairly high carbonate concentrations. For Fe^{3+} carbonate complexes, no temperature data are available, and there is no suitable chemical analogue for an empirical estimation of the complexation constants.

Stability constants and temperature parameters are available for all relevant oxide and hydroxide solids i.e. for brucite, $Mg(OH)_2$, portlandite, $Ca(OH)_2$, gibbsite, $Al(OH)_3$, and boehmite, AlOOH, hematite, Fe_2O_3, goethite, α-FeOOH, lepidocrocite, γ-FeOOH, magnetite, Fe_3O_4, manganosite, MnO, pyrochroite, $Mn(OH)_2$, bixbyite, Mn_2O_3, manganite, MnOOH, hausmannite, Mn_3O_4, and pyrolusite, MnO_2.

In the case of fluoride solids only fluorite, CaF_2, is important in ground and pore water models. The other fluoride solids, some of them known as rare minerals, are not relevant for repository systems as CaF_2 usually limits the concentration of F^- in water and all the other fluoride solids are much more soluble than CaF_2.

All chloride salts of the metals shown in Tab 7.1 are very soluble, and they may only play a role in concentrated brines.

Thermodynamic data for carbonate solids are available for magnesite, $MgCO_3$, calcite, $CaCO_3$, (and aragonite and vaterite, the metastable variants of $CaCO_3$), dolomite, $CaMg(CO_3)_2$, strontianite, $SrCO_3$, witherite, $BaCO_3$, rhodochrosite, $MnCO_3$, siderite, $FeCO_3$, and dawsonite, $NaAlCO_3(OH)_2$.

Thermodynamic data for sulphate solids are limited to anhydrite, $CaSO_4$, gypsum, $CaSO_4 \cdot 2H_2O$, celestite, $SrSO_4$, and barite, $BaSO_4$. All other sulphate solids are highly soluble salts.

Tab. 7.1: Thermodynamic data for aqueous species and solids in TDB 2020 containing the metals Li, Na, K, Mg, Ca, Sr, Ba, Mn(II,III,IV), Fe(II,III), Al and the ligands OH^-, F^-, Cl^-, CO_3^{2-}, HCO_3^- and SO_4^{2-}. Coloured fields: at least $log_{10}K°$ data available at 25°C; ΔH*: temperature data available, ΔH in italics: estimated values.*

Aqueous species in TDB 2020

	Li	Na	K	Mg	Ca	Sr	Ba	Mn (II)	Mn (III)	Fe (II)	Fe (III)	Al
hydroxide	ΔH	ΔH	ΔH	ΔH	ΔH	ΔH	ΔH	ΔH	ΔH	ΔH	ΔH	ΔH
fluoride	ΔH	ΔH		ΔH	ΔH	ΔH	ΔH	ΔH	*ΔH*	*ΔH*	ΔH	ΔH
chloride								ΔH	*ΔH*	ΔH	ΔH	
carbonate		ΔH	*ΔH*	ΔH	ΔH	ΔH	ΔH	ΔH		*ΔH*		
sulphate	*ΔH*	ΔH	ΔH	ΔH	ΔH	ΔH	*ΔH*	ΔH		ΔH	*ΔH*	ΔH

Solids in TDB 2020

	Li	Na	K	Mg	Ca	Sr	Ba	Mn (II)	Mn (III)	Mn (IV)	Fe (II)	Fe (III)	Al
(hydr)oxide				ΔH	ΔH			ΔH	ΔH	ΔH		ΔH	ΔH
fluoride					ΔH								
chloride													
carbonate				ΔH	ΔH	ΔH	ΔH	ΔH			ΔH		*ΔH*
sulphate					ΔH	ΔH	ΔH						

7.2.2 Solubility of fluorite, CaF_2

The solubility data for fluorite, CaF_2(cr), are presented here as an example of the recent review work.

Nordstrom et al. (1990) selected a $\log_{10}K_s°$ and a $\Delta_rH_m°$ value as well as a temperature function (dashed line in Fig. 7.1) for the solubility of fluorite with the remark: "based on Nordstrom & Jenne (1977) but forced to go through $\log_{10}K_s° = -10.6$ at 298.15 K to be in agreement with the solubility data of Macaskill & Bates (1977) and Brown & Roberson (1977)".

Note that Macaskill & Bates (1977) report $\log_{10}K_s°$ (298.15 K) = –10.51 and Brown & Roberson (1977) report $\log_{10}K_{s0}°$ (298.15 K) = –10.58 ± 0.17 while the value originally derived by Nordstrom & Jenne (1977) is $\log_{10}K_s°$ (298.15 K) = –10.96. The temperature function of Nordstrom & Jenne (1977) has been derived from solubility data at room temperature, calorimetric data and, at that time, the only available solubility data measured at elevated temperatures by Strübel (1965) (dot-dashed line in Fig. 5.1). As it seems, "forced to go through $\log_{10}K_s° = -10.6$ at 298.15 K" just meant that Nordstrom et al. (1990) shifted the temperature function of Nordstrom & Jenne (1977) by a constant value of +0.36 log-units (dashed line in Fig. 7.1).

Hummel et al. (2002) remark "the mineral fluorite, CaF_2, is common in aqueous systems, and may influence groundwater chemistry. In spite of the ubiquity and simple chemistry of this mineral, values for its thermodynamic properties differ widely. Values given by CODATA (Cox et al. 1989), Nordstrom et al. (1990, Table I) and other data bases differ by as much as 0.55 in $\log_{10}K_s°$. Hence, fluorite is included as supplemental data only, and reaction data for this mineral are taken from Nordstrom et al. (1990)". Supplemental data are of low quality or based on estimation.

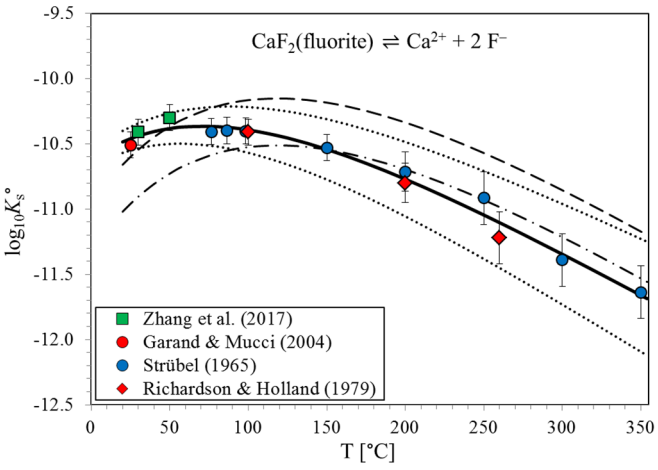

Fig. 7.1: The solubility product $\log_{10}K_s°$ for fluorite as function of temperature in the range 25 – 350°C. Solid line: unweighted regression of all data. Dotted lines: lower and upper limits using $\log_{10}K_s°$ (298.15 K) = –10.46 ± 0.09, $\Delta_rH_m°$(298.15 K) = (7.8 ± 1.9) kJ · mol^{-1} and $\Delta C_{p,m}°$(298.15 K) = –(170 ± 15) J · K^{-1} · mol^{-1} and extrapolated to higher temperatures. Dashed line: temperature function selected by Nordstrom et al. (1990); dot-dashed line: temperature function derived by Nordstrom & Jenne (1977); both shown for comparison.

This review considered the solubility data of Garand & Mucci (2004) at 25°C, Zhang et al. (2017) at 30 and 50°C, Richardson & Holland (1979) at 100, 200 and 260°C, and Strübel (1965) at >70°C. It seems that due to the short equilibration times the solubility experiments of Strübel (1965) did not reach equilibrium at temperatures below 70°C. Therefore, these data have not been used.

The value $\log_{10}K_s°$ (298.15 K) = –10.51 of Macaskill & Bates (1977), extrapolated from measurements at 1 mol·kg^{-1} KCl to zero ionic strength by an undefined extrapolation procedure, has not been considered by this review, although it is numerically identical to the value obtained by Garand & Mucci (2004) at the same temperature.

Brown & Roberson (1977) measured the solubility products of two samples of natural fluorite, at very low (0.0007 mol·L^{-1}) to low (0.1 mol·L^{-1}) ionic strengths resulting from impurities in the samples. The authors tried many different variants of extrapolation to zero ionic strength and finally reported $\log_{10}K_{s0}°$ (298.15 K) = –10.58 ± 0.17 as their "more correct value" derived from one sample, while the values derived from the second sample were always +0.2 log-units or more at variance. Also these values have not been considered in this review.

All data shown in Fig. 7.1 join relatively smoothly across the whole temperature range. An unweighted regression of all data resulted in $\log_{10}K_{s0}°$ (298.15 K) = –10.46 ± 0.09, $\Delta_rH_m°$(298.15 K) = (7.8 ± 1.9) kJ · mol^{-1} and $\Delta_rC_{p,m}°$(298.15 K) = –(170 ± 15) J · K^{-1} · mol^{-1}. These values are included in TDB 2020.

7.3 Supplementary sorption data for the update of the cement sorption database

A new update of the cement sorption database has to be developed by the end of 2022 for use in safety assessments in SGT-E3. In preparation for this report, an experimental study was launched in 2019 to determine the sorption values (R_d) for some safety-relevant radionuclides that had not been taken into account in previous sorption databases. These include ^{26}Al, ^{32}Si and ^{41}Ca. The approach used to assess the sorption behaviour of these radionuclides is based upon the hypothesis that their retention by cementitious

materials is controlled by isotopic exchange with stable Al, Si and Ca during recrystallisation of the main cement minerals, such as C-(A)-S-H phases (Ca, Si, Al), portlandite (Ca), ettringite (Ca, Al) and AFm phases (Ca, Al). To confirm this hypothesis, the sorption of ^{32}Si and ^{45}Ca on the above-mentioned cement minerals is investigated as function of time in batch sorption experiments. The observed kinetic sorption behaviour should reveal whether or not the uptake is controlled by isotope exchange and recrystallisation processes. Sorption experiments with ^{26}Al are not planned because this radionuclide cannot be purchased. R_d values for ^{26}Al in the sorption database will be estimated by assuming that the isotopic exchange behaviour with stable Al in ettringite and AFm phases is identical to that of ^{45}Ca. Isotopic exchange of the latter radioisotope can be determined experimentally.

In 2019, the sorption kinetic behaviour of ^{45}Ca was determined on C-S-H phases with three different Ca:Si (C:S) ratios, on portlandite and on hardened cement paste in the second degradation stage (pH = 12.5, solution composition in equilibrium with portlandite). In addition, ^{32}Si sorption kinetic experiments on one C-S-H phase having a C:S ratio of 1.0 was carried out.

The sorption of ^{45}Ca onto C-S-H phases increases as a function of time for a period of at least 180 days (Fig. 7.2). Furthermore, ^{45}Ca sorption onto C-S-H phases strongly depends on their composition (Fig. 7.2a). After 180 days equilibration, an R_d value of ~0.1 m^3 kg^{-1} was measured for ^{45}Ca sorption onto a C-S-H phase with a high C:S ratio of 1.7, whereas the R_d value for ^{45}Ca sorption onto a C-S-H phase with a low C:S ratio of 0.7 amounts to 1.7 m^3 kg^{-1}. The difference in the aqueous Ca concentrations at equilibrium with the different C-S-H phases may explain at least qualitatively the trend in the observations: The high aqueous Ca concentration (0.02 M) in the case of C-S-H phases with a C:S ratio of 1.7, results in a low Ca solid-to-solution ratio and thus, in a low Rd value. Conversely, a low aqueous Ca concentration (~5·10-5 M) in the case of C-S-H phases with low C:S ratio results in a high Ca solid-to-solution ratio and thus in a high Rd value. ^{45}Ca sorption onto C-S-H phases was also observed to decrease with increasing solid-to-liquid (S:L) ratio used in the batch sorption experiments (Fig. 7.2b). The latter finding cannot be explained by simple isotopic exchange with stable Ca in the solid and liquid phase and is not understood at present.

Sorption of ^{32}Si onto C-S-H phases is also slow with R_d values increasing from 30 m^3 kg^{-1} after 1 day equilibration to 45 m^3 kg^{-1} after 180 days equilibration (Fig. 7.2c). Note that the R_d values for ^{32}Si sorption are approximately a factor 100 higher than those for ^{45}Ca sorption onto a C-S-H phase with the same composition (C:S = 1.0) and using the same S:L ratio in the experiment (10 g L^{-1}) (Fig. 7.2c). To evaluate the effect of the aqueous Si concentration on the R_d value, sorption experiments on C-S-H phases with different C:S ratios have to be performed. This is presently not possible due to high cost of ^{32}Si tracer and thus the very limited amounts of ^{32}Si tracer activities available. Interpretation of these experimental observations is still ongoing. In 2020, the project will be continued with ^{45}Ca sorption measurements onto AFm phases and ettringite and ^{32}Si sorption experiments onto degraded hardened cement paste.

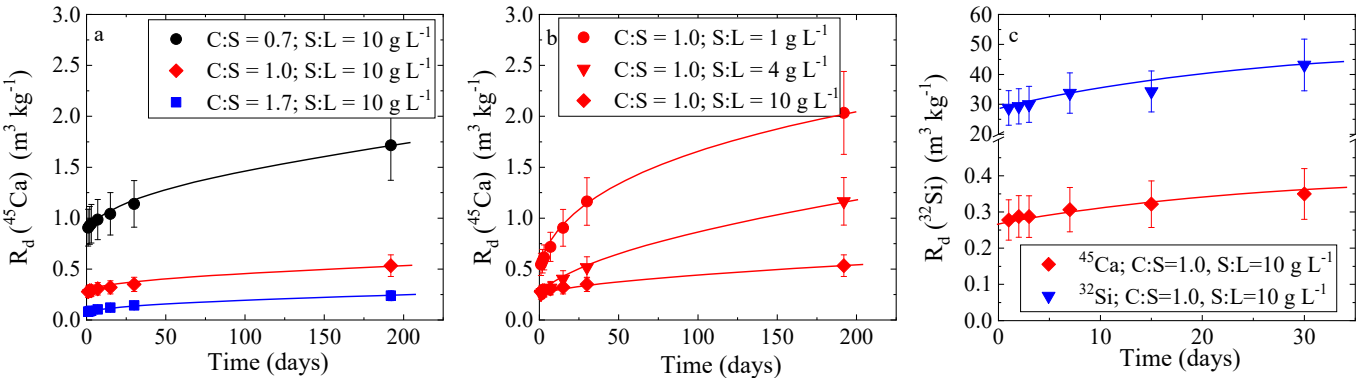

Fig. 7.2: Sorption kinetics of ^{45}Ca (a, b) and ^{32}Si (c) onto C-S-H phases, a) effect of the C-S-H composition (C:S ratio), b) effect of the S:L ratio, c) comparison of ^{32}Si and ^{45}Ca sorption kinetics on a C-S-H phase with a C:S ratio of 1.0. The S:L ratio used in the experiment is 10.0 g L^{-1}. Solid lines are added to guide the eye.

7.4 Extension of the multi-site C-S-H solid-solution model for Al uptake and for retention of radionuclides (U, Np) and fission products (Ba, Sr)

The currently developed structurally consistent CNKASH+ sublattice solid solution model (Kulik et al. 2018) has been incrementally extended to be able to describe the incorporation of aluminium, as well as the retention of some relevant cationic radionuclides and fission products. This model allows more accurate thermodynamic description of cement-waste interaction for radioactive waste disposal. The model was extended with end members corresponding to the incorporation of aluminium on the bridging tetrahedral (BT) and interlayer cation (IC) structural sites. Considering all possible exchange combinations, 7 aluminium-containing end members were generated. To consider possible non-ideal interactions at these two structural sites, 6 regular interaction parameters were considered. Initial guesses for the Gibbs energy of end members G^o_j were retrieved from solid exchange reactions with previously fitted end members from the base C-S-H subsystem. Using the GEMSFITS code (Miron et al. 2015), the G^o_j values of these end members and the interaction parameters were optimised against the selected literature data (L'Hôpital et al. 2015) and the new experimental data retrieved in the CASH-2 project. The sensitivity of parameters to the experimental data was monitored, and the case when Al was allowed to enter only BT sites was tested. The experimental data seem to be better reproduced, if Al is allowed to enter both the BT and the IC sites (Fig. 7.3). Additional fitting exercises will be done to test the uptake of Al in these two sites using more experimental data retrieved in the CASH 2 project.

Spectroscopic studies suggest that the retention of Sr, Ba, Ra in C-S-H occurs mostly in IC sites (Tits et al. 2006; Missana et al. 2017), while actinides and rare earth elements can also enter BT sites or form surface precipitates (Tits et al. 2003; Tits et al. 2014). Using this information, the C-S-H model was extended with the necessary end members and interaction parameters for each cation, and their properties were fitted against the uptake isotherms at different Ca/Si ratios. GEMSFITS fits to experimental data by Tits et al. (2006) are good at close to ideal mixing behaviour of Sr on the IC site (using 3 end members and 4 interaction parameters). In practical sense, no Sr on BT sites is needed (Fig 7.4a). For the uptake of Ba, initial estimates for the properties of end members were calculated from exchange reactions with Sr, assuming that all reaction excess free energy contributions are equal to zero. An applied correction of -5.6 kJ/mol to all 3 Ba-C-S-H end members results in a good agreement with the experimental data (Fig 7.4b). Preliminary work has been done to extend the model for the incorporation of U(VI) in C-S-H. Uranyl is considered to enter both BT and IC site, resulting in eight additional end members that were added to the original C-S-H model. The predicted isotherms compare well with the experimental data (Tits et al. 2007; Fig 7.4c) at Ca/Si ratio >0.96 but over-predicts data at Ca/Si < 0.75. The CNKASH+ model describes well the uptake of cations tried so far (Ca, Na, K, Al, Sr, Ba, U(VI), Np(V)) and can be extended incrementally and in consistency with PSI-Nagra and Cemdata TDBs. More work has to be done on the extension and parameterisation of CNKASH+ model for sorption/ uptake of relevant cations and anions using the available experimental data.

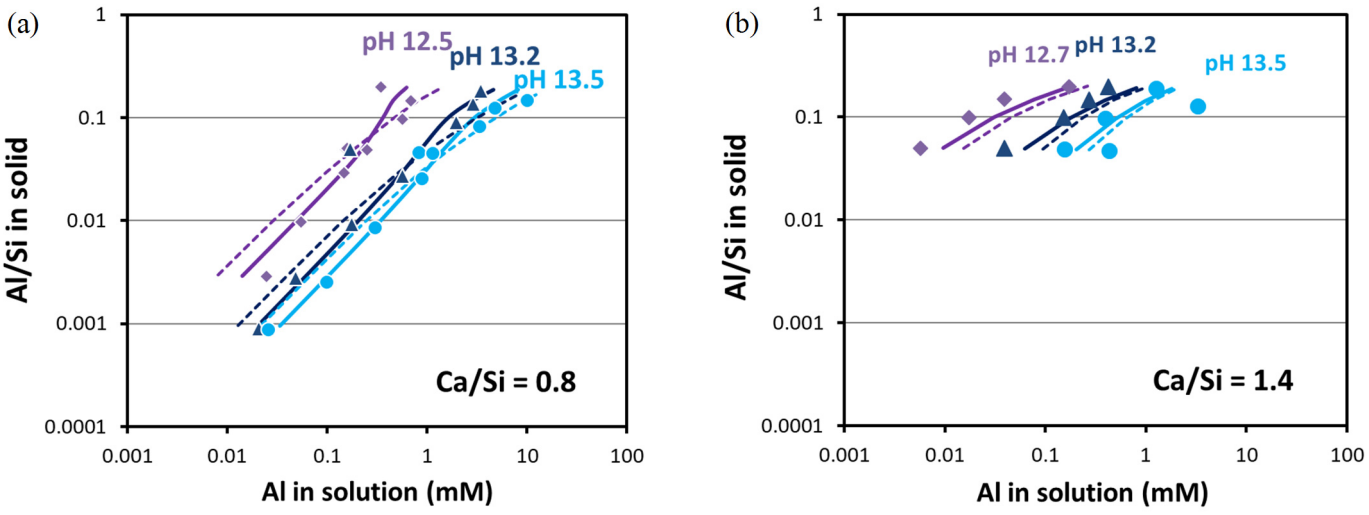

Fig. 7.3: Uptake of aluminium in C-S-H at 0.8 (a) and 1.4 (b) Ca/Si ratios. Experimental data (symbols) against modelled values allowing Al to enter both BT and IC sites (solid lines) and only BT sites (dotted lines).

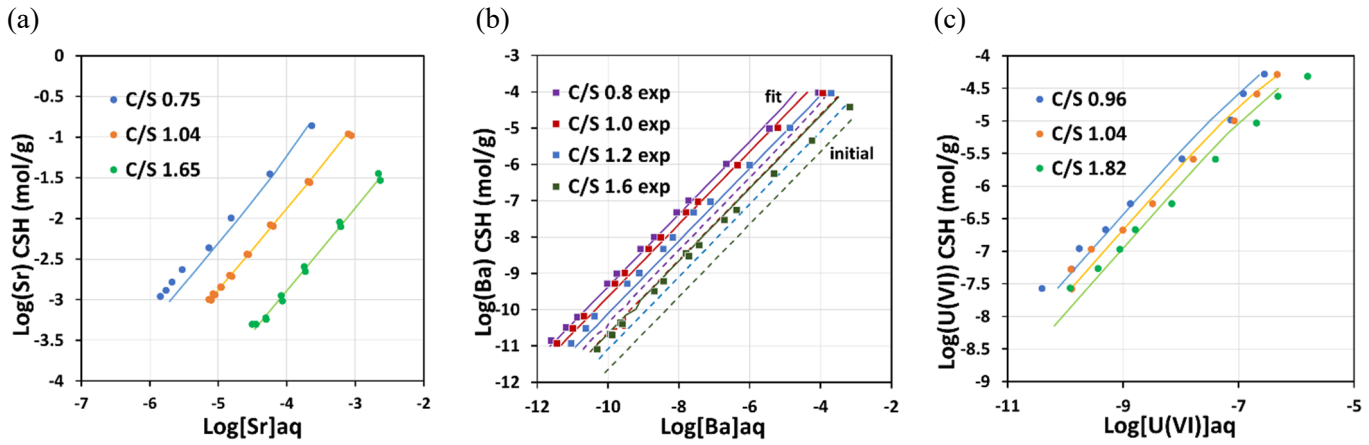

Fig. 7.4: Uptake of Sr (a), Ba (b), and U(VI) (c) in C-S-H. Experimental data (symbols) compared with calculated values using optimised end members (solid lines) and using initial estimates for Ba end members (dashed lines).

7.5 References

Brown D. E., Roberson C. E. (1977)
Solubility of natural fluorite at 25°C. Journal of Research of the U.S. Geological Survey 5, 509–517.

Cox J. D., Wagman D. D., Medvedev V. A. (1989) CODATA Key Values for Thermodynamics. Hemisphere Publishing, New York.

Garand A., Mucci A. (2004)
The solubility of fluorite as a function of ionic strength and solution composition at 25°C and 1 atm total pressure. Marine Geochemistry 91, 27–35.

Hummel W. (2017a)
The PSI Chemical Thermodynamic Database 2020: Data selection for mercury. PSI Internal Report, TM-44-17-04, Paul Scherrer Institut, Villigen PSI, Switzerland.

Hummel W. (2017b)
The PSI Chemical Thermodynamic Database 2020: Data Selection for Lead. PSI Internal Report, TM-44-17-06, Paul Scherrer Institut, Villigen PSI, Switzerland.

Hummel W. (2017c)
The PSI Chemical Thermodynamic Database 2020: Data Selection for Polonium. PSI Internal Report, TM-44-17-08, Paul Scherrer Institut, Villigen PSI, Switzerland.

Hummel W. (2018a)
The PSI Chemical Thermodynamic Database 2020: Data Selection for Silver. PSI Internal Report, TM-44-18-09, Paul Scherrer Institut, Villigen PSI, Switzerland.

Hummel W. (2018b)
The PSI Chemical Thermodynamic Database 2020: Data Selection for Actinium. PSI Internal Report, TM-44-18-11, Paul Scherrer Institut, Villigen PSI, Switzerland.

Hummel W. (2018c)
The PSI Chemical Thermodynamic Database 2020: Data Selection for Protactinium. PSI Internal Report, TM-44-18-14, Paul Scherrer Institut, Villigen PSI, Switzerland.

Hummel W. (2018d)
The PSI Chemical Thermodynamic Database 2020: Data Selection for Californium. PSI Internal Report, TM-44-18-13, Paul Scherrer Institut, Villigen PSI, Switzerland.

Hummel W. (2019a)
The PSI Chemical Thermodynamic Database 2020: Data Selection for Cadmium. PSI Internal Report, TM-44-19-02, Paul Scherrer Institut, Villigen PSI, Switzerland.

Hummel W. (2019b)
The PSI Chemical Thermodynamic Database 2020: Data Selection for Data for Ground and Pore Water Models. PSI Internal Report, TM-44-19-03, Paul Scherrer Institut, Villigen PSI, Switzerland.

Hummel W., Berner U., Curti E., Pearson F.J., Thoenen T. (2002)
Nagra/PSI Chemical Thermodynamic Data Base 01/01. Nagra Technical Report NTB 02-16, Nagra, Wettingen, Switzerland, and Universal Publishers, Parkland, Florida.

Lothenbach B., Kulik D.A., Matschei T., Balonis M., Baquerizo L., Dilnesa B., Miron G.D., Myers R.J. (2019)
Cemdata18: A chemical thermodynamic database for hydrated Portland cements and alkali-activated materials. Cement and Concrete Research 115, 472–506.

Kulik D. A., Miron G. D., Lothenbach B. (2018)
A realistic three-site solid solution model of C-S-H. Goldschmidt 2018 Conference, Boston MA, USA (2018).

L'Hôpital E., Lothenbach B., Le Saout G., Kulik D., Scrivener K. (2015)
Incorporation of aluminium in calcium-silicate-hydrates. Cement and Concrete Research 75, 91–103.

Macaskill J. B., Bates R. G. (1977)
Solubility product constant of calcium fluoride. The Journal of Physical Chemistry 81, 496–498.

Miron G. D., Kulik D. A., Dmytrieva S. V., Wagner T. (2015)
GEMSFITS: Code package for optimisation of geochemical model parameters and inverse modeling. Applied Geochemistry 55, 28-45.

Missana T., García-Gutiérrez M., Mingarro M., Alonso U. (2017)
Analysis of barium retention mechanisms on calcium silicate hydrate phases. Cement and Concrete Research 93, 8-16.

Nordstrom D. K., Jenne A. E. (1977)
Fluorite solubility equilibria in selected geothermal waters. Geochimica et Cosmochimica Acta 41, 175-188.

Nordstrom D. K., Plummer L. N., Langmuir D., Busenberg E., May H. M., Jones B. F., Parkhurst D. L. (1990)
Revised chemical equilibrium data for major water-mineral reactions and their limitations. ACS Symposium Series 416, 398-413.

Pearson F. J., Berner U. (1991)
Nagra Thermochemical Data Base I. Core Data. Nagra Technical Report NTB 91-17, Nagra, Wettingen, Switzerland.

Pearson F. J., Berner U., Hummel W. (1992)
Nagra Thermochemical Data Base II. Supplemental Data 05/92. Nagra Technical Report NTB 91-18, Nagra, Wettingen, Switzerland.

Richardson C. K., Holland H. D. (1979)
The solubility of fluorite in hydrothermal solutions, an experimental study. Geochimica et Cosmochimica Acta 43, 1313–1325.

Strübel G. (1965)
Quantitative Untersuchungen über die hydrothermale Löslichkeit von Flußspat (CaF_2). Neues Jahrbuch für Mineralogie / Monatshefte, Monatshefte 83-95.

Thoenen T. (2017a)
The PSI Chemical Thermodynamic Database 2020: Data Selection for Copper. PSI Internal Report, TM-44-17-05, Paul Scherrer Institut, Villigen PSI, Switzerland.

Thoenen T. (2017b)
The PSI Chemical Thermodynamic Database 2020: Data Selection for Iron. PSI Internal Report, TM-44-17-07, Paul Scherrer Institut, Villigen PSI, Switzerland.

Thoenen T. (2018a)
The PSI Chemical Thermodynamic Database 2020: Data Selection for Tin. PSI Internal Report, TM-44-18-08, Paul Scherrer Institut, Villigen PSI, Switzerland.

Thoenen T. (2018b)
The PSI Chemical Thermodynamic Database 2020: Data Selection for Niobium. PSI Internal Report, TM-44-18-10, Paul Scherrer Institut, Villigen PSI, Switzerland.

Thoenen T. (2018c)
The PSI Chemical Thermodynamic Database 2020: Data Selection for Titanium. PSI Internal Report, TM-44-18-12, Paul Scherrer Institut, Villigen, PSI, Switzerland.

Tits J., Fujita T., Harfouche M., Dähn R., Tsukamoto M., Wieland E. (2014)
Radionuclide uptake by calcium silicate hydrates: case studies with Th(IV) and U(VI). PSI Bericht 14-03, Paul Scherrer Institut, Villigen PSI, Switzerland.

Tits J., Fujita T., Tsukamot, M., Wieland E. (2007)
Uranium(VI) uptake by synthetic calcium silicate hydrates. Material Research Society Symposium Proceedings 1107, 467–474.

Tits J., Stumpf T., Rabung T., Wieland E., Fanghänel T. (2003)
Uptake of Cm(III) and Eu(III) by calcium silicate hydrates: a solution chemistry and time-resolved laser fluorescence spectroscopy study. Environmental Science and Technology 37, 3568-3573.

Tits J., Wieland E., Müller C. J., Landesman C., Bradbury M. H. (2006)
Strontium binding by calcium silicate hydrates. Journal of Colloid and Interface Science 300, 78-87.

Zhang W., Zhou L., Tang H., Li H., Song W., Xie G. (2017)
The solubility of fluorite in Na-K-Cl solutions at temperatures up to 260 °C and ionic strengths up to 4 mol/kg H_2O. Applied Geochemistry 82, 79-88.

8 FUNDAMENTAL ASPECTS OF MINERAL REACTIVITY AND STRUCTURAL TRANSFORMATIONS

Churakov S.V., Cametti G., Di Lorenzo F., Giordani M., Adams D., Schliemann R. (PhD student)

8.1 Introduction

Since 2015, PSI/LES and the Institute for Geological Science at the University of Bern (UBERN/IfG) have established research collaboration in the field of mineralogy, crystallography and environmental geochemistry. The research field of the Mineralogy group at the University of Bern covers fundamental aspects of mineral dissolution and precipitation mechanisms, chemical aspects of crystal structure stability and temperature driven phase transitions in minerals. The dedicated laboratories operated by the group are equipped with powder and single-crystal diffractometers for structural studies of minerals and an atomic force microscopy laboratory for in-situ characterisation of mineral surfaces. The experimental studies are widely supported by modelling activities. Main research activities are focused on the characterisation of mineral structure transformations in natural and synthetic zeolite materials as result of dehydration and cation exchange processes. These structural characterisation studies are conducted combining single crystal X-ray diffraction experiments, spectroscopic measurements, and molecular simulations. *Ab initio* molecular dynamics simulations are further used to elucidate the mechanism of clay minerals dissolution at an atomic-scale. Dedicated laboratory nucleation and re-crystallisation experiments, surface characterisations and geochemical modelling are applied to develop sustainable strategies for heavy metal extraction from contaminated water via carbonates precipitation.

8.2 Structural changes and thermal stability in heavy-metal exchanged zeolites

Heavy-metal-exchanged zeolites are attractive materials that find applications in several research fields, from environmental remediation to catalysis. In the SNF-AMBIZIONE project lead by Dr. G. Cametti, the structural changes taking place in natural zeolites as a function of heavy-metal uptake are investigated by combing experimental methods (X-ray diffraction, X-ray absorption spectroscopy) and theoretical computations (Molecular dynamics). This complementary approach is found to be highly successful in structural characterisation of complex systems where the charge compensating cations are usually affected by strong positional disorder.

A medium-microporous zeolite (stellerite) with STI framework type (dimension of channels 2.7×5.6 and 4.7×5.0 Å for those parallel to [001] and [100], respectively) was used as starting material. Two heavy-metal exchanged forms were produced: i) fully-exchanged Ag^{+}-stellerite (Ag-STI) and ii) fully–exchanged Cd^{2+}-stellerite (Cd-STI).

The average structures were determined at room-temperature by single-crystal X-ray diffraction. In contrast, to solve the strong disorder of the extraframework cations (EF) and H_2O and to have a better understanding of their local environment inside the zeolitic cages, molecular dynamic simulations and X-ray absorption spectroscopy experiments were performed.

The structural changes were also monitored as a function of increasing temperature, to ascertain the effect of the EF cations on the thermal stability of the newly-produced zeolite forms. Both *in situ* high-temperature single crystal X-ray diffraction (HT-SCXRD) and X-ray absorption data were collected between 25 and 500°C to track the evolution of the aluminosilicate framework and of the metal sites.

The results obtained by different techniques were consistent with each other and demonstrated that the thermal stability is strongly influenced by the nature of the EF cations. In particular, different phases with different structural topologies formed upon heating. Most important, the thermal stability of the metal-exchanged forms is reduced compared to the pristine material.

The main outcomes of the study are summarised in Fig. 8.1. The heavy-metal exchanged zeolites at RT undergo a monoclinic distortion that can be related to the electronic structure and strength of chemical bounding of the EF cations with H_2O and framework oxygen atoms. On the other hand, the charge of the extraframework cation seems to affect the structural topology which forms upon heating.

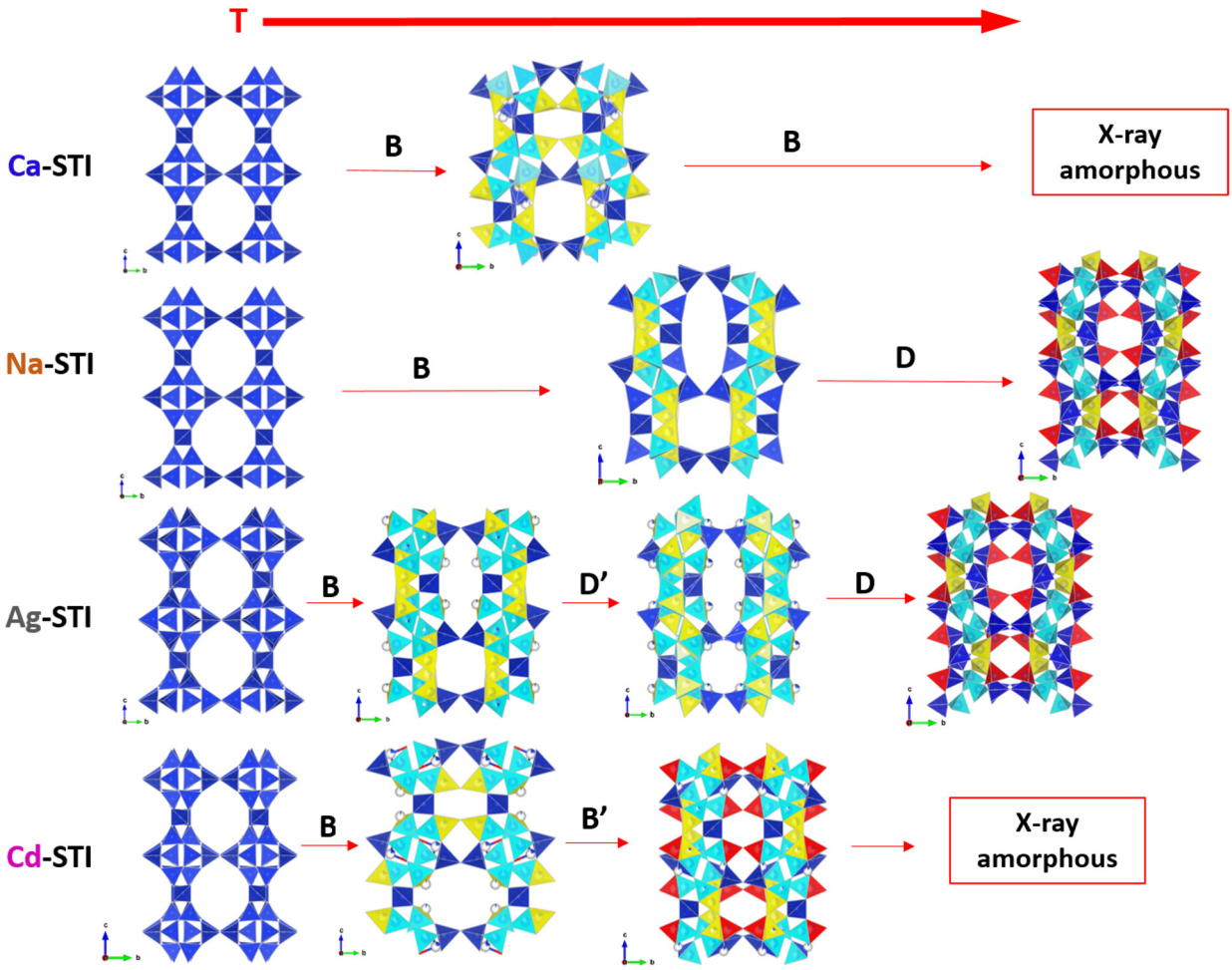

Fig. 8.1: Summary of the main structural modifications of Ca-, Na-, Ag-, and Cd-stellerite occurring as a function of temperature. Each phase is indicated with a capital letter. Different structural topologies can be recognised by the different arrangement of the tetrahedra of the aluminosilicate framework.

8.3 Dissolution mechanism of pyrophyllite from the (110) edge surface: An *ab initio* study

The molecular-scale understanding of clay minerals dissolution is essential for the development of mechanistic models for toxic metals and radionuclides retention in soils and waste disposal sites. In the framework of the SNF PhD project (PhD student R. Schliemann) the *ab initio* metadynamics simulations approach (Laio 2002) is applied to investigate the free energy surface (FES) and the reaction mechanism associated with the removal of tetrahedral and octahedral units from pristine edge faces of smectite minerals. The results of the simulations show a complex FES with multiple local minima corresponding to the intermediate reaction products formed during the dissolution process. The saddle point connecting the local minima represent the energies of the activated complexes corresponding to the individual reaction steps. Analysis of data for different edge surfaces indicate that a complete detachment of silanol and aluminol groups can be represented by at least four elementary reaction steps.

Detailed analysis of the simulation trajectories indicates that the dissolution process is often activated through a nucleophilic attack of a water molecule on the corresponding surface complex. The nucleophilic interaction leads to local increase of the coordination polyhedra and elongation of one or more oxygen-metal bonds (see Fig. 8.2). Finally, when the elongated bonds break, the neo-formed reaction intermediates are stabilised by proton transfer reaction and rearrangement of hydrogen bonds.

The only exception to this kind of mechanism arises from a sterically hindered structure, which does not allow for a water molecule to approach the surface complexes site. In this case the activation is supported by a nearby protonated bridging oxygen, adding to the coordination shell (similar to the water molecule) and eventually breaking one of the initial bonds.

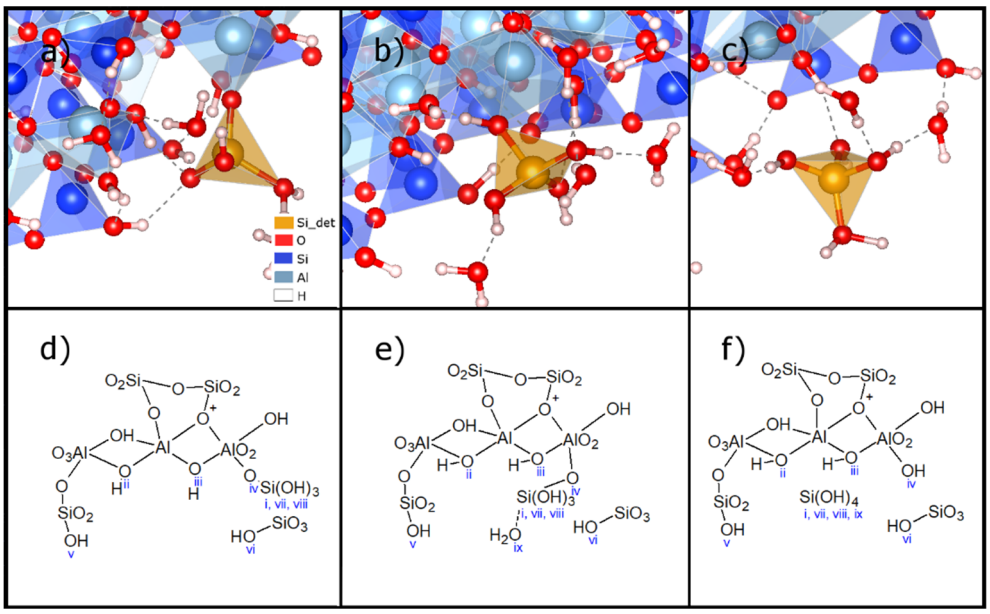

Fig. 8.2: Final detachment step of a silicon tetrahedra from the (110) edge surface of pyrophyllite. The top row shows snapshots from the simulation, while the bottom row represent a simplified schematic description of the reaction mechanism. The reaction step starts with a monodentate structure (a and d), when a water molecule enters the Si coordination shell (intermediate structure in b and e) the silicon is attracted by the oxygen and breaks the remaining bond to the surface oxygen. After that, the excess proton is transferred to the dangling surface oxygen site. That results in a dissolved silicic acid molecule and the altered surface (see c and f).

8.4 The effect of calcium carbonate polymorphism on lead uptake

The two most common calcium carbonate minerals (calcite, CAL, trigonal; and aragonite, ARG, orthorhombic) have been proposed as a remediation agent for water contaminated with lead (Pb). (Godelitsas et al. 2003; Yuan et al. 2016). Accordingly, batch recrystallisation experiments have been performed to assess the efficiency of these materials (Di Lorenzo et al. 2019). Despite the similar solubility of aragonite and calcite (i.e. similar negative Gibbs free energy variation for the reaction), our experiments demonstrate that the efficiency is substantially different (Fig. 8.3(A)). The reason is in the crystallographic relationships between substrates and product. ARG and cerussite ($PbCO_3$, orthorhombic) share the same crystallographic structure. This favours the formation of a continuous layer of cerussite that hinders reaction and prevent the replacement of the whole substrate grains (Fig. 8.3(B)). In the case of calcite, the absence of the crystallographic match between the substrate and the precipitate allows the process to proceed further. The conversion rate of calcite and aragonite into cerussite was 15 ± 2 % for calcite and 5 ± 1 % for aragonite after 10 days of interaction (maximum theoretical conversion yield of 50%: 1 mmol of aqueous Pb^{2+} interacting with 2 mmol of $CaCO_3$ powder). The atomic-scale mechanism of calcite dissolution in presence of $Pb(NO_3)_2$ solutions was revealed using flow-through AFM. We observed the change in the morphology of dissolving CAL surface due to Pb^{2+}. The rhombic etch pits typical for CAL dissolving in water change into elongated pits due to the stabilisation of steps parallel to [010] direction. The experimental conditions of the AFM experiments made pH raise and the formation of hydrocerussite (HCER, $Pb_3(CO_3)_2(OH)_2$) was observed. The hexagonal crystals of hydrocerussite were observed growing via the formation of hillocks (Fig. 8.3(C)). The measurements of the step height matched the dimension of the crystalline structure of HCER along the c-axis.

The study of kinetic properties of carbonate minerals bearing heavy metals could make possible the development of fast and cheap techniques for water decontamination. The presence of heavy metals in wastewater is a serious health risk and prevents reutilisation (Chipasa 2003; Khan et al. 2008). Wastewater contains large quantities of phosphorus and nitrogen that makes it suitable for agricultural use (Li et al. 2015). Our work aims to provide the fundamental knowledge about heavy metal uptake processes by carbonate minerals that could play a role to achieve safe reutilisation of wastewater.

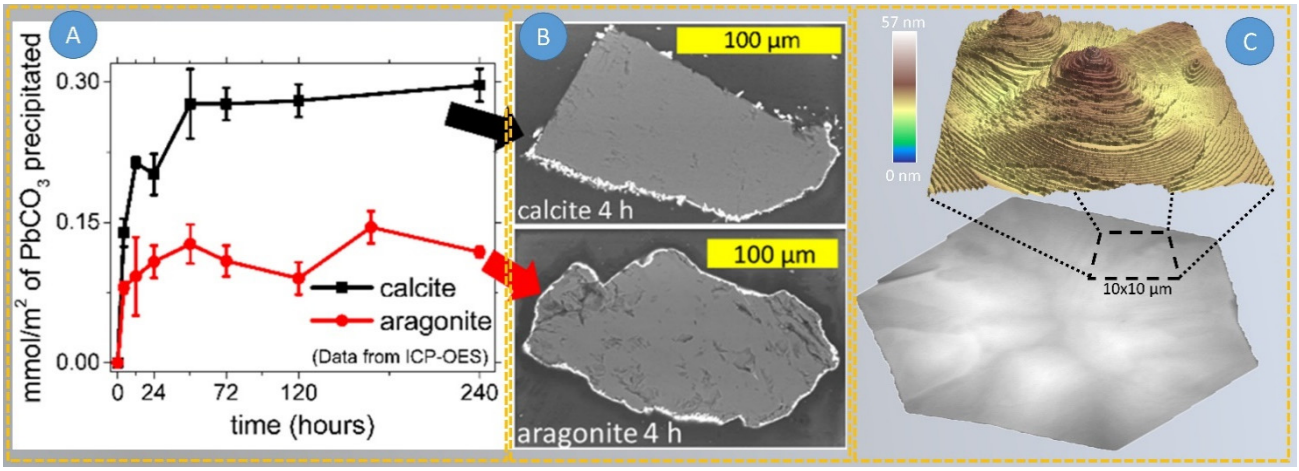

Fig. 8.3: (A) The ICP-OES analysis of the final solution showing the uptake efficiency. (B) Calcite and aragonite showed a different behavior, the cross sections of reaction product observed with SEM (backscattered electrons) revealed the formation of a homogenous layer of cerussite on aragonite (isostructural phases). (C) During AFM flow-through experiments the formation of hydrocerussite occurred. We observed the growth of the hexagonal crystals with a spiral mechanism.

8.5 References

Cametti G., Scheinost A. C., Churakov S. V. (2019) Structural modifications and thermal stability of Cd-$^{2+}$ exchanged stellerite, a zeolite with STI framework type. The Journal of Physical Chemistry C 123, 25236-25245.

Cametti G., Scheinost A. C., Giordani M., Churakov S. V. (2019)
Framework modifications and dehydration path of a Ag^{+}-modified zeolite with STI framework type. The Journal of Physical Chemistry C 123, 13651-13663.

Chipasa K.B. (2003)
Accumulation and fate of selected heavy metals in a biological wastewater treatment system. Waste Management 23, 135-143.

Di Lorenzo F., Ruiz-Agudo C., Churakov S. V. (2019)
The key effect of polymorphism during Pb^{II} uptake by calcite and aragonite. Crystal Engineering Communications 21, 6145-6155.

Godelitsas A., Astilleros J. M., Hallam K., Harissopoulos S., Putnis A. (2003)
Interaction of calcium carbonates with lead in aqueous solutions. Environmental Science and Technology 37, 3351-3360.

Khan S., Cao Q., Zheng Y. M., Huang Y. Z., Zhu Y. G. (2008)
Health risks of heavy metals in contaminated soils and food crops irrigated with wastewater in Beijing, China. Environmental Pollution 152, 686-692.

Li W. W., Yu H.Q., Rittmann B. E. (2015)
Reuse water pollutants. Nature 528, 29-31.

Laio A., Parrinello M. (2002)
Escaping free-energy minima. Proceedings of the National Academy of Sciences of the United States of America 99, 12562-12566.

Schliemann R., Churakov S. V. (2019)
Dissolution mechanism of 2:1 clay minerals: *Ab initio* simulations of Pyrophyllite as reference model. Geochimica et Cosmochimica Acta (in preparation).

Yuan K., Lee S. S., De Andrade V., Sturchio N. C., Fenter P. (2016)
Replacement of calcite ($CaCO_3$) by cerussite ($PbCO_3$). Environmental Science and Technology 50, 12984-12991.

9 GEOCHEMICAL ASPECTS OF CONVENTIONAL WASTE MATERIALS AND THEIR DISPOSAL

Eggenberger U., Churakov S.V., Weibel G., Glauser A. (PhD student), Wolffers M. (PhD student), Camesi L., Fromm S., Zappatini A., Zucha W., Ulrich M. (MSc student)

9.1 Introduction

The Competence Centre for Secondary Raw Materials at the Institute of Geological Sciences conducts applied research in the field of environmental geochemistry and secondary raw materials. The core competences of the Centre cover the topics of circular economy and disposition quality of conventional non-radioactive waste materials. Sustainable implementation of recycling technology is waste type specific and requires a detailed knowledge of the material composition, long-term behaviour and process couplings controlling the material degradation. For the replacement of mass raw materials, e.g. the use of gravel mud in cement production, the whole process of cement production must be kept under control and inline with chemical and structural analytical methods. For the metal recycling from the residues of municipal solid waste incineration (MSWI) and wood incineration (WI), a detailed knowledge about formation and composition of the incineration residues (bottom ash, fly ash, wood ash) is essential to optimise metal recovery. Within the framework of the recent Swiss Waste Ordinance (Swiss Confederation 2015), the requirements for residues have increased and metal recovery must be implemented by 2021 for municipal solid waste incineration fly ash and by 2023 for waste wood ash.

Zero waste concept is a long-term vision of circular economy. In practice, the implementation of sustainable recycling technologies will take several decades, during which the waste disposal in landfill sites will continue. Long-term stability of the wastes material under disposed conditions is essential for the environmental protection. Corresponding waste acceptance criteria and suitable test methods have to be developed for different waste types. One of the main activities of the Competence Centre for Secondary Raw Materials is thus the development of leaching tests and monitoring of newly build waste deposits to better understand the corresponding waste-water interaction processes and to set up the scientific basis needed for geochemical modelling in the future.

9.2 Recycling of gravel wash mud in cement production

In Switzerland about 3.3 Mio tons of gravel wash mud (GWM) has been deposited in Type A or B deposits every year (Fisch & Eggenberger 2017). In a pilot project, GWM have been collected and analysed from 47 national production sites. The results show that GWM materials can be used as raw material substitutes for the cement production process since their composition fall on the mixing line (Figure 9.1) for conventional raw material composition. In the framework of a follow-up environmental technology promotion project, the development and implementation of a concept for the utilisation of several 100'000 tons of GWM as a raw material additive or raw material substitute in the clinker production has been investigated in cooperation with the Cornaux cement plant of Jura-Cement-Fabriken AG.

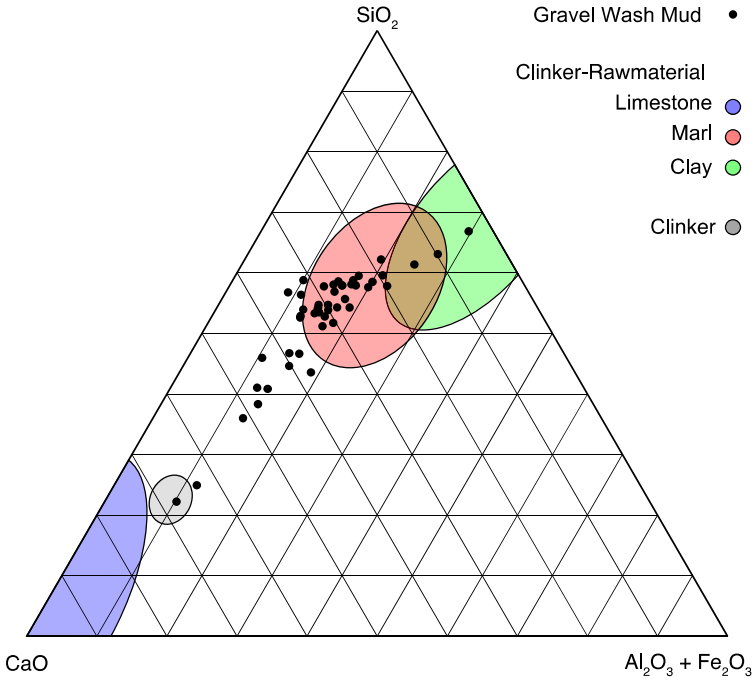

Fig. 9.1: Chemical composition of investigated Swiss Gravel Wash Mud samples (dots) and the compositional range (coloured areas) of typical primary raw material for cement manufacturing.

Within this project, a numerical tool was developed, which provides optimal mixing recipe for the cement plant, based on material properties and chemical composition of components. Boundary conditions for the target composition can be defined within the tool and mixing ratios of the raw mixture are optimised for material costs and transport. A number of additional criteria, such as chemical and mineralogical composition, sum of primary and secondary materials can be included to optimise the mixture for the specific operational conditions in the specific plants. All the parameters necessary for clinker production (e.g. lime saturation factor, alkali ratio, sulfate resistance, Na-equivalent, particle size distribution) are calculated and displayed in real time. In the benchmarking phase, this tool was used to evaluate performance of numerous materials as well as their mixtures, and to select 13 recipes for laboratory tests. The laboratory scale tests for the synthesis of clinker were tuned to the firing conditions specific to a Lepol-type kiln at the Cornaux plant. Both the X-ray diffraction phase analysis and the electron microscopic examinations of the products showed that all mixtures are in the range of clinker phase compositions to be expected and are found suitable for factory tests. The observed difference lies in the formation of the aluminate phases. In the laboratory mainly, the cubic form (aluminat-C) is dominant, whereas in the plant the orthorhombic form (aluminat-O) is mostly identified (Figure 9.2). This is mainly attributed to the different furnace atmosphere conditions in the laboratory compared to the plant where fossil fuel is used.

On the basis of numerous laboratory investigations, 2 mixtures were selected for factory tests. A "conservative" one with 50% clay replacement (total 10% replacement of primary raw material) and an "extreme" one with 100% clay replacement (total 20% replacement of raw material) and two recipes for a daily production of 1'200 tons each were defined. For the quantitative phase analysis of the GWM and the mixtures during the factory trials, an automated, user-independent XRD evaluation method (Rietveld refinement) was installed in the Cornaux plant test facility. Both tests have been performed and completed in 2019. The main challenge was logistics and technical adaption for the material handling because of differences in water content and granularity of the secondary raw material. The testing results (clinker composition, different aspects of quality management, economic and ecological benefit) are being evaluated.

9.3 Characterisation of bottom ash and fly ash from MSWI and WI plants

At present 4.2 Mio tons of municipal solid waste (MSW) are incinerated in Switzerland every year. The incineration allows mass and volume reduction, destruction of organic compounds, energy recovery and transformation of waste into inert residues. Per year 750,000 t of bottom ash (BA) and 75,000 t of fly ash (FA) are produced in incineration plants. In addition, similar quantities of wood ash (WA) from wood-burning stoves are produced. All these waste residuals are subject to the same waste treatment requirements defined by the Swiss Waste Ordinance.

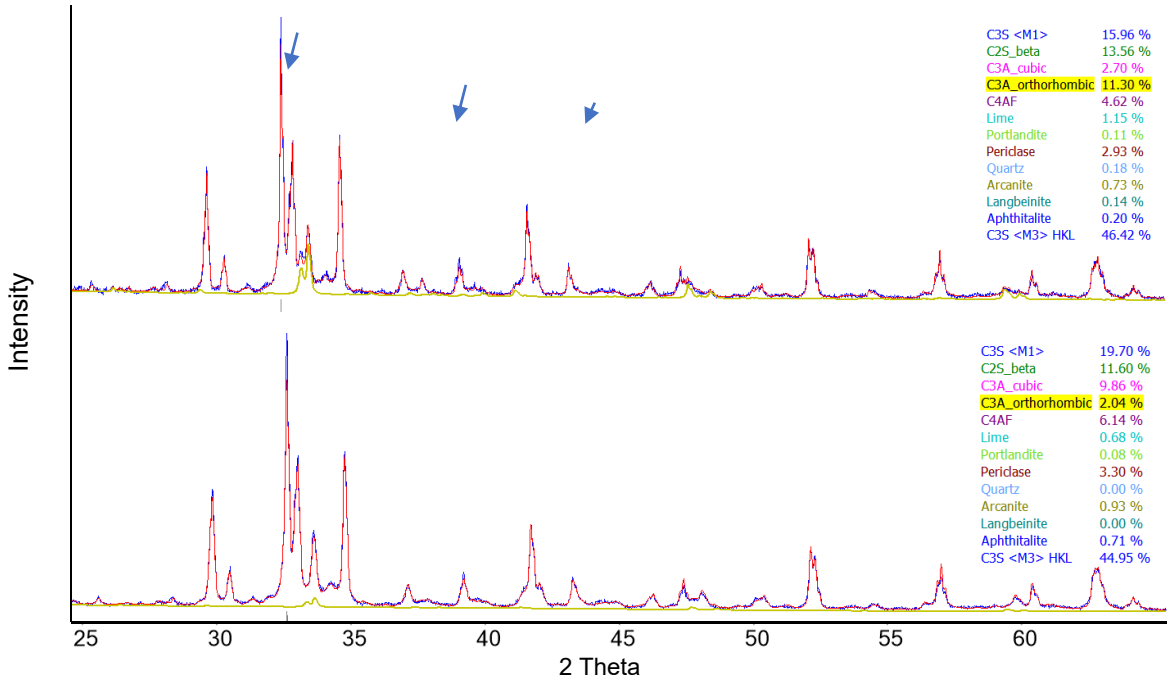

Fig. 9.2: XRD patterns showing different aluminat polymorphs from cement kiln (top, aluminat-O dominating – olive line) and from laboratory experiment (bottom, aluminat-C).

9.3.1 Bottom Ash from MSWI plants

The composition of bottom ash (BA) is dominated by crystalline (35-40%) and amorphous (50%) compounds, ferrous (10%) and non-ferrous metals (2.5%). The Swiss Waste Ordinance requests the recovery of metals before landfilling with limit value for the non-ferrous metals below 1 wt.-%. In most MSWI plants in Switzerland BA is wet discharged with subsequent conventional BA treatment for metal recovery. Individual plants, however, use enhanced techniques for metal recovery (ZAV Recycling AG, supersort®technologie, RecuLAB, Selfrag). However, about 85-90% of initial BA remains after metal separation regardless of the applied technique. The aim of this study is to evaluate the potential for deposition of BA residues with limited aftercare or their use as secondary raw material.

In contrast to conventional BA treatment, where only one residual fraction arises, enhanced BA treatment produces two BA fractions: fine fractions, which are separated prior to metal recovery and coarse fractions that undergo additional treatment. This multistep process leads to fractionation trends within fine fractions containing elevated concentrations of carbonates, sulphates, total organic carbon (TOC) and heavy metals (Fig. 9.3). The coarse fraction show elevated contents of silicates.

Deposition with low aftercare is permissible for the materials with low emissions, which is controlled by batch (Federal Office for the Environment 2017) and up-flow column leaching tests (CEN 2017). Column tests reveal the dynamics of mobilisation with increasing liquid-to-solid ratio (L/S) as is shown in Fig. 9.4 for dissolved organic carbon (DOC) of the three types of residual BA fractions. DOC is related to leaching of heavy metals (e.g. Cu) forming organic complexes at alkaline pH conditions (Comans et al. 1993; Johnson et al. 1996; Chandler et al. 1997; van Zomeren and Comans 2004; Dijkstra et al. 2006). All fractions show high initial concentrations, which decrease rapidly, so that at L/S 2 already 90% of the DOC is mobilised (Fig. 9.4a). As has been observed for total carbon contents, the leaching of DOC from the coarse fraction is smaller and elevated from the fine fraction, with respect to BA from conventional treatment (Fig. 9.4b).

The use of residual BA fractions as secondary raw material requires compliance with threshold values of the Swiss Waste Ordinance for total concentrations. Characterisation of residual BA fraction has shown that heavy metal concentrations for all fractions is too high for recycling, e.g. for the use in concrete industry. However, coarse fractions showing the lowest heavy metal concentrations are predestined for the further treatment. The most promising results were obtained by density separation, reducing the concentrations of most heavy metals in the light mineral fraction close to or below the relevant limit values (Fig. 9.2). However, Cu and especially Sb concentrations remain elevated and further tests on a laboratory scale are required.

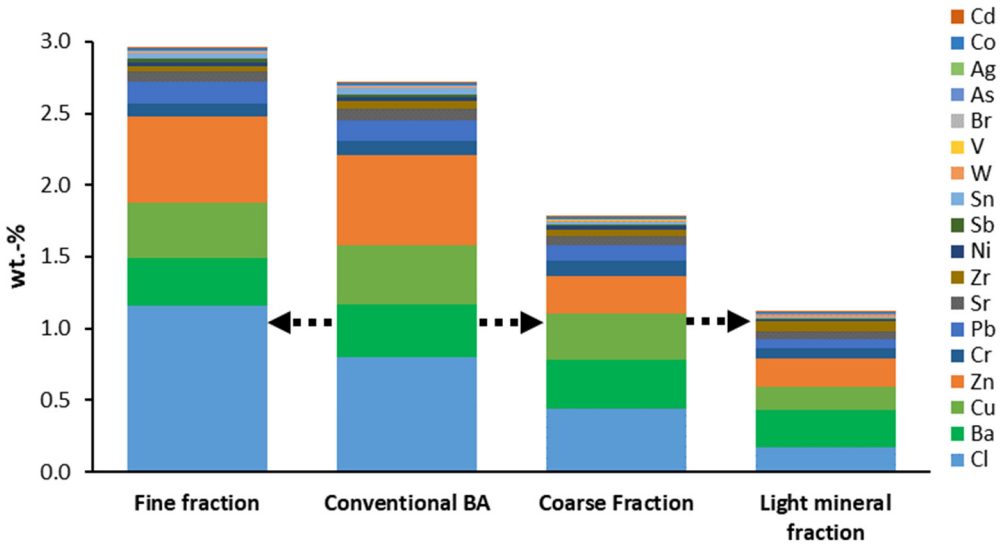

Fig. 9.3: Element concentrations of BA fractions after conventional metal recovery. The fine fraction shows a general metal enrichment, while the coarse and light mineral fractions are depleted.

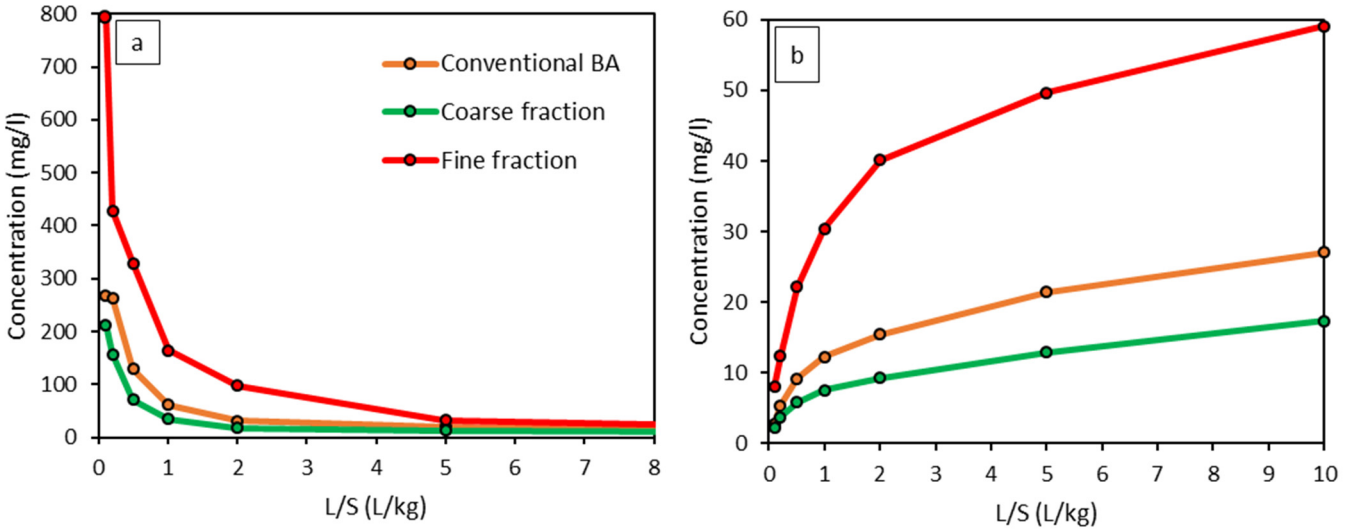

Fig. 9.4: a) Development of DOC concentrations from column experiments at increasing L/S ratio for different BA fractions (left) and the cumulated DOC release (right).

9.3.2 Fly ash from MSWI

The second mass stream remaining from waste incineration, the fly ash (FA), shows elevated concentrations of toxic constituents and heavy metals. The Swiss Waste Ordinance prescribes heavy metal extraction from FA. Commonly applied acid fly ash leaching produces a depleted filter cake (FC) for discharge. Heavy metal depletion rates are currently defined for Zn and Pb - dependent on the respective concentration in the FA, as well as technical and economic feasibility.

FA is composed by a mix of two ash materials: Electrostatic precipitator ash (ESPA; ~70-75%) and boiler ashes (BOA; ~25-30%), originating from up to 6 different boiler sections. All ash types were collected separately from three different Swiss MSWI plants, in order to characterise their formation conditions and mineralogical composition. The investigation was aimed at the identification of the binding forms of heavy metals that control the heavy metal leaching potential. Chemical and mineralogical analysis reveals that BOA and ESPA are two geochemically distinct materials. The BOAs from different boiler sections have very similar chemical and mineralogical composition despite their different formation conditions (between 600 and 250°C). They consist of the less volatile compounds of the flue gas and have comparably low heavy metal concentrations (~3% Zn), similar to the fine-grained fraction of the bottom ash (BA). An increased concentration of toxic compounds (Zn, Pb, Cd, Sb) had been observed at the superheater section of the boiler (BOA 3), as seen in Figure 9.5. Also, a trend of increasing concentration of the toxic PCDD/F phases can be observed towards the cooler end of the boiler, which is consistent with their formation at temperatures below 300°C (Zhang & Buekens 2016). PCDD/F concentrations are expected to be over the given threshold limit (1000 ng/kg; ADWO, 2016) in ESPA.

BOA is composed of anhydrite, quartz, lime, calcite, as well as different Ca/Al-silicates and shows a high content of amorphous phases (up to 40%). The ESPA is dominated by high Cl, S, Na, K and Zn (~8%) elements and is further enriched in Pb, Cu, Cd, Sb, Sn compared to BOA. The ESPA is mainly composed of very fine grained newly precipitated heavy metal bearing Cl^- and SO_4^{2+} salts, such as K_2ZnCl_4 or $Na_{21}Zn(SO_4)_{10}Cl_3$.

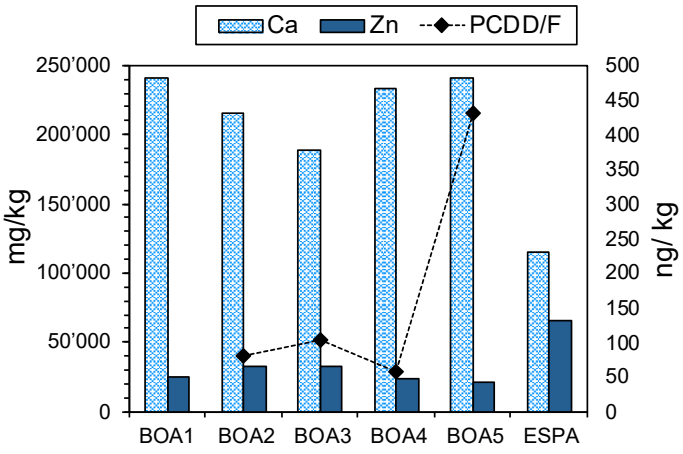

Fig. 9.5: Exemplary plot of the geochemical characteristics of the different BOAs and ESPA. BOAs are enriched in less volatile compounds and dust particles (such as Ca) and show lower concentrations in heavy metals (Zn) and toxic compounds (PCDD/F) compared to ESPA.

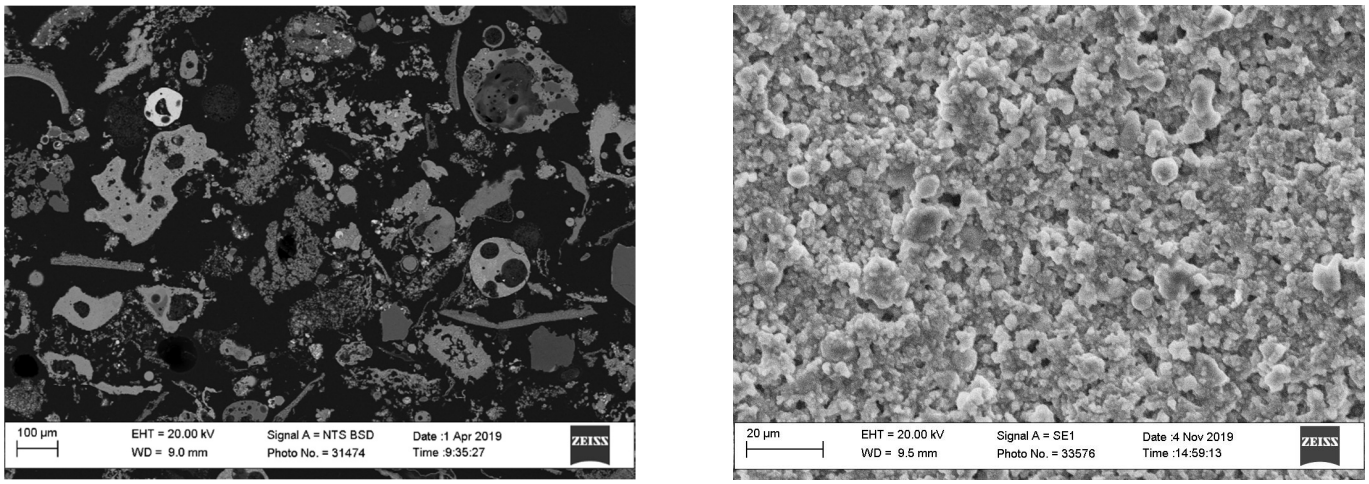

Fig. 9.6: Two geochemically distinct materials form the FA: coarse-grained, low crystalline BOA (left) and salt-dominated, fine-grained ESPA (right).

BOA has a high pH and redox buffering capacity because of the high concentration of "matrix" element (Ca, Si, Al^0). These chemical composition of BOA and cementation processes (Weibel et al. 2017) complicate leaching of redox sensitive heavy metal (Cu, Pb), even with high dosages of H_2O_2 added as oxidising agent. ESPA shows low pH and redox buffering capacity, which promises even higher Cu and Pb depletion after acid leaching compared to acid leaching of FA. Acid leaching experiments will be performed on the different ash types in order to evaluate whether the required heavy metal depletion rates can be achieved with reasonable effort. The results of this study helps to reveal whether BOA should be treated as BA or FA in terms of heavy metal depletion.

9.3.3 Fly ash from wood incineration

Wood ash (WA) produced by combustion of waste wood may have elevated concentrations of heavy metals (up to ~4 % Zn, ~1 % Pb) depending on the amount of co-incinerated contaminated wood. Out of ~60'000 tons of yearly produced wood ash in Switzerland, around 12'000 tons are highly polluted. The chemical and mineralogical composition of WA is comparable to MSWI fly ash (Fig. 9.7) for which, heavy metals recovery prior the disposal is prescribed by the Swiss Waste Ordinance from the year 2023.

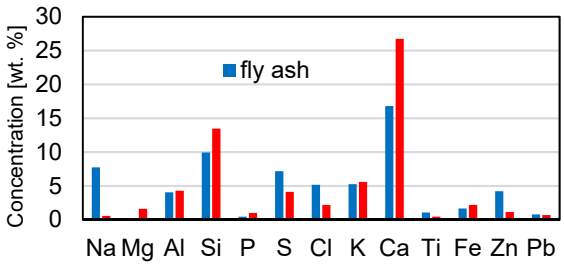

Fig. 9.7: Comparison of major chemical constituents in fly ash and wood ash.

However, WA generally has a higher content of metallic aluminium and calcium oxide. Thus, acidic leaching becomes less efficient and more complex. The high acid neutralising capacity of the WA requires a large amount of acid for the leaching at low pH condition in order to optimise metal recovery (Fig. 9.8). The recovery is also reduced by metallic aluminium as it causes reductive cementation of Cu and Pb. This can be countered by the usage of an oxidising agent (e.g. H_2O_2) which raises the operating costs of the whole process (Weibel 2017).

Another problem is the high amount of toxic Cr(VI) in wood ash. Chemically pre-treated wood (e.g. impregnation) WA may show Cr(VI) concentrations of

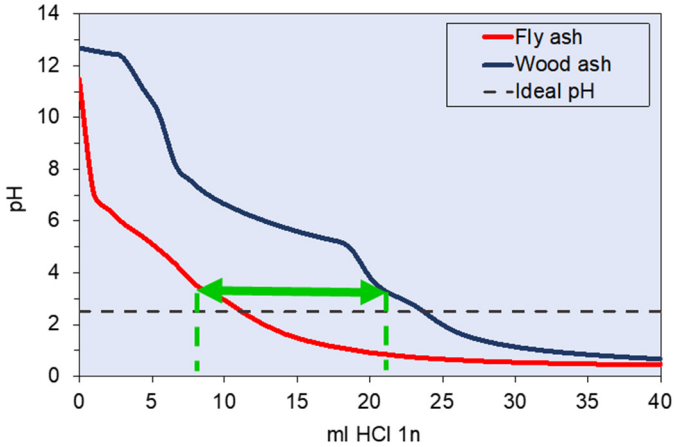

Fig. 9.8: Titration curve of 2 g fly/wood ash with a liquid/solid ratio of 10. The wood ash requires more than double the amount of acid to reach a pH value of 2.

up to 100 ppm, exceeding the threshold concentration for Swiss landfills (0.5 ppm) by the factor of 200. Fortunately, the acidic leaching does not only deplete heavy metals but also seems to successfully reduce Cr(VI) to Cr(III). This process takes place at very low pH conditions even when an oxidising agent is used to enhance the depletion of heavy metals (Wolffers 2019).

Currently, only acidic leaching fulfils the requirement of the Waste Ordinance even though the acidic treatment of wood ash is more demanding than that of MWSI fly ash and higher operating costs are expected. In September 2019 an extended study was launched to assess the technical feasibility and economic viability of treating the WA by acidic leaching and other processes as well as their combinations.

9.4 Thermal destruction of dioxins and furans in acid-leached fly ash from MSWI (ReFire)

In addition to metals, FA also contain various organic compounds, in particular polychlorinated dibenzo-p-dioxins and dibenzofurans (PCDD and PCDF). Dioxins are formed in the boiler area according to the de novo synthesis and accumulate in the FA. It is known from extensive monitoring studies that the dioxin content is subjected to high concentration fluctuations due to waste input, combustion conditions and process conditions during exhaust gas purification. The temperature curve and the heavy metal content in the gas phase can promote synthesis and increase the dioxin content.

PCCD/PCDF are not soluble during acid fly ash leaching (FLUWA) and remain in the leached filter cake (FC). In addition to external thermal treatment (Marb et al. 2004), two possible methods are currently available for reducing the dioxin loads in leached FC: a) ExDiox process (Fierz & Bunge 2006) by flotation of the dioxin-containing light particles and subsequent thermal destruction by returning them to the furnace of the MSWI, or b) return of the entire acid-leached FC to the furnace for complete thermal destruction of the dioxin load (ReFire). The project was financed by Environmental Technology Promotion and industrial partners and was carried out in cooperation with the development centre for sustainable management of recyclable waste and resources (ZAR). ReFire tests with the acid-leached FC from the FLUWA process were carried out at KEBAG and KEZO (2018-2019). This allowed the investigation of plants with dry and wet exhaust gas treatment as well as bottom ash (BA) treatment, which allows recommendation to be made with respect to all plant configurations currently used in Switzerland.

A fully automatic return feed of the FC was developed in one of the kiln lines at KEBAG, where one of the other lines served as a reference line, so that a direct comparison was guaranteed over the entire duration of the test. The recycled amount of FC corresponded proportionally to the amount of FA produced in the respective kiln line.

BA samples from the ReFire process and from reference furnace lines of KEBAG and KEZO were sampled and stored for a period of several weeks. The untreated BAs were processed after 3 months of storage at KEWU in Krauchthal and the mineral residual fraction was analysed for dioxins. Total 9 and 5 tons of BA per furnace line of tons (KEBAG) and (KEZO) respectively, were processed. Representative mineral fractions, 700 kg for each line, were taken and divided into 2 laboratory samples (A and B) of 30 kg each.

During recirculation, the measured dioxin contents in the reference FC were found to be 560 ng/kg and 580 ng/kg in dry matter (DM) from KEZO and KEBAG, respectively. The resulting dioxin contents in the ReFire BA did not differ from those of the reference line. They were between 4 and 9 ng/kg DM (Table 9.1). If no dioxin destruction had occurred during incineration, the added dioxin load by FC would have to be found again in the BA of the ReFire lines by its proportionate contribution of approx. 30 ng/kg DM. A corresponding increase in dioxin concentration was not observed in any of the ReFire BAs. No carry-over of dioxins into the FA or into the BA was observed (Table 9.1). A complete thermal destruction of the dioxin load of the FC could thus be demonstrated.

Tab. 9.1: Dioxin contents in ng/kg dry matter of the ReFire and reference BA samples. Samples A and B are the two independently collected and prepared laboratory samples.

	Slag A PCDD ng/kg	Slag B PCDD ng/kg
KEBAG *ReFire*	6.6	9.0
KEBAG *Reference*	8.7	5.8
KEZO *ReFire*	5.9	3.7
KEZO *Reference*	6.0	3.9

The ReFire process does not produce FA. Instead, the BA contains a corresponding proportion of “re-fired” ash. No negative effects were observed when recovering metals from BA. In the case of other elements - due to the different thermal stability - accumulation occurred in the ReFire BA compared to the reference BA. In particular, this concerned the three elements antimony, lead and tin (Table 9.2).

Tab. 9.2: Selected element enrichment and depletion in the ReFire BA compared to the reference BA. Numerical values >100% correspond to an increase, values <100% to a decrease. Standard deviation ±10%; Statistically changes are therefore only significant if <90% or >110%.

	KEBAG	KEZO		KEBAG	KEZO
Al	100%	101%	Ni	118%	102%
Ba	101%	93%	P	110%	99%
Ca	105%	102%	Pb	129%	115%
Cr	93%	109%	S	99%	112%
Cu	94%	89%	Sb	153%	133%
Fe	104%	101%	Si	99%	98%
K	102%	97%	Sn	108%	124%
Mg	99%	105%	Ti	103%	102%
Mn	97%	98%	Zn	98%	96%
Na	95%	97%			

Antimony shows strong increase of the concentration in the ReFire BA because Sb is enriched about ten fold in the FC incorporated in the reference BA in comparison to the ReFire BA. The increase of lead in the ReFire BA was due to the lower immobilisation of lead in the FLUWA process and the precipitation of lead sulfate. For sulphur, a statistically significant increase could only be observed in the KEZO ReFire BA. For KEZO, this corresponds to the specifically lower additional consumption of neutralisation chemicals in comparison to KEBAG where sulphur transfer into the exhaust gas is smaller. A separate treatment (discharge) of the neutral, sulfate-containing scrubber sludge is therefore recommended.

It has been shown that PCDD/PCDF can be completely destroyed by returning it to the furnace of the MSWI. The ReFire process eliminates the material flow of the FC and only BA remains as residue to be landfilled. On the other hand, the increased SO_2 load in the waste gas stream caused a significant increase in the consumption of neutralisation chemicals. An optimised design of the flue gas cleaning system of the MSWI should be implemented and enable further improvements in the future.

9.5 Assessment of quality criteria for solidified hazardous waste

Currently, a number of hazardous wastes produced in Switzerland are exported and disposed in underground depositories abroad. If, for any reason, this disposal route is no longer feasible, these materials will have to be treated or deposited in Switzerland. To fulfil the requirements of the Swiss Waste Ordinance, solidification/stabilisation of such waste materials need to be implemented. Solidification of waste aims at converting a liquid or semi-solid waste to a solid, monolithic form that allows for an easier handling and disposal. Stabilisation on the other hand focuses on producing a less toxic or less mobile form of the contaminant. As the aim of these procedures is the minimisation of contaminant release, both solidification and stabilisation are usually implemented in one single process.

The Swiss Waste Ordinance defines waste acceptance criteria for the Type C landfills based on threshold values in the leaching tests. The current study evaluates monitoring and testing methods for the estimation of the long-term environmental impact of Type C landfills containing solidified waste satisfying the Swiss Waste Ordinance and existing international norms. These methods are being applied and tested on a set of hazardous wastes originating from Switzerland, which were stabilised and solidified with Portland cement.

The integral assessment protocol comprise four "modules" aiming to provide a fundamental understanding of the processes and mechanisms promoting or inhibiting contaminant release: a) compressive strength, b) availability of contaminant release, c) long-term elution and d) computer modelling.

The compressive strength of a waste body is important for assessing its fundamental suitability for disposal in a landfill, where usually, the material is exposed to physical stress by the material dumped on top of it as well as the top lining of the landfill. A broad range of storage conditions have to be considered for assessing the potential for long-term contaminant release. The availability test thus investigates the release of metals over a wide pH range of 2-12. In these tests the resistance of the sample bodies against acid or base attack together with the pH dependence of contaminant release. The long-term test adapts the original batch eluate test according to the Waste Ordinance for a monolithic sample body and a time period of 64 days. Samples are taken at different times where the eluent is replaced at every step (batch reactor). Parallel to this test, a percolation test (column test) according to EU standard CEN/TS 14405 (CEN, 2017) with distilled water is done. Model calculations will be used to illustrate diffusion and solution processes in order to describe long-term system behaviour. Currently the results of the four “modules” from two solidified waste materials are being evaluated. First results (Fig. 9.9) show big differences in e.g. sulphur- and Cu mobilisation from two Portland cement-stabilised waste materials belonging to the same “class of waste”.

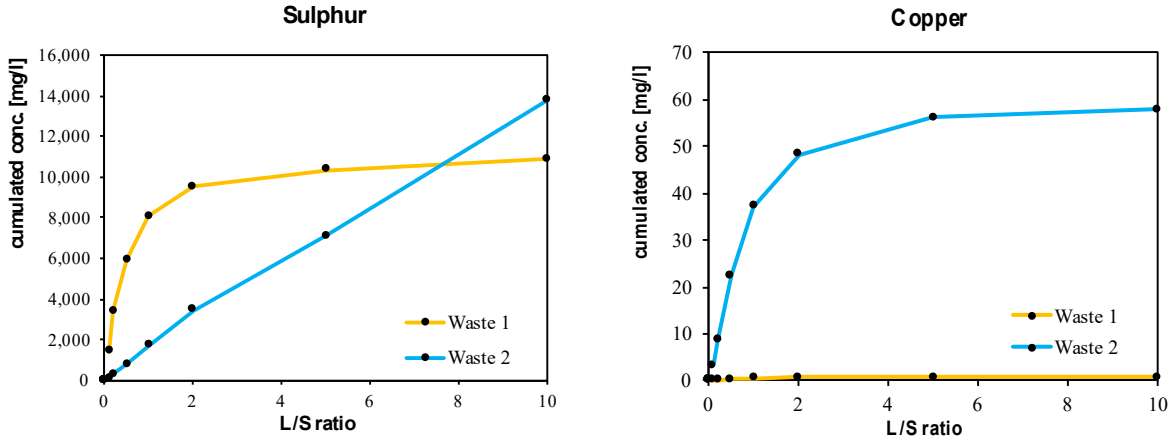

Figure 9.9: Cumulated leaching from the percolation tests. The sulphur concentrations of waste 1 and the copper concentrations of waste 2 show a decreasing release over time, whereas the sulphur in waste 2 has not (yet) reached a mobilisation plateau.

9.6 Landfill monitoring of dry-processed residual bottom ash

In recent years, research and development has mainly focused on returning as many metals as possible from BA from MSWI to the material cycle. Today, great attention is paid to the treatment and aftercare of the residual BA (85-90%) to be deposited at Type D landfill after metal separation. In addition to conventionally wet discharged BA, dry discharged BA has been increasingly processed and landfilled in Switzerland in recent years. In contrast to BA from wet discharge, the dry BA has a higher reactivity and a larger specific surface. A comprehensive monitoring of a dry BA landfill compartment was started in October 2018 to study the behaviour of the material and to make statements about the aftercare of the landfill. A central basis for the risk assessment of a landfill is the evaluation of the actual state based on investigations of solid material, leachate and gas emissions in the surrounding of the landfill.

The results of the monitoring show a temperature gradient from 90°C a few meters below the surface to about 40°C near the base of the landfill (Fig. 9.7). Last year, a temperature-decrease of 18% was measured over the entire depth profile. Increased temperatures in BA bodies are a known phenomenon (Speiser 2001). Metastable phases formed in the furnace react with water and oxygen from the air to form more stable compounds.

The monitored emissions via the gas and leachate path are in the range of data observed for other BA landfills in the early disposal stage. On average, 35% of the precipitation is discharged as leachate. The determined transfer coefficients of the substances analysed in the leachate show that 99.7% of the total organic carbon (TOC) and more than 99.9% of the heavy metals are currently still in the landfill body. Only for chlorine a relevant discharge can already be observed. Within 3 years approx. 14% of the chlorine present in the BA has been mobilised via the leachate. The discharge of dissolved nitrogen compounds has so far mobilised approx. 6% of the total amount of nitrogen. Short-term increases in leachate volumes play an important role in landfill dynamics. The continuous measurement of conductivity shows that an increased leachate

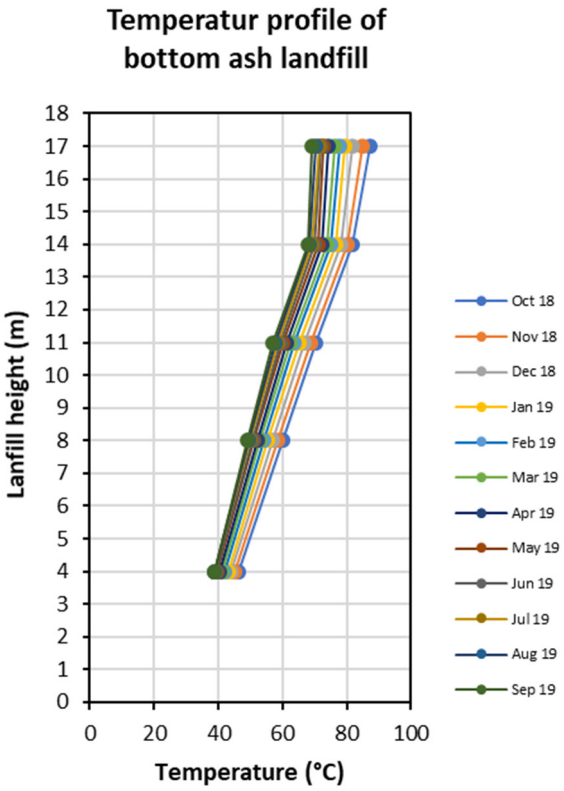

Fig. 9.7: Temperature development on different horizons of the bottom ash compartment between October 2018 and October 2019.

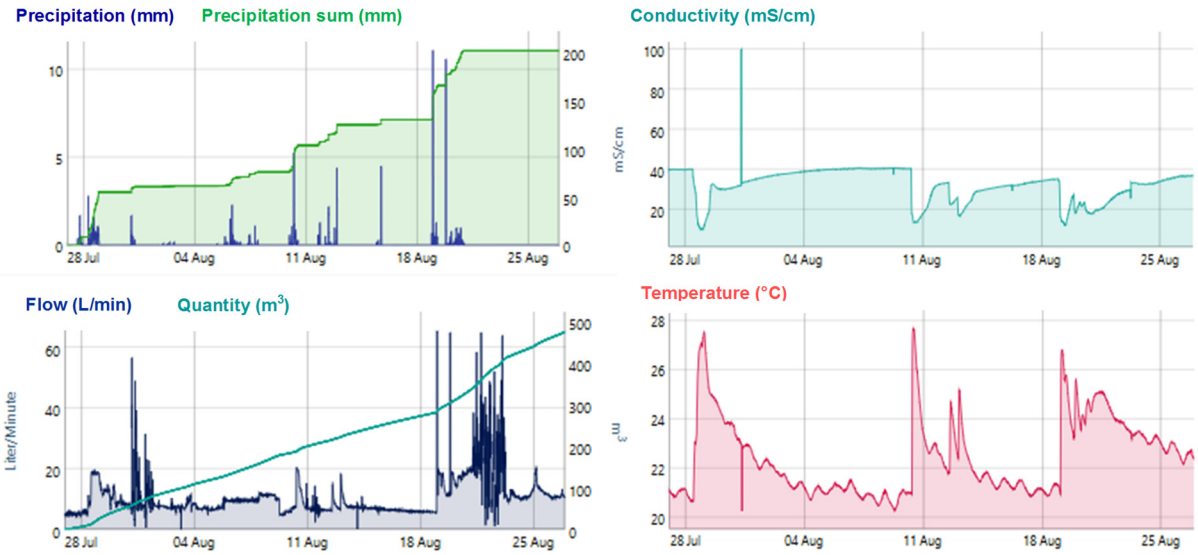

Fig. 9.8: Temperature development on different horizons of the bottom ash compartment between October 2018 and October 2019.

discharge is associated with a short-term decrease in conductivity from 35-40 mS to 10-15 mS (Fig. 9.8). On the other hand, an increased leachate discharge leads to an increase in temperature from approx. 20°C to approx. 27°C. Concentration development at different flow rate regimes shows that a short-term increased flow due to precipitation events leads to an increase of the pH value, dissolved organic carbon (DOC), copper and ammonium. An increase in temperature and pollutant concentration in the leachate are an indication that partially saturated zones are washed out of the BA body.

In order to develop a reliable forecast of the long-term behaviour of dry BA deposits, longer time series of landfill data must be evaluated. Since these time series are still missing for dry BA, the results of this study should be compared with long-term time series of wet BA landfills. For a risk assessment, a long-term prognosis has to be carried out under consideration of changing conditions. The influences of temperature, pH value, redox conditions, sorption and biological activity are planned to be investigated in a follow-up project using reactive transport models.

9.7 References

CEN (2017)
TS 14405, Characterisation of waste - Leaching behaviour tests - Up-flow percolation test (under specified conditions). European Committee for Standardization.

Chandler A. J., Eighmy T. T., Hjelmar O., Kosson D., Sawell S., Vehlow J., Van der Sloot H., Hartlén J. (1997)
Municipal solid waste incinerator residues. Studies in Environmental Science 67, Elsevier, Amsterdam.

Comans R., Van der Sloot H., Bonouvrie P. (1993) Geochemical reactions controlling the solubility of major and trace elements during leaching of municipal solid waste incinerator residues, Proceedings of the International Conference on Municipal Waste Combustion, 667-679.

Dijkstra J. J., Van Der Sloot H. A., Comans R. N. (2006)
The leaching of major and trace elements from MSWI bottom ash as a function of pH and time. Applied Geochemistry 21, 335-351.

Federal Office for the Environment (2017)
Messmethoden im Abfall- und Altlastenbereich: Umwelt-Vollzug Nr. 1715, 1-82.

Fierz R., Bunge R. (2006)
Schlussbericht exDIOX - Dioxinentfernung aus sauer gewaschener KVA-Filterasche, UMTEC.

Fisch M., Eggenberger U. (2017)
Inventar der Schweizerischen Kieswaschschlämme. Studie im Auftrag Fachverband der Schweizerischen Kies- und Betonindustrie FSKB.

Johnson C., Kersten M., Ziegler F., Moor H. (1996) Leaching behaviour and solubility-controlling solid phases of heavy metals in municipal solid waste incinerator ash. Waste Management 16, 129-134.

Marb C., Bogner C., Schindler M., Schuller M. (2004) Aufgabe eines sauer extrahierten Kessel-Elektrofilterasche-Gemischs am MHKW Kempten, Bayerisches Landesamt für Umweltschutz.

Speiser C. (2001)
Exothermer Stoffumsatz in MVA-Schlackendeponien: Mineralogische und geochemische Charakterisierung von Müllverbrennungsschlacken, Stoff- und Wärmebilanz. Technische Universität München, 1-262.

Swiss Confederation (2015)
Ordinance on the Avoidance and the Disposal of Waste (ADWO), 1-46.

Van Zomeren A., Comans R. N. (2004)
Contribution of natural organic matter to copper leaching from municipal solid waste incinerator bottom ash. Environmental Science and Technology 38, 3927-3932.

Weibel G., Eggenberger U., Schlumberger S., Mäder U.K. (2017)
Chemical associations and mobilization of heavy metals in fly ash from municipal solid waste incineration. Waste Management 62, 147-159.

Wolffers M. (2019)
The impact of wood ash and acid fly ash leaching regarding heavy metal recovery a and Cr(VI) reduction. Master thesis, University of Bern, Bern, Switzerland.

Zhang M., Buekens A. (2016)
De novo synthesis of dioxins: a review'. International Journal of Environment and Pollution 60, 63-110.

10 PUBLICATIONS

10.1 Peer reviewed journals

Afroughsabet V.[1], Geng G., Lin A.[2], Biolzi L.[1], Ostertag C.P.[2], Monteiro P.J.M.[2]
The influence of expansive cement on the mechanical, physical, and microstructural properties of hybrid-fiber-reinforced concrete. Cement and Concrete Composites 96, 21-32 (2019).
[1]Politecnico di Milano, Milan, Italy
[2]University of California, Berkeley, USA

Cametti G.[1], Scheinost A.C.[2, 3], Churakov S.V.
Structural modifications and thermal stability of Cd^{2+}-exchanged stellerite, a zeolite with STI framework type. Journal of Physical Chemistry C 123, 25236-25245 (2019).
[1]Institute of Geological Sciences, University of Bern, Bern, Switzerland
[2]IRE, Helmholtz-Zentrum Dresden-Rossendorf, Dresden, Germany
[3]ROBL, ESRF, Grenoble, France

Cametti G.[1], Scheinost A.C.[2, 3], Giordani M.[1], Churakov S.V.
Framework modifications and dehydration path of a Ag^{+}-modified zeolite with STI framework type Journal of Physical Chemistry C 123, 13651-13663 (2019).
[1]Institute of Geological Sciences, University of Bern, Bern, Switzerland
[2]IRE, Helmholtz-Zentrum Dresden-Rossendorf, Dresden, Germany
[3]ROBL, ESRF, Grenoble, France

Curti E., Xto J.[1, 2], Borca C.N.[1], Henzler K.[1], Huthwelker T.[1], Prasianakis N.I.
Modelling Ra-bearing baryte nucleation/precipitation kinetics at the pore-scale: application to radioactive waste disposal. European Journal of Mineralogy 31, 247-262 (2019).
[1]SLS, Paul Scherrer Institut, Villigen, Switzerland
[2]Department of Chemistry, Swiss Federal Institute of Technology (ETHZ), Zürich, Switzerland

Di Lorenzo F.[1], Ruiz-Agudo C. [2], Churakov S.V.
The key effects of polymorphism during Pb-II uptake by calcite and aragonite. Crystal Engineering Communications 21, 6145-6155 (2019).
[1]Institute of Geological Sciences, University of Bern, Bern, Switzerland
[2]University of Konstanz, Germany

Fazeli H.[1], Patel R.A., Ellis B.R.[2], Hellevang H.[1]
Three-dimensional pore-scale modeling of fracture evolution in heterogeneous carbonate caprock subjected to CO_2-enriched brine. Environmental Science and Technology 53, 4630-4639 (2019).
[1]University of Oslo, Oslo, Norway
[2]University of Michigan, Ann Arbor, USA

Gautschi A.[1], Gaus I.[1], Gimmi T., Mazurek M.[2], Wersin P.[2], Cathelineau M.[3], Bath A.[4]
Preface: Applied Geochemistry Special Issue on "Geochemistry of clays and clay rocks in the context of radioactive waste disposal". Applied Geochemistry 105, 127–129 (2019).
[1]Nagra, Wettingen, Switzerland
[2]Institute of Geological Sciences, University of Bern, Bern, Switzerland
[3]Laboratoire GeoResources, Université de Lorraine, Nancy France
[4]Intellisci, Willoughby on the Wolds, Loughborough, United Kingdom

Gimmi T., Churakov S.V.
Water retention and diffusion in unsaturated clays: Connecting atomistic and pore-scale simulations. Applied Clay Science 175, 169-183 (2019).

Giordani M. [1], Cametti G. [1], Di Lorenzo F. [1], Churakov S.V.
Real-time observation of fibrous zeolites reactivity in contact with simulated lung fluids (SLFs) obtained by atomic force microscope (AFM). Minerals 9, 83 (2019).
[1]Institute of Geological Sciences, University of Bern, Bern, Switzerland

Hummel W., Filella M.[1], Rowland D.[2]
Where to find stability constants? Science of the Total Environment 692, 49-59 (2019).
[1]University of Geneva, Geneva, Switzerland
[2]University of Western Australia, Crowley, Australia

Kéri A., Dähn R., Krack M., Churakov S.V.
Characterisation of structural iron in smectites - an *ab initio* based X-ray absorption spectroscopy study. Environmental Science and Technology 53, 6877-6886 (2019).

Li J.[1], Geng G., Myers R. [2], Yu Y.-S.[3], Shapiro D.A.[3], Carraro C. [1], Maboudian R. [1], Monteiro P.J.M.[1]
The chemistry and structure of calcium (alumino) silicate hydrate: A study by XANES, ptychographic imaging, and wide- and small-angle scattering. Cement and Concrete Research 115, 367-378 (2019).
[1]University of California, Berkeley, California, USA
[2]University of Edinburgh, Edinburgh, UK
[3]ALS/LBNL, Berkeley, USA

Li J.[1], Geng G., Zhang W. [1], Yu Y.-S.[2], Shapiro D.A.[2], Monteiro P.J.M.[1]
The hydration of β- and α′H-dicalcium silicates: an X-ray spectromicroscopic study. ACS Sustainable Chemistry and Engineering 7, 2316-2326 (2019).
[1]University of California, Berkeley, USA
[2]ALS/LBNL, Berkeley, USA

Liu L.[1], Sun C.[1], Geng G., Feng P.[2], Li J.[3], Dähn R.
Influence of decalcification on structural and mechanical properties of synthetic calcium silicate hydrate (C-S-H). Cement and Concrete Research 123, 105793 (2019).
[1]Hohai University, Nanjing, China
[2]Southeast University, Nanjing, Jiangsu, China
[3]University of California, Berkeley, USA

Liu X.[1, 2], Vinograd V.L.[3], Nichenko S., Kulik D.A., Lu X.[1], Winkler B.[2]
Emulation of short-range ordering within the Compound Energy Formalism: Application to the calcite-magnesite solid solution. Calphad 64, 115-125 (2019).
[1]State Key Lab for Mineral Deposits Research, School of Earth Sciences and Engineering, Nanjing University, China
[2]Institute of Geosciences, Goethe Universität Frankfurt am Main, Germany
[3]Institute of Energy and Climate Research (IEK-6), Forschungszentrum Jülich, Germany

Lothenbach B.[1], Kulik D.A., Matschei T.[2], Balonis M.[3], Baquerizo L.[4], Dilnesa B.[5], Miron G.D., Myers R.J.[6]
Cemdata18: A chemical thermodynamic database for hydrated Portland cements and alkali-activated materials. Cement and Concrete Research 115, 472-506 (2019).
[1]Empa, Dübendorf, Switzerland
[2]HTW Dresden, Dresden, Germany
[3]University of California, Los Angeles, USA
[4]Lafarge Centre de Recherche, Lyon, France
[5]BASF, Basel, Switzerland
[6]University of Sheffield, Sheffield, United Kingdom

Marques Fernandes M., Baeyens B.
Cation exchange and surface complexation of lead on montmorillonite and illite including competitive adsorption effects. Applied Geochemistry 100, 190-202 (2019).

Miron G.D., Leal A.M.M. [1], Yapparova A.[1]
Thermodynamic properties of aqueous species calculated using the HKF model: How do different thermodynamic and electrostatic models for solvent water affect calculated aqueous properties? Geofluids 2019, 5750390 (2019).
[1]ETH Zurich, Zurich, Switzerland

Nedyalkova L., Lothenbach B.[1], Renaudin G.[2], Mäder U.[3], Tits J.
Effect of redox conditions on the structure and solubility of sulfur- and selenium-AFm phases. Cement and Concrete Research 123, 105803 (2019).
[1]Empa, Dübendorf, Switzerland
[2]Université Clermont Auvergne, Clermont-Ferrand, France
[3]University of Bern, Bern, Switzerland

Poonoosamy J.[1], Westerwalbesloh C.[2], Deissmann G.[1], Mahrous M., Curti E., Churakov S.V., Klinkenberg M.[1], Kohlheyer D.[2], von Lieres E.[2], Bosbach D.[1], Prasianakis N.I.
A microfluidic experiment and pore-scale modelling diagnostics for assessing mineral precipitation and dissolution in confined spaces. Chemical Geology 528, 119264 (2019).
[1]Institute of Energy and Climate Research (IEK-6): Nuclear Waste Management and Reactor Safety, Forschungszentrum Jülich, Jülich, Germany
[2]Institute of Bio- and Geosciences (IBG-1): Biotechnology, Forschungszentrum Jülich, Jülich, Germany

Safi M.A.[1], Mantzaras J.[1], Prasianakis N.I., Lamibrac A.[2], Büchi F.N.[2]
A pore-level direct numerical investigation of water evaporation characteristics under air and hydrogen in the gas diffusion layers of polymer electrolyte fuel cells. International Journal of Heat and Mass Transfer 129, 1250-1262 (2019).
[1]Laboratory for Scientific Computing and Modelling, LSM-NES, Paul Scherrer Institut, Villigen, Switzerland
[2]Laboratory for Electrochemistry, LEC - ENE, Paul Scherrer Institut, Villigen, Switzerland

Shi Z.[1], Geng G., Leemann A.[1], Lothenbach B.[1]
Synthesis, characterisation, and water uptake property of alkali-silica reaction products. Cement and Concrete Research 121, 58-71 (2019).
[1]Empa, Dübendorf, Switzerland

Soler J.M.[1], Steefel C.I.[2], Gimmi T., Leupin O.X.[3], Cloet V.[3]
Modelling the ionic strength effect on diffusion in clay. The DR-A experiment at Mont Terri. ACS Earth and Space Chemistry, 3, 442-451 (2019).
[1]IDAEA-CSIC, Barcelona, Spain
[2]Lawrence Berkeley National Laboratory, Berkeley, USA
[3]Nagra, Wettingen, Switzerland

Yang Y.[1], Patel R.A., Churakov S.V, Prasianakis N.I., Kosakowski G., Wang M.[1]
Multiscale modeling of ion diffusion in cement paste: electrical double layer effects. Cement and Concrete Composites 96, 55–65 (2019).
[1]Department of Engineering Mechanics and CNMM, Tsinghua University, Beijing, China

Yapparova A.[1], Miron G.D., Kulik D.A., Kosakowski G., Driesner T.[1]
An advanced reactive transport simulation scheme for hydrothermal systems modelling. Geothermics 78, 138–153 (2019).
[1]Institute of Geochemistry and Petrology, ETH Zurich, Zurich, Switzerland

Zhou Y.[1], Orozco C.A.[2], Duque-Redondo E.[3], Manzano H.[3], Geng G., Feng R.[1], Monteiro P.J.M.[2], Miao C.[1]
Modification of poly(ethylene glycol) on the microstructure and mechanical properties of calcium silicate hydrates. Cement and Concrete Research 115, 20-30 (2019).
[1]Southeast University, Nanjing, China
[2]University of California, Berkeley, USA
[3]University of the Basque Country UPV/EHU, Leioa, Spain

10.2 Technical reports

Jenni A., Wersin P., Thoenen T., Baeyens B., Ferrari A., Gimmi T., Mäder U., Marschall P., Hummel W., Leupin O.
Bentonite backfill performance in a high-level waste repository: a geochemical perspective. Nagra Technical Report NTB 19-03 (2019).

Prasianakis N.I., Kimura S., Churakov S.V., Van Loon L., Wigger C., Kikura H.
Measurement of water saturation level in Opalinus Clay via non-destructive ultrasound apparatus, basis for a monitoring technique. Mont Terri Technical Note TN2017-07 (2019).

10.3 Conference proceedings

Geng G., Dähn R., Wieland E., Monteiro P.J.M. Molecular-scale mechanical property of calcium silicate/aluminate hydrates studied with synchrotron-based XRD, Proceedings of 15th International Congress of the Chemistry of Cements, Prague, Czech Republic, 16-20 September 2019.

Mancini A., Wieland E., Lothenbach B., Dähn R., Geng G., Wehrli B.
Fe in GGBFS: New insights from laboratory experiments and synchrotron-based investigations, Proceedings of the 15th International Congress of the Chemistry of Cements, Prague, Czech Republic, 16-20 September 2019.

10.4 Invited talks

Churakov S.V.
Multiscale mechanistic modelling of reactive transport phenomena in nuclear waste disposal systems, Nuklearchemie, Dresden, Germany, 25-27 September 2019 (Key Note).

Gimmi T., Jenni A., Alt-Epping P., Krejci P.
Ion transport in clays: Comparing ion-exchange, surface-diffusion, and diffuse-layer modelling approaches, EUROCLAY 2019, Paris, France, 1-5 July 2019.

Glaus M.A., Van Loon L.R.
Diffusive transport of strongly sorbing radionuclides in argillaceous media: Effect of solution composition and compaction. 14th Biennial Symposium on Nuclear and Radiochemistry (NUCAR-2019), Mumbai, India, 15-19 January 2019.

Glaus M.A., Van Loon L.R.
Diffusive transport of strongly sorbing radioelements in argillaceous media: old wines in new bottles.
17th International Conference on the Chemistry and Migration Behavior of Actinides and Fission Products in the Geosphere, Kyoto, Japan, 15−20 September 2019.

Kéri A., Cametti G., Dähn R., Krack M., Churakov S.V.
Atomistic modelling approach for interpretation of spectroscopic data, 29th Goldschmidt Conference, Barcelona, Spain, 18-23 August 2019.

Marques Fernandes M.F., Scheinost A.C., Baeyens B. Reduction of NpO_2^+ and TcO_4^- at the Fe^{II}-montmorillonite-water interface. 29th Goldschmidt Conference 2019, Barcelona, Spain, 18-23 August 2019.

Miron G.D., Kulik D.A., Thoenen T.
Estimating temperature dependence of Ln and An complexes using isocoulombic reactions. 29th Goldschmidt Conference, Barcelona, Spain, 18-23 August 2019.

Prasianakis N.I.
Cross-scale reactive transport modelling: prediction of porous media evolution due to dissolution and precipitation processes. CECAM-FR-RA Current Challenges in transport, growth and dissolution at mineral-fluid interfaces, Lyon, France, 3-5 April 2019.

10.5 Conferences/workshops/presentations

Baeyens B., Marques Fernandes M.
Validation of experimental radionuclide adsorption data on argillaceous rocks by mechanistic models. 17th International Conference on the Chemistry and Migration Behavior of Actinides and Fission Products in the Geosphere, Kyoto, Japan, 15-20 September 2019.

Cametti G., Churakov S.V.
Structural modifications and thermal stability of Cd^{2+}-exchanged stellerite, a zeolite with STI framework type. Jointly meeting of the Italian Zeolite Association (AIZ) Czech-Italian-Spanish (CIS) Conference Italian Interdivisional Catalysis Group (GIC), Amantea (CS), Italy, 11-14 June 2019.

Cametti G., Scheinost A.C., Churakov S.V.
Crystal structure and dehydration behavior of Ag+-exchanged levyne. 32nd European Crystallographic Meeting, Vienna, Austria, 18-23 August 2019.

Claret F., Bracke G., Pepin G., Cances C., Kolditz O., Prasianakis N.I., Baksay A., Lukin D.
Development and improvement of numerical methods and tools for modelling coupled processes: a R&D initiative within EURAD, 9th European Commission Conference on EURATOM Research and Training in Safety of Reactor Systems and EURADWASTE '19, Pitesti, Romania, 4-7 June 2019.

Curti E., Kulik D.A.
Effect of Cr-doping on UO_2 spent fuel thermodynamics: preliminary data and results, 2nd Annual Meeting of the DISCO project, Cologne, Germany, 27-29 May 2019.

Di Lorenzo F., Ruiz-Agudo C., Churakov S.V.
Cadmium and lead coprecipitation during replacement of calcium carbonate minerals, 7th Granada Münster Discussion Meeting on Mineral Reactivity: from biomineralization and Earth's climate evolution to CO2 capture and built heritage conservation, Granada, Spain, 27-29 November 2019.

Di Lorenzo F., Ruiz-Agudo C., Churakov S.V.
Uptake of Pb^{II} by $CaCO_3$: the influence of polymorphism on the process, 29th Goldschmidt Conference, Barcelona, Spain, 18-23 August 2019.

Dähn R.
State-of-the-art microspectroscopic characterisation of cementitious materials used for the engineered barrier of a deep geological repository. EUROSAFE 2019, Cologne, Germany, 4-5 November 2019.

Geng G.
Microscale chemistry of C_3A hydration – evidences from recent synchrotron experiments. Nanocem Workshop "Tribute to Ellis Gartner", Villars sur Ollon, Switzerland, 17-19 June 2019.

Guillemot T., Wieland E., Kunz D., Cvetković B.Z.
Corrosion of irradiated steel in cementitious environment: Speciation of carbon-14. 5th International Workshop on Mechanisms and Modelling of Waste/Cement Interactions, Karlsruhe, Germany, 25-27 March 2019.

Guillemot T., Wieland E., Kunz D., Cvetković B.Z.
Understanding the carbon speciation during iron corrosion in alkaline anoxic conditions for safety assessment of radioactive waste repositories, 7th International Workshop on Long-term Prediction of Corrosion Damage in Nuclear Waste Systems, Nancy, France, 19-21 November 2019.

Hummel W.
Mission impossible: Building the all-purpose chemical thermodynamic database. COST Action TD1407 Network on Technology-Critical Elements: Advanced Workshop on Solution Chemistry of TCEs, Białystok, Poland, 22-23 January 2019.

Hummel W.
Metal-humic binding models: Make them as simple as possible, but not simpler. COST Action TD1407 Network on Technology-Critical Elements: Advanced Workshop on Solution Chemistry of TCEs, Białystok, Poland, 22-23 January 2019.

Kosakowski G., Lothenbach B.
Influence of temperature pulse on a cementitious near field. 5th International Workshop on Mechanisms and Modelling of Waste/Cement Interactions, Karlsruhe, Germany, 25-27 March 2019.

Kosakowski G., Lothenbach B.
Influence of temperature pulse on a cementitious near field. EGU General Assembly, Vienna, Austria, 7-12 April 2019.

Krejci P., Gimmi T., Van Loon L.
Modelling diffusion of sorbing cations in Opalinus Clay. 29th Goldschmidt Conference, Barcelona, Spain, 18-23 August 2019.

Kulik D.A., Miron G.D., Lothenbach B.
Thermodynamic modelling of An and FP uptake in C-S-H. 5th International Workshop on Mechanisms and Modelling of Waste/Cement Interactions, Karlsruhe, Germany, 25-27 March 2019.

Kulik D.A., Miron G.D., Tits J., Lothenbach B.
Geochemical modelling of retention of radionuclides in C-S-H. 17th International Conference on the Chemistry and Migration Behavior of Actinides and Fission Products in the Geosphere, Kyoto, Japan, 15-20 September 2019.

Lösch H., Tits J., Marques Fernandes M., Baeyens B., Krüger S., Stumpf T., Huittinen N.
Uranium(VI) complexation with aqueous silicates in the acidic to alkaline pH-range. 17th International Conference on the Chemistry and Migration Behavior of Actinides and Fission Products in the Geosphere 2019, Kyoto, Japan, 15-20 September 2019.

Luraschi P., Gimmi T.
Long-term evolution of porosity and mineralogy at cement-clay interfaces. 29th Goldschmidt Conference, Barcelona, Spain, 18-23 August 2019.

Luraschi P., Gimmi T., Van Loon L.R, Shafizadeh A., Churakov S.V.
5 years of monitoring of cement-clay interfaces: HTO and ^{36}Cl diffusivity and its relation to porosity changes. 5th International Workshop on Mechanisms and Modelling of Waste/Cement Interactions, Karlsruhe, Germany, 25-27 March 2019.

Mahrous M., Poonoosamy J., Curti E., Churakov S.V., Prasianakis N.I.
Microfluidic numerical diagnostics for the interpretation of lab-on-a-chip mineral precipitation experiments, 16th International Conference for Mesoscopic Methods in Engineering and Science (ICMMES 2019), Edinburgh, UK, 22-26 July 2019.

Mahrous M., Sultan S., Liao Q., Prasianakis N.I., Curti E., Churakov S.V.
Approaches for initial porosity permeability distribution parametrisation in continuum-scale reactive transport simulations. 29th Goldschmidt Conference, Barcelona, Spain, 18-23 August 2019.

Maier M.L., Patel R.A., Prasianakis N.I., Churakov S.V., Nirschl H., Krause M.J.
Fully coupled multiscale lattice Boltzmann-discrete element model for dense reactive particulate flows, 16th International Conference for Mesoscopic Methods in Engineering and Science (ICMMES 2019), Edinburgh, UK, 22-26 July 2019.

Mancini A., Wieland E., Lothenbach B., Dähn R., Geng G., Wehrli B.
Interaction of Fe(III) with calcium-silicate-hydrates, 5th International Workshop on Mechanisms and Modelling of Waste/Cement Interactions, Karlsruhe, Germany, 25-27 March 2019.

Marafatto F.F., Ferreira-Sanchez D., Dähn R., Grolimund D., Voegelin A.
Thallium redox speciation in soil Mn concretions by X-ray imaging. 29th Goldschmidt Conference, Barcelona, Spain, 18-23 August 2019.

Marafatto F.F., Ferreira-Sanchez D., Dähn R., Grolimund D., Voegelin A.
Hard X-ray imaging of trace elements in environmental samples. Eawag Symposium, Dübendorf, Switzerland, 13 September 2019.

Marques Fernandes M., Scheinost A.C., Huittinen N., Baeyens B.
Sorption of U^{VI} and Eu^{III} by illite: The deceptive role of trace phosphate minerals. 17th International Conference on the Chemistry and Migration Behavior of Actinides and Fission Products in the Geosphere 2019, Kyoto, Japan, 15-20 September 2019.

Molins S., Soulaine C., Prasianakis N.I., Abbasi A., Poncet P., Ladd A.J.C., Starchenko V., Roman S., Trebotich D., Tchelepi H.A., Steefel C.I.
A benchmark problem set for the simulation of mineral dissolution at the pore-scale with evolving fluid-solid interfaces, American Geophysical Union, AGU Fall Meeting, San Francisco, USA, 9-13 December 2019.

Patel R. A.
Ion transport in cement paste: Perspective from pore-scale modelling. 2nd ERICA modelling workshop, EPFL, Lausanne, Switzerland, 16-17 January 2019.

Pellegrini D., Detillieux V., Swahn J., Pfingsten W., Zeleznik N.
The sitex initiative, 9th European Commission Conference on EURATOM Research and Training in Radioactive Waste Management, Pitesti, Romania, 4-7 June 2019.

Poonoosamy J., Deissmann G., Mahrous M., Curti E., Churakov S.V., Klinkenberg M., Bosbach D., Prasianakis N.I.
A microfluidic experiment and pore-scale modelling for assessing mineral precipitation and dissolution in confined spaces. 29th Goldschmidt Conference, Barcelona, Spain, 18-23 August 2019.

Prasianakis N.I.
Technical R&D, Modelling and simulation of multiphysics multiscale processes. GlaxoSmithKline Vaccines, Rixensart, Belgium, 13 November 2019.

Schliemann R., Kurganskaya I., Churakov S.V.
Molecular mechanism of dissolution, growth and ion uptake at the clay mineral/water interface 29th Goldschmidt Conference, Barcelona, Spain, 18-23 August 2019.

Schliemann R., Kurganskaya I., Churakov S.V.
Molecular mechanism of dissolution, growth and ion uptake of clay minerals at the mineral/water interface, EuroClay 2019, Paris, France, 1-5 July 2019.

Soler J.M., Steefel C.I., Gimmi T., Leupin O.X., Cloet V.
The effect of ionic strength on diffusion in clay. Modeling solute transport and retention in the DR-A experiment at Mont Terri. 17th International Conference on the Chemistry and Migration Behavior of Actinides and Fission Products in the Geosphere, Kyoto, Japan, 15-20 September, 2019.

Tits J., Wieland E.
Formate and acetate stability under repository relevant conditions: What can we learn from the literature? 5th International Workshop on Mechanisms and Modelling of Waste/Cement Interactions, Karlsruhe, Germany, 25-27 March 2019.

Wieland E.
Long-term chemical evolution of wasteforms predicted by geochemcial modelling, EUROSAFE 2019, Cologne, Germany, 4-5 November 2019.

Wieland E., Kosakowski G., Lothenbach B., Kulik D.A.
A geochemical modelling approach for predicting long-term waste-cement interactions, 5th International Workshop on Mechanisms and Modelling of Waste/Cement Interactions, Karlsruhe, Germany, 25-27 March 2019.

Wieland E., Guillemot T., Kunz D., Tits J., Salazar G., Szidat S.
Corrosion of irradiated steel in cementitious environment: Speciation of carbon-14, 7th International Workshop on Long-term Prediction of Corrosion Damage in Nuclear Waste Systems, Nancy, France, 19-21 November 2019.

10.6 Teaching

Churakov S.V.
Master course: Atomistic simulations of geomaterials, Institut für Geologie, Universität Bern. Fall semester.

Churakov S.V.
Bachelor course: Kristallographie I+II, Institut für Geologie, Universität Bern, March 22, 2019. Institut für Geologie, Universität Bern, Spring and Fall Semester.

Churakov S.V.
Bachelor course: Kristalloptik. Institut für Geologie, Universität Bern, Fall Semester.

Curti E.
Lecturer for master course: Geological Disposal of Radioactive Waste, Institut für Geologie, Universität Bern, 22 March 2019.

Emmerich K., Gimmi T., Jaeggi D.
Water content in clays and clay rocks and implications for radioactive waste repositories, 5. Herbstschule, Material – Prozesse – Systeme, Karlsruhe Institut of Technology KIT, 8-11 October 2019.

Gimmi T., Alt-Epping P.
Geochemical Modelling II: Reactive Transport, Lecture and examinations, University of Bern, Master course in Environmental and Resource Geochemistry, Spring semester 2019.

Gimmi T.
Ausbreitung von Schadstoffen in Böden und Grundwasser: Von der Realität zum Modell – und zurück, Lecture Weiterbildungskurs Verhalten der organischen und anorganischen Schadstoffe in der Umwelt, University of Bern, 13-15 June 2019.

Hummel W., Plötze L.M.
Master course: Landfilling, Contaminated Sites and Radioactive Waste Repositories, ETH Zurich.

Kosakowski, G.
Master course: Geostatistics, Institute for Geological Sciences, University of Bern, Spring semester 2019.

Kulik D.A.
GEMS training at PSI NES, Villigen PSI, Switzerland, 14-15 January 2019.

Kulik D.A., Gysi A.
GEMS training at the Department of Geology & Geological Engineering, Colorado School of Mines, Golden CO, USA, 21-22 May 2019.

Kulik D.A.
GEMS training on thermodynamic modeling of cementitious and water-sediment systems, Department of Civil and Environmental Engineering, Hiroshima University, 24-27 September 2019.

Lothenbach B., Winnefeld F., De Weerdt K., Kulik D.A., Kunther W.
6th GEMS Workshop on thermodynamic modelling of cementitious systems, Empa, Dübendorf, Switzerland, 18-21 June 2019.

Miron G.D.
GEM-Selector workshop on geochemical modeling. Departement of Mineralogy - Petrology, Albert Ludwig University, Freiburg, Germany, 18 and 23 July 2019.

Pfingsten W., Furrer G.
Master course: Modelling of Processes in Soils and Aquifers, ETH Zurich

Prasser H.-M., Günther-Leopold I., Hummel W.
Master course: Nuclear Energy Systems, ETH Zurich.

10.7 PhD thesis defenses

Shafizadeh A.
Neutron imaging study of evolution of structural and transport properties of cement-clay interfaces. University of Bern, Bern, Switzerland, 30 July 2019.

Kéri A.
Mechanism of metal uptake by clay minerals - X-ray spectroscopy and molecular modelling study. University of Bern, Bern, Switzerland, 14 June 2019.

Nedyalkova L.
A structural and thermodynamic study of the intercalation of selenium, sulfur and iodine in AFm phases. University of Bern, Bern, Switzerland, 8 November 2019.

10.8 Other

Churakov S.V.
Examination of PhD of B. Zareeipolgaradani ”Surface reactivity of soft minerals at atomic-scale“, University of Lyon, Lyon France, 14 February 2019.

Dähn R, Churakov S. V.
Examination of PhD thesis of A. Kéri “Mechanism of metal uptake by clay minerals - X-ray spectroscopy and molecular modelling study”, University of Bern, Bern, Switzerland, 14 June 2019.

T. Gimmi
Associate Editor of Applied Geochemistry.

T. Gimmi
Examination of PhD thesis of S. Le Crom, “Modélisation à l'échelle microscopique des fluides et des solutés dans des argiles saturées et insaturées”, Sorbonne Université, Paris, France, 28 October 2019.

Gimmi T., Van Loon L.R., Churakov S.V.
Examination of PhD thesis of A. Schafizadeh “Neutron imaging study of evolution of structural and transport properties of cement-clay interfaces”, University of Bern, Bern, Switzerland, 8 November 2019.

Kulik D.
Associate Editor of Applied Geochemistry.

Miron G.D.
Improved modeling of low density fluids. SNF Scientific Exchanges grant. 1 Month exchange at the Departement of Mineralogy - Petrology, Albert Ludwig University, Freiburg, Germany, 1-31 July 2019.

Patel R.
Active member RILEM technical committee TC 281-CCC.

Patel R.
Active member RILEM technical committee TC 270-CIM.

Pfingsten W.
Secretary General of SITEX_Network Association.

Tits J., Churakov S.V.
Examination of PhD thesis of L. Nedyalkova “A structural and thermodynamic study of the intercalation of selenium, sulfur and iodine in AFm phases”, University of Bern, Bern, Switzerland, 8 November 2019.

Paul Scherrer Institut :: Forschungsstrasse 111 :: 5232 Villigen PSI :: Switzerland :: Tel. +41 56 310 21 11 :: www.psi.ch